Cell-free-synthesized voltage-gated proton channels: Approaches to the study of protein dynamics

Dissertation

zur Erlangung des Doktorgrades

der Naturwissenschaften

vorgelegt beim Fachbereich

Biochemie, Chemie und Pharmazie (FB14)

der Johann Wolfgang Goethe-Universität

in Frankfurt am Main

von

Beate Hoffmann

aus Halle (Saale)

Frankfurt am Main (2018)

D(30)

vom Fachbereich Biochemie, Chemie und Pharmazie (FB14) der

Johann Wolfgang Goethe-Universität als Dissertation angenommen.

Dekan: Prof. Dr. Clemens Glaubitz

Gutachter: Prof. Dr. Volker Dötsch

Prof. Dr. Klaas Martinus Pos

Datum der Disputation:

Table of contents

List of figures

List of tables

Abbreviations

2D ..... two-dimensional

2GBI 2-guanidinobenzimidazole

5FP ..... pentafluoro-L-phenylalanine

aa ..... amino acids

Abs ..... absorption

ACMA 9-amino-6-chloro-2-methoxyacridine

AcP ..... acetyl phosphate lithium potassium salt

amino acid nitroxide ..... (S)-2-amino-6-((((1-oxy-2,2,5,5-tetramethylpyrroline-3-yl)methoxy)carbonyl)amino)hexanoic acid

Anzergent3-14 ..... n-tetradecyl-N,N-dimethyl-3-ammonio-1-propanesulfonate

AOA ..... O-(carboxymethyl)hydroxylamine hemihydrochloride

ApoA1 ..... apolipoprotein A1

APS ..... ammonium persulfate

ATP ..... adenosine-5‘-triphosphate

BLAST ..... basic local alignment search tool

BSA ..... bovine serum albumin

CAI ..... codon adaptation index

CCCP ..... cyanide m-chlorophenyl hydrazone

CD ..... circular dichroism

CECF ..... continuous-exchange cell-free

CHAPS ..... 3-((3-cholamidopropyl) dimethylammonio)-1-propanesulfonate

CHARMM ..... Chemistry at Harvard Molecular Mechanics

CiH_V1 ..... *ciona intestinalis* voltage-gated proton channel

CiVSD ..... *ciona intestinalis* voltage-sensing phosphatase voltage-sensor domain

CiVSP ..... *ciona intestinalis* voltage-sensing phosphatase

cmc ..... critical micellar concentration

CPM ..... 7-diethylamino-3-(4’-maleimidylphenyl)-4-methylcoumarin

CTP ..... cytidine 5’-triphosphate di-sodium salt

D_2O ..... deuterium oxide

D-CF ..... detergent-based cell-free

DDM ..... n-dodecyl β-D-maltoside

DH(7)PC 1,2-diheptanoyl-sn-glycero-3-phosphocholine

DLS.....dynamic light scattering
DMPC.....1,2-dimyristoyl-sn-glycero-3-phosphocholine
DMPG.....1,2-dimyristoyl-sn-glycero-3-phospho-(1'-rac-glycerol)
DMSO..... dimethylsulfoxide
DOPC.....1,2-dioleoyl-sn-glycero-3-phosphocholine
DOPE.....1,2-dioleoyl-sn-glycero-3-phosphoethanolamine
DOPG.....1,2-dioleoyl-sn-glycero-3-phospho-(1'-rac-glycerol)
DPC..... n-dodecylphosphocholine
DrVSD.....zebrafish voltage-sensing phosphatase voltage-sensor domain
DrVSP.....zebrafish voltage-sensing phosphatase
DSS.....3-(trimethylsilyl)-1-propanesulfonic acid sodium salt
DTT..... 1,4-dithiothreithol
EDTA.....ethylenediaminetetraacetic acid
EF.....elongation factors
EGTA.....ethylenglycol-bis(aminoethylether)-N,N,N',N'-tetraacetic acid
EPC..... 1,2-dipalmitoyl-sn-glycero-3-ethylphsophocholine
EPR.....electron paramagnetic resonance
FbAA..... fluorescence-based activity assay
FM.....feeding mixture
Fos14.....n-tetradecylphosphocholine
FPLC.....fast protein liquid chromatography
FRET.....Förster resonance energy transfer
GTP.....guanosine 5'-triphosphate di-sodium salt
HABA..... hydroxyl-azophenyl-benzoic acid
HEPES.....2-[4-(2-hydroxyethyl)piperazin-1-yl]ethanesulfonic acid
hH_V1.....human voltage-gated proton channel
hH_V1-VSD.....human voltage-gated proton channel voltage-sensor domain
HMQC..... heteronuclear multiple quantum coherence
HPLC.....high-performance liquid chromatography
HPSF.....high purity salt free
HRP.....horseradish peroxidase
HSQC..... heteronuclear single quantum coherence
HT.....high-tension voltage
H_V1.....voltage-gated proton channels

IMAC ..... immobilized metal ion affinity chromatography
IP ..... isoelectric point
IPTG ..... isopropyl-β-D-thiogalactopyranosid
ITC ..... isothermal titration calorimetry
KOAc ..... potassium acetate
K_VAP ..... voltage-dependent potassium channel
L-CF ..... lipid-based cell-free
LDAO ..... N,N-dimethyldodecylamine N-oxide
LILBID ..... laser-induced liquid bead ion desorption
LMPG ..... 1-myristoyl-2-hydroxy-sn-glycero-3-phospho-(1'-rac-glycerol)
LPPG ..... 1-palmitoyl-2-hydroxy-sn-glycero-3-phospho-(1'-rac-glycerol)
M. barkeri ..... *methanosarcina barkeri*
M. mazei ..... *methanosarcina mazei*
MALDI ..... matrix-assisted laser desorption/ionization
MBP ..... maltose-binding protein
MD ..... molecular dynamic
$Mg(OAc)_2$ ..... magnesium acetate
MOPS ..... 3-(N-morpholino)propanesulfonic acid
MS ..... mass spectrometry
MSP ..... membrane scaffold protein
MTS ..... methanethiosulfonate
MWCO ..... molecular weight cut-off
NADPH ..... nicotinamide adenine dinucleotide phosphate
NAMD ..... nanoscale molecular dynamics
ND ..... nanodisc
NiEDDA ..... nickel ethylenediamine-N,N'-diacetic acid
NMR ..... nuclear magnetic resonance
NS ..... number of scans
NTA ..... nanoparticle tracking analysis
NTCB ..... 2-nitro-5-thiocyanatobenzoic acid
OAc ..... acetate
OD_{600} ..... optical density at 600 nm
p.A. ..... pro analysi
PAGE ..... polyacrylamide gel electrophoresis

P-CF ..... precipitate-based cell-free
PCR ..... polymerase-chain reaction
PEG ..... polyethylene glycol
PEP ..... phosphoenol pyruvic acid monopotassiumsalt
PIP phosphatidylinositol-4-phosphate
PIP2 ..... phosphatidylinositol-4,5-bisphosphate
PMSF ..... phenylmethylsufonyl fluoride
POPC 1-palmitoyl-2-oleoyl-sn-glycero-3-phosphocholine
POPE 1-palmitoyl-2-oleoyl-sn-gylcero-3-phosphoethanolamine
POPG ..... 1-palmitoyl-2-oleoyl-sn-gylcero-3-phospho-(1´-rac-gylcerol)
PPM ..... parts per million
PRE ..... paramagnetic relaxation enhancement
PVDF ..... polyvinylidene difluoride
PylRS ..... pyrrolysyl-tRNA-synthetase
RM ..... reaction mixture
RMM ..... resonant mass measurements
ROS ..... reactive oxygen species
RT ..... room temperature
SAXS ..... small-angle X-ray scattering
SDS ..... sodium dodecyl sulfate
SEC ..... size-exclusion chromatography
T7RNP T7-RNA-polymerase
TCA ..... trichloroacetic acid
TD1 ..... delay time
TEM ..... transmission electron microscopy
TEMED ..... tetramethylethylenediamine
TEV ..... tobacco etch virus
T_m ..... melting temperature
TOF ..... reflectron time of flight
Tris ..... tris(hydroxymethyl)aminomethane
UTP ..... uridine 5’-triphosphate tri-sodium salt
VSD ..... voltage sensing domain
VSP ..... voltage-sensing phosphatase
β-OG ..... n-octyl-β-D-glucoside

Summary

We often only realize how important health is when diseases manifest themselves through their symptoms and, ultimately, in a diagnosis. Over time, we suffer from many diseases starting with the first childhood disease to colds to gastrointestinal infections. Most diseases pass harmlessly and symptoms fade away. However, not all diseases are so harmless. Alzheimer's disease, breast cancer, Parkinson's disease, and colorectal cancer usually cause severe illness with high mortality rates. In pharmaceutical research, efforts are therefore being made to determine the molecular basis of them in order to provide patients with potential relief and, at best, healing. A special group of regulators, involved in the previously mentioned diseases, are voltage-gated proton channels. Thus, the understanding of their structure, function, and potential drug interaction is of great importance for humanity.

Voltage-gated proton channels are localized in the cell membrane. As their name indicates, they are controlled by voltage changes. Depolarization of the cell membrane induces conformational changes that open these channels allowing protons to pass through. Here, the transfer is based on a passive process driven by a concentration gradient between two individual compartments separated by the cell membrane. Voltage-gated proton channels are highly selective for protons and show a temperature- and pH-dependent gating behavior. However, little is known about their channeling mechanism. Previous experimental results are insufficient for understanding the key features of proton channeling.

In this thesis, for the first time, the cell-free production of voltage-sensing domains (VSD) of human voltage-gated proton channels (hH_V1) and zebrafish voltage-sensing phosphatases (DrVSP) is described. Utilizing the cell-free approach, parameters concerning protein stability, folding and labeling can be easily addressed. Furthermore, the provision of a membrane mimetic in form of detergent micelles, nanodiscs, or liposomes for co-translational incorporations of these membrane proteins is simple and efficient. Both VSDs were successfully produced up to 3 mg/ml. Furthermore, the cell-free synthesis enabled for the first time studies of lipid-dependent co-translational VSD insertions into nanodiscs and liposomes. Cell-free-produced VSDs were shown to be active, and to exist mainly as dimers. In addition, also their activation was stated to be lipid-dependent, which has not been described so far. Solution-state NMR experiments were performed with fully

and selectively labeled cell-free produced VSDs. With respect to the development of potential drug candidates, I could demonstrate the inhibition of the VSDs by 2-guanidinobenzimidazole (2GBI). Determined K_D-values were comparable to literature data for the human construct. For the first time, a low affinity for 2GBI of the zebrafish VSD could be described.

In future, the combination of a fast, easy and cheap cell-free production of fully or selectively labeled VSDs and their analysis by solution-state NMR will enable structure determinations as well as inhibitor binding studies and protein dynamic investigations of those proteins. The results of these investigations will serve as a basis for example for the development of new drugs. In addition, a detailed description of the lipid-dependent activity might be helpful in controlling the function of voltage-gated proton channels in cancer cells and thereby reducing their growth or disturbing their cell homeostasis in general.

Zusammenfassung

Zellfrei-synthetisierte spannungsgesteuerte Protonenkanäle:

Ansätze zur Untersuchung von Proteindynamiken

Oft merken wir erst, wie wichtig Gesundheit ist, wenn sich Krankheiten durch ihre Symptome und letztlich durch eine Diagnose manifestieren. Mit der Zeit leiden wir an vielen Krankheiten, beginnend mit der ersten Kinderkrankheit über Erkältungen bis hin zu Magen-Darm-Infektionen. Die meisten Krankheiten sind heilbar und die Symptome verschwinden. Jedoch sind nicht alle Krankheiten so harmlos. Beispielsweise Alzheimer, Brustkrebs, Parkinson und Kolorektalkrebs bringen meist schwere Krankheitsverläufe mit hoher Sterblichkeitsrate mit sich. In der pharmazeutischen Forschung gibt es daher Bestrebungen, die molekularen Ursachen solcher Krankheiten und deren Grundlagen genauer zu verstehen, um Patienten eine potentielle Linderung der Beschwerden und bestenfalls Heilung zu verschaffen. Eine spezielle Gruppe von Regulatoren, die an den zuvor erwähnten, aggressiv verlaufenden Krankheiten beteiligt sind, sind spannungsgesteuerte Protonenkanäle. Daher ist das Verständnis ihrer Struktur, ihrer Funktion und ihrer Interaktion mit potentiellen Arzneimitteln für die Menschheit von hoher Bedeutung.

Der aktuelle Wissensstand als Ausgangspunkt der vorliegenden Arbeit lässt sich wie folgt beschreiben. Spannungsgesteuerte Protonenkanäle sind in der Zellmembran verschiedenster Zellen lokalisiert, vor allem aber in denen von Zellen des menschlichen Immunsystems. Wie ihr Name andeutet, werden sie durch Spannungsänderungen gesteuert. Im Speziellen ist eine Domäne der Proteine, die spannungserfassende Domäne (VSD), dafür zuständig. Die Depolarisierung der Zellmembran induziert Konformationsänderungen in der VSD, wodurch diese geöffnet wird und Protonen passieren lässt. Die Übertragung basiert hier auf einem passiven Prozess, der durch einen Konzentrationsgradienten zwischen zwei, durch die Zellmembran getrennten, einzelnen Kompartimenten gesteuert wird. Die VSD besteht aus vier Transmembranhelices, welche über Loop-Strukturen miteinander verbunden sind. In Helix vier befinden sich mehrere positive Ladungen in Form von Argininseitenketten, die auf Spannungsänderung reagieren können. Folglich wird diese Helix auch als der Spannungssensor bezeichnet. Die vier membranständigen Helices der VSD bilden die Pore aus, welche die Protonen passieren lässt. Spannungsgesteuerte Protonenkanäle sind

hochselektiv für Protonen und zeigen ein temperatur- und pH-abhängiges Kanalisierungsverhalten. Über dessen Mechanismus ist jedoch wenig bekannt. Bereits publizierte, experimentelle Ergebnisse sind teils widersprüchlich und ergeben noch kein klares Bild. Es existieren mehrere Theorien, in welcher Form die Ionen die Pore durchqueren. Zum einen vermutet man eine wassergefüllte Pore, durch die die Protonen in Form von Hydroniumionen hindurchgeschleust werden. Auf der anderen Seite wird spekuliert, dass ein Mechanismus vorliegt, in dem die Protonen durch das Wechselspiel zwischen Wasserstoffbrückenbindungsbildung und -lösung transportiert werden. Die dreidimensionale Struktur der Kanäle konnte ebenfalls noch nicht ins Detail beschrieben werden. Es wurden Kristallstrukturen von Chimären und Artverwandten sowie Computersimulationsmodelle präsentiert, welche auf Daten verschiedenster Publikationen basieren. Es konnte jedoch bislang keine Struktur eines *in vivo* oder *in vitro* produzierten humanen spannungsgesteuerten Protonenkanals basierend auf den natürlichen Aminosäureprimärsequenzen gezeigt werden.

In dieser Doktorarbeit werden eine Vielzahl von Experimenten vorgestellt, um den molekularen Bauplan und die damit verbunden proteinspezifischen Eigenschaften der VSDs zu verstehen. Dabei lag das Hauptaugenmerk auf der Durchführung von Kernspinresonanzspektroskopie (NMR) Experimenten zur Bestimmung der Struktur und Analyse von Dynamiken innerhalb der VSDs. Im Speziellen wird die zellfreie Produktion von VSDs aus humanen Protonenkanälen (hH_V1) und denen von spannungserfassenden Phosphatasen aus Zebrafisch (DrVSP) beschrieben. Die zellfreie Proteinsynthese bietet hier entscheidende Vorteile gegenüber der Proteinproduktion in Zellen. Parameter bezüglich Proteinstabilität, Faltung und insbesondere Markierung mittels Isotopen können wesentlich einfacher adressiert werden, da keine physischen Barrieren in Form einer Zellmembran überwunden werden müssen. Die Ansätze können somit jeder Zeit von außen kontrolliert und gesteuert werden. Darüber hinaus ist die Bereitstellung eines Membranmimetikums, essentiell in der Arbeit mit Membranproteinen, in Form von Detergenz-Mizellen, Nanodiscs oder Liposomen, für die direkte Proteineinbettung nach erfolgter Translation, einfach und effizient umsetzbar.

In dieser Arbeit wird erstmals die erfolgreiche, zellfreie Produktion der zu erforschenden VSDs beschrieben. Unter Anwendung der zellfreien Proteinsynthese konnten die VSDs mit

hohen Ausbeuten von über 3 mg/ml hergestellt werden. Im Zuge von NMR Experimenten sind Messungen bei erhöhten Temperaturen über einen längeren Zeitraum notwendig. Dementsprechend mussten zunächst Aussagen über die Stabilität und Faltung der Konstrukte gesammelt werden. Die Untersuchungen begannen mit VSDs rekonstituiert in Detergentien als membranvortäuschende Umgebung. Der Einfluss verschiedenster Detergentien (LPPG, DHPC, DPC, DPC/LDAO, LDAO, Fos14) wurde mittels SDS-Polyacrylamidgelelektrophorese, Western Blot, Massenspektrometrie (LILBID), Größenausschlusschromatographie (SEC), NMR, und Circulardichroismus (CD) -Spektroskopie untersucht. Der Nachweis der Existenz von α-Helices in VSDs und deren nativer oligomerer Zustand (LILBID) deuteten auf gefaltete Proteine hin. Unerwarteter Weise traten erhebliche Stabilitätsverluste bei hohen Konzentrationen und hohen Temperaturen in Form von Aggregationsbildungen auf. Mit Hilfe von dynamischer Lichtstreuung (DLS), Resonanzmassenmessung (RMM) und *Nanoparticle Tracking Analysis* (NTA) wurde die Aggregationsproblematik genauer beleuchtet. In zellfrei produzierten, gereinigten VSD-Proben wurden eindeutig Aggregate identifiziert. Auch wenn diese nur in sehr geringer Konzentration vorlagen erwiesen sie sich zum Problem im Hinblick auf die Erhöhung der Temperatur und/oder Konzentration in NMR Messungen, da sie hier als eine Art Keim wirkten und die vollständige Aggregation der Probe zur Folge hatten. Die bestehenden Aggregate konnten nicht mit Hilfe von Zentrifugations-, Ultrazentrifugations- oder Filtrierungsschritten abgetrennt werden. Es stellte sich die Frage, ob man die Bildung der Aggregate umgehen kann, in dem man direkt am Punkt der Proteinsynthese naturnahere Membranumgebungen präsentiert, um somit die eventuelle Falschfaltung in Detergenz-Mizellen, welche zur Aggregatbildung beitragen könnte, zu verhindern. Nanodiscs und Liposomen wurden als Umgebung für die hydrophoben VSDs ausgewählt. Beide weisen eine Lipiddoppelschicht auf, deren Lipide variabel zusammengesetzt werden können. Zunächst wurden beide Systeme in Bezug auf ihre VSD-Insertionseigenschaften hin untersucht, um eine durch Nichteinbau hervorgerufene Falschfaltung und dadurch bedingte Aggregation auszuschließen.

Erstmals konnte eine erfolgreiche co-translationale Insertion der VSDs in Liposomen und Nanodiscs gezeigt werden. Die anschließende SEC Analyse bestätigte die Homogenität und Stabilität der VSD-Nanodiscs. Dabei waren die Nanodiscs in der Lagerung bei 4 °C für

mindestens einen Monat stabil. Mit Hilfe einer passenden Strategie in der LILBID Technik, wobei hH_V1-VSD mittels Markierung mit schweren Isotopen in seinem Molekulargewicht angehoben wurde, konnte dessen natives Dimer in Nanodiscs nachgewiesen werden. Zusätzlich zeigten NMR Experimente Signale in Bereichen, die typisch für gefaltete Proteine sind. Zusammenfassend war von einer erfolgreichen Insertion eines gefalteten VSD-Konstruktes in Nanodiscs auszugehen. Dennoch wurden in Transmissionselektronen-mikroskopieaufnahmen erneut Aggregate detektiert, deren Konzentration zwar durch eine Ultrazentrifugation verringert, aber sie nicht vollständig entfernt werden konnten. Unabhängig davon sollten weitere NMR Experimente zu strukturellen Aussagen führen. Dafür wurden die Konstrukte auch mittels erfolgreicher Selektivmarkierung untersucht. Die Gesamtauflösung, der unter den genannten Bedingungen, erhaltenen Spektren und deren Peakverteilung waren dennoch ungenügend für eine finale Peakzuordnung zu einzelnen Aminosäuren im Protein sowie für Experimente bezüglich der Analyse von Dynamiken. Erneut stand die mögliche Falschfaltung der VSDs als Ursache der Aggregationsneigung im Raum. Aktivitätsstudien sollten weitergehende Aussagen über die Faltungseigenschaften machen.

Erstmalig wurde die Aktivität und Inhibierung für zellfrei produzierte VSDs beschrieben. Nur VSDs, die ihre native Struktur vorweisen, sind in der Lage, Spannungsänderungen zu detektieren, darauf zu reagieren und gegebenenfalls Protonen zu kanalisieren. Des Weiteren sollten nur richtig gefaltete VSDs auf Inhibitorzusätze mittels verminderter Kanalisationsleistung reagieren können. Der durchgeführte Fluoreszenz-basierte Aktivitätstest erforderte hierbei eine Kompartimentierung zur Gewährleistung eines messbaren, passiven Protonenflusses nach erfolgter Spannungsänderung an der Membran/Lipiddoppelschicht. Demzufolge mussten die VSDs in Liposomen rekonstituiert werden. Proteoliposomen mit einer definierten Lumenzusammensetzung wurden in Fluoreszenzpuffer mit einer geringen Kaliumkonzentration verdünnt. Durch Zugabe des Kalium-selektiven Ionophors Valinomycin erfolgte ein Ausstrom dieser Ionen aus dem Lumen der Liposomen. In dessen Folge wurde eine Spannungsänderung über die Membran induziert, welche zur Aktivierung vorhandener, gerichtet insertierter und gefalteter VSDs führte. Die Kanalisierung von Protonen wurde mittels des Fluoreszenzfarbstoffes ACMA gemessen. Durch Protonierung dessen, im Inneren der Liposomen, kam es zur

Fluoreszenzlöschung, welche detektiert werden konnte. Unter Anwendung dieses Assays konnte die Protonen-kanalisierende Aktivität für beide Konstrukte gezeigt werden. Zusätzlich wurde sogar erstmals eine Lipidabhängigkeit attestiert. Dabei konnte gezeigt werden, dass VSDs humanen und zebrafisch Ursprungs Phosphatidylglycerol (PG) Kopfgruppen in Kombination mit Phosphatidylethanolamin (PE) oder Phosphatidylcholine (PC) Kopfgruppen sowie ungesättigte Fettsäuren im Schwanzabschnitt der Lipide zur Ausbildung ihrer Aktivität benötigten. Mittels des Fluoreszenz-basierten Aktivitätstests konnte zusätzlich die Inhibierung der Protonenkanalisierung der VSDs durch den Inhibitor 2-Guanidinobenz-imidazol (2GBI) gezeigt werden. Unerwarteter Weise, war die inhibitorische Wirkung für die VSD der spannungserfassenden Phosphatase prägnanter als für die VSD des humanen Protonenkanals. Um einen detaillierten Einblick in die Ursachen zu erlangen, wurden isothermale Titrationskalorimetriemessungen (ITC) durchgeführt. Diese ergaben Affinitäten (K_D-Werte) von 2GBI zu ~50 µM für das humane und ~2.6 mM für das Konstrukt aus Zebrafisch. Die Ergebnisse verdeutlichen eine wesentlich schwächere Bindung des Inhibitors an die VSD der spannungserfassenden Phosphatase mit einer gleichzeitig höheren hemmenden Wirkung. In Summe kann dies nur durch bessere Zugangsmöglichkeiten des Inhibitors an die Wirkstelle im Protein oder auf zwei grundverschiedene Inhibierungs-mechanismen zurückzuführen sein. Gleichwohl ließ die Summe aller Ergebnisse der Aktivitätsstudien den Schluss zu, dass die VSDs in Liposomen gefaltet sein mussten. Nachteilig können Liposomen aufgrund ihrer Größe mittels Lösungs-NMR nicht untersucht werden. Hier bieten sich nur Studien mittels Festkörper-NMR an, wobei die Proben in einem kryogenen Zustand vorliegen, welcher die Untersuchungen von dynamischen Prozessen erheblich erschweren würde. Es stellte sich nun die Frage, wie man den Liposomenzustand, in dem die Faltung gezeigt werden konnte, auflösen kann, unter Aufrechterhaltung des Faltungszustandes bis zu einer mittels Lösungs-NMR detektierbaren Größe.

In einem Kooperationsprojekt wurden die VSDs erstmalig einer Art Rückfaltung unterzogen. Präzipitierte, zellfrei synthetisierte VSDs wurden durch Zugabe eines harschen Detergenz solubilisiert und anschließend in Liposomen rekonstituiert. Durch Lipidkontakte und den allgemeinen Einfluss der Lipiddoppelschicht (seitlicher Druck, Krümmung) wurde die Faltung ermöglicht. Anschließend konnten die VSDs durch Behandlung der Proteoliposomen mit einem milden Detergenz unter Beibehaltung ihres nativen oligomeren Zustandes extrahiert

werden. Die solubilisierten VSDs zeigten neben der Dimerstruktur auch eine deutlich erhöhte Stabilität und Homogenität gegenüber Proben, die ausschließlich in einer Detergenzumgebung untersucht worden sind. Unerwarteter Weise zeigte sich keine Verbesserung im Hinblick auf die Peakverteilung und Auflösung der NMR Spektren der rückgefalteten Konstrukte. Die detektierten Größenverhältnisse in NMR Experimenten sowie Auswertungen von SEC Läufen dieser Proben nach erfolgten NMR Messungen wiesen erneut auf gebildete Aggregate hin.

Die Ergebnisse der vorgelegten Arbeit bringen Hinweise und Anregungen für weitere Forschungen.

Zukünftig gilt es die Aggregationsbildung zu unterbinden, um den molekularen Bauplan der spannungsgesteuerten Domänen von Protonenkanälen entschlüsseln zu können. Verlängerte Ultrazentrifugationsläufe, optimierte Pufferbedingungen, die experimentelle Arbeit mit Volllängenproteinen ohne jegliche Mutationen sowie deren Einbettung in noch naturnahere Membranumgebungen bzw. deren zellfreie Synthese mittels Zellextrakten aus deren Wirtszellen könnten die Aggregation der Proben verhindern. Perspektivisch gesehen, werden zellfreie Plattformen zur Verfügung stehen, bei denen Komponenten noch leichter ausgetauscht und manipuliert werden können. Diese werden hohe Produktausbeuten bei gleichzeitiger, ausgezeichneter Probenqualität gewährleisten. Die hiermit synthetisierten Proteine stehen dann für unterschiedliche Analysen zur Verfügung, um Antworten auf verschiedene Fragen wie z.B. den Kanalisierungsmechanismen zu erhalten.

Die Analyse der Dynamiken in spannungsgesteuerten Protonenkanälen bleibt aber auch zukünftig eine sehr anspruchsvolle Aufgabe.

1 Introduction

Life is always out of equilibrium! A living cell, as a high complex system, needs to maintain homeostasis by simultaneously being out of equilibrium. Consequently, control mechanisms and regulators are essential. Here, membrane structures of the cell enable the formation of compartments, which can be controlled individually. The membranes determine exchange processes between different environments of a variety of substances including small ions, lipids, messenger molecules, or energy metabolites in form of e.g. adenosine triphosphate (ATP). Small ions are able to diffuse across this barrier directly, but not as effective as required to take part in regulatory processes. To ensure this, the cell membranes contain specialized proteins for the regulation of the cell homeostasis. Here, exchange processes across the membrane are realized by transporters, pumps, and channels reacting on concentration gradients and/or signaling molecules in an active or passive manner. The translocation of substrates by channels, embedded in the cell membrane, is driven by a concentration gradient caused by different ion compositions in two individual compartments. Mostly, this process is energy independent, which determines the flow direction to be along the chemical gradient. However, channels can be controlled in their opening and closing probabilities by other mechanisms. For example, ubiquitous voltage-sensing membrane proteins channel their substrates during voltage-dependent changes of the membrane potential. These specific membrane proteins and properties of the membrane potential will be discussed in the next section.

1.1 Voltage-sensing membrane proteins

Small ions in- and outside the cell generate an electrochemical gradient whereby charges are separated by the cell membrane. This charge difference can be translated into the membrane potential V_m of each cell (mostly at -70 mV inside). Typically, Na^+, K^+, Ca^{2+}, Cl^-, and H^+ determine the electrochemical potential (Hille, 2001). In detail, the chemical potential is caused by a concentration gradient of these ions. The electrical gradient is a result of the charge separation by the cell membrane. An ion can reach its electrochemical equilibrium, known as the Nernst potential, when electrical and concentration gradients are equal (described by the Nernst equation, Equation 1), resulting in no net ion diffusion across the membrane (Nernst, 1888, 1889).

$$V_{eq} = \frac{RT}{zF} ln \frac{[X]_o}{[X]_i}$$ Equation 1

In the Nernst equation, V_{eq} symbolizes the equilibrium potential for a given ion, R is the universal gas constant, T the temperature, z the valence of the ion, F the Faraday's constant, $[X]_o$ the ion concentration outside the cell, and $[X]_i$ the ion concentration inside the cell. Under physiological conditions, the Nernst potential of protons with an intracellular concentration $[H]_i$ of 63 nM (pH 7.2) and an extracellular concentration $[H]_o$ of 40 nM (pH 7.4) can be calculated as -12 mV (DeCoursey, 1991). As another example, the Nernst potential for potassium ions is calculated as -97 mV if $[K]_i$ is 150 mM and $[K]_o$ is 4 mM (Hille, 2001; Boron & Boulpaep, 2012). Consequently, different types of regulatory proteins are necessary for maintaining the cell homeostasis. Specific membrane proteins (channels, transporters, pumps etc.) are either responsible for maintaining the cell's resting potential (e.g. Na^+/K^+-ATPase) or responding donors of membrane potential changes. Second are known as voltage-sensing membrane proteins. This kind of proteins was first described in 1973 when they measured currents for a sodium-potassium pump (Armstrong & Bezanilla, 1973).

First, the nomenclature for voltage-sensing membrane proteins is based on basic principles. The first letter(s) of each name represents the organism in which the protein was found (e.g. h for human and Dr for *danio rerio*). The following capital letter denotes the transported or channeled ion (e.g. H for protons and K for potassium). Most importantly, the following V, written as subscript, indicates the regulation of this protein by voltage changes in the membrane.

On a molecular level, voltage-sensing membrane proteins react to changes in the membrane potential by switching the conformational state, which results in the transmission of signals. Several mechanisms exists which can lead to voltage-induced conformational changes. The electric field can have an influence on side chains (e.g. Tyr) or entire α-helices with an intrinsic dipole moment, which is reoriented during electrochemical gradient changes (Bezanilla, 2008). Some proteins contain cavities filled with ions, which start moving because of a certain current. Furthermore, charged side chains are supposed to be the modulating factors during the gating process of a special group of voltage-sensing proteins, the voltage-gated proton channels. Here, the opening and closing of voltage-gated ion channels is based on a change in the protonation state of charged residues like Arg, Glu, Asp, Lys and His in response to a membrane depolarization (Bezanilla, 2008).

1.2 Voltage-gated proton channels

The permeation of protons through the membrane of a cell is proposed to be either ensured by transient water wires, weak bases or acid shuttles, phospholipid flip-flop or transport proteins (channels, carriers, pumps) (Boron, 1983; Gutknecht, 1988; DeCoursey, 2003). Important representatives of this group are voltage-gated proton channels (H_V1), which are specialized voltage-gated cation channels designed to control the movement of protons across membranes. Thereby, they are highly selective for protons (Hille, 2001; Smith *et al.*, 2011; DeCoursey, 2013).

Voltage-gated proton channels were first postulated in 1972 and identified in snail neurons in 1982 under patch-clamp recording conditions (Fogel & Hastings, 1972; Nealson *et al.*, 1972; Thomas & Meech, 1982). Proton currents in human cells were not reported before 1993 (Demaurex *et al.*, 1993; DeCoursey & Cherny, 1993). Proton channels could be identified in various organisms and different tissues, in which they fulfill multiple functions. In mammals, they are mainly localized in the plasma membrane of cells of the immune system (function: maintain cell homeostasis) (Babcock & Pfeiffer, 1987; DeCoursey, 1991; DeCoursey & Cherny, 1993; Kapus *et al.*, 1993; Musset *et al.*, 2008; Capasso *et al.*, 2010). Here, these channels are known to participate in acid extrusion. In addition, they are involved in reactive oxygen species production by nicotinamide adenine dinucleotide phosphate (NADPH) oxidase, a membrane-embedded enzyme in phagocytes, whereby a created proton current compensates for the electron efflux (Henderson *et al.*, 1987; DeCoursey, 2003; Ramsey *et al.*, 2009). Consequently, by transporting the protons out of the cell, the specific channels prevent a massive acidification or depolarization of the cell over time. Additionally, H_V1 were found in sperm cells (function: triggering capacitation), in coccolithophores (function: calcium skeleton formation) and in different dinoflagellates (function: triggering bioluminescence flash, pH homeostasis) (Lishko *et al.*, 2010; Lishko & Kirichok, 2010; Smith *et al.*, 2011; Taylor *et al.*, 2011; Bach *et al.*, 2013; Berger *et al.*, 2017; Kigundu *et al.*, 2018).

Structurally, voltage-gated proton channels are composed of four transmembrane helices (S1-S4) forming the so-called voltage-sensing domain (VSD). In contrast to voltage-gated cation channels, the pore is formed solely by the four transmembrane helices of the VSD (Figure 1).

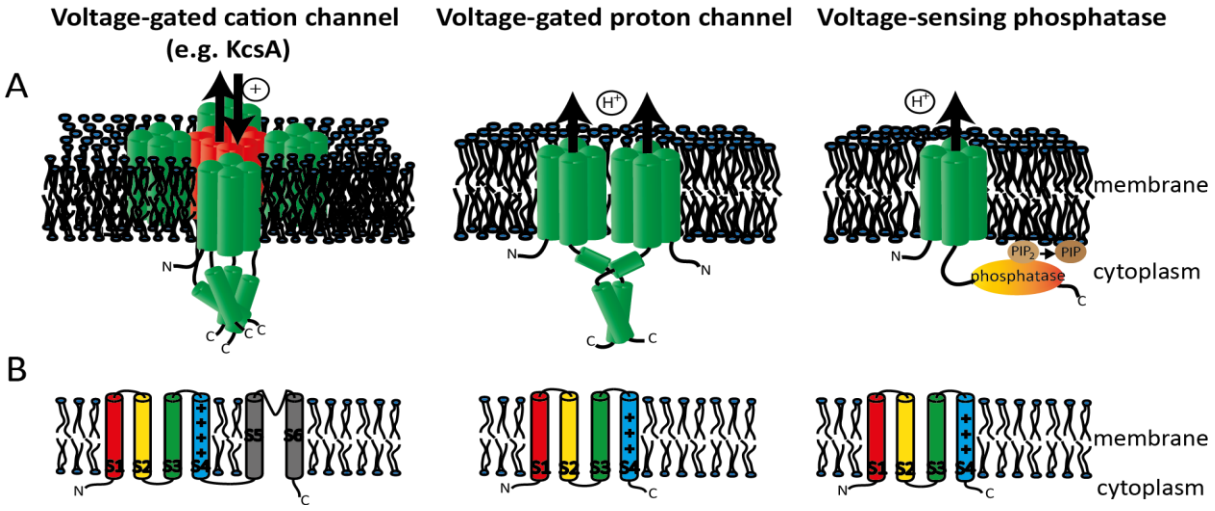

Figure 1: Schematic representation of different voltage-gated ion channels in the cell membrane. A Predominantly, voltage-gated cation channels are composed of six transmembrane helices whereby the first four (S1-S4) record changes in the membrane potential (VSD) and helices S5 and S6 form the central pore of a tetrameric channel responsible for ion permeation. Helices are drawn as cylinders in green and highlighted in red to demonstrate the pore formation in a tetrameric channel. In contrast, voltage-gated proton channels exist as dimers (1.2). Each VSD, composed of the four transmembrane helices, forms an individual pore through which protons are channeled. Likewise, the VSD of a voltage-sensing phosphatase is formed by four transmembrane helices and responsible for proton channeling and the regulation of the coupled phosphatase activity (1.2.2). Here, the lipid head group phosphatidylinositol-4,5-bisphosphate (PIP_2) gets dephosphorylated generating phosphatidylinositol-4-phosphate (PIP), shown as an example (Iwasaki *et al.*, 2008). N- and C-termini of the different channels are indicated, lipids are represented as pictograms, and black arrows illustrate the main direction of cation movement. **B** The pictures show a schematic representation of the pore forming unit of each channel (S1-S6 or S1-S4) by highlighting the four- or three-times positive charges in S4 (+), reacting to changes in the membrane potential by conformational changes of the entire helices. Helices are shown as cylinders and lipids are represented by pictograms. N- and C-termini of the different channels are indicated.

Voltage-gated proton channels lack the helices S5 and S6 as well as the loop forming the pore domain in the tetrameric quaternary structure of other voltage-gated cation channels (Figure 1) (Berger & Isacoff, 2011). However, H_V1 occurs as dimers mainly triggered by the C-terminal cytoplasmic coiled-coil domain and by the helices S1 and S4 (Koch *et al.*, 2008; Lee *et al.*, 2008b; Li *et al.*, 2010b; Smith & DeCoursey, 2013; Fujiwara *et al.*, 2013; Li *et al.*, 2015; Boonamnaj & Sompornpisut, 2018). Dimer formation occurs due to cooperativity reasons (Gonzalez *et al.*, 2010; Tombola *et al.*, 2010; Musset *et al.*, 2010b; Musset *et al.*, 2010c). However, each monomer is able to conduct protons independently. Charged residues, responsible for the opening and closing of the VSD, are located in S4 (three conserved arginine residues) (Figure 1B).

As mentioned, the proton channel gating-pore is built up only by the VSD. Furthermore, the transmembrane helices, mostly composed of hydrophobic amino acids (aa), contain charged residues like Arg, Asp and Glu, known to be involved in channeling processes (Carmona *et*

al., 2018; DeCoursey, 2018a, b). Concerning functional properties, voltage-gated proton channels can be subdivided into four or five varieties, with respect to their different gating kinetics (channel opening and closing), although all are activated by membrane depolarization and are sensitive to pH (DeCoursey, 1998, 2003). Two different proton channels are under investigation in this thesis, the VSD of the human voltage-gated proton channel (hH_V1) and the VSD of the zebrafish voltage-sensing phosphatase (DrVSD).

1.2.1 The human H_V1

Proton currents in human granulocytes were first reported in 1993 (1.2) (Demaurex *et al.*, 1993). Why is a proton current necessary at all in these specialized immune cells and how is this process controlled? Granulocytes become activated in response to microbial contact. The bacteria are engulfed and killed by an increasing cytosolic acidification. In order to maintain the cell homeostasis the excess of cytosolic protons (low pH_i) has to be regulated by a massive proton efflux. These outward currents were measured for cells overexpressing H_V1 channels. These channels are opened due to membrane depolarization and pH changes. Until now, many more functions of the human H_V1 channel (hH_V1) were described, which will be introduced in the next paragraphs.

The human genome encodes only one H_V1 gene. Nevertheless, different isoforms exist due to alternative splicing events (DeCoursey, 2015). Channels are localized in the plasma membrane of human basophils (Musset *et al.*, 2008), sperm cells (Lishko *et al.*, 2010; Lishko & Kirichok, 2010), B lymphocytes (Capasso *et al.*, 2010), microglia (Eder & DeCoursey, 2001) and others. As mentioned, their common function is the restoring of the cytoplasmic pH. This is of particular importance in cancer cells. Here, their extensive growth is enabled by a 10 times higher anaerobic glycolysis compared to normal tissue cells. The resulting acidification by increased concentrations of lactic acid due to the Warburg effect (Warburg, 1924) is most likely counteracted by the outward extrusion of protons by voltage-gated proton channels, thus, maintaining high proliferation rates of cancer cells (Wang *et al.*, 2011; Wang *et al.*, 2012; Wang *et al.*, 2013a; Wang *et al.*, 2013b). Especially the synthesis of a shorter isoform, missing the first 20 N-terminal amino acids, was found to be upregulated in these cells (Capasso *et al.*, 2010). An inhibition of hH_V1 in malignant cells by polyvalent cations induced their apoptosis, which demonstrates its significant role in drug development

(Wang *et al.*, 2013b). As an example, the information that two Histidine residues are supposed to coordinate a zinc ion, His140 and His193, can be used for future developments of new blocking reagents (Figure 2B) (Ramsey *et al.*, 2006). Furthermore, these channels are involved in the production of reactive oxygen species (ROS), which can cause severe tissue damage. As a result, hH_V1 channels play a role in a variety of diseases like Alzheimer's disease, ischemic stroke, Parkinson's disease, Crohn's disease, cystic fibrosis, breast cancer, colorectal cancer, and chronic lymphocytic leukemia underlining its importance for pharmaceutical research (Eder & DeCoursey, 2001; Haglund *et al.*, 2013; Conese *et al.*, 2014; Wang *et al.*, 2012; Morgan *et al.*, 2015; Wang *et al.*, 2013a). Further knowledge with regard to the protein structure and/or gating mechanism will accelerate future drug development to mitigate or even prevent the mentioned diseases.

Structurally, the hH_V1 is composed of 273 amino acids (UniProtKB-Q96D96, [Consortium, 2017]). A model representing the voltage-sensing domain of hH_V1 (hH_V1-VSD) (amino acids 84-214) embedded in the membrane is shown in Figure 2.

The hH_V1 is composed of a short N-terminal intracellular domain, four transmembrane helices connected by small loops and a large intracellular C-terminal domain. The latter is known to participate in dimer formation and is involved in the channeling process by influencing the S4 movement (Lee *et al.*, 2008b; Li *et al.*, 2010b; Fujiwara *et al.*, 2012; Fujiwara *et al.*, 2014). The four transmembrane helices form the VSD. Based on the homology model **S1** includes amino acids 99-120, **S2** 133-156, **S3** 172-186 and **S4** 194-210. The VSD responds to membrane depolarization by the movement of the S4 helix enabling the channeling of protons across the membrane barrier. Here, the countercharge positions of three arginine residues localized in S4 (Figure 1, Figure 2) (R205, R208 and R211) are supposed to be exchanged. In detail, countercharges D112, E119, D123 and D185 are described to be involved in the opening process whereas E153 and D174 stabilize the closed-state of hH_V1 (Ramsey *et al.*, 2010; Li *et al.*, 2015; DeCoursey *et al.*, 2016). A special role is assumed for the amino acids F150, V109 and V178 function as a plug, closing the pore as described for other voltage-gated cation channels (DeCoursey *et al.*, 2016; Li *et al.*, 2014; Lacroix *et al.*, 2014; Li *et al.*, 2015). Potential phosphorylation sites are located in the N-terminal region of the channel, T29 and S97. Phosphorylation of T29 by protein kinase C enhances the channeling process in leukocytes (Morgan *et al.*, 2007; Musset *et al.*, 2010a).

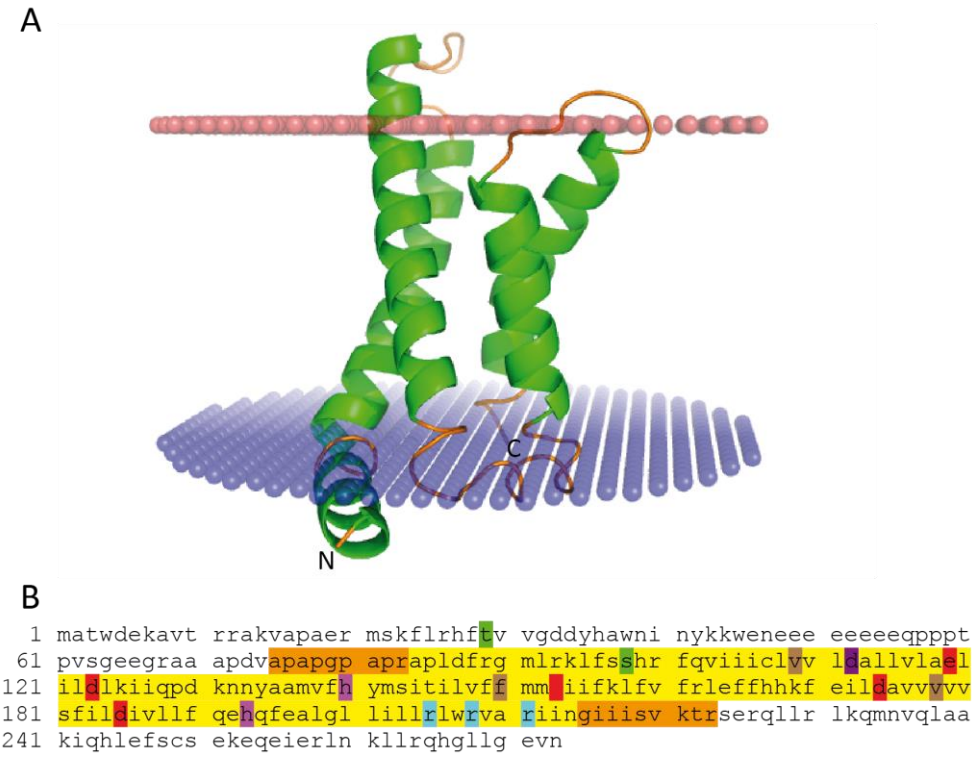

Figure 2: Homology model and sequence information of the hH$_V$1-VSD embedded in the membrane. A A homology model of the hH$_V$1-VSD (amino acids 75-223 applied for modeling, 84-214 shown), under investigation in this thesis, was created by SWISS-MODEL (Arnold *et al.*, 2006; Benkert *et al.*, 2011; Biasini *et al.*, 2014). The X-ray structure of the voltage-sensor containing phosphatase from *ciona intestinalis* (4G7V, rcsb.org [Berman *et al.*, 2000]) was used as the template with a sequence similarity of 33 % and sequence identity of 24.4 %. Subsequently, the resulting hH$_V$1-VSD structure was embedded in a model membrane of 1,2-dioleoyl-*sn*-glycero-3-phosphocholine (DOPC) lipid molecules (Lomize *et al.*, 2012). Helices are shown in green and loop regions in orange. N- and C-terminus of the VSD are labeled. The membrane is represented by dots whereby the cytoplasmic barrier is shown in blue and the extracellular membrane part is shown in red. **B** The hH$_V$1 sequence with highlighted residues is shown. The yellow box indicates the complete sequence of the modeled VSD structure (84-214), extended by the orange boxes which show the hH$_V$1-VSD sequence used in this thesis (75-223) (Figure 2A). The green boxes represent possible phosphorylation sites, the light purple boxes a potential coordination site for polyvalent cations and the dark purple box residue D112, known to be involved in gating processes. The brown boxes show residues, which determine proton accessibility, and the red boxes additional potential countercharges for the three arginine residues, known as the voltage-sensors, here highlighted in blue.

Despite numerous attempts involving crystallization and computational modeling, the structure of the hH$_V$1 could not be solved so far (Li *et al.*, 2010b; Musset *et al.*, 2010c; Wood *et al.*, 2012; Kulleperuma *et al.*, 2013; Takeshita *et al.*, 2014; Pupo *et al.*, 2014; DeCoursey *et al.*, 2016; Randolph *et al.*, 2016). Referring to the channel presence in a variety of different diseases, the knowledge of the structure and/or of the channeling mechanism is of tremendous importance for pharmaceutical research in drug development. If we understand how protons pass through the channel and also how conformational changes lead to its closing or opening, inhibitors could be designed that block proton extrusion e.g. from cancer cells.

Consequently, the cells would die due to massive cytosolic acidification. These considerations were the basis of the present work.

In this thesis, I worked with a truncated version of hH_V1 including amino acids 75-223, referred as **hH_V1-VSD**, which was cut off shortly before the first intracellular helix and four amino acids after the calculated fourth transmembrane helix (Figure 3) (7.1). As the VSD was the preferred target for my studies, the C-terminal domain was left out to generate a construct of decent size for solution-state NMR studies.

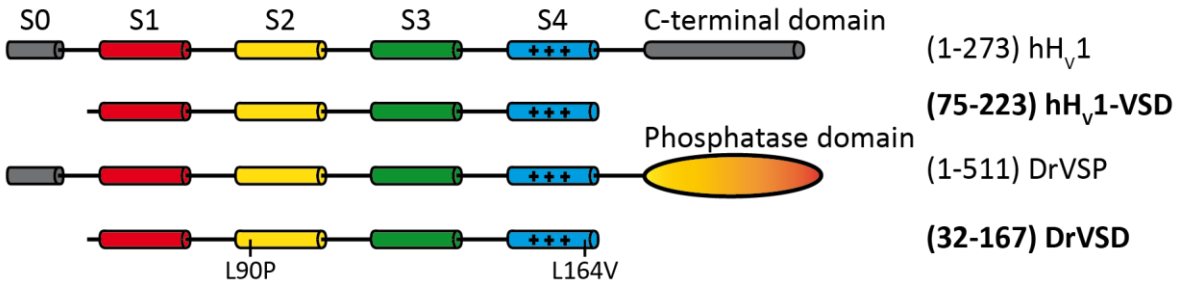

Figure 3: Schematic representation of examined voltage-gated proton channels. The figure illustrates the different constructs under investigation in this thesis (hH_V1-VSD and DrVSD) in comparison to the respective full-length proteins (hH_V1 and DrVSP). Helices are displayed as cylinders and named according their order S0-S4. The C-terminal helix domain of hH_V1 is shown as a grey cylinder. The phosphatase domain of the zebrafish voltage-sensing phosphatase (DrVSP) is shown as an orange ellipse. Three plus symbols represent the three positive charged arginine residues, which are described to be the voltage-sensor unit. L90P and L164V indicate substitutions in the DrVSD construct compared to the wild-type protein.

A similar procedure was used for the second analyzed VSD from the zebrafish phosphatase construct, which will be introduced in the next section.

1.2.2 The zebrafish voltage-sensing phosphatase

Voltage-sensing phosphatases (VSP), as special voltage-gated channels, are composed of two different subunits, the voltage-sensing domain recognizing changes in the membrane potential and the cytosolic phosphatase domain responsible for the dephosphorylation of membrane phospholipids (Figure 1). The level of PIP_2 in the membrane determines the activity of other ion channels or transporters, thereby regulating several different biological processes (Suh & Hille, 2005). Thus, electrical signals can be translated into intracellular responses. Additionally and of main importance in this thesis, VSDs of these phosphatases are described to channel protons (Li *et al.*, 2015).

In this thesis, the voltage-sensing domain of the zebrafish (*danio rerio*) voltage-sensing phosphatase was studied (DrVSD). The full-length protein (wild-type) is composed of 511

amino acids (UniProtKB-B3IUN7, [Consortium, 2017]) (Figure 4). This is reflected in the tertiary structure by a short N-terminal intracellular domain followed by four transmembrane helices, a linker region, and a large intracellular C-terminal-attached phosphatase domain (Figure 3). I worked with a truncated (amino acids 32-167) version of the DrVSP, named **DrVSD** (Figure 3, Figure 4).

As described for the hH_V1-VSD construct (1.2.1), exclusively the voltage-sensor domain of this protein was under investigation. The DrVSD shows 25 % sequence identity and 54 % sequence similarity with the hH_V1-VSD calculated with the basic local alignment search tool (BLAST).

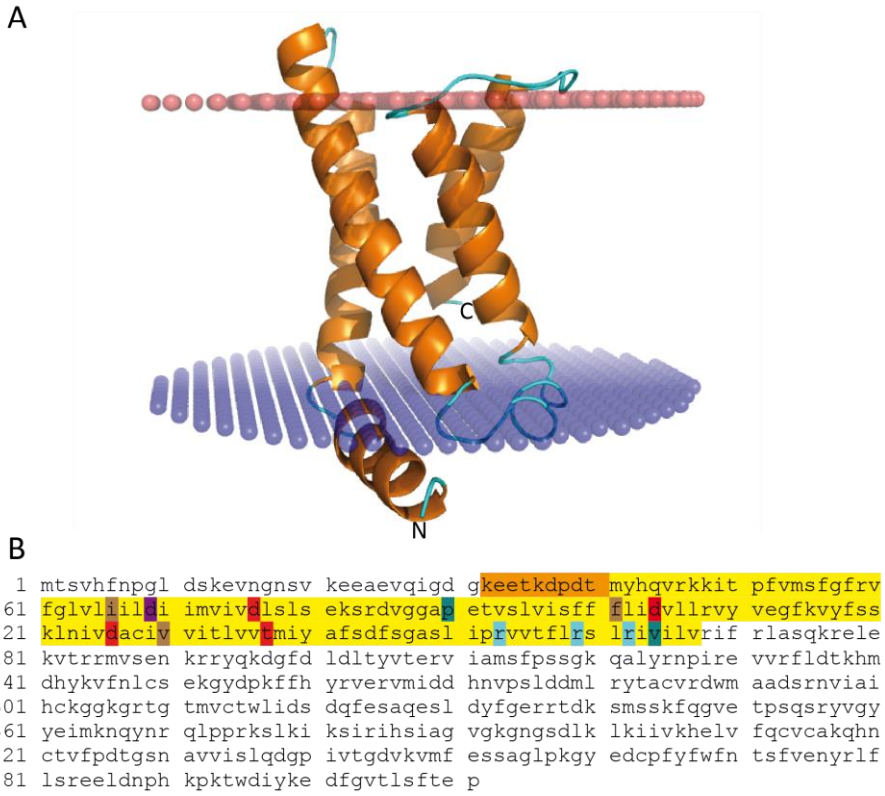

Figure 4: Homology model and sequence information of the DrVSD embedded in the membrane. A A homology model of the DrVSD with two mutations L90P and L164V (amino acids 32-167 applied for modeling, 41-167 shown), was created by SWISS-MODEL (Arnold *et al.*, 2006; Benkert *et al.*, 2011; Biasini *et al.*, 2014) The X-ray structure of the voltage-sensor containing phosphatase from *ciona intestinalis* (4G7V, rcsb.org, [Berman *et al.*, 2000]) was used as the template with a sequence similarity of 37 % and sequence identity of 36 %. Subsequently, the resulting DrVSD structure was embedded in a model membrane of DOPC lipid molecules (Lomize *et al.*, 2012). Helices are shown in orange and loop regions in cyan. N- and C-terminus of the VSD are labeled. The membrane is represented by dots whereby the cytoplasmic barrier is shown in blue and the extracellular membrane part is shown in red. **B** The DrVSP sequence with highlighted residues is shown. The yellow box indicates the start and end position of the modeled VSD structure (41-167), extended by the orange box which shows the DrVSD sequence used in this thesis (32-167) (Figure 2A). The dark purple box represents the countercharge D69, aligned residue to D112 in hH_V1 known to be involved in gating processes. The brown boxes show residues, which might be responsible for proton accessibility, and the red boxes additional potential countercharges for the three arginine residues, known as the voltage-sensors, here highlighted in blue. Mutations in the DrVSD construct, L90P and L164V, are shown in cyan.

Leucine90 was exchanged to proline to stabilize the beginning of S2 as it was described for other α-helical proteins (Kim & Kang, 1999). The sea squirt protein, *ciona intestinalis* VSP (CiVSP), contains the only VSD of a voltage-sensing proton channel from which a reliable structure is known so far (Li *et al.*, 2014). Hence, it was used as a kind of model system for other VSDs. For this reason, Leucine164 in DrVSD was exchanged to valine. Valine represents the complement in the CiVSP sequence, which was shown to be stable enough for structural investigations.

Based on the homology model **S1** includes amino acids 58-78, **S2** 84-109, **S3** 124-140 and **S4** 151-166, respectively (Figure 4). S4 movement in response to voltage changes in the membrane is supposed to be enabled by three arginines localized in S4 (R153, R159 and R162) (Figure 1, Figure 4). In this case, too, countercharge positions have to be present as well as side chains forming the hydrophobic gasket, which regulates proton channeling. Due to the absence of a detailed description of structural insight of DrVSP, these regions with the crucial aa residues are not classified so far. However, the protein sequence of the *ciona intestinalis* voltage-sensor domain (CiVSD), from which the crystal structure is known (Li *et al.*, 2014), and hH_V1 can be used for sequence alignments and homology model calculations to gain information of potential countercharge residue candidates in DrVSD (Figure 2, Figure 4). Table 1 shows the proposed amino acid positions in different VSDs based on the alignment of hH_V1 (aa 75-223) and DrVSP (aa 1-200) with CiVSP (aa 89-260) as template.

Table 1: Alignment results of hHV1-VSD and DrVSD with CiVSD as template are shown. Important residues are compared, which are involved in proton flux regulation.

species[1]	residues[2]							
hH_V1	V109	D112	E119	D123	H140	F150	E153	D174
DrVSP	I66	D69	-	D76	E91	F101	D104	D126
CiVSP	I126	D129	-	D136	D151	F161	D164	D186
species[1]	residues[2]							
hH_V1	V178	D185	H193	-	R205	R208	R211	
DrVSP	V130	T137	S146	R153	R159	R162	I165	
CiVSP	I190	T197	T210	R217	R223	R226	R229	

[1]VSDs of different species aligned with BLAST (hHv1 75-223, CiVSP 89-260 and DrVSP 1-200).
[2]The color code is identical to Figure 2 and Figure 4 (brown – residues forming a hydrophobic plug, dark purple – most studied countercharge of the arginines and classified as the selectivity filter for protons in hH_V1, red – potential countercharges, light purple – residues involved in polyvalent cation binding, blue – arginines known as the voltage sensor).

Based on the crystal structures, solved for the CiVSD channel (Li *et al.*, 2014), behavior on voltage stimuli of VSDs from voltage-sensing phosphatases can be described, which is equally expected for DrVSD. In detail, it was shown that the monomeric CiVSD is functional without the phosphatase subunit (Murata *et al.*, 2005; Kohout *et al.*, 2008; Okamura *et al.*, 2009). Comparison of a structure in the down (R217E mutant, R153 in DrVSP) and the up conformation (wild-type) allowed a more detailed description of S4 movement. Perozo and co-workers proposed a 5 Å upward and 60 °rotational reorientation of the entire helix without a significant change in the neighboring helix S3 as well as their connecting loop upon membrane depolarization (Li *et al.*, 2014). To this end, arginines were always stabilized by countercharges in S1 and S3 (potential candidates: D69, D76, D104, D126) (Table 1). Depending on the amino acid pair distances in other voltage-gated proton channels, the S4 movement parameters can be different to the proposed ones. Furthermore, the effect of S4 reorientation might be more significant in voltage-dependent phosphatases as in voltage-gated proton channels, because the conformational change has to activate the phosphatase unit instead of only open the passage for proton flux. In conclusion, a detailed description of gating properties of the zebrafish and human voltage-sensing domains is highly desired and was the aim of this work. However, speculated mechanisms of proton channeling in voltage-gated proton channels are discussed in the next chapter.

1.2.3 Mechanism of voltage-dependent gating in proton channels

Protons in open voltage-gated proton channels diffuse down the electrochemical gradient in a passive manner. The high turnover rate of $10^5\ H^+\ s^{-1}$ of this process defines them as real channels instead of being a carrier protein (DeCoursey, 2003, 2017). Mainly, depolarization of the cell membrane from -70 mV resting potential to 40 mV induces a conformational change in the VSD, activating the channeling of protons. Thereby, H_V1 gating is dependent on ΔpH and on the membrane polarization (DeCoursey, 2015). A special role is described for dinoflagellates where the electrochemical driving force is inward upon membrane depolarization contrary to the usual outward proton flux (Smith *et al.*, 2011). Consequently, these channels were thought to have different functions.

The mechanism of proton flux through voltage-gated proton channels is controversially discussed (Bennett & Ramsey, 2017; DeCoursey, 2017). Based on different experimental data two mechanisms were postulated.

First, protons can diffuse from the intracellular to the extracellular matrix by a Grotthus-type mechanism (Agmon, 1995). As described for the ion channel gramicidin A, the pore is filled with water where protons are transported via hopping along the water wire without direct involvement of amino acid sidechains (Myers & Haydon, 1972; Ramsey *et al.*, 2010; Wood *et al.*, 2012; Pupo *et al.*, 2014; Randolph *et al.*, 2016). Evidence is given by atomistic and homology models as well as molecular dynamic (MD) simulations where water filled crevices are detected (Ramsey *et al.*, 2010; Wood *et al.*, 2012; Pupo *et al.*, 2014; van Keulen *et al.*, 2017). Additionally, experts argue that more than 50 amino acid exchanges in the central pore of the H_V1 channel still result in measurable currents, which is an indication that no amino acid side chains are involved in channeling processes (Bennett & Ramsey, 2017; Ramsey *et al.*, 2010; Randolph *et al.*, 2016).

In contrast, the second hypothesis is based on the participation of amino acid side chains in proton transport in form of a hydrogen bonded chain mechanism (DeCoursey & Cherny, 1994, 1997; DeCoursey, 1998; DeCoursey & Cherny, 1998; DeCoursey, 2003). Here, the carboxyl group of a highly conserved aspartate in helix S1 (D112 in hH_V1, potentially D69 in DrVSD) is protonated and deprotonated, acting as a proton shuttle (Musset *et al.*, 2011; Morgan *et al.*, 2013; Dudev *et al.*, 2015). The theory is based on different experimental results. First, the H_V1 channel is highly selective for protons. A mutation of Asp112 (in hH_V1) to a neutral amino acid converts the selectivity of the channel to anions (Musset *et al.*, 2011). In a reduced quantum mechanical model of the H_V1 selectivity filter, a hydrogen bond network between this Asp, neutral water and Arg side chains was observed, which occludes other ions from entering the pore (Dudev *et al.*, 2015). Second, the observed isotope effect is contrary to the effect observed for protons in a water-filled gramicidin A channel and for protons in bulk solution (DeCoursey & Cherny, 1997). Furthermore, H_V1 has a much higher temperature-dependence than observed for other ion channels or for protons in solution (DeCoursey & Cherny, 1998; Kuno *et al.*, 2009), which can be explained by e.g. rotational processes of protonated side chains like described for the M2 influenza A virus proton channel (Lin & Schroeder, 2001; Hu *et al.*, 2010). Fourth, kinetic measurements of transport rates in the H_V1 gave evidence for an involved generic hydrogen bonded chain when compared with literature data (Nagle & Morowitz, 1978; DeCoursey, 2017).

In addition to the two hypotheses of proton channeling, the inhibition of VSDs is controversially discussed too. H_V1 channels coordinate Zn^{2+} by two histidine residues in the crystal structure (Mahaut-Smith, 1989; Takeshita *et al.*, 2014). Nevertheless, homology models could not support this thesis completely (Musset *et al.*, 2010c). Furthermore, voltage-gated proton channels in coccolithophores miss any His residues, but still show an inhibition by Zn^{2+} (Taylor *et al.*, 2011). In sum, so far it is unclear which details are responsible for the H_V1 channel inhibition by polyvalent cations.

Another inhibition by guanidine derivatives was intensively studied by mutational experiments and MD simulations, but no holo-structure is reported so far (Hong *et al.*, 2013; Hong *et al.*, 2014a; Hong *et al.*, 2015; Gianti *et al.*, 2016). Nevertheless, potential residues in hH_V1 are described, which are involved in intracellular e.g. 2-guanidinobenzimidazole (2GBI) binding with a K_D of 38 µM (Hong *et al.*, 2013; Hong *et al.*, 2014a; Gianti *et al.*, 2016). Computational docking studies of hH_V1 with 2GBI revealed a benzimidazole ring stabilization by the aa V109, L108, I146, I105, V178, F150, D112 and R211 (Gianti *et al.*, 2016). Furthermore, F182 is described to stabilize the guanidine moiety. Docking experiments were performed with an active model of hH_V1 based on the mouse H_V1 crystal structure. Transferring the data to my homology models reveals slightly different results (Figure 5).

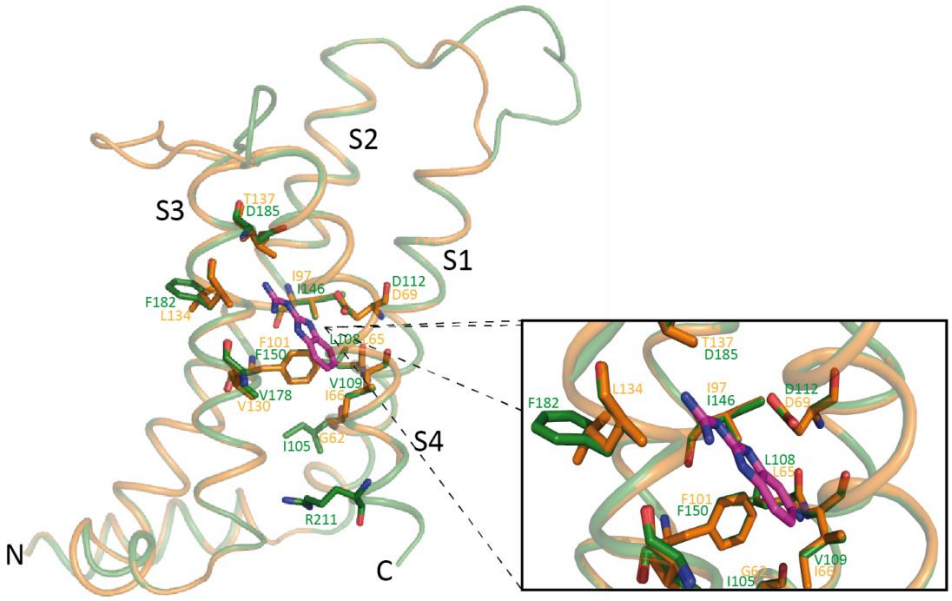

Figure 5: PyMOL-based 2GBI docking in modeled VSD structures. Structures of hH_V1 (green) and DrVSD (orange) were modeled using SWISS-MODEL and the open CiVSD structure as template (Figure 2, Figure 4). The four transmembrane helices (S1-S4) as well as N- and C-terminal parts are displayed. Published residues involved in inhibitor binding (Gianti *et al.*, 2016; Hong *et al.*, 2014a) are shown as stick representations colored by element (O-red, N-blue). 2GBI is shown in a pink stick representation colored by element. The dotted lines represent a zoom of all atoms 6 Å within the 2GBI selection to highlight possible interaction partners.

Interestingly, my applied model could not show any interaction of 2GBI with residues F182 and R211 in parallel although the other contacts could be identified. This demonstrates again the difficulties in detailed analysis of the binding and channeling mechanism. Nevertheless, the binding region of 2GBI deep inside the channel promotes the theory of active-state inhibitor binding (Hong *et al.*, 2013; Hong *et al.*, 2014a; Hong *et al.*, 2015). Furthermore, the remarkable role of residue F150 in inhibitor binding can be shown, as the inhibitor has to pass this barrier to be able to bind to the channel. For example, mutational studies revealed an increased inhibition when F150 was exchanged to alanine (Hong *et al.*, 2013; Hong *et al.*, 2014a; Gianti *et al.*, 2016).

In summary, there is an ongoing discussion about the proton channeling mechanism, the binding site for polyvalent cations and for guanidine derivatives in VSDs. However, a general mechanistic description for the proton flux through a voltage-gated proton channel is missing but of importance especially for future drug developments.

1.3 Techniques for the investigation of dynamic processes in VSDs

Why are we asking for the mechanistic details of proton transport? Voltage-gated proton channels are involved in cancer cell development and growth as mentioned earlier (1.2). The knowledge of their activation and deactivation properties would help to develop new drug candidates for reducing or even preventing abnormal cell growth, especially focusing on compounds acting from the extracellular site. The next chapter will highlight a selection of suitable methods, which were or can be used to get access to mechanistic details of proton channeling activities in voltage-gated proteins.

1.3.1 Patch-clamp recordings and EPR measurements

For electrophysiologists, patch-clamp recordings are the method of choice for studying ion channels (Neher & Sakmann, 1976). Membrane patches are analyzed concerning their response to different membrane voltages induced by changes in the ion composition of the pipette solution or the patch external environment. In detail, the membrane potential V_m and equilibrium potential V_{eq} for a given ion are unequal in a real cell. Consequently, an electrochemical driving force V_{DF} pushes each contributing ion into its equilibrium state (Equation 2).

$$V_{DF} = V_m - V_{eq}$$ Equation 2

The arithmetic sign of the driving force in combination with the valence of the ion under investigation is used to define the direction of ion movement across the membrane. Additionally, the driving force can be used for measuring currents I_m of specific voltage-sensing membrane proteins, for calculating the ion conductance G, known as a function of the total number of open channels for a specific ion, and for determining the reversal potential V_{rev} of an ion channel (equal to the resting potential V_{rest} of a cell) (Figure 6).

Currents can be measured and translated to single channel activities. To this end, measured currents are plotted against the different membrane potentials (Figure 6). Currents were normalized (I/I_{max}) and fitted by a two-state Boltzmann equation to determine the voltage at which half of the channels are open (V_{mid}) to estimate their opening probability. Patch-clamp experiments enable a direct analysis of measurable currents and flow directions.

H_V1 channels were extensively studied using the patch-clamp technology. To this end, channels were overexpressed in different cell types (COS/HEK cells, *xenopus leavis* oocytes) and analyzed concerning their gating behavior (Ramsey *et al.*, 2010; Musset *et al.*, 2011; Morgan *et al.*, 2013; Hong *et al.*, 2014a; Mony *et al.*, 2015).

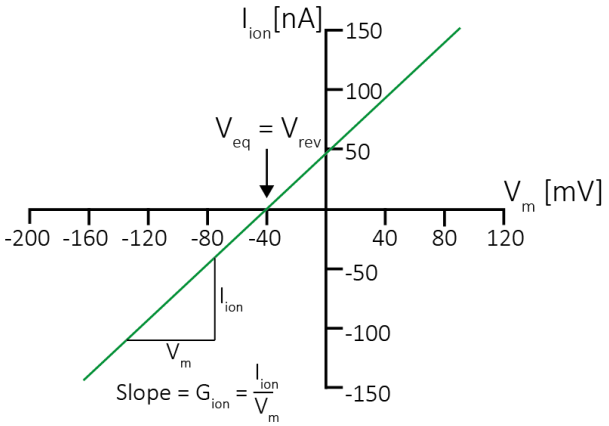

Figure 6: Hypothetical current-voltage (I-V) relationship for studying voltage-sensing membrane proteins. The plot represents measured currents I_{ion} in a voltage-clamp recording under changes in the membrane potential V_m (-160 to 80 mV). To this end, the intersection with the X-axis is defined as the reversal potential V_{rev}. If the measured currents are caused by one defined ionic species the reversal or resting potential corresponds to the V_{eq} of this ion ($I_{ion} = G_{ion} (V_m-V_{eq})$). Consequently, the ionic species channeled/transported can be analyzed and the direction of ion flow can be determined. For values smaller than $V_{eq,}$ the ion enters the cell whereas at more positive values than V_{eq} the ion flows out.

I-V-curves of hundreds of mutants were recorded and evaluated (Ramsey *et al.*, 2006; Sasaki *et al.*, 2006; Tombola *et al.*, 2008; Musset *et al.*, 2010a; Ramsey *et al.*, 2010; Tombola *et al.*, 2010; Gonzalez *et al.*, 2010; Musset *et al.*, 2011; Smith *et al.*, 2011; Berger & Isacoff, 2011; Hong *et al.*, 2013; Morgan *et al.*, 2013; Hondares *et al.*, 2014; Hong *et al.*, 2014a; Fujiwara *et al.*, 2014; Cherny *et al.*, 2015; Chamberlin *et al.*, 2015; Mony *et al.*, 2015; Chaves *et al.*, 2016; Okuda *et al.*, 2016; DeCoursey *et al.*, 2016). For example, experiments with hH_V1 revealed a change in cation to anion selectivity when D112 was exchanged to a neutral charged aa (1.2.1) (Musset *et al.*, 2011; Morgan *et al.*, 2013). Mutations of aspartate to glutamate retain cation selectivity (DeCoursey *et al.*, 2016). Further electrophysiology studies highlighted different countercharge positions in the transmembrane residues in the closed or open state of the channel (DeCoursey *et al.*, 2016). Nevertheless, the patch-clamp technique cannot be used exclusively to determine mechanistic details. For example, the complexation of polyvalent cations by two His residues in hH_V1 is controversially discussed (1.2.3). In patch-clamp recordings, it was shown that, a mutation of His to Ala prevented Zn^{2+} binding (Cherny & DeCoursey, 1999; Ramsey *et al.*, 2006). Nevertheless, later, homology models revealed a much more complex binding event whereby the dimer interface in combination with the His residues acts as the anchor point for zinc binding (Musset *et al.*, 2010c).

Voltage-clamp fluorometry as a further development of the patch-clamp technology, enables the simultaneous preservation of structural and functional data of the protein under investigation (Kalstrup & Blunck, 2017; Wulf & Pless, 2018), making it an ideal tool for studying H_V1 channels. The H_V1 channel from *ciona intestinalis* (CiH_V1) labeled with Alexa-488 maleimide revealed cooperative gating in dimeric channels. Furthermore, detailed analysis of the Zn^{2+} inhibition properties supposed the existence of two Zn^{2+} coordination sites in a monomeric channel (Qiu *et al.*, 2013; Qiu *et al.*, 2016). The Zn^{2+} binding blocks the channeling of protons in one site and hinders the movement of S4 in another (Qiu *et al.*, 2016).

Information about the tertiary or even quaternary protein structure can be gained by using the patch-clamp technique in combination with paramagnetic agents. To this end, accessibility studies have been performed with single-cysteine mutants of H_V1 overexpressed in cells. Here, the rate of e.g. methanethiosulfonate (MTS) binding to cysteine residues is proportional to their accessibility. The results suggested a parallel movement of S1 and S4 (Gonzalez *et al.*, 2010; Mony *et al.*, 2015).

Additionally, paramagnetic agents can be used to study oligomeric states in combination with amino acid exchanges by applying the electron paramagnetic resonance (EPR) spectroscopy technique. Here, electron spins of radicals are exposed to microwaves by concurrent increase of the magnetic field strength and measuring their resonance absorption. To this end, the motion of a spin label attached to a cysteine residue of a single-cysteine mutant (protein) can be calculated, known as the mobility (ΔH_o^{-1}). A high mobility is a hint for loop regions. Additional paramagnets like e.g. nickel ethylenediamine-N,N'-diacetic acid (NiEDDA) and oxygen are used for accessibility (Π) screenings. In this case, high ΠO_2 values indicate lipid contacts, high ΠNiEDDA values, indicate contact to solvent outside the membrane, mostly loop regions (low ΠNiEDDA indicate the transmembrane region). Analyzing such data for single-cysteine mutants of hH_V1 reconstituted in liposomes revealed the non-lipid contacts of D112, R205, R208 and R211, the individual length of each helix in the given membrane environment and the presence of water-filled crevices (Li *et al.*, 2015).

Nevertheless, movements can occur in any direction of the x-, y- and z-axis, whereby the accessibility will always be changed, which would hamper a precise interpretation. Therefore, often the EPR-obtained information are combined with MD simulations.

1.3.2 Molecular dynamic simulations and other computer-based models

Computer simulations of proteins embedded in a membrane environment, proteins in ligand binding studies or transport/channeling processes in proteins use experimental data as structural restraints to build a model. Often these models are based on template structures, which were derived from e.g. crystallographic data. For example, the group of E. Perozo modeled hH_V1 embedded in a POPC bilayer using nanoscale molecular dynamics (NAMD) simulation with Chemistry at Harvard Molecular Mechanics (CHARMM) 36 as force field for lipid and protein and the TIP3P model for water. As a template the wild-type CiVSD crystal structure in the resting conformation (Li *et al.*, 2015) was used. The result showed that upon activation S4 moves and rotates three residues up whereby a countercharge exchange from D112-R205-D185 to D112-R208-D185 occurs and additionally, R211 is no longer connected to E153 and D174.

Another all-atom MD simulation with NAMD of hH_V1 used the active $K_V1.2$–$K_V2.1$ paddle-chimera VSD crystal structure (2R9R; rcsb.org; Berman *et al.*, 2000) (Long *et al.*, 2007) as a template (CHARMM22, CHARMM32 and TIP3P) (Wood *et al.*, 2012). Study revealed that a static water wire inside the channel exists where protons are channeled in a Grotthus-type mechanism (1.2.3). Interestingly, the group of R. Pomès evaluated the existing water wire differently and stated that further kinetic analyses were necessary to distinguish between the two proposed models (Kulleperuma *et al.*, 2013). Here, three VSD crystal structures in the open state (1ORS; 3RVY; 2R9R; rcsb.org; Berman *et al.*, 2000) were applied to the software program Gromacs (Groningen Machine for Chemical Simulations) (OPLS-AA as force field for protein and octane and TIP3P for water). Hence, the homology model was based on a clustering of different protein conformation. Study revealed a water-filled channel with specific salt bridges, e.g. D112-R208 similar to the results of the Perozo lab (Kulleperuma *et al.*, 2013; Li *et al.*, 2015).

In summary, defined interaction clusters in H_V1 channels could be so far only identified by MD simulations rather than using mutational analyses (Wood *et al.*, 2012; Kulleperuma *et al.*, 2013; Chamberlin *et al.*, 2014; Li *et al.*, 2015). Nevertheless, the same question arises consistently. Is the model correct? Direct measurements are required, which are not based on protein models, for analyzing channeling mechanisms in more detail. One suitable method is nuclear magnetic resonance (NMR) spectroscopy.

1.3.3 Nuclear magnetic resonance spectroscopy

In 1945, first radio-frequency signals of the nuclei of atoms could be measured and observed (Purcell *et al.*, 1946; Bloch *et al.*, 1946). This event denotes the birth of nuclear magnetic resonance spectroscopy. NMR is based on the principle of the alignment of atomic nuclei with a magnetic moment in a strong, homogenous magnetic field. Directed radio-frequency pulses allow these nuclear spins to be tilted out of their equilibrium position. During the return to the equilibrium state, referred as relaxation, the nuclei emit signals with their own resonance frequencies. NMR enables their detection and interpretation. Resonance frequencies of NMR-active nuclei are strongly dependent on the chemical surrounding. The environment like solvent molecules, amino acid side chains, bound inhibitors and many more affect the actual magnetic field to which each individual nucleus is exposed. Hence, the

resonance frequency of these nuclei shifts. The value of this chemical shift in ppm (parts per million) refers to the resonance frequency of a reference substance whose chemical shift value is set equal to zero (Stordeur, 2007).

NMR-active nuclei in proteins are protons (^{1}H), nitrogen atoms (^{15}N), and carbon atoms (^{13}C). However, the natural abundance of ^{15}N and ^{13}C nuclei is too low, so that they need to be artificially enriched in the protein of interest. Thus, the recombinant protein production is essential. As described by Stordeur, 2007, one problem in solution-state NMR recordings is the signal of protons from water. As they are represented in a higher concentration than the proteins NMR-active nuclei, their signals mask signals of the protein. The proton signal of water can be suppressed with the help of certain pulse sequences. However, proton signals that originate from the protein but lie in the resonance range of the water are also suppressed here and thus cannot be detected in the spectrum. Another possibility to avoid the presence of signals from water is to record spectra in proton-free solvents like deuterium oxide (D_2O). Deuterium is a quadrupole nucleus and shows a far more reduced NMR-sensitivity than ^{1}H. Consequently, the water signal should be suppressed. However, amide protons of the protein are in permanent exchange with deuterium, which causes again an increase of the water signal in the spectrum while at the same time reducing the signals of the amides. Only inert amides, like those in a hydrogen-bond network, are shielded. In summary, complete data sets can only be obtained when spectra in both solvents, water and deuterium oxide, are recorded (Stordeur, 2007).

Normally, the first heteronuclear two-dimensional (2D) spectrum recorded for the assignment of resonances in protein NMR is the heteronuclear single quantum coherence (HSQC) spectrum (or the heteronuclear multiple quantum coherence (HMQC) spectrum with increased sensitivity but lower dispersion). Every observed peak can be assigned to a particular residue of the protein. Furthermore, indications for folded protein species can be gained by analyzing the dispersion and distribution of recorded peaks. Well-dispersed spectra without any clustering of signals point towards folded protein species under investigation. The HSQC experiment is based on two insensitive nuclei enhanced by polarization transfer (INEPT) pulses, which transfer the magnetization of the protons to the directly-attached heteronucleus (^{15}N or ^{13}C) and back to the proton where signals evolve. The HSQC experiment is sensitive and can be recorded in a relatively short time. Thus, it

makes it an ideal tool for initial screening purposes concerning sample stability and folding issues. Additionally, the experiment can be used for screening of binding interfaces when inhibitors or other binding partners are present. Here, spectra of holo- and apo-state of the protein are compared concerning their chemical shift properties. Furthermore, this kind of experiment can be used for the analysis of molecular dynamics in proteins by relaxation studies. In sum, HSQC experiments are particularly suited to investigate the mechanism behind proton channeling in VSDs.

Up to now, there is only one solution-state NMR data set for the hH_V1 channel available (Letts, 2014). J. A. Letts worked with a shortened, 138 aa version of hH_V1 with a truncated N- and C-terminus. He recorded [^{15}N,^{1}H]-HSQC spectra of uniformly ^{2}H,^{15}N-labeled $\Delta N\Delta Ch H_V1$ and assigned 82 % of the residues by ^{15}N-selective labeling of the protein with 12 from 20 aa. Interestingly, paramagnetic relaxation enhancement (PRE) measurements, used for distance restraint determination, revealed an unfolded protein structure in LPPG micelles although the initial HSQC-peak distribution looked quite promising. This means, NMR is subject to a constant back and forth between sample and spectra quality that is not necessarily compliant. Intensive screening procedures are necessary. Expression host systems, purification strategies, detergent properties and many more parameters have to be adjusted to obtain folded protein species with well-dispersed peaks in NMR spectra recordings. However, it could be demonstrated that studying the VSDs by solution-state NMR is possible.

To sum up, the description and analysis of mechanistic features of channeling processes has to be based on a variety of different techniques to explain nature as close as possible. For all the above-mentioned experimental approaches, cell-free protein synthesis offers numerous advantages over the conventional *in vivo* expression systems, which includes an easier handling of protein labeling (e.g. with heavy isotopes), ligand/inhibitor additions promoting protein folding and stability, scrambling inhibitor suppressions and, especially for membrane proteins, the direct addition and easy screening of membrane mimetics. This makes it an ideal tool to study voltage-gated proton channels. The cell-free synthesis of this protein class is not described in the literature so far. Nevertheless, the synthesis of other voltage-gated channels could be successfully shown. Obtained membrane protein batches were correctly folded, stable, and functional (Deniaud *et al.*, 2010; Kovácsová *et al.*, 2015; Renauld *et al.*, 2017).

1.4 Protein synthesis using cell-free gene expression

Proteins can be synthesized under non-native conditions using a variety of different techniques. Protein characteristics like folding and stability, time- and money-issues as well as lab equipment availabilities determine which method will be finally applied. The conventional protein synthesis in host cells requires many different steps including vector transfection into those cells, their inoculation and growth, cell cultivation, cell harvest and breakage to obtain the protein of interest. In contrast, using the cell-free expression platform the proteins of interest are synthesized outside of a living cell. Hence, steps like cell growth, cultivation, harvest, and breakage can be skipped, making the overall procedure faster and easier (Hein *et al.*, 2014). In detail, it means that the environment of protein production is controllable and can be adapted to requirements of each individual protein under investigation. Cell-free protein production can be performed in an one-tube format in less than 24 h, often including the purification steps. Supplementations can be performed at any point of the reaction (Schneider *et al.*, 2010). High product yields in mg quantities can be obtained. To this end, a defined cell extract containing the core components of the protein translation/transcription machinery is mixed with an energy source, precursors like amino acids and nucleoside triphosphates, tRNA and the DNA of the protein of interest. Further additives are necessary for prolonging and promoting protein synthesis (2.6.1, 3.1.8, 3.1.9).

The extract sources can be varied depending on the target protein and the aim of the project (Hodgman & Jewett, 2013; Buntru *et al.*, 2014). Currently available extracts, are produced from *E. coli* cells, wheat germ cells, *Leishmania*, rabbit reticulocyte cells, insect cells (Sf9, Sf21), mammalian cells (HeLa cells, Chinese hamster ovary [CHO] cells, mouse embryonic fibroblasts, human embryonic kidney [HEK] 293 cells), archaea, protozoans, yeast and tobacco BY-2 cells (Hoffmann *et al.*, 2018). As a first step in cell-free protein synthesis, strains for lysate production have to be evaluated. Most common extracts use *E. coli* strains as raw material. The most prominent *E. coli*-based extract is named S30, based on the centrifugal force used during extract preparation (30,000xg). Protocols for extract production can be found in a variety of reviews and papers (Spirin, 2004; Kigawa *et al.*, 2004; Schwarz *et al.*, 2007; Schneider *et al.*, 2010; Shrestha *et al.*, 2012; Harbers, 2014; Fujiwara & Doi, 2016). Our protocol of S30 extract preparation includes an additional step at the final stage to remove endogenous mRNA from the produced *E. coli* lysate. To this end, the extract

is incubated for 45 min at 42 °C under high-salt conditions prior to dialysis (3.1.8). Consequently, we can guarantee the exclusive synthesis of the protein of interest in subsequent cell-free expressions.

In a next step, the cell-free configuration has to be chosen. “Two basic configurations are commonly used for cell-free expression reactions. The simpler of the two is the one-compartment batch configuration, which uses microplates as reaction containers and is excellent for high-throughput applications.” (Hoffmann *et al.*, 2018) Literature examples using this kind of cell-free expression conditions for voltage-gated proteins show pure protein concentrations of 20-300 µg per ml expression (Deniaud *et al.*, 2010; Kovácsová *et al.*, 2015; Renauld *et al.*, 2017). “Yields of the protein of interest can be significantly increased by using the two-compartment continuous-exchange cell-free (CECF) configuration, in which the reaction compartment, containing all high molecular weight components necessary for transcription/translation, is separated from a feeding compartment holding a reservoir of low molecular weight precursors by a membrane” (Hoffmann *et al.*, 2018) (Figure 7). Up to now, no literature data about concentrations of voltage-gated proteins in CECF reactions are available, but they are one focus of my thesis. “A further beneficial effect of this arrangement is that inhibitory byproducts such as pyrophosphate are continuously diluted out from the reaction compartment and protein production is therefore ongoing for a longer period. The CECF system mimics the working principle of a whole cell, where compounds are continuously supplied and reaction products removed. However, any additives, smaller than the membrane molecular weight cut-off, need to be added into both compartments. The ratios of reaction compartment (RM) to feeding compartment (FM) sizes are usually between 1:10 and 1:20. Common reaction volumes are between 0.05 and 100 ml, and even high-throughput approaches are suitable for the CECF system.” (Hoffmann *et al.*, 2018)

The cell-free production platform can be used for any kind of protein but is of particular importance for the synthesis of membrane proteins, like for the VSDs under investigation in this thesis. Here, the cell-free gene expression can be influenced in many ways to support the folding and stability of membrane proteins directly during their synthesis. Three different modes exist (Figure 7) (Schwarz *et al.*, 2008; Reckel *et al.*, 2010; Junge *et al.*, 2011; Hein *et al.*, 2014).

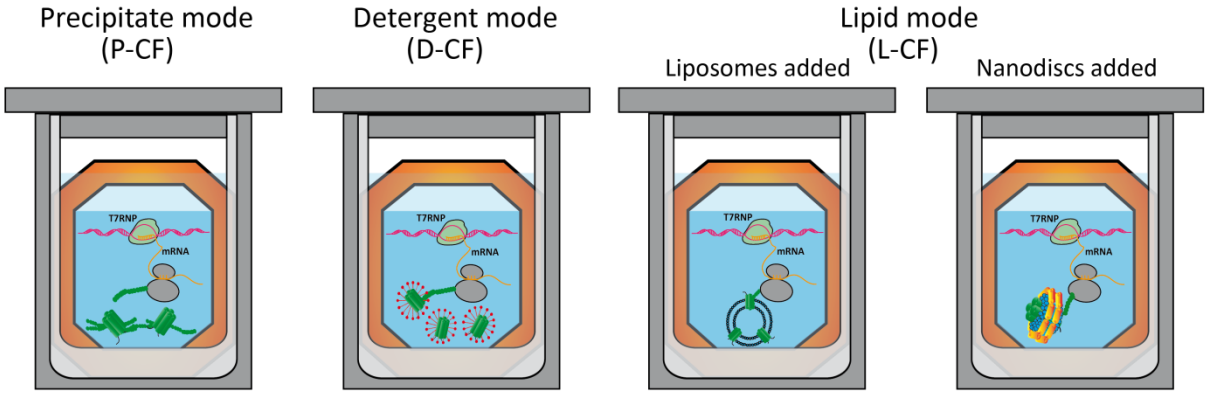

Figure 7: Different cell-free expression modes for membrane proteins in a preparative scale home-made continuous-exchange reaction container. The figure shows cell-free expression containers (grey) filled with the feeding mix and an inserted dialysis cassette (orange) in which the *in vitro* protein transcription/translation process occurs (reaction mix). Plasmid DNA (pink) is transcribed by T7-RNA-polymerase (T7RNP) into the mRNA (yellow) which binds the ribosomal complex (grey circles) for subsequent protein sequence translation. In the precipitate-based cell-free (P-CF) mode, no hydrophobic environment for the synthesized membrane protein (green) is provided. Hence, the protein precipitates in form of a white protein pellet. When detergent molecules (red) are supplied the protein stays soluble caused by a direct shielding of hydrophobic residues by amphiphilic detergent moieties in a detergent-based cell-free (D-CF) mode. In the lipid-based cell-free (L-CF) mode, any kind of lipid-containing compound can be added for direct membrane protein solubilization. Here, the addition of pre-formed liposomes and nanodiscs, as used in this thesis, are shown (modified and reprinted with permission from Hoffmann *et al.*, 2018).

In the precipitate (P-CF) mode, no supplements, keeping the membrane protein soluble, are added. Consequently, the synthesized polypeptide chain precipitates (Figure 7, P-CF). Nevertheless, it could be shown that the precipitated proteins are partially folded (Maslennikov *et al.*, 2010). The protein pellets can be solubilized in a defined detergent while maintaining their native structure without the implementation of time-intense refolding steps (Klammt *et al.*, 2012; Boland *et al.*, 2014). Here, only the detergent properties (mild/harsh, chain length, charge) have to be screened regarding the fold, yield, and stability of the cell-free-produced protein. The P-CF mode is often used for initial screening processes.

In the detergent (D-CF) mode, detergent molecules solubilize the membrane protein directly during its synthesis (Figure 7, D-CF). The amphiphilic nature of the detergent shields hydrophobic protein parts and keeps the whole, synthesized protein in solution. Folded protein species can be obtained (Reckel *et al.*, 2011; Matthies *et al.*, 2011; Wada *et al.*, 2011). Nevertheless, also here the detergent type is extremely important. Too harsh detergents, like n-octyl-β-D-glucoside (β-OG), n-dodecylphosphocholine (DPC) or other Fos-cholines inhibit the cell-free expression machinery when they are supplied in too high concentrations (Proverbio *et al.*, 2014). Attempts were made to supply them as mixed micelles in combination with 3-((3-cholamidopropyl) dimethylammonio)-1-propanesulfonate

(CHAPS) (Genji *et al.*, 2010). Mild detergents like Brij®-derivatives, digitonin, or n-dodecyl-β-D-maltoside (DDM) could be successfully used for membrane protein solubilization during cell-free expression (Schwarz *et al.*, 2007; Proverbio *et al.*, 2014; Hein *et al.*, 2014). The range of detergent molecules used in D-CF mode has been extended over the last few years by amphipols, amphiphilic polymers and nonionic amphipols (NAPols) (Tribet *et al.*, 1996; Bazzacco *et al.*, 2012). Unfortunately, also some amphipols, like A8-35 inhibit the cell-free expression (Bazzacco *et al.*, 2012). However, they can be used after P-CF expression for protein solubilization with the advantage over detergent micelles that no free surfactant molecules could be detected in solution (mainly important for further analytical studies) (Elter *et al.*, 2014).

In the third mode, lipid-bilayer-containing supplements were provided which allow a co-translational insertion of the membrane proteins in a more native, but anyhow artificial membrane environment (Roos *et al.*, 2012; Roos *et al.*, 2014), called the lipid (L-CF) mode (Figure 7, L-CF). Additives can be pre-formed liposomes (Abdine *et al.*, 2011; Long *et al.*, 2012; Niwa *et al.*, 2015), bicelles (Uhlemann *et al.*, 2012) or nanodiscs (NDs). More recently, a specialized L-CF mode was described, where the liposomes were not added but contained the whole cell-free machinery allowing protein synthesis inside with simultaneous fusion with the liposomal membrane after translation (Deng *et al.*, 2016). Referring to ion channels, the spontaneous integration of functional, well-folded potassium channel KcsA during L-CF expression could be demonstrated (Ando *et al.*, 2016). Hence, this mode is of tremendous importance for the synthesis of VSDs. The conventional VSD synthesis includes the expression in a host cell organism. Produced proteins were either directly integrated into the cell membrane or they precipitated in form of inclusion bodies. Afterwards, VSDs were solubilized by detergent treatment and subsequently, transferred into liposomes to assist folding and analyze function (Li *et al.*, 2015; Lee *et al.*, 2008b, 2009). Using the L-CF expression, critical steps such as detergent exposure by direct transfer of the VSDs into the lipid bilayer of either liposomes or NDs can be avoided. Additionally, again, the open nature of cell-free expression enables screening of different lipid composition. Lipid chemical properties based on their length, saturation, and head group can have a great influence on membrane protein insertion as well as on their folding and stability (Boggs, 1987; Cybulski & de Mendoza, 2011; Rues *et al.*, 2016). For example, for prokaryotic proteins lipids

predominant in *E. coli* membranes might be a good promoter of obtaining correctly folded cell-free-synthesized membrane proteins (van der Does *et al.*, 2000).

The L-CF mode is favored for all kind of membrane proteins as it provides a hydrophobic environment for protein insertion in form of a lipid bilayer, which is closer to nature than a detergent micelle. Furthermore, detergent contacts often cause the loss of the native structure and/or the loss of function of the membrane proteins under investigation (Shenkarev *et al.*, 2010a). The lipid contact in form of a liposome, bicelle, or ND supports protein folding by enabling direct protein-lipid-interactions. Such kind of lipid-dependent protein folding could be observed for voltage-sensor domains of other *E: coli*- and cell-free-expressed cation channels (Shenkarev *et al.*, 2009; Shenkarev *et al.*, 2010a; Lyukmanova *et al.*, 2012; Shenkarev *et al.*, 2013). However, dynamic studies of membrane proteins reconstituted in liposomes using solution-state NMR spectroscopy are un-imaginable due to size limitations of this method. But, NDs provide a lipid bilayer, support lipid-protein contacts, are smaller in size than liposomes, were successfully used in NMR applications (Shenkarev *et al.*, 2009; Hagn *et al.*, 2013) and can be added in L-CF mode for direct incorporation of membrane proteins without any prior detergent contact (Roos *et al.*, 2012; Roos *et al.*, 2013; Paramonov *et al.*, 2017). Hence, NDs would be an ideal tool to study cell-free-synthesized VSDs of voltage-gated proton channels.

1.4.1 Nanodiscs in L-CF expression

Nanodiscs are particles composed of a lipid bilayer surrounded in a belt-like manner by a membrane scaffold protein (MSP) (Carlson *et al.*, 1997; Bayburt *et al.*, 1998; Bayburt & Sligar, 2003). The MSP is derived from the naturally occurring apolipoprotein A1 (ApoA1) (Matz & Jonas, 1982; Bayburt *et al.*, 2002). Its amphiphilic nature enables the enclosure of a lipid bilayer in a defined size depending on the MSP variant (Figure 8). Different MSPs vary in length thereby defining the size of the overall ND to between 5 and 15 nm and even bigger (Denisov *et al.*, 2004; Ritchie *et al.*, 2009; Grinkova *et al.*, 2010; Hagn *et al.*, 2013). A variety of different techniques is available to form NDs. The website of the Sligar lab who invented this technology provides fantastic overviews (http://sligarlab.life.uiuc.edu/nanodisc.html; 11.03.2018, 3:30 pm). However, a schematic representation of the strategy used in this thesis is represented in Figure 8.

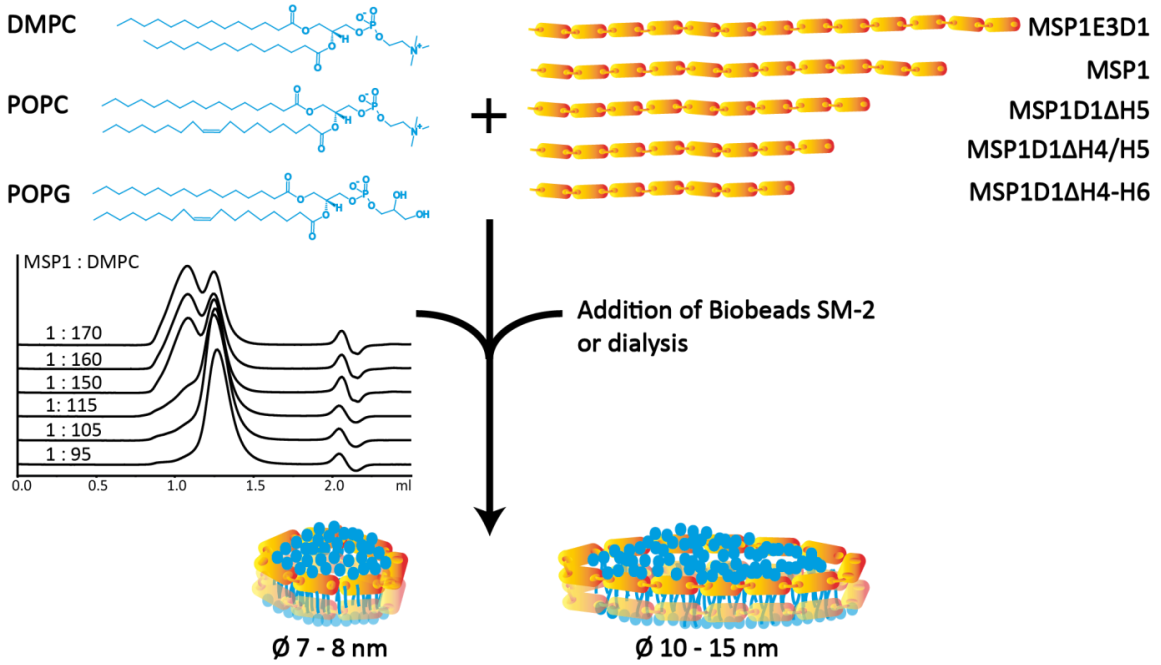

Figure 8: Schematic workflow of a nanodisc preparation procedure. The ND preparation starts with an incubation of specific lipids with a MSP. Thereby, lipids like 1,2-dimyristoyl-sn-glycero-3-phosphocholine (DMPC), 1-palmitoyl-2-oleoyl-sn-glycero-3-phosphocholine (POPC) or 1-palmitoyl-2-oleoyl-sn-gylcero-3-phospho-(1´-rac-gylcerol) (POPG) can be used. MSPs can vary in length by insertion or deletion of amphiphilic helices (Ritchie *et al.*, 2009; Hagn *et al.*, 2013). After the addition of Biobeads SM-2 or a performed dialysis step NDs were formed because of detergent removal. Different sized NDs were built (5 to 15 nm). The SEC chromatogram represents necessary screening processes of different lipid to MSP ratios. Ratios with which homogenous NDs can be formed (e.g. 1:95 in the example) were chosen for preparative scale reconstitution approaches. Membrane helices are shown as orange ovals connected by short loops. Lipids are shown as blue pictograms. Black lines with depicted MSP1:DMPC ratios represent elution profiles of different NDs in a SEC chromatogram.

First, lipids were incubated with the MSP in defined ratios in small-scale reactions. The treatment of the solution with Biobeads SM-2 or a performed dialysis step removed the detergent prior used for lipid solubilization and therewith forming the ND structure. Formed NDs were analyzed by size-exclusion chromatography (SEC) in terms of homogeneity, aggregation tendency, and stability. Best performing MSP to lipid ratios were used for further preparative approaches. Pre-formed NDs were provided in the reaction mix (RM) of a cell-free reaction enabling the co-translational membrane protein insertion (Roos *et al.*, 2012; Roos *et al.*, 2014; Laguerre *et al.*, 2016; Henrich *et al.*, 2017a; Henrich *et al.*, 2017b; Rues *et al.*, 2017; Waberer *et al.*, 2017). Here, screenings of optimal lipid contents, size (by varying the MSP properties) and final concentrations in the RM are extremely important to increase protein yield and activity.

However, up to now no successful co-translational insertion of VSDs could be shown, but will be of tremendous importance regarding structural and analytical investigations of the channeling mechanism e.g. by solution-state NMR (Lyukmanova *et al.*, 2012; Paramonov *et al.*, 2017).

1.4.2 Cell-free protein production and NMR spectroscopy

The open nature of CF protein production allows an easy, cheap, and efficient screening of different additives or system compositions to ensure optimal protein folding, stability and functionality, which is necessary for obtaining high quality NMR spectra. Such supporters can be the provision of a redox-shuffling system for disulfide bond-containing proteins (Goerke & Swartz, 2008; Knapp *et al.*, 2007; Rues *et al.*, 2018), additives which support post-translational modifications (Guarino & DeLisa, 2012), chaperones to ensure correct protein folding (Ryabova *et al.*, 1997; Niwa *et al.*, 2012; Foshag *et al.*, 2018), co-factors (Reckel *et al.*, 2011), metal ions (Matsuda *et al.*, 2006; Waberer *et al.*, 2017) and other binding partners as well as inhibitors (Laguerre *et al.*, 2016).

In addition to high-throughput screening applications, cell-free protein synthesis offers the possibility of easy protein labeling with heavy nuclei (fully or selectively) (Guignard *et al.*, 2002; Klammt *et al.*, 2004; Klammt *et al.*, 2006) (1.3.3) and with unnatural amino acids (Goerke & Swartz, 2009; Bundy & Swartz, 2010; Albayrak & Swartz, 2013a, b; Hong *et al.*, 2014b; Hong *et al.*, 2014c; Yanagisawa *et al.*, 2014; Chemla *et al.*, 2015; Worst *et al.*, 2016; Ogawa *et al.*, 2016; Ozer *et al.*, 2017). Here, labels can be added directly to the reaction mix without the necessity of passing any barrier like the cell membrane compared to other *in vitro* expression systems. Furthermore, scrambling inhibitors can be added to avoid the transfer of the heavy nuclei between different amino acids. Varieties of papers describe different sample labeling strategies for cell-free-produced proteins (Kigawa *et al.*, 1995; Staunton *et al.*, 2006; Su *et al.*, 2011; Tonelli *et al.*, 2011; Yokoyama *et al.*, 2011; Laguerre *et al.*, 2015; Hoffmann *et al.*, 2018). Label introduction can be easily screened as purification steps can often be avoided and final experiments related to the differently attached labels can be performed (Guignard *et al.*, 2002; Klammt *et al.*, 2012). Furthermore, the reduced complexity of the given cell extracts reduces the scrambling of labels as well as their degradation. As an example, in a cell-free system all amino acids in a protein can be labeled with ^{15}N by supplementing a commercially available ^{15}N-labeled amino acid mix. Because the only protein synthesized is the protein of interest, all signals appearing in an HSQC NMR spectrum belong to the protein under investigation. In contrast, cells expressing the protein of interest have to be supplemented with precursors like ^{15}N-labeled ammonia (to ensure membrane uptake), which will later be introduced in a variety of different proteins due to metabolic issues. Hence, extensive purification steps are necessary before analyzing the protein of interest. Another benefit of cell-free protein synthesis in

combination with solution-state NMR spectroscopy is that the strategy of selective labeling can be easily applied (Reckel *et al.*, 2008; Löhr *et al.*, 2012; Löhr *et al.*, 2014; Löhr *et al.*, 2015; Lazarova *et al.*, 2018). Here, the supplemented pool of labeled amino acids can be controlled precisely and is independent of passing a membrane barrier. This enables the analysis of high-molecular weight proteins by solution-state NMR as only parts of the protein are displayed with high resolution even though the rotational correlation times are drastically increased.

In conclusion, the cell-free protein production for VSDs offers numerous advantages for the characterization of mechanistic features of the channeling process when studying the proteins by solution-state NMR.

1.5 Motivation of this thesis

For thousands of years we have been trying to understand nature and the world around us. We need explanations for everything. Why? We try to make our world a better one for the next generation. New technologies enable the production of energy without being dependent on coal and oil. Robotic systems support our daily life and new vaccines, antibiotics, and drugs facilitate having a long and healthy life. Often scientists gain the knowledge for new drug developments by studying defined metabolic pathways or specific proteins, involved in the respective diseases. Human voltage-gated proton channels, as mentioned earlier, are known to participate in many different diseases including cancer, Alzheimer's disease, and cystic fibrosis (1.2.1). Getting to know their opening and closing probabilities as well as their channeling mechanism is essential for designing new drug molecules interacting with this protein class. Attempts have been made to solve this question but are currently not sufficient. In this thesis, I focused on the cell-free production of two different voltage-sensing domains of human and zebrafish origin. I analyzed them later on by solution-state NMR with respect to their structural rearrangements as a response to environmental changes. Here, the zebrafish construct was used for comparative purposes as another example for voltage-sensing domains with proton channeling function from vertebrates with high sequence similarity to the human construct. The zebrafish as a model system is widely used in scientific research. Hence, it was hoped that the *in vitro* produced VSD might be more stable compared to the human version, which would have made dynamic studies much easier. Results and their classification in the literary context can be found in the following sections of this thesis.

2 Materials

2.1 Primer list

The primers listed were used for vector modification and/or amplification of the indicated constructs (Table 2). Primer 1, 2, 3, 8, 9, 16, 17, 18 and 19 were purchased from Biomers and purified by a cartridge (<60 bp) or by high-performance liquid chromatography (HPLC) (>60 bp). Primer 15, 20, 21, 22, 23, 24, and 25 were ordered from Eurofins and purified by cartridge high purity salt free (HPSF).

Table 2: List of primers used for molecular biological experiments.

Name	Sequence (5'->3')
Primer 1 (pET21a amplification reverse)	**ATAATTCTCGAGTCCTGATCCGGATCCACGGGTC TTCACGCTAATGATGATGC**
Primer 2 (pET21a introduction 10xHis-tag forward)	**TTACTACTCGAGCATCATCACCATCACCACCATC ACCATCATTAGTGAGATCCGGCTGCTAACAAAGC**
Primer 3 (pET21a introduction StrepII-tag forward)	**TTACTACTCGAGTGGAGTCACCCTCAGTTTGAAA AGTAGTGAGATCCGGCTGCTAACAAAGC**
Primer 15 (introduction of a C-terminal StrepII-tag in His-DrVSD in pET15b reverse)	**CTGAGGGTGACTCCATCCTGATCCAACCAGAATG ACGATGCGC**
Primer 16 (introduction of a C-terminal StrepII-tag in His-hH_V1-VSD in pET15b forward)	**GAGTCACCCTCAGTTTGAAAAGTAGGGATCCGGC TGCTAACAAAG**
Primer 17 (introduction of a C-terminal StrepII-tag in His-hH_V1-VSD in pET15b reverse)	**CTGAGGGTGACTCCATCCTGATCCACGGGTCTTC ACGCTAATGATG**
Primer 18 (exchange N-terminal His-tag against StrepII-tag in hH_V1-VSD in pET15b reverse)	**CTGAGGGTGACTCCAGCTGCTGCCCATGGTATAT CTCC**
Primer 19 (exchange N-terminal His-tag against StrepII-tag in hH_V1-VSD in pET15b forward)	**GGCACCAGGCCGCTGCTCTTTTCAAACTGAGGGT GACTC**
Primer 20 (amplification DrVSD1 forward)	**GGAATTCCATATGAAGGAGGAAACC**
Primer 21 (amplification DrVSD1 reverse)	**CGCGGATCCTTAAACCAAAATTACG**
Primer 22 (PylRS-tRNA amplification forward)	**GCTTTTAGATCTTAATACGACTCACTATAGGGAG AC**
Primer 23 (PylRS-tRNA amplification reverse)	**TGGCGGAAACCCCGGGAATC**
Primer 24 (introduction of a *Nco* I restriction site into the PylRS *M. mazei* construct in pBH4 forward)	**ATATTACCATGGATAAAAAACCGCTGAATACCCT GATTAGCG**
Primer 25 (introduction of a *Nco* I restriction site into the PylRS *M. mazei* construct in pBH4 reverse)	**TAATATGGATCCTTACAGGTTGGTGCTAATACCA TTGTAATAGC**

2.2 Construct list

The DNA and protein sequences of the listed constructs in Table 3 can be found in the appendix (7.1). The hHV1-VSD and DrVSD constructs in pET15b with 6x N-terminal His-tags were sent to our lab by the group of E. Perozo (institute for biophysical dynamics, University of Chicago). A DNA-string for DrVSD1 was ordered including the *Nde* I/*Bam*H I restriction sites for further transfer in the pET15b vector from Thermo Fisher Scientific.

Table 3: List of all construct used in the experiments with their lengths, corresponding vector systems, and restriction sites with which they were cloned.

Protein	UniProtKB	Length	Construct	Vector system	Cloning procedure
hH_V1-VSD	Q96D96	75-223	6xHis-tag::Thrombin-site::hH_V1-VSD	pET15b	*Nde* I/*Bam*H I
		75-223	hH_V1-VSD::10xHis-tag	pET21a*	*Nde* I/*Bam*H I
		75-223	hH_V1-VSD::StrepII-tag	pET21a*	*Nde* I/*Bam*H I
		75-223	6xHis-tag::Thrombin-site::hH_V1-VSD::StrepII-tag	pET15b	QuickChange primer16/17 His-hH_V1-VSD in pET15b
		75-223	StrepII-tag::Thrombin-site::hH_V1-VSD	pET15b	QuickChange primer18/19 His-hH_V1-VSD in pET15b
DrVSD (L90P, L164V)	B3IUN7	32-167	6xHis-tag::Thrombin-site::DrVSD	pET15b	*Nde* I/*Bam*H I
		32-167	6xHis-tag::Thrombin-site::DrVSD::StrepII-tag	pET15b	QuickChange primer15/16 His-DrVSD in pET15b
		32-167	6xHis-tag::Thrombin-site::DrVSD1	pET15b	*Nde* I/*Bam*H I
GFP (F64L, S65T, Q80R, F99S, V163A)	A0A193CK14	37-273	GFP::6xHis-tag	pET21a	*Nde* I/*Hind* III
GFP (F64L, S65T, Q80R, F99S, Y151*, V163A)	A0A193CK14	37-273	GFP::6xHis-tag	pET21a	*Nde* I/*Hind* III
KcsA	P0A334	3-160	6xHis-tag::Thrombin-site::KcsA::StrepII-tag	pET28a	
MraY	Q03521	1-324	AC-tag::MraY::10xHis-tag	pET21a	
MSP1E3D1[1]		255 aa	6xHis-tag::TEV-site::MSP1E3D1	pET28a	
MSP1[1]		200 aa	6xHis-tag::TEV-site::MSP1	pET28a	
MSP1D1 ΔH4/H5[2]		145 aa	6xHis-tag::TEV-site::MSP1D1 ΔH4H5	pET28a	
MSP1D1 ΔH4-H6[2]		123 aa	6xHis-tag::TEV-site::MSP1D1 ΔH4-H6	pET28a	
MSP1D1 ΔH5[2]		167 aa	6xHis-tag::TEV-site::MSP1D1 ΔH5	pET28a	
MSP1D1 ΔH5(-)[2]		167 aa	MSP1D1 ΔH5	pET28a	

Protein	UniProtKB	Length	Construct	Vector system	Cloning procedure
PylRS *M. barkeri* (D76G, N143S, N194D, N311G, Y349F)	Q6WRH6	1-419	10xHis-tag::TEV-site::PylRS	pBH4	*Bam*H I/*Xho* I
		1-419	MBP::8xHis-tag::TEV-site::PylRS	pMAL	*Bam*H I/*Xho* I
PylRS *M. mazei* (Y306A, Y384F, I413L)	Q8PWY1	1-454	10xHis-tag::TEV-site::PylRS	pBH4	*Bam*H I/*Xho* I
		1-454	10xHis-tag::Ub19::TEV-site::PylRS	pET39_Ub19	*Nco* I/*Bam*H I (primer24/25)
		1-454	MBP::8xHis-tag::TEV-site::PylRS	pMAL	*Bam*H I/*Xho* I
PylRS-tRNA			Hammerhead ribozyme::tRNA	pUC57	*Xba* I/*Bam*H I

[1]Constructs are similar to what was described previously (Ritchie *et al*., 2009).
[2]Constructs are similar to what was described previously (Hagn *et al*., 2013).

The lab of Dr. C. Ahern (department of molecular physiology and biophysics, Carver College of Medicine, University of Iowa) provided us with information about the DNA sequence of the *M. barkeri* pyrrolysyl-tRNA-synthetase with defined mutated sites, which ensure the recognition of the substrate pentafluoro-L-phenylalanine. Introduction of this substrate will enable ^{19}F-NMR experiments. Dr. Andrzej Rajca (department of chemistry, University of Nebraska-Lincoln) provided us with the self-synthesized amino acid nitroxide useful for PRE measurements (3.1.9, 3.1.10, 3.2.11, 7.1). The radical as well as the associated synthetase were described in the literature (Yanagisawa *et al.*, 2008b; Plass *et al.*, 2011; Schmidt *et al.*, 2014a). Here, the DNA sequence information for the PylRS-SL1 from *M. mazei* was used. The gene constructs for both pyrrolysyl-tRNA-synthetases were ordered and transferred to different expression vectors (pBH4, pET39(+)_Ub19 and pMAL). Both PylRSs load the different substrates onto the same tRNA, which contains the anticodon that recognizes the TAG stop-codon. The tRNA-synthetase from *M. barkeri* with *Bam*H I/*Xho* I restriction sites and the corresponding tRNA were purchased in an *E. coli* codon-optimized version from GenScript in a pUC57 vector. The tRNA-synthetase from *M. mazei* was ordered as an *E. coli* codon-optimized DNA-string with *Bam*H I/*Xho* I restriction sites from Thermo Fisher Scientific.

2.3 Bacterial strains

The bacterial strains were used for cell-free extract preparation, protein production and for plasmid replication. All used bacterial strains are listed in Table 4 with their respective genotypes.

Table 4: Bacterial strains used for different experiments.

Strain	Genotype	Reference
***E. coli* A19**	*rna-19*, *gdhA2*, *his-95*, *relA1*, *spoT1*, *metB1*	*E. coli* Genetic stock center (New Haven, USA)
***E. coli* BL21 Star™ (DE3)**	F⁻*omp*T *hsd*S_B (r_B^-, m_B^-) *galdcmrne*131 (DE3)	Thermo Fisher Scientific
***E. coli* DH5α**	*fhuA2 Δ(argF-lacZ)U169 phoA glnV44 Φ80 Δ(lacZ)M15 gyrA96 recA1 relA1 endA1 thi-1 hsdR17*	NEB C29871

2.4 Equipment

2.4.1 Equipment for cloning procedures and gene expression

- 24-well microplates Greiner bio-one (Frickenhausen, Germany)
- Agarose gel electrophoresis system Peqlab (Erlangen, Germany)
- Customized cell-free expression containers for analytical (55 µl) and preparative (3 ml) applications (Schwarz *et al.*, 2007) (University Frankfurt a.M., Germany)
- Fermenter Biostat ED, 10 l B. Braun Biotech (Braunschweig, Germany)
- Incubator LB-plates Memmert (Schwabach, Germany)
- Injekt® Solo disposable syringes 1 ml, 2 ml, 5 ml, 10 ml B. Braun (Melsungen, Germany)
- Plastic LB-plates Nerbe (Winsen, Germany)
- Polymerase-chain reaction (PCR) thermocycler pEQStar 96 universal gradient Peqlab (Erlangen, Germany)
- Shaking devices: Infors HT Infors (Bottmingen, Switzerland), Infors HT Multitron Infors (Einsbach, Germany), InnovaTM 4330 New Brunswick Scientific (Nürtingen, Germany)
- Slide-A-lyzer dialysis cassette, 10 kDa molecular weight cut-off (MWCO) Thermo Fisher Scientific (Langenselbold, Germany)
- Sterican® standard needles B. Braun (Melsungen, Germany)
- Thermostatic Cabinet Lovibond (Amesbury, UK)

2.4.2 Equipment for protein downstream processing and analyses

- 96F Nunc™ non-treated black microwell polystyrene plates Thermo Fisher Scientific (Langenselbold, Germany)
- ÄKTA prime fast protein liquid chromatography (FPLC) system GE Healthcare (Munich, Germany)
- ÄKTA purifier FPLC system GE Healthcare (Munich, Germany)
- Amicon ultra-0.5 centrifugal filter units (10 kDa MWCO), Amicon ultra-4 centrifugal filter units (10, 30 and 50 kDa MWCO), Amicon ultra-15 centrifugal filter units (10, 30 and 50 kDa MWCO) Merck Millipore (Darmstadt, Germany)
- Avanti mini-extruder Avanti Polar Lipids (Alabaster, USA)
- Bio-Beads SM2 Bio-Rad (Munich, Germany)
- Centripreps (10 kDa MWCO) Merck Millipore (Darmstadt, Germany)
- Cuvettes: QS high precision cell 160 µl and 1 ml fluorescence cuvette Hellma Analytics (Müllheim, Germany), 100-QS 1 mm thickness 350 µl cuvette for circular dichroism (CD) measurements Hellma Analytics (Müllheim, Germany)
- Desalting columns: PD MidiTrap G-25 and PD-10 desalting columns GE Healthcare (Munich, Germany), Bio-Spin® 6 columns Bio-Rad (Munich, Germany)
- Econo-Pac® chromatography columns Bio-Rad (Munich, Germany)
- Fluorescence spectrophotometer Cary Eclipse Varian (Palo Alto, USA)
- French pressure cell disruptor SLM Aminco Instruments (Irvine, USA)
- GeniosPro microplate spectrophotometer Tecan (Crailsheim, Germany)
- HisTrap FF 5 ml column GE Healthcare (Munich, Germany)
- Immobilized metal ion affinity chromatography (IMAC) sepharose 6 fast flow resin GE Healthcare (Munich, Germany)
- Immobilon-P polyvinylidene difluoride (PVDF) membrane (0.45 µm) Merck Millipore (Darmstadt, Germany)
- Ismatec Vario pump systems Cole-Parmer GmbH (Wertheim, Germany)
- Jasco J-810 spectropolarimeter Jasco (Gross-Umstadt, Germany)
- Lumi-Imager F1 Roche (Penzberg, Germany)
- Mini-protein electrophoresis system Bio-Rad (Munich, Germany)
- NanoDrop 1000 Peqlab (Erlangen, Germany)

- Omnifit® glass column Sigma-Aldrich (Taufkirchen, Germany)
- OptimaTM TLX ultracentrifuge (rotors: TLA-55, TLA-100 and TLA-110) Beckman Coulter (Krefeld, Germany)
- Sonifier Labsonic U B. Braun Biotech (Braunschweig, Germany), UP100H Sonifier Hielscher Ultrasound technology (Teltow, Germany)
- Standard disposable polystyrene cuvettes Bio-Rad (Munich, Germany)
- Strep-Tactin® sepharose® 50 % suspension IBA (Goettingen, Germany)
- Superdex 200 3.2/30 gel-filtration column GE Healthcare (Munich, Germany)
- Superdex 200 3.2/30 increase gel-filtration column GE Healthcare (Munich, Germany)
- Trans-Blot® Turbo™ blotting system Bio-Rad (Munich, Germany)
- Ultracentrifugation tubes: thickwall, polypropylene, 200 µl/1 ml/4 ml and with snap-oncap, polypropylene, 1.5 ml Beckman Coulter (Krefeld, Germany)
- UV-Vis spectrometer SpectroStar^{Nano} BMG Labtech (Ortenberg, Germany)
- Wet/Tank western blot system (miniProteanIV) Bio-Rad (Munich, Germany)
- Whatman^{TM} Nuclepore^{TM} track-etched membrane, 0.2 µm pore size, 19 mm diameter GE Healthcare (Munich, Germany)
- Zeba micro spin desalting columns (MWCO 7 kDa) Thermo Fisher Scientific (Langenselbold, Germany)

2.4.3 General equipment

- Autoclave Gettinge (Rastatt, Germany)
- Balances: Sartorius CP1245-OCE balance Sartorius (Goettingen, Germany)
- Cellulose acetate filter 0.22 µm and 0.45 µm Sartorius (Goettingen, Germany)
- Centrifuges: centrifuge 5415 R Eppendorf (Hamburg, Germany), centrifuge 5810 R Eppendorf (Hamburg, Germany), centrifuge Sorvall RC5B Thermo Fisher Scientific (Langenselbold, Germany), Sorvall RC5C Thermo Fisher Scientific (Langenselbold, Germany), RC12BP^{+} Thermo Fisher Scientific (Langenselbold, Germany), cooled table top centrifuge Micro 22R Hettich (Tuttlingen, Germany), Megafuge 16R Heraeus Thermo Fisher Scientific (Langenselbold, Germany), Biofuge 13 Heraeus Sepatech Gemini^{BV} (Apeldoorn, Netherlands), micro centrifuge Roth (Karlsruhe, Germany)

- Dialysis tubes type 27/30, 12-14 kDa MWCO Spectrum Laboratories (Rancho Dominguez, USA),
- Glas and plastic accessories Carl Roth and VWR (Karlsruhe and Darmstadt, Germany)
- Haake Fisons C1 water bath Thermo Fisher Scientific (Langenselbold, Germany)
- Magnetic stirring devices IKAMAG (Staufen, Germany)
- Membrane pump Vacuumbrand GmbH (Wertheim, Germany)
- Microwave Bosch (Munich, Germany)
- Milli-Q water purification systems Merck Millipore (Darmstadt, Germany)
- MS2 minishaker IKA (Staufen, Germany), vortexing device Bender&Hobein (Munich, Germany)
- Orbital shaker: Revolver™ adjustable rotator Labnet International Inc. (Edison, USA), RS-60 Tube rotator BioSan (Riga, Latvia)
- PHM 210 standard pH-meter Radiometer Copenhagen (Brønshøj,Denmark)
- Pipettes Eppendorf Research Plus (Hamburg, Germany)
- Pipetus® Hirschmann (Eberstadt, Germany)
- Rotavapor RE120 Buechi (Essen, Germany)
- Rotors: SS34, GSA, GS3, H12000 Thermo Fisher Scientific (Langenselbold, Germany)
- Shaking devices:, Promax 2020 reciprocating platform shaker Heidolph Instruments (Schwabach, Germany), shaker 3005 GFL (Burgwedel, Germany),
- Sonorex Super RK 510 water bath Bandelin electronics (Berlin, Germany)
- Standard heat block VWR (Darmstadt, Germany)
- Sublimater Vaco10 Zirbus (Osterode, Germany)
- Thermomixer 5436 Eppendorf (Hamburg, Germany)

2.4.4 Kits

The different Kits listed were used for molecular biological and protein biochemistry work.

- Midi/Maxi DNA preparation kit Macherey-Nagel (Dueren, Germany)
- QIAprep spin miniprep kit Qiagen (Hilden, Germany)
- QIAquick gel extraction kit Qiagen (Hilden, Germany)
- QIAquick PCR purification kit Qiagen (Hilden, Germany)
- Trans-Blot® Turbo™ RTA transfer kit Bio-Rad (Munich, Germany)

2.4.5 Software

- Adobe Creative Suite 6
- Chromas Lite
- CLC Sequence Viewer6
- Clone Manager
- EndNote X6
- ImageJ
- Microsoft Office 2010
- PyMOL
- SigmaPlot 11.0
- Sparky
- TECAN Magellan 5.03
- TopSpin 3.2
- UNICORN 5.11
- Vector NTI

2.5 Chemicals and reagents

2.5.1 General chemicals

Unless otherwise stated, the listed chemicals were purchased from Carl Roth (Karlsruhe, Germany) and exhibit a degree of purity of *pro analysi* (p.A.).

- (S)-2-amino-6-((((1-oxy-2,2,5,5-tetramethylpyrroline-3-yl)methoxy)carbonyl)amino)-hexanoic acid (amino acid nitroxide) synthesized by A. Rajca (1.1)
- 1,4-Dithiothreithol (DTT)
- 2-[4-(2-Hydroxyethyl)piperazin-1-yl]ethanesulfonic acid (HEPES)
- 2-Guanidinobenzimidazole (2GBI) Sigma-Aldrich (Taufkirchen, Germany)
- 2-Mercaptoethanol
- 2-Nitro-5-thiocyanatobenzoic acid (NTCB) Sigma-Aldrich (Taufkirchen, Germany)
- 3-(N-morpholino)propanesulfonic acid (MOPS) Sigma-Aldrich (Taufkirchen, Germany)
- 3-(Trimethylsilyl)-1-propanesulfonic acid sodium salt (DSS)
- 9-Amino-6-chloro-2-methoxyacridine (ACMA) Sigma-Aldrich (Taufkirchen, Germany)
- Acetic acid
- Acetyl phosphate lithium potassium salt (AcP) Sigma-Aldrich (Taufkirchen, Germany)
- Adenosine-5’-triphosphate (ATP)
- Agarose Biozym (Hessisch Oldendorf, Germany)
- Amino acids (except: E,K and T)
- Amino acids E, K, T Sigma-Aldrich (Taufkirchen, Germany)

- Ammonium persulfate (APS)
- Antifoam Y-30 emulsion Sigma-Aldrich (Taufkirchen, Germany)
- Bovine serum albumin (BSA)
- Bromophenol blue
- Calcium chloride
- Chloroform
- Complete protease inhibitor cocktail Roche (Penzberg, Germany)
- Coomassie brilliant blue G-250
- Cyanide m-chlorophenyl hydrazone (CCCP) Sigma-Aldrich (Taufkirchen, Germany)
- Cytidine 5'-triphosphate di-sodium salt (CTP) Sigma-Aldrich (Taufkirchen, Germany)
- D(+)-saccharose
- Desthiobiotin IBA (Goettingen, Germany)
- Dimethyl sulfoxide (DMSO)
- Dipotassium hydrogen phosphate
- Di-sodium hydrogen phosphate
- Ethanol 96 % (denatured)
- Ethylenediaminetetraacetic acid (EDTA)
- Ethylenglycol-bis(aminoethylether)-N,N,N',N'-tetraacetic acid (EGTA)
- Folinic acid calcium salt Sigma-Aldrich (Taufkirchen, Germany)
- Glucose monohydrate
- Glycerol 98 %
- Guanosine 5'-triphosphate di-sodium salt (GTP) Sigma-Aldrich (Taufkirchen, Germany)
- Hydrochloric acid 37 %
- Hydrogen peroxide 30 %
- Hydroxyl-azophenyl-benzoic acid (HABA), ready to use solution from IBA (Goettingen, Germany)
- Imidazole ≥ 99 % Sigma-Aldrich (Taufkirchen, Germany)
- Isopropanol
- Isopropyl-β-D-thiogalactopyranosid (IPTG)
- Luminol Sigma-Aldrich (Taufkirchen, Germany)

- Magnesium acetate ($Mg(OAc)_2$) tetrahydrate
- Magnesium chloride hexahydrate
- Magnesium sulfate heptahydrate
- Manganese II sulfate monohydrate
- Methanol
- Nickel(II) sulfate
- p-Cumaric acid Sigma-Aldrich (Taufkirchen, Germany)
- Pentafluoro-L-phenylalanine (5FP) Tokyo chemical industry Co., Ltd. (Zwijndrecht, Belgium)
- Phenylmethylsufonyl fluoride (PMSF) Sigma-Aldrich (Taufkirchen, Germany)
- Phosphoenol pyruvic acid monopotassiumsalt (PEP) Sigma-Aldrich (Taufkirchen, Germany)
- Polyethylene glycol (PEG) 8000
- Potassium acetate (KOAc)
- Potassium chloride ≥ 99 %
- Potassium dihydrogenphosphate
- Potassium hydroxide
- Pyruvate kinase Roche (Penzberg, Germany)
- Restriction enzymes NEB (Frankfurt, Germany)
- RiboLock RNase inhibitor Fermentas, Thermo Fisher Scientific (Langenselbold, Germany)
- Rotiphorese Gel 30 (37.5:1)
- Skim milk powder Sigma-Aldrich (Taufkirchen, Germany)
- Sodium acetate
- Sodium azide
- Sodium carbonate decahydrate
- Sodium chloride ≥99.9 %
- Sodium hydrogen phosphate-dihydrate
- Sodium hydroxide
- T4 DNA-ligase NEB (Frankfurt, Germany)
- Tetramethylethylenediamine (TEMED)

- Trichloroacetic acid (TCA) ≥99.0 % Sigma-Aldrich (Taufkirchen, Germany)
- Tricine
- Tris(hydroxymethyl)aminomethane (Tris)
- tRNA *E. coli* MRE 600 Roche (Penzberg, Germany)
- Tryptone
- Turbo-Pfu DNA polymerase Stratagene (Waldbronn, Germany)
- Urea
- Uridine 5'-triphosphate tri-sodium salt (UTP) Sigma-Aldrich (Taufkirchen, Germany)
- Valinomycin Sigma-Aldrich (Taufkirchen, Germany)
- VentDNA polymerase NEB (Frankfurt, Germany)
- Yeast extract
- Zinc chloride

2.5.2 Antibodies and markers

The following antibodies were used as primary and secondary antibodies in western blot analyses. They were solved in blocking buffer. Their recommended dilutions are indicated. The different markers were used as references for agarose and polyacrylamide gel analyses.

- Monoclonal mouse anti-hexa His-antibody (1:2000 dilution) Sigma-Aldrich (Taufkirchen, Germany)
- Anti-mouse IgG (Fab specific)-peroxidase antibody from goat (1:5000 dilution, 800-2200 ng/ml) Sigma-Aldrich (Taufkirchen, Germany)
- Anti-StrepII-tag IgG from mouse Qiagen (1:2000, 100 ng/ml) (Hilden, Germany)
- Monoclonal mouse apoA-I (A5.4) antibody (1:200, 1 µg/ml) Santa Cruz Biotechnology (Dallas, USA)
- Precision Protein™ StrepTactin-horseradish peroxidase (HRP) conjugate (1:5000 dilution) Bio-Rad (Munich, Germany)
- Gene ruler 100 bp, 1 kb DNA ladder Fermentas Thermo Fisher Scientific, (Langenselbold, Germany)
- Precision plus protein dual color standard Bio-Rad (Munich, Germany)
- Unstained protein molecular weight marker Thermo Fisher Scientific, (Langenselbold, Germany)
- Roti®-Mark 10-150 PLUS His-marker Carl Roth (Karlsruhe, Germany)

2.5.3 Detergents

The detergents used for different experiments are listed here.

- 1,2-diheptanoyl-sn-glycero-3-phosphocholine (DH(7)PC) Avanti Polar Lipids (Alabaster, USA)
- 1-palmitoyl-2-hydroxy-sn-glycero-3-phospho-(1'-rac-glycerol) (LPPG) Avanti Polar Lipids (Alabaster, USA)
- Cholic acid Sigma-Aldrich (Taufkirchen, Germany)
- N,N-dimethyldodecylamine N-oxide (LDAO) Sigma-Aldrich (Taufkirchen, Germany)
- n-Dodecylphosphocholine (DPC, Fos-12) Avanti Polar Lipids (Alabaster, USA)
- n-Dodecyl-β-D-maltoside (DDM) Anatrace (Santa Clara, USA)
- n-Tetradecyl-N,N-dimethyl-3-ammonio-1-propanesulfonate (Anzergent3-14) Anatrace (Santa Clara, USA)
- n-Tetradecylphosphocholine (Fos14) Anatrace (Santa Clara, USA)
- Sodium dodecyl sulfate (SDS) Carl Roth (Karlsruhe, Germany)
- Triton X-100 Sigma-Aldrich (Taufkirchen, Germany)
- Tween20 Carl Roth (Karlsruhe, Germany)

2.5.4 Lipids

The following lipids were used for nanodisc/liposome preparations or for producing mixed micelles/bicelles.

- 1,2-Dimyristoyl-sn-glycero-3-phospho-(1'-rac-glycerol) (DMPG) Avanti Polar Lipids (Alabaster, USA)
- 1,2-Dimyristoyl-sn-glycero-3-phosphocholine (DMPC) Avanti Polar Lipids (Alabaster, USA)
- 1,2-Dioleoyl-sn-glycero-3-phospho-(1'-rac-glycerol) (DOPG) Avanti Polar Lipids (Alabaster, USA)
- 1,2-Dioleoyl-sn-glycero-3-phosphocholine (DOPC) Avanti Polar Lipids (Alabaster, USA)
- 1,2-Dioleoyl-sn-glycero-3-phosphoethanolamine (DOPE) Avanti Polar Lipids (Alabaster, USA)

- 1,2-Dioleoyl-sn-glycero-3-phospho-monomethyl-ethanolamine (DOPMME) De Kroon group Utrecht University self-synthesized
- 1,2-Dipalmitoyl-sn-glycero-3-ethylphsophocholine (EPC) chloride salt Avanti Polar Lipids (Alabaster, USA)
- 1-Palmitoyl-2-oleoyl-sn-glycero-3-phosphocholine (POPC) Avanti Polar Lipids (Alabaster, USA)
- 1-Palmitoyl-2-oleoyl-sn-gylcero-3-phospho-(1´-rac-gylcerol) (POPG) Avanti Polar Lipids (Alabaster, USA)
- 1-Palmitoyl-2-oleoyl-sn-gylcero-3-phosphoethanolamine (POPE) Avanti Polar Lipids (Alabaster, USA)
- Asolectin Sigma-Aldrich (Taufkirchen, Germany)
- Total lipid extract from bovine brain Avanti Polar Lipids (Alabaster, USA)

2.5.5 Labeled amino acids and scrambling inhibitors

The listed labeled amino acids and scrambling inhibitors were used in cell-free protein synthesis for NMR and mass spectrometry sample preparations. They were ordered from CIL (Tewksbury, USA) if not stated otherwise.

- ^{13}C-methyl-labeled methionine Sigma-Aldrich (Taufkirchen, Germany)
- ^{15}N,^{13}C6-labeled isoleucine
- ^{15}N,^{2}H-labeled alanine
- ^{15}N,^{2}H-labeled algal amino acid mix Sigma-Aldrich (Taufkirchen, Germany)
- ^{15}N,^{2}H-labeled cell-free amino acid mix
- ^{15}N,^{2}H-labeled glycine
- ^{15}N-labeled L-asparagine:H_2O
- ^{15}N-labeled L-glutamine
- ^{15}N-labeled L-tryptophan
- ^{2}H-labeled algal amino acid mix Sigma-Aldrich (Taufkirchen, Germany)
- D-(+)-malic acid Sigma-Aldrich (Taufkirchen, Germany)
- D-cycloserine Sigma-Aldrich (Taufkirchen, Germany)
- O-(carboxymethyl)hydroxylamine hemihydrochloride (AOA) Sigma-Aldrich (Taufkirchen, Germany)

2.6 Composition of frequently used buffers and solutions

2.6.1 Buffers and solutions for protein upstream processing

Different buffers and solutions used for molecular biological experiments were listed in Table 5. All solutions and buffers were prepared with ultra-pure, desalted water.

Table 5: List of all different buffers and solutions used for protein upstream processing.

Name	Composition
Buffers and media for cell cultivation, growth and storage	
LB medium:	10 g/l tryptone, 5 g/l yeast extract, 10 g/l NaCl
2xYTPG medium (S30 extract preparation):	16 g/l tryptone, 10 g/l yeast extract, 5 g/l NaCl, 2.99 g/l KH_2PO_4, 6.97 g/l K_2HPO_4, 19.8 g/l glucose
TB medium (MSP fermentation):	12 g/l tryptone, 24 g/l yeast extract, 5 g/l glycerin, 4.8 g/l KH_2PO_4, 25 g/l K_2HPO_4, 19.8 g/l glucose
ZYM-5052 medium (auto-induction of PylRS):	Studier, 2005
SOC medium:	20 g/l tryptone, 5 g/l yeast extract, 0.6 g/l NaCl, 0.2 g/l KCl, 10 mM $MgCl_2$, 10 mM $MgSO_4$, 20 mM glucose
DB-salt:	5.22 mM $(NH_4)H_2PO_4$, 0.049 mM magnesium sulfate, 0.101 mM KCl, 86 % glycerin (w/v)
TFB1 buffer:	100 mM KCl, 100 mM manganese II sulfate monohydrate, 30 mM KOAc, 10 mM $CaCl_2$, 15 % glycerol (v/v), glacial acetic acid for pH 5.8
TFB2 buffer:	10 mM MOPS, 10 mM KCl, 75 mM $CaCl_2$, 15 % glycerol (v/v), NaOH for pH 7.0
$MgCl_2$:	1 M
IPTG:	1 M
Ampicillin (1000x):	100 mg/ml solved in 50 % EtOH (v/v)
Kanamycin (1000x):	30 mg/ml solved in water
Stock solutions for cell-free protein synthesis	
tRNA from *E. coli*:	40 mg/ml
AcP[1]:	1 M, pH 7.0 (adjusted with KOH)
Pyruvate kinase[1]:	10 mg/ml
NTP mix (75x)[1]:	90 mM ATP, 60 mM each CTP, GTP and UTP, pH 7.0, (adjusted with NaOH)
Folinic acid:	10 mg/ml
DTT:	500 mM
HEPES/EDTA (24x):	2.4 M HEPES, pH 8.0 (adjusted with KOH), 20 mM EDTA pH 8.0

Name	Composition
$Mg(OAc)_2$:	1 M
KOAc:	10 M
PEG 8000:	40 % (w/v)
NaN_3:	10 % (w/v)
Amino acid mix:	25 mM each (20 *L*-amino acids)
RCWMDE mix:	25 mM each
Complete (50x):	1 tablet/ml
RiboLock RNase inhibitor (50x):	40 U/µl
T7 RNA-polymerase[1]:	Different batches: 3.2 U/µl, 3.62 U/µl, 5.4 U/µl, 6.5 U/µl
PEP[1]:	1 M, pH 7.0 (adjusted with KOH)
DNA aminoacyl-tRNA:	50-170 ng/µl in H_2O
Amino acid nitroxide:	100 mM in H_2O
5FP:	100 mM in 1 M NaOH
Agarose gel electrophoresis	
TAE buffer:	40 mM Tris, 20 mM acetic acid, 1 mM EDTA, pH 8.3
Agarose (1 % w/v):	0.5 g/50 ml TAE buffer, 2.5 µl Roti-GelStain
DNA loading buffer (6x):	30 % glycerol (v/v), 0.25 % bromophenol blue (w/v), 0.1 M EDTA

[1]These ingredients were kindly prepared and provided by other members of the institute for biophysical chemistry.

2.6.2 Buffers and solutions for protein downstream processing

The following Table 6 lists different buffers and solutions used for the protein biochemical experiments. All solutions and buffers were prepared with ultra-pure, desalted water.

Table 6: List of all different buffers and solutions used for protein downstream processing.

Name	Composition
S30 extract preparation	
S30 buffer A:	10 mM Tris-OAc, 14 mM $Mg(OAc)_2$, 60 mM KCl, 6 mM β-mercaptoethanol, pH 8.2 @ 25 °C
S30 buffer B:	10 mM Tris-OAc, 14 mM $Mg(OAc)_2$, 60 mM KCl, 1 mM DTT, 1 mM PMSF, pH 8.2 @ RT
S30 buffer C:	10 mM Tris-OAc, 14 mM $Mg(OAc)_2$, 60 mM KOAc, 0.5 mM DTT, pH 8.2

Name	Composition
MSP purification, cleavage and ND preparation	
MSP-A buffer:	40 mM Tris-HCl pH 8.0 @ 4 °C, 300 mM NaCl, 1 % Triton X-100 (v/v)
MSP-B buffer:	40 mM Tris-HCl pH 8.9 @ 4 °C, 300 mM NaCl, 50 mM sodium cholate
MSP-C buffer:	40 mM Tris-HCl pH 8.0 @ 4 °C, 300 mM NaCl
MSP-D buffer:	40 mM Tris-HCl pH 8.0 @ 4 °C, 300 mM NaCl, 50 mM imidazole
MSP-E buffer:	40 mM Tris-HCl pH 8.0 @ 4 °C, 300 mM NaCl, 300 mM imidazole
MSP-F buffer:	40 mM Tris-HCl pH 7.4 @ 4°C, 300 mM NaCl, 0.5 mM EDTA, 10 % glycerol (w/v)
TEV digestion buffer:	50 mM Tris-HCl pH 8.0 @ 4 °C, 0.5 mM EDTA, 1 mM DTT
TEV equilibration buffer:	20 mM Tris-HCl pH 8.0 @ 4 °C, 100 mM NaCl, 20 mM imidazole
TEV elution buffer:	20 mM Tris-HCl pH 8.0 @ 4 °C, 100 mM NaCl, 300 mM imidazole
ND-A buffer:	10 mM Tris-HCl pH 8.0 @ 4 °C, 100 mM NaCl
Lipid solutions:	50 mM of the appropriate lipid, ≥100 mM sodium cholate (for DMPG 300 mM)
Protein purification and analysis[a]	
5x standard buffer:	500 mM Tris-HCl pH 8.0 @ 4 °C, 750 mM NaCl
Solubilization buffer:	1x standard buffer, variable detergent (2 % DH(7)PC, 1 % DPC, 1 % LPPG, 1 % Fos14)
Equilibration buffer:	1x standard buffer, 10 mM imidazole, (variable detergent (0.1 % DH(7)PC, 0.2 % DPC, 0.2 % LPPG, 0.07 % Fos14])
Wash buffer:	1x standard buffer, 30 mM imidazole, (variable detergent [0.1 % DH(7)PC, 0.2% DPC, 0.2 % LPPG, 0.07 % Fos14])
Wash buffer W2:	1x standard buffer, 0.15 % DPC, 0.05 % DH(7)PC
Wash buffer W3:	1x standard buffer, 0.1 % DPC, 0.1 % DH(7)PC
Wash buffer W4:	1x standard buffer, 0.2 % DH(7)PC
Elution buffer:	1x standard buffer, 250 mM imidazole, (variable detergent [0.2 or 0.5 % DH(7)PC, 0.5 % DPC, 0.2 % LPPG, 0.07 % Fos14])
Buffer W:	100 mM Tris-HCl pH 8.0 @ 4 °C, 150 mM NaCl, 1 mM EDTA, (variable detergent [0.1 % DH(7)PC, 0.08 % DPC])
Buffer E:	Buffer W, 2.5 mM desthiobiotin (variable detergent [0.1 % DH(7)PC, 0.08 % DPC])

Name	Composition
Buffer R:	Buffer W, 1 mM HABA
IMAC stripping buffer:	20 mM sodium phosphate, 0.5 M NaCl, 50 mM EDTA, pH 7.4
CD buffer:	10 mM K_2HPO_4 pH 7.0, 0.08 % DPC
Sucrose:	64 %, 25 %, 5 % (w/v) in liposome buffer
Mass spectrometry buffer:	50 mM NH_4OAc pH 6.8
Sodium carbonate precipitation buffer:	100 mM Na_2CO_3 pH 11.5, 20 mM HEPES, 150 mM NaCl
Lysis buffer PylRS:	50 mM HEPES-NaOH pH 7.5, 300 mM NaCl, 10 mM imidazole
Wash buffer PylRS:	50 mM HEPES-NaOH pH 7.5 or 50 mM Tris-HCl pH 8.0 @ 4 °C, 300 mM NaCl, 10 mM imidazole, 3 mM β-mercaptoethanol
Elution buffer PylRS:	50 mM HEPES-NaOH pH 7.5 or 50 mM Tris-HCl pH 8.0 @ 4 °C, 300 mM NaCl, 300 mM imidazole, 3 mM β-mercaptoethanol
Storage buffer PylRS:	50 mM HEPES-NaOH pH 7.5 or 50 mM Tris-HCl pH 8.0 @ 4 °C, 10 mM $MgCl_2$, 30 mM KCl, 5 mM DTT, 40 % glycerol (v/v)
PBS buffer:	137 mM NaCl, 2.7 mM KCl, 10 mM Na_2HPO_4, 1.8 mM KH_2PO_4, pH 7.4
Size-exclusion chromatography (SEC) protein standards:	3 mg/ml aprotinin, 3 mg/ml ribonuclease, 3 mg/ml carbonic anhydrase, 0.4 mg/ml ovalbumin, 3 mg/ml conalbumin, 4 mg/ml aldolase, 0.3 mg/ml ferritin, 5 mg/ml thyroglobulin, 1 mg/ml blue dextran2000
SEC calibration buffer:	50 mM sodium phosphate, 150 mM NaCl, pH 7.2
ITC buffer/ Malvern buffer:	50 mM K_2HPO_4 pH 7.0, 0.08 % DPC
GFP buffer:	20 mM Tris-HCl pH 7.8, 150 mM NaCl

[a] The detergent concentration is always referred to w/v.

Fluorescence-based activity assay	
Liposome buffer:	20 mM HEPES-NaOH pH 7.0, 150 mM KCl, 10 % glycerol (v/v), 0.2 mM EGTA, 2 mM β-mercaptoethanol
Flux buffer:	20 mM HEPES-NaOH pH 7.0, 150 mM NaCl, 0.2 mM EGTA, 2 mM β-mercaptoethanol, 10 % glycerol (v/v), 0.5 mg/ml BSA, 7.5 mM KCl, 2 µM ACMA
CCCP:	100 mM in DMSO
Valinomycin:	1 mg/ml in DMSO

Name	Composition
Protein refolding	
Solubilization buffer refolding:	50 mM HEPES-NaOH pH 7.5, 0.2 M NaCl, 1 % SDS (w/v), 0.1 M DTT
Asolectin liposomes:	20 mg/ml in 50 mM HEPES-NaOH pH 7.0, 200 mM NaCl, 10 mM DTT
Equilibration buffer refolding:	20 mM Tris-HCl pH 8.0 @ 4 °C, 150 mM NaCl, 0.07 % Fos14 or 0.08 % DPC (w/v)
Elution buffer refolding:	20 mM Tris-HCl pH 8.0 @ 4 °C, 150 mM NaCl, 0.07 % Fos14 or 0.08 % DPC (w/v), 250 mM imidazole
SDS-polyacrylamide gel electrophoresis (PAGE) analysis	
4x SDS sample-loading buffer:	0.1 M Tris-HCl pH 6.8 @ 4 °C, 8 M urea, 15 % glycerol (v/v), 20 % SDS (w/v), 0.12 % bromophenol blue (w/v), 20 % β-mercaptoethanol (v/v)
Tricine gels	
3x gel buffer:	3 M Tris, 1 M HCl, 0.3 % SDS, pH 8.45
Anode buffer (25x):	2.5 M Tris, 0.5625 M HCl, pH 8.9
Cathode buffer (10x):	1 M Tris, 1 M tricine, 1 % SDS (w/v), pH~8.25
Tris-glycine gels (Laemmli-SDS-PAGE)	
TGS buffer:	25 mM Tris, 192 mM glycine, 0.1 % SDS, pH 8.3
Staining solution:	10 % acetic acid (v/v), 0.25 % Coomassie brilliant blue G-250 (w/v)
Western blot analysis	
Western blot transfer buffer:	25 mM Tris, 192 mM glycine, 10 % ethanol (v/v), pH 8.3
TBST-buffer:	50 mM Tris-HCl pH 7.6, 150 mM NaCl, 0.05 % Tween20 (v/v)
Blocking solution:	5 % milk powder (w/v) in TBST
ECL 1 solution:	100 mM Tris-HCl pH 8.5 @ RT, 2.5 mM luminol solved DMSO, 0.4 mM p-cumaric acid solved in DMSO
ECL 2 solution:	100 mM Tris-HCl pH 8.5 @ RT, 0.0183 % H_2O_2 (v/v)

For SDS-PAGE analyses precast 4-15 % Tris-glycine gels from Bio-Rad, 12 % Tris-glycine and 11 % Tricine gels were used. The composition of separating and stacking gel for the self-made ones is listed in Table 7.

Table 7: Composition of the used SDS-polyacrylamide gels (volume for two gels).

Ingredients	12 % Tris-glycine gel	4 % Tris-glycine gel	11 % Tricine gel	4 % Tricine gel
Acrylamide[1]	4 ml	0.65 ml	4.4 ml	0.825 ml
3x gel buffer	-	-	4 ml	2 ml
50 % glycerol	-	-	2 ml	-
1.5 M Tris-HCl pH 8.8	2.5 ml	-	-	-
0.5 M Tris-HCl pH 6.8	-	1.25 ml	-	-
10 % SDS (w/v)	100 µl	50 µl	-	-
Water	3.4 ml	3.05 ml	1.6 ml	3.175 ml
10 % APS (w/v)	50 µl	25 µl	100 µl	50 µl
TEMED	5 µl	5 µl	10 µl	10 µl
	≈ 10 ml	≈ 5 ml	≈ 12 ml	≈ 6 ml

[1]30 % acrylamide/bisacrylamide (37.5:1)

3 Methods

3.1 Molecular biological methods

3.1.1 Preparation of chemically competent cells

Competent *E. coli* cells were required for the chemical transformation of plasmid DNA into the new host cell. A pre-culture of 10 ml LB medium was inoculated with one colony of BL21 Star™ (DE3) cells, which was picked from an agar plate, and grown over night at 37 °C. The next day, 37 °C-pre-warmed LB medium was inoculated with 1.5 ml of the overnight culture (optical density of 2 at 600 nm [OD_{600}]). Cells were grown at 37 °C, harvested at an OD_{600} of 0.5, and cooled for 10 min on ice. Afterwards, they were transferred to ice-cooled Falcon tubes (2x 50 ml) and centrifuged at 2,000xg for 10 min at 4 °C. Pellets were carefully resuspended in 7.5 ml TFB1 buffer, combined, and incubated on ice for 1 h. The suspension was centrifuged at 2,000xg for 10 min at 4 °C and the pellet was carefully resuspended in 4 ml ice-cooled TFB2 buffer. Aliquots to 100 µl competent cells were prepared, shock frozen in liquid nitrogen and stored at -80 °C.

3.1.2 Transformation, storage and growth of bacterial cells

50 µl to 100 µl chemically competent *E. coli* cells (DH5α or BL21 Star™ (DE3)) were thawed on ice for 20 min before they were incubated for minimum 30 min with 1 µl foreign plasmid DNA (10 µl DNA from a ligation or QuickChange were used) on ice. Afterwards, the cells were applied to a 45 s heat shock at 42 °C and directly incubated with 450 µl pre-warmed SOC medium at 37 °C for 1 h under shaking conditions. The cell suspension was centrifuged (1,000xg, 1 min, RT). 400 µl of the supernatant were removed. The residual volume was pipetted on pre-warmed agar plates with the defined antibiotics. The plates were incubated overnight at 37 °C. The next day, one clone was picked, plated onto another LB plate with the defined antibiotics, and afterwards directly used for inoculation of 5 ml LB medium (1:1000 dilution of the defined antibiotics). Both cultures were incubated overnight at 37 °C. Cells of the agar plates were transferred to 1 ml sterile DB salt medium and stored at -80 °C as cryo stocks. The 5 ml LB cultures were applied to plasmid DNA preparation procedures (QIAprep spin miniprep kit). The obtained plasmid DNA was sent for sequencing to Seqlab.

200 ml LB medium with a 1:1000 dilution of the defined antibiotics was inoculated with positive clones of a transformed cryo stock by using a pipette tip without thawing the cells. Overnight cultures of transformed cells were incubated at 37 °C under constant shaking at 180 rpm and harvested the next day by centrifugation (6,000xg, 10 min, 4 °C). They were either applied to DNA preparation using the Midi/Maxi DNA preparation kit from Macherey-Nagel or used for inoculation of fermentation processes or gene expression in shaking flasks (3.1.7, 3.1.10).

3.1.3 Agarose gel electrophoresis

Agarose gel electrophoresis describes a method to separate DNA or RNA by size. The gels were prepared by solving 0.5 g agarose in 50 ml TAE buffer. The mixture was boiled and cooled to 60 °C prior to the addition of 0.5 µl/10 ml Roti-GelStain. Digested DNA constructs and amplified PCR products were analyzed and referenced to marker nucleotides of a defined size. To this end, the DNA was mixed with 6x DNA loading dye and loaded onto the 1 % agarose gel placed in the running chamber filled with 1x TAE buffer. The run was performed at 120 V for 45 min for an insert and 1:30 h for a linearized vector. UV light was used for detection. Higher agarose percentages were used for smaller fragments (≤100 bp).

3.1.4 Codon optimization

The gene expression in different host organisms is not trivial. Rare codons could hamper the translation/transcription process. Codon optimization tools help to improve the DNA sequence of interest by avoiding rare codons and/or sequence parts that are known to fold in a manner, which disables ribosome-binding events. The constructs used in this thesis were optimized for the codon usage of *E. coli* K12. The constructs were either sent to us by our cooperation partners in a codon-optimized manner, optimized during the gene synthesis by GenScript or Thermo Fisher Scientific, or manually modified using the computer algorithm from IDT (https://eu.idtdna.com/CodonOpt; 10.06.2017, 2:26 pm). This tool is based on the codon adaption index (CAI) which describes the percentage of how well the codon usage of the host organism is affected. Consequently, each new iteration procedure produces a new optimized sequence. Newly designed genes were ordered as strings from Thermo Fisher Scientific, transferred into the pET15b vector, and analyzed in cell-free reactions.

3.1.5 DNA concentration determination and sequencing

Quantification of the DNA was performed by spectrophotometric measurements at a NanoDrop instrument at 260 nm against an appropriate reference solution. Absorption of one is equivalent to a concentration of double-stranded DNA of 50 µg/ml. The DNA quality was determined by analyzing the 260 nm/280 nm value. The ratio should be ~1.8 for pure DNA.

Sequencing reactions were performed by Seqlab Sequence Laboratories Göttingen GmbH (Goettingen, Germany). To this end, purified DNA with a known concentration was sent under compliance of manufacturer's instructions.

3.1.6 Cloning procedures

Different cloning procedures were necessary to introduce or exchange affinity tags of the protein of interest, to transfer the gene of interest into different vector systems or to multiply DNA fragments.

For cloning with restriction enzymes, 0.1 µg/µl of template DNA were digested with 0.6-1 U/µl of the specific restriction enzymes following the manufacturer's indications (NEB) for double digestion at 37 °C for 3 h. Simultaneously, linearized vector fragments were dephosphorylated at the 5' end by the addition of 0.1-0.2 U/µl Antarctic phosphatase from shrimp (SAP) or calf intestine (CIAP) in NEB-recommended buffers. On the one hand, digested construct were mixed with 6x DNA loading dye and applied to 1 % agarose gel electrophoresis (3.1.3). Gel extraction was performed using the QIAquick gel extraction kit from Qiagen. On the other hand, the restriction enzymes were first heat inactivated by incubation for 20 min at 65 °C if recommended. Afterwards, digested fragments were purified using the QIAquick PCR purification kit from Qiagen. In both cases, the DNA was eluted in 30 µl water. The linearized vectors to 2-2.5 ng/µl were ligated with 3x or 5x excess of insert by addition of 20 U/µl T4 DNA ligase. The mixture was incubated in the recommended T4 buffer overnight at 7 °C or for 1 h at room temperature (RT). Afterwards 10 µl of the new plasmid and a control (ligated linearized vector only) were transformed into competent cells, plasmids were prepared and quality-checked by sequencing (3.1.2, 3.1.5).

Tag-variations or amplification strategies were based on different primers (2.1). Primers were designed according to certain rules. Thereby, the annealing part of the primer was used for property checks. The length should be around 13-20 nucleotides that are GC rich. The calculated melting temperature should be higher than 55 °C to allow a specific PCR reaction. The ΔG value for primer annealing should be smaller than -30 kcal/mol and if dimers or hairpins were present, their ΔG value should be bigger than -5 kcal/mol to avoid side reactions. Finally, the full-length primer was always checked with the software Clone Manager for additional annealing sites. Primers were used to 0.5 µM in a standard PCR reaction with 0.02 U/µl Phusion polymerase (additional 3 % DMSO were added if using the GC buffer) or 0.025 U/µl Pfu-polymerase (for QuickChange protocols) in the appropriate buffer, 0.2 mM dNTPs and 0.2 ng/µl or 1 ng/µl template DNA, respectively. A typical protocol for DNA amplification by PCR using the different polymerases is shown in Table 8.

Table 8: Protocols used for PCR reactions with different polymerases.

Steps	**Phusion polymerase**			**Pfu-turbo polymerase**		
	T [°C]	t [s]		T [°C]	t [s]	
Denaturation	98	30		95	120	
Denaturation	98	10		95	30	
Annealing	Primer T_m[a]	15-30	30 cycles	Primer T_m[a]	30	18 cycles
Elongation	72	15-30 s/kb		68	2 min/kb	
Elongation	72	600		68	600	

[a] The primer melting temperature (T_m) is indicated in the following description of the different cloning procedures.

The amplified constructs were applied to PCR purification. *Dpn* I treatment to 1 U/µl for 1 h at 37 °C was performed to digest parental DNA strands, which are methylated. Afterwards the PCR products were ligated and transformed in competent cells as mentioned before (3.1.2).

Cloning of hH_V1-VSD with a C-terminal 10xHis- or StrepII-tag

First, pET21a was chosen as the final vector system. The vector and hH_V1-VSD in pET15b were digested with *Nde* I/*Bam*H I, purified using the gel extraction procedure, and ligated. Afterwards, the hH_V1-VSD in pET21a was amplified in a PCR reaction with primers 1/2

(10xHis-tag introduction; T_m = 66.9 °C) or 1/3 (StrepII-tag introduction; T_m = 63.4 °C) using the Phusion polymerase. The amplified DNA was purified using the PCR purification kit and digested with *Xho* I/*Dpn* I. Next, the single stranded fragments were purified again, ligated, and transformed into competent cells.

Cloning of VSDs with N-terminal and C-terminal StrepII-tag in pET15b

The initial constructs 6xHis-hH_V1-VSD and 6xHis-DrVSD in pET15b were used as templates for primer design. In a QuickChange reaction primers 16/17 (hH_V1-VSD C-terminal StrepII-tag, T_m = 62 °C), 18/19 (hH_V1-VSD N-terminal StrepII-tag; T_m = 62 °C) or 15/16 (DrVSD C-terminal StrepII-tag, T_m = 62 °C) were elongated by the Pfu-turbo polymerase. The mixtures were incubated for 4 h at 37 °C with *Dpn* I and directly transformed into competent cells.

Transfer of DrVSD1 into pET15b

The new *E. coli*-optimized version of DrVSD was ordered as a string and multiplied in a standard PCR reaction using primers 20/21 (T_m = 55 °C) and the Phusion polymerase. The elongated fragments were purified using the PCR purification kit. Vector and PCR product were digested with *Nde* I/*Bam*H I in the appropriate buffer overnight at 37 °C. Simultaneously, the vector was dephosphorylated by addition of 0.2 U/µl Antarctic phosphatase. A heat inactivation step was followed by another PCR purification procedure. The ligation was performed at 16 °C for 3 h and the DNA was transformed into competent cells.

Transfer of tRNA-aminoacyl-synthetases into the pBH4 and pMAL vector

After initial gene synthesis, whereby an additional *Xho* I restriction site in the PylRS sequence from *M. mazei* was removed by exchange of CTC against CTG, without changing the amino acid sequence, the PylRS genes were digested with *Bam*H I/*Xho* I, gel purified and ligated with the digested, dephosphorylated pBH4/pMAL vector and transformed into competent cells.

Transfer of the PylRS from *M. mazei* into pET39b_Ub19

Primers 24/25 (T_m = 61 °C) were applied to a PCR using the Pfu-turbo polymerase to introduce an *Nco* I restriction site into the PylRS in pBH4. Following gel extraction, the construct was digested with *Nco* I/*Bam*H I and purified using the PCR purification kit. The pET39b_Ub19 vector was digested, dephosphorylated, and purified using the gel extraction procedure. Insert and vector were ligated and transformed into competent cells (3.1.2).

tRNA amplification from pUC57

Primers 22/23 (T_m = 55 °C) were designed to amplify and multiply the DNA of the tRNA construct in a standard PCR reaction using the Phusion polymerase. The DNA was purified using the PCR purification kit whereby four PCR reactions were loaded on one column to increase the final DNA concentration.

3.1.7 Production of MSP variants

The different MSP variants used in this thesis were listed in Table 3 (Denisov *et al.*, 2004; Ritchie *et al.*, 2009; Hagn *et al.*, 2013). All plasmids containing the MSP genes and a kanamycin resistance cassette were transformed into *E. coli* BL21 Star™ (DE3) cells. 2x 200 ml LB medium of an overnight culture were inoculated with cells from a cryo stock and incubated at 37 °C. Next day, cells were harvested by centrifugation (5,800xg, 10 min, 4 °C) and gently resuspended in 100 ml sterile, filtered tap water. The fermenter was filled with 10 l TB medium, 30 µg/ml kanamycin, 1 ml antifoam and inoculated with the resuspended cells. The temperature was set to 37 °C, the stirrer to 300 rpm, an air pressure of 1.6 bar and an airflow of 30 l/min. Process tracking was performed by measuring the pH and OD_{600} every 30 min. Furthermore, the foam level was monitored and additional antifoam was added if necessary. At an OD_{600} between 7-10, the gene expression was induced by the addition of 1 mM sterile-filtered IPTG. The fermentation process was stopped 1 h after induction. Cells were harvested and centrifuged (6,700xg, 20 min, 4 °C). Afterwards the cells were transferred into falcon tubes and stored at -80 °C until further processing. The amount of cells for each MSP variant was around 20 g/l.

3.1.8 Cell-free extract preparation

E. coli A19 cells were used as the source for cell-free extract preparations. 2x 200 ml LB medium were inoculated with a cryo stock of A19 cells and incubated overnight at 37 °C without any antibiotics. Next day, the fermenter was filled with 10 l 2xYPTG medium, 1 ml antifoam and inoculated with 200 ml of the overnight culture. The fermentation process was performed at a temperature of 37 °C. The stirrer was set to 500 rpm, the air pressure to 1.6 bar and the airflow was adjusted to 30 l/min. Process tracking was performed by measuring the OD_{600} every 30 min. When the mid-log phase of growth at an OD_{600} between

3-3.5 was reached, the temperature was switched off and the cell suspension was cooled to 22 °C. Afterwards cells were harvested and centrifuged (6,700xg, 20 min, 4 °C). The cells were resuspended in 300 ml S30 buffer A and combined in one centrifuge tube, followed by another centrifugation (8,200xg, 10 min, 4 °C). This procedure was repeated twice with the last centrifugation step extended to 30 min. Afterwards the pellet was weighted and resuspended in 110 % (v/w) S30 buffer B. Cells were disrupted using a French press, followed by another centrifugation step (30,000xg, 30 min, 4 °C). The supernatant was transferred to another centrifuge tube and was centrifuged again (30,000xg, 30 min, 4 °C). The clear supernatant was carefully collected, adjusted drop-by-drop to 400 mM NaCl and incubated for 45 min at 42 °C. This run-off step was performed to remove endogenous mRNA. Afterwards the extract was dialyzed for 2 h, followed by an overnight step at 4 °C against 5 l S30 buffer C in dialysis tubing (12-14 kDa MWCO). The dialyzed lysate was centrifuged again (30,000xg, 30 min, 4 °C), aliquoted to 0.5-1 ml, shock frozen in liquid nitrogen and immediately stored at -80 °C until further processing.

3.1.9 Cell-free protein synthesis

In vitro production of proteins was performed using the published S30-extract-based protocols for a CECF set-up (Schwarz *et al.*, 2007; Schneider *et al.*, 2010). Analytical scale reactions were performed in 24-well plate format with 55 µl RM in home-made dialysis containers. They were used for initial screening procedures, e.g. defining the optimal magnesium concentration or performing screens for the incorporation of unnatural amino acids. The reactions were always performed in duplicates. The RM:FM ratio was set to 1:17. Preparative scale reactions were performed in home-made dialysis containers capable of fixing a slide-A-lyzer dialysis cassette of maximum 3 ml RM. Cell-free protein synthesis was carried out by incubation of the set-up for 16 h at 30 °C under constant, gentle shaking conditions. Expressions were performed in P-CF and L-CF mode whereby e.g. NDs, liposomes and substrates were exclusively added to the RM reducing the final water addition (1.4). Scrambling inhibitors were always added as powder to RM and FM in their final concentrations. Labeled amino acids replaced the amino acid mix and RCWMDE mix and were added to a final concentration of 1.5 mg/ml. To this end, a stock concentration of 30 mg/ml was used where each of the 20 amino acids (labeled or not) was present to 1.5 mg/ml. An exemplarily composition of RM and FM for a CECF reaction is shown in Table 9. Stock concentrations of the different components are listed in Table 5.

Table 9: Composition of a standard CECF reaction.

Component	Reaction mix	Feeding mix
RCWMDE-mix	1 mM	1 mM
Amino acid mix	0.55 mM	0.55 mM
AcP	20 mM	20 mM
PEP	20 mM	20 mM
NTPs	1x	1x
DTT	2 mM	2 mM
Folinic acid	0.1 mg/ml	0.1 mg/ml
Complete	1x	1x
HEPES/EDTA buffer	1x	1x
$Mg(OAc)_2$	16-24 mM	16-24 mM
KOAc	290 mM	290 mM
PEG 8000	2 %	2 %
NaN_3	0.05 %	0.05 %
S30 buffer C	-	0.35x
S30 extract	0.35x	-
Plasmid DNA	5-15 ng/µl	-
RiboLock	0.3 U/µl	-
T7 RNA-polymerase	0.06-0.16 U/µl	-
tRNA *E. coli*	0.5 mg/ml	-
Pyruvate kinase	0.04 mg/ml	-

The substrates for unnatural amino acid synthesis were provided to 1 mM final concentration in RM and FM. Purified aminoacyl-tRNA-synthetases replaced the complete residual volume of water to ensure the highest final concentration possible. Aminoacyl-tRNA-synthetases were also used as plasmid DNA between 15-20 ng/µl. The double-stranded, PCR-amplified DNA of the aminoacyl-tRNA reached a final concentration of 5 ng/µl in the RM.

3.1.10 Synthesis of aminoacyl-tRNA-synthetases in bacterial cells

As aforementioned, the genes for the specific aminoacyl-tRNA-synthetases derived from the pyrrolysyl system were codon-optimized and synthesized either as a DNA string by Thermo Fisher Scientific (PylRS from *M. mazei*) or in a pUC57 cloning vector by GenScript (PylRS from *M. barkeri*) (3.1.6). Initially, both genes were transferred into the pBH4 vector and transformed into *E. coli* BL21 Star™ (DE3) cells for *in vitro* protein synthesis. 2x 1 l ZYM-5052 medium, supplemented with 100 µg/ml ampicillin, were prepared in 2 l shaker flasks. The auto-induction medium was prepared following the protocol of Studier, 2005 and 1:100 inoculated with an overnight culture. Cells were grown overnight at 37 °C under gentle shaking at 180 rpm and harvested the next day by centrifugation (6,000xg, 10 min, 4 °C).

For another *in vitro* approach, the gene constructs were cloned into the pMAL vector system and transformed into *E. coli* BL21 Star™ (DE3) cells. 2x 1 l LB medium, supplemented with 0.5 % glucose (w/v) and 100 µg/ml ampicillin, was prepared in 2 l shaker flasks and inoculated 1:100 with an overnight culture. Cells were grown at 20 °C under gentle shaking at 180 rpm and gene expression was induced at an OD_{600} of 0.6 by the addition of 1 mM IPTG. The cells were grown overnight at 20 °C and harvested the next day by centrifugation (6,000xg, 10 min, 4 °C). The pellets were solved in 50 ml/1 l lysis buffer PylRS and immediately stored at -80 °C until further processing.

3.1.11 Subfractionation of synthesized aminoacyl-tRNA-synthetases

During cell growth and protein synthesis in *E. coli* cells (3.1.10), samples for a subfractionation procedure were taken, prior induction, 1 h, and 2 h after induction and at the point of cell harvest. The cells were normalized to OD 1 ml to ensure the analysis of the same amount of cells. Afterwards, the samples were centrifuged (16,100xg, 10 min, 4 °C) and the pellet was solved in 500 µl lysis buffer PylRS. 40 µl were removed and mixed with 20 µl 4x SDS sample-loading buffer to analyze the whole-cell protein synthesis. Afterwards, the cells were disrupted via sonication for 4 cycles of 20 s with 20 s incubation time on ice in between. Another centrifugation step (16,100xg, 10 min, 4 °C) separated soluble and insoluble produced proteins, which were analyzed by SDS-PAGE later on (3.2.1).

3.2 Protein biochemistry methods

3.2.1 SDS-PAGE analysis

SDS gel electrophoresis is used for separating proteins under denaturing conditions by their molecular weights (Laemmli, 1970; Schägger & von Jagow, 1987). Samples were diluted or solved in 2x or 4x SDS sample-loading buffer with urea. It was decided not to boil the samples at 95 °C prior to loading onto the gel as it could be observed, especially for membrane proteins, that they tend to aggregate at the stated temperature (Schägger, 2006). They were loaded to maximum 20 µl in a volume to volume referenced manner to allow comparison between different samples. In every figure legend, the SDS-PAGE system is indicated. They were based on either the Tris-glycine gel or Tricine gel system (Table 7). The recommended running buffers were listed in Table 6. Tris-glycine gels were either prepared as 12 % or used as pre-cast 4-15 % gels. They were run for 90 min at 120 V. Tricine-gels were prepared to 11 % and run for 20 min at 80 V, followed by another 50 min at 150 V. Afterwards, the acrylamide gels were either applied to western blot analysis (3.2.2) or stained with Coomassie using the listed staining solution for minimum 15 min. For destaining, the gels were rinsed 3x in tap water, overlaid with water and boiled for 1 min at 800 W in a microwave oven. This procedure was repeated until the gel background color was completely removed with incubation times in between to cool the gels.

3.2.2 Western blot analysis

Western blot analysis is used to detect specific signals of proteins by antibody-binding and its visualization. To this end, proteins, separated by size during SDS-PAGE, were transferred to a PVDF membrane. Either the transfer was performed in a wet-tank blot procedure or as a semi-dry variant using the Trans-Blot® Turbo™ RTA transfer kit and the corresponding blotting instrument from Bio-Rad. PVDF membranes were activated by incubation for minimum 1 min in 100 % methanol. Wet-tank blotting was exclusively used for Tricine gels and performed for 30 min at 340 mA and 4 °C using the western blot transfer buffer. The semi-dry blotting was performed with pre-cast gels according to the manufacturer's instructions for the turbo protocol of mixed molecular weight proteins (1.3 A, 7 min).

Afterwards, the membrane was blocked for 1 h at RT in blocking solution, incubated for another 1 h at RT or overnight at 4 °C with the primary antibody diluted in blocking solution and washed for 3x 20 min in TBST buffer. Afterwards, the membrane was treated with the secondary antibody solved in blocking solution for 1 h at 4 °C and washed 3x for 10 min in TBST buffer (2.5.2). Signal visualization was performed using the chemiluminescence technique by treating the membrane with 1 ml ECL1 and 1 ml ECL2 for minimum 2 min and illuminating it using the Lumi-Imager from Roche. Thereby the light exposure time was step-wise decreased from 8 min to obtain the best resolution. As reference signals, either pre-stained protein ladders were visualized by top illumination or protein ladders with specific tags recognized by the first or secondary antibody were used.

The antibodies from a western blot membrane were stripped by 10 min equilibration at RT in 100 mM glycine-HCl pH 2.8. Afterwards, the membrane was washed 2x 5 min with TBST, followed by 1 h blocking in blocking solution and repetition of the antibody incubation procedure as previously described.

3.2.3 Immobilized metal affinity chromatography (IMAC) purification

In this thesis, the purification process by an IMAC was performed with Ni^{2+} ions (Porath & Olin, 1983). Poly-histidine tags in a deprotonated state can bind specifically to resin-chelated Ni^{2+} ions. Consequently, tagged proteins will bind to the column material and impurities can be removed. Purification procedures were either performed with gravity flow columns or using the ÄKTA system with self- or pre-packed columns (sepharose 6 fast flow resin GE Healthcare in an Omnifit® column body or a HisTrap FF 5 ml column GE Healthcare). All buffers used were filtered (0.22 µm) and degassed. The chromatography steps were performed at 4 °C or with ice-cooled buffers at RT to ensure the correct pH when working with Tris buffers. Prior to protein loading, the columns were washed with 10 CV water, followed by 10 CV equilibration buffer. 600 µl resin per 1 ml protein sample were used for the purification procedure. Under gravity flow conditions, the protein solutions were incubated with the resin in batch mode for 1 h at 4 °C. On the other hand, prior to connecting the columns to the ÄKTA systems the protein solutions were loaded onto the columns using a peristaltic pump with a flow rate of maximum 2 ml/min. Afterwards, the protein-bound resins were washed with 10 CV wash buffer. Additional washing steps are

indicated in the particular sections of this thesis. Finally, the proteins were eluted in 10 CV elution buffer containing 250 mM imidazole. Fractions were collected to 0.5 CV. Subsequently, they were analyzed by SDS-PAGE or western blot and the protein concentration was determined (3.2.1, 3.2.2, 3.2.6). Protein-containing fractions were pooled and applied to further analyses. The columns were washed with 10 CV water, stripped by the addition of 10 CV IMAC stripping buffer (after 5x usage), washed with 10 CV water and incubated with 2 CV 0.5 M NaOH for maximum 30 min. Next, the column was washed with 10 CV water, 10 CV 20 % (v/v) ethanol and stored under this conditions at 4 °C. Recharging was performed by washing the column with 10 CV water, loading 0.5 CV of 0.1 M $NiSO_4$ and washing the column again with 10 CV water prior to the next purification procedure.

3.2.4 StrepII-tag purification

Engineered streptavidin (Strep-Tactin) resin is capable of binding StrepII-tagged fusion proteins as another type of a protein purification procedure. The gravity flow handling protocol from IBA was used for the purification of Strep-tagged proteins. Chromatography steps were performed at 4 °C or with ice-cooled buffers at RT. In brief, 600 µl resin per 1 ml sample were equilibrated with 2 CV buffer W. The protein solution was loaded and washed with 5 CV buffer W. Prior to protein loading the detergent and buffer compatibility of the Strep-Tactin resin was checked by analyzing manufacturer's instructions. If necessary, the initial protein solution was either diluted or dialyzed against buffer W to reduce the detergent concentration. Furthermore, to increase the binding capacity the flow through after protein loading was reloaded up to 5 times or the protein solution was incubated with the resin in batch mode for 30 min at 4 °C. Finally, proteins were eluted by adding 6x 0.5 CV buffer E and fractions were collected and subsequently analyzed by SDS-PAGE or western blot. The column was regenerated by adding either 3x 5 CV buffer R or 3 CV 0.5 M NaOH. HABA or NaOH were removed by washing the column extensively with buffer W until the pH reached 8.0 or the orange color of HABA was completely removed. The columns were stored overlaid with 2 CV buffer W at 4 °C.

3.2.5 Buffer exchange procedures

Buffer exchange procedures were performed in different ways. Protein solutions, without any detergents or small compounds present, were dialyzed against the appropriate buffer in

minimum 1:1000 dilutions as the sum of all dialysis steps. Depending on their initial sample volume, they were dialyzed either in slide-A-lyzer cassettes (up to 12 ml; MWCO 10 kDa) or in dialysis tubings (MWCO 12-14 kDa). Dialysis procedures were performed for minimum 8 h for each dilution step under constant stirring conditions.

Dialysis processes for detergent-containing samples are expensive when detergent molecules can pass the dialysis membrane. Consequently, they were excluded for this kind of samples. Here, desalting columns or Amicon centrifugal filter units were used for buffer exchanges. PD MidiTrap G-25 (1 ml sample volume), PD-10 desalting columns (2.5 ml sample volume) or Bio-Spin 6 columns (100 µl sample volume) were used for desalting procedures following the manufacturer's instructions (gravity flow protocol for the PD columns). In Amicon centrifugal filter units, the initial sample was concentrated (5,000xg, 10 min, 4 °C) and refilled with the appropriate new buffer. This procedure was repeated until a dilution of minimum 1:1000 was reached. Afterwards, buffer exchanged samples were always centrifuged (at minimum 16,100xg, 10 min, 4 °C) to remove potential aggregates.

3.2.6 Determination of protein concentrations

Quantification of the proteins was performed by spectrophotometric measurements either at a NanoDrop instrument or at a UV-Vis spectrometer in standard disposable polystyrene cuvettes at 280 nm against an appropriate reference solution. The concentration was determined using Lambert-Beer's law whereby $A_{280\,nm}$ denotes the measured absorption at 280 nm, c the protein concentration in M, d the path length in cm and $\varepsilon_{280\,nm}$ the extinction coefficient in $M^{-1}cm^{-1}$ when all cysteine residues are reduced (Equation 3).

$$A_{280nm} = c \cdot d \cdot \varepsilon_{280nm} \qquad \text{Equation 3}$$

The following table lists the molecular weights and extinction coefficients of the constructs used in this thesis, determined with the web-based tool ProtParam based on the method developed by Gill and Hippel (Gill & von Hippel, 1989).

Table 10: List of molecular weights and extinction coefficients of constructs under investigation.

Construct	Molecular weight [g/mol]	$\varepsilon_{280\ nm}$ [$M^{-1}cm^{-1}$]
His-hH_V1-VSD	19555.5	8480
His-hH_V1-VSD-Strep	20796.8	13980
His-DrVSD/His-DrVSD1	17638.9	5960
His-DrVSD-Strep	18880.2	11460
His-KcsA-Strep	21326.5	40450
MraY-His	38209.3	47900
MSP1E3D1	31962.0	28420
MSP1	25309.5	25440
MSP1D1 ΔH4H5	18582.8	11460
MSP1D1 ΔH4-H6	16086.0	11460
MSP1D1 ΔH5	21468.1	19940
MSP1D1 ΔH5(-)	19488	18450
PylRS *M. barkeri*	50037.3	35870
MBP-PylRS *M. barkeri*	91969.6	100730
PylRS *M. mazei*	53438.0	32890
MBP-PylRS *M. mazei*	95370.3	97750

As an approximation, concentrations of empty NDs were determined by using 2x the extinction coefficient of the MSP variant as one ND contains two MSP molecules. The calculated VSD amounts in NDs after purification, concentration, and centrifugation of the samples always represented a rough estimation. The sample absorbance was measured at 280 nm and the concentration was calculated based on the ideal theorem that one ND contained two MSP and one VSD molecule ($\varepsilon_{ND} = 2 \cdot \varepsilon_{MSP} + \varepsilon_{VSD}$). In further analysis, protein-loaded ND concentrations were estimated from signal intensities in NMR measurements.

The protein sample quality was determined by analyzing the 260 nm/280 nm ratio. The ratio should be ~0.6 for a pure protein sample without any DNA/RNA contamination. However, the ratio of the VSDs in detergent was always higher caused by the high number of phenylalanines in the protein sequence absorbing light at 260 nm. Furthermore, often the

detection limit of 0.1 mg/ml BSA of the NanoDrop instrument, equated with an absorption of 0.06, was reached because of the low extinction coefficients of some of the constructs (Table 10).

Spectroscopic concentration determinations based on extinction coefficients are exclusively valuable for purified proteins. In contrast, the fluorescence detection of GFP in comparison to a recorded standard curve with known GFP concentrations was used to determine the protein concentrations in crude extract. To this end, the supernatant of a CF reaction was diluted 1:100 or 1:30 in GFP buffer in a black 96 well-plate format as triplicates. The fluorescence was measured with a GeniosPro microplate spectrophotometer from Tecan at an excitation wavelength of 485 nm and an emission wavelength of 510 nm at 20 °C. The valid signal range was between 160-1000 RU. The GFP concentration in µg/ml was determined using the corresponding calibration curve (Equation 4).

$$F_{510\,nm} = c_{GFP} \cdot 3.4197\ ml/\mu g \qquad \text{Equation 4}$$

Whereby, $F_{510\,nm}$ denotes the detected fluorescence signal at 510 nm, the value 3.419 ml/µg the slope of the linear regression curve and c_{GFP} the GFP concentration in µg/ml.

3.2.7 Purification of MSP variants

20-30 g of the MSP cell pellet from fermentation (3.1.7) were resuspended in 45 ml MSP-C buffer supplemented with freshly prepared 1 mM PMSF (solved in ethanol) and one tablet complete protease inhibitor. Triton X-100 was added to a final concentration of 1 % (v/v) and cells were disrupted by ultrasonication for 3x 60 s and 5x 45 s with 60 s cooling time between each cycle. Afterwards, the suspension was centrifuged (38,000xg, 30 min, 4 °C). The supernatant was filtered through a syringe filter (0.45 µM) prior to loading onto a pre-equilibrated, self-packed 20 ml IMAC sepharose 6 FF column by a peristaltic pump at a flow rate of 1 ml/min. Afterwards the column was connected to an ÄKTA system (16 °C or RT with ice-cooled buffers). The program included one washing step with 5 CV MSP-A buffer, followed by 5 CV MSP-B buffer, 5 CV MSP-C buffer and 5 CV MSP-D buffer. The flow rate was set to maximum 3 ml/min and the pressure limit to 0.15 MPa. MSP was eluted by adding 5 CV MSP-E buffer and collecting fractions to 2 ml. MSP-containing fractions were pooled and dialyzed immediately against 5 l MSP-F buffer overnight with one buffer exchange after 2 h. Next day, the MSP was centrifuged (20,780xg, 30 min, 4 °C), the concentration

determined (e.g. 18 ml of 400 µM ΔH5(-)), shock frozen in liquid nitrogen and stored until further processing at -80 °C.

Additionally, the His-tag of the MSP variants was removed by tobacco etch virus (TEV) protease digestion. To this end, the MSP solution (1 ml) was set to 1 mM DTT and His-tagged TEV protease was added in a molar ratio of 1:25. The mixture was dialyzed overnight against the TEV digestion buffer. Next day, the solution was centrifuged (16,100xg, 10 min, 4 °C) and the supernatant was loaded onto pre-equilibrated 2 ml IMAC resin (TEV equilibration buffer) in a gravity flow column. In batch mode, they were incubated for 1 h at 4 °C. The flow through was collected and the resin was washed with additional 10 CV TEV equilibration buffer. Both fractions were combined as they contained the cleaved MSP constructs and dialyzed again against the MSP-F buffer overnight with one buffer exchange after 2 h. Next day, the sample was centrifuged (16,100xg, 10 min, 4 °C) and the concentration was determined (e.g. 44 ml of 167 µM ΔH5(-)). Cleaved MSP was shock frozen in liquid nitrogen and stored at -80 °C until further processing. The TEV protease was eluted by adding 10 CV TEV elution buffer. The cleavage was always quantified by SDS-PAGE analyses.

3.2.8 Nanodisc preparation

The ND preparation procedure was performed as described previously with minor changes (Roos *et al.*, 2012; Denisov *et al.*, 2005). In brief, 50 mM lipids were solved in minimum 100 mM sodium cholate. A detailed list can be found in the aforementioned publication (e.g., DMPG lipids require 300 mM sodium cholate) (Roos *et al.*, 2012). MSP was rapidly thawed and used in a defined molar MSP : lipid ratio for empty ND preparations. The best ratio was either described previously or determined by screening processes whereby empty ND were prepared with different ratios and analyzed by SEC concerning their peak homogeneity and hydrodynamic radii (Table 11).

MSP and lipids were incubated for 1 h at RT in an overhead shaker. The addition of DPC was omitted if the cholate concentration in the mixture was above the critical micellar concentration (cmc) (between 9-14 mM). Afterwards the mixtures were either dialyzed against 5 l ND-A buffer overnight, followed by two exchanges for 1 h each against 1 l ND-A buffer the next day (dialysis procedure) or 0.5 mg/ml Bio-Beads were added in two proportions after a 45 min delay time and incubated overnight in a shaking device (Bio-Beads procedure). Prior, the Bio-Beads were solubilized in ND-A buffer, degassed for 30 min and stored at 4 °C.

Table 11: Listed ratios of MSP to lipid for ND preparations applying the indicated procedures.

MSP variant	Lipid	Ratio	ND preparation method	ND size
MSP1E3D1	DMPC	1:140	Bio-Beads	12-13 nm
	DMPC	1:115	Dialysis	
	DOPC	1:80	Dialysis	
	DMPG	1:110	Dialysis	
MSP1	DMPC	1:95	Bio-Beads	10-11 nm
MSP1D1 ΔH5(-)	POPE/POPG (3:1)	1:50	Bio-Beads	8-9 nm
	DMPG	1:45	Dialysis	
MSP1D1 ΔH4/H5	DMPC	1:20	Bio-Beads	6-7 nm

The incubation temperatures were based on the lipid transition temperatures (T_m) (Table 12). For example, NDs that were prepared with DMPC lipids (T_m = 24 °C) were incubated at RT.

Table 12: Phase transition temperatures (T_m) of different lipids used and their corresponding incubation temperatures during the reconstitution procedure.

Lipid	T_m [°C]	Incubation temperature [°C]
POPE	25	RT
POPG	-2	4
POPC	-2	4
DOPE	-16	4
DOPG	-18	4
DOPC	-17	4
DMPC	24	RT

Afterwards, the pre-formed NDs were centrifuged (16,100xg, 10 min, 4 °) and concentrated in ND-A buffer pre-equilibrated Centriprep concentration devices (MWCO 10 kDa) following the manufacturer's instructions. Afterwards, the concentrated NDs were centrifuged (16,100xg, 10 min, 4 °) and stored at either 4 °C or shock frozen in liquid nitrogen and stored at -80 °C until further processing. ND concentrations of 100-300 µM in 500 µl buffer could be obtained.

3.2.9 Purification of VSD constructs

After CF protein synthesis, the VSD samples were centrifuged (16,100xg, 10 min, 4 °C). The pellet fraction produced in P-CF mode was washed once in RM-volume S30 buffer C and afterwards resuspended and incubated for 1 h at RT in the RM-volume of the particular solubilization buffer containing 1-2 % detergent followed by an additional centrifugation step (16,100xg, 10 min, 4 °C). The supernatant of the solubilized or of the L-CF-produced ND samples were incubated with the pre-equilibrated Ni^{2+}-resin beads and an IMAC purification step was performed as previously described (3.2.3). To this end, the appropriate detergent was added additionally to the different buffers as stated in Table 6. The column was washed with 10 CV equilibration buffer, followed by 10 CV wash buffer. Additional performed washing steps are indicated in the particular sections in this thesis. Elution fractions containing the VSDs were pooled and either applied directly to buffer exchange procedures and concentration processes, dialyzed against 1 l buffer W for 1 h at 4 °C (VSD samples in NDs) or diluted 1:10 (VSD samples in detergent) prior to the Strep-purification procedure (3.2.4).

The tandem purification strategy was only applied to ND samples and samples with the indicated detergents (Table 6). Strep-column elution fractions were combined, ultracentrifuged (100,000xg, 1 h, 4 °C) and concentrated in Amicon centrifugal filter units (MWCO 30 kDa) following the manufacturer's instructions. Afterwards, the concentrated samples were centrifuged as indicated (16,100xg, 30 min, 4 °C or 100,000xg, 1 h, 4 °C). The supernatant was either used for further activity studies or buffer exchanged. VSD-NDs were dialyzed for 1 h followed by overnight against the appropriate buffer volumes (minimum 1:100 dilution each). Detergent-containing samples were buffer exchanged using desalting columns following the manufacturer's instructions (3.2.5). Afterwards the samples were centrifuged (16,100xg, 30 min, 4 °C or 100,000xg, 1 h, 4 °C). For NMR investigation purposes the final protein solutions were set to 5 % D_2O/DSS and transferred to a NMR tube.

L-CF-produced VSD-liposomes were not purified at all. The supernatant from a CF expression set-up was directly applied to further investigative analyses.

3.2.10 Post-translational ND insertion of purified VSDs

The post-translational refolding procedure was performed based on protocols published on the Sligar lab homepage (http://sligarlab.life.uiuc.edu/nanodisc/protocols.html, May 30, 2017, 5:42 pm). To this end, MSP was present in an excess of 5 compared to the target protein and the final lipid concentration was chosen between 3-20 mM. Different MSP to lipid ratios were tested (1:50, 1:60, 1:70, 1:80, 1:166, 1:333). The final cholate concentration was set to 70 mM. IMAC-purified hH_V1-VSD in 0.2 % LPPG (final concentration of 12 µM) was mixed with ΔH5(-), POPE/POPG (3:1) lipids and cholate in a defined volume, incubated for 1 h at RT and treated with finally 1 g/ml Bio-Beads (pre-equilibrated and degassed in ND-A buffer). The Beads were added in three steps after 1 h, overnight and again after 1 h incubation. Afterwards, the ND solution was removed from the Bio-Beads via pipetting and centrifugation (16,100xg, 10 min, 20 °C). The supernatant was loaded onto ND-A buffer pre-equilibrated Ni^{2+}-resin beads and incubated for 1 h at RT. The beads were transferred into an empty gravity flow column body, washed with 7 CV ND-A buffer and eluted with 10 CV buffer containing 250 mM imidazole. Protein-containing fractions were combined, mixed with SDS sample-loading buffer, and analyzed by SDS-PAGE (3.2.1). Reconstitution efficiencies were estimated comparing the SDS-PAGE results of the initial VSD sample in LPPG with reconstituted ones using the software ImageJ.

3.2.11 Purification of aminoacyl-tRNA-synthetases

The aminoacyl-tRNA-synthetase purification strategy was based on the protocol of Polycarpo *et al.* (Polycarpo *et al.*, 2004). Cell pellets, which were stored at -80 ° C and solved in lysis, buffer PylRS, were thawed on ice and immediately applied to 10x sonication cycles á 30 s with 30 s cooling periods in between. Afterwards, the supernatant after centrifugation (40,000xg, 1 h, 4 °C) was loaded onto a pre-equilibrated HisTrap FF 5 ml column using a peristaltic pump with a flow rate of 2 ml/min. The pre-loaded column was connected to an ÄKTA system. The run was performed with a flow rate of 1 ml/min at 16 °C. Initially, the column was washed with 5 CV wash buffer PylRS. All purification steps for the PylRS *M. barkeri* were performed at pH 8.0, as the isoelectric point (IP) of the MBP-fusion is 7.6, and at pH 7.5 for the PylRS *M. mazei* MBP-fusion with an IP of 7. The synthetases were eluted in 10 CV elution buffer PylRS whereby fractions of 2 ml were collected.

Protein-containing fractions, visualized by real-time detection of the extinction at 280 nm, were combined and concentrated in Amicon centrifugal filter units (MWCO 50 kDa) to a final volume of 2.5 ml. After a centrifugation step (16,100xg, 10 min, 4 °C), the supernatant was loaded onto a PD10 desalting column following the manufacturer's instructions. The sample was buffer exchanged to storage buffer PylRS, centrifuged (16,100xg, 10 min, 4 °C) and stored at -80 °C until further processing. The concentration was determined as previously described to be 4 mg/ml for the MBP-PylRS *M. barkeri* construct and 11 mg/ml for the MBP-PylRS *M. mazei* sample (3.2.6).

3.2.12 Proving co-translational ND-insertion

Various strategies have been pursued for analyzing the co-translational insertion of VSDs into NDs.

Sodium carbonate precipitation

The procedure of removing partially bound proteins from the surface of a membrane by a pH change to 11 was described previously (Fujiki *et al.*, 1982; Long *et al.*, 2012). The purified VSD-ND samples were treated in a 1:1 (v/v) ratio with sodium carbonate precipitation buffer and incubated for 30 min at 4 °C. Afterwards, a centrifugation step (16,100xg, 10 min, 4 °C) separated supernatant and pellet fraction, which were solved in SDS sample-loading buffer and analyzed by SDS-PAGE (3.2.1).

Enzymatic cleavage

The ExPASy tool PeptideCutter was used for the identification of specific cleavage sites in the VSD constructs (Wilkins *et al.*, 1999). A protease had to be selected, which specifically cleaves the VSD and not the MSP variant to determine differences in the cleavage profile of an inserted or only partially attached protein. Two thrombin cleavage sites were determined for the DrVSD construct whereby one was located directly after the His-tag in the N-terminal, soluble part and the other one present in the fourth transmembrane domain of the VSD. Thrombin was solved in PBS buffer, aliquoted to 100 µl and stored at -80 °C until further usage. 1 U cleaves more than 90 % of 100 µg protein. Thrombin was added to 1 U/100 µg protein and incubated overnight at 4 °C. Next day, the sample was centrifuged (16,100xg, 10 min, 4 °C) and supernatant and pellet fraction were analyzed by SDS-PAGE (3.2.1). As a control DrVSD in detergent and empty ND were analyzed too.

NTCB treatment

NTCB is known to cyanylate reduced cysteine thiols at pH 8.0. The resulting chain can then be cleaved under alkaline conditions by cyclization. Hence, the N-terminus becomes modified by the iminothiazolidine carboxyl group during the cleavage reaction. Only VSDs can be studied, as my MSP variants do not contain cysteines and are therefore not affected by the cleavage reaction. 4.5 mg/ml NTCB were solved in 1x standard buffer. VSD samples of 1.25 - 2.5 pmol/µl pH 8.0 were treated with finally 1 mM DTT and incubated for 2 h at RT to reduce all cysteines. Afterwards, 4 mM NTCB were added and incubated for 1 h at 30 °C. The cleaved proteins were purified using the Bio-spin 6 columns and buffer exchanged to 20 mM Tris pH 9.0 at 4 °C and 150 mM NaCl following the manufacturer's instructions. The solutions were incubated for 1 h at RT. The reactions were stopped by adding SDS sample-loading buffer and performing a SDS-PAGE analysis. As controls, the samples were always analyzed in a treated and non-treated form. Furthermore, the VSDs in detergent micelles were analyzed whereby the different buffers contained the appropriate detergent.

3.2.13 Liposome reconstitution

Proteins were either co-translationally-inserted into liposomes by adding pre-formed liposomes to the RM of a CF expression or post-translationally after cell-free protein synthesis and purification in detergent micelles.

First, lipids were solved to 20 mg/ml in 1 ml chloroform. Using a rotary evaporator the chloroform was removed resulting in a thin lipid film, which was subsequently suspended in liposome buffer by pipetting up and down and incubating the solution for 20 min in an ultrasonication bath. The lipid suspension was extruded 11x to 200 nm using an Avanti mini-extruder with the specific membrane pore size. Empty liposomes were either used directly in L-CF expression approaches or screened for highest insertion efficiency. To this end, empty liposomes were destabilized by adding a 1 % Triton X-100 solution in 1 µl steps to 80 µl 2.5 mg/ml liposomes whereby the scattering light at 540 nm was recorded in real-time after 1 min incubation on a UV-Vis spectrometer SpectroStar^{Nano}. First, the liposomes start to swell caused by detergent molecule insertion into the lipid bilayer before they are destroyed. An initial raise in the scattering light followed by a massive reduction describes this process. The 80 % value of swelling was used to destabilize the empty liposomes prior to

protein addition (for 2.5 mg/ml liposomes 0.08 % Triton X-100 was determined as the final concentration).

Next, 900 µl of 2.5 mg/ml empty liposomes were treated with the appropriate amount of Triton X-100 and liposome buffer in a total volume of 915 µl. The mixture was incubated for 30 min in an overhead shaker above the transition temperature of the lipid (in a lipid mixture the highest T_m was important) (Table 12).

The purified proteins were added in a lipid to protein mass ratio of 100:1 in a total volume of 1 ml (0.0225 mg/ml protein) and incubated for 30 min in an overhead shaker above the lipid-T_m. As a negative control, a sample was prepared where no protein was added, but only the specific protein-sample storage buffer. The detergents were removed by adding 4x 40 mg/ml Bio-Beads (after 1 h, overnight, 2 h, 2 h). Previously, the beads were washed with 100 % methanol, resuspended in liposome buffer and degassed for 30 min. Finally, the suspension was transferred in an empty gravity flow column body with a filter unit at the bottom and was washed 3x with liposome buffer. The elution was collected in an ultracentrifuge tube and proteoliposomes were harvested via an ultracentrifugation step (300,000xg, 1 h, above T_m). Afterwards, the liposomes were resuspended in the appropriate volume of liposome buffer (usually 200 µl).

3.2.14 Density gradient centrifugation

Liposome reconstitution efficiencies were proven by density gradient centrifugation. To this end, liposomes (pre-treated with sodium carbonate or not [3.2.12]) were mixed with 64 % sucrose in a total volume of 250 µl to a final sucrose concentration of 40 %. This mixture was overlaid with 250 µl 25 % sucrose, followed by 250 µl 5 % sucrose and 250 µl liposome buffer in an ultracentrifuge tube. The ultracentrifugation step was performed at 300,000xg above the T_m of the lipid for 1 h. Afterwards, a photo was taken and the fractions were collected from top to bottom in 250 µl steps. Each fraction was treated with 100 % ice-cooled acetone to precipitate the proteins. TCA precipitation was not successful, as the sugar molecules precipitated too. After a centrifugation step (30,000xg, 30 min, 4 °C) the pellets were washed once in liposome buffer and then solubilized in comparable volumes of SDS sample-loading buffer. Next, the fractions were analyzed by SDS-PAGE (3.2.1).

3.2.15 Refolding of cell-free-produced proteins

The refolding strategy used was invented in a cooperation with the Valiyaveetil lab from the Oregon health and science university (Valiyaveetil *et al.*, 2002a; Valiyaveetil *et al.*, 2002b; Focke *et al.*, 2016). In brief, P-CF-synthesized protein pellets were washed twice with RM-volume S30 buffer C, resuspended under denaturing conditions in 1 ml solubilization buffer refolding and incubated for 10-15 min under gentle shaking at 45 °C. *In vitro* folding was carried out by a 1:10 dilution of the unfolded protein into pre-formed asolectin liposomes. The solution was sonicated for 30 s in a water bath sonicator and incubated overnight at RT in an overhead shaker. Next day, the folding mixture was dialyzed 2x against 1 l 20 mM HEPES-NaOH pH 7.5 and 150 mM NaCl to decrease the initial DTT concentration previously to the purification procedure. Proteoliposomes were treated with either 1 % Fos14, 1 % DPC (hH_V1-VSD, DrVSD) or 1 % Anzergent3-14 as described for the membrane solubilization of proteins produced in *E. coli* cells (Li *et al.*, 2012; Li *et al.*, 2015). The mixture was incubated for 2 h at RT in an overhead shaker and centrifuged at 30,000xg for 15 min at 4 °C. The supernatants were loaded onto pre-equilibrated Ni^{2+}-beads (equilibration buffer refolding) whereby the flow through was reloaded 6 times, followed by the previously described IMAC purification procedure whereby the initial detergent was either exchanged or its concentration reduced to 0.08 % for DPC and 0.07 % for Fos14 (3.2.3, 3.2.9). Combined elution fractions in elution buffer refolding were concentrated in Amicon centrifugal filter units (MWCO 10 kDa), centrifuged (30,000xg, 30 min, 4 °C) and applied to further analyses.

Asolectin liposome preparation

1 g asolectin powder was dissolved in a minimal amount of cyclohexane and lyophilized to obtain a fine powder, which was instantly solved in 50 ml 50 mM HEPES-NaOH pH 7.5, 0.2 M NaCl and 10 mM DTT. The 20 mg/ml mixture was stirred for 1 h at RT. Afterwards, small unilamellar vesicles were formed by sonication for 10x 30 s at 80 % power with a resting period of 30 sec on ice (UP100H Sonifier). The liposomes were stored at -20 °C until further usage.

3.2.16 Size-exclusion chromatography (SEC)

SEC runs were performed using an ÄKTA purifier system at 16 °C with a Superdex 200 3.2/30 gel-filtration column in the basic or increase version following the manufacturer's instructions. The running buffers, injection volumes and flow rates used were always indicated in the figure legends. Buffers were filtered (0.22 µm) and degassed for 30 min prior to usage. First, the column was washed with 3 CV water followed by 3 CV of the appropriate running buffer. The backpressure limit was always set to 1.2 MPa. SEC samples were centrifuged prior to loading onto the column (16,100xg, 10 min, 4 °C). Protein-containing fractions were monitored at 215 nm, 260 nm and 280 nm and collected in a sample size of 100 µl. Temperature-screens were performed by incubating the appropriate samples for a defined period at the indicated temperatures. Afterwards, they were centrifuged (16,100xg, 10 min, 4 °C) and the supernatant was applied to SEC analyses at 16 °C. After finishing all runs, the columns were washed with 3 CV water, followed by 3 CV 20 % ethanol and stored in 20 % ethanol. Once the column pressure raised or more than 30 runs were performed, a cleaning-in-place procedure, described in the column manual, was performed (1 M NaOH contact time for 1-2 h, 5-10 ml water at a flow rate of 0.04 ml/min, 5 ml 70 % EtOH at 0.02 ml/min, 5-10 ml water at 0.04 ml/min, 5-10 ml 20 % EtOH at 0.04 ml/min).

Calibration runs were performed to determine the molecular weight of a protein sample of interest. To this end, the column was equilibrated with SEC calibration buffer following the manufacturer's recommendations. Three runs were performed with 40 µl kit protein (globular proteins) injections (1^{st} run: 0.3 mg/ml ferritin, 3 mg/ml conalbumin, 3 mg/ml ribonuclease; 2^{nd} run: 5 mg/ml thyroglobulin, 4 mg/ml aldolase, 0.4 mg/ml ovalbumin; 3^{rd} run: 1 mg/ml blue dextran2000). Calibration curves were determined whereby K_{AV} represents the partition coefficient, MW the molecular weight, V_e the elution volume, V_o the void volume and V_c the column volume (Table 13). The void volume for the increase column was determined to 0.93 ml (used for ND screenings) and for the basic superdex200 (used as detergent column) to 0.89 ml. The column volume was 2.4 ml.

Table 13: Calibration curves for the different SEC columns determined with the calibration kit standards.

Detergent column	ND column
$K_{AV} = 1.854 - 0.1307 \cdot lnMW$	$K_{AV} = 1.9475 - 0.1416 \cdot lnMW$
$K_{AV} = \frac{V_e - V_o}{V_c - V_o}$	

Peak symmetry and performance calculation was done by injecting 2 % (v/v) acetone at the maximum flow rate in a water-equilibrated system. The determined column performances were excellent.

Oligomeric states of the VSDs were determined by analyzing their elution volumes in SEC experiments. To this end, calculated molecular weights were subtracted with molecular weights of detergent micelles in water or empty NDs in SEC analysis to obtain molecular weight values only for the VSDs (Table 14).

Table 14: Detergent micelle and ND sizes in the protein-free state used for the calculation of oligomeric species of voltage-gated proton channels in SEC analysis.

Hydrophobic environment	Monomer molecular weight	Aggregation number	Size
DH(7)PC	-	-	20-80 kDa[a]
DPC	351.5 Da	~54	19 kDa
LPPG	507 Da	~125	63 kDa[b]
Fos14	379.5 Da	~108	41 kDa
ΔH5(-)-DMPG-ND	-	-	95-125 kDa

[a] Tausk *et al.*, 1974; [b] Lipfert *et al.*, 2007

Here, detergent micelle molecular weights were either determined by light-scattering and ultracentrifugation (Tausk *et al.*, 1974) or by a simple multiplication of their monomer molecular weight with their number of aggregation. However, the detergent aggregation number cannot be stated as constant when comparing a membrane protein being surrounded by the molecules and a detergent micelle being formed in buffer solutions without any protein contact. Thus, the listed values for detergent micelle sizes can only be used for a rough estimation of the VSDs molecular weights in SEC and mass specrometry analysis.

3.2.17 TCA precipitation of proteins

The TCA precipitation of proteins was used for a fast detergent exchange without any necessity of a new protein synthesis and/or purification. The method used, was described previously for membrane proteins under NMR investigations (Shenkarev *et al.*, 2010b). In brief, ice-cooled 0.1 volume 100 % TCA was added to the purified VSD solutions (in 0.07 % Fos14), thoroughly mixed, and incubated for 15 min at -20 °C. After a centrifugation step (16,100xg, 15 min, 4 °C) the pellet was washed with ice-cooled acetone, incubated for 15 min at -20 °C, and centrifuged again. This procedure was repeated thrice. The pellet was dried at RT, weighted to calculate the protein mass, and solved in the appropriate detergent-containing buffer whereby the detergent concentration was set to at least 100x molar excess relative to the protein concentration (Shenkarev *et al.*, 2010b). The mixture was centrifuged (16,100xg, 15 min, 4 °C), the pH was checked, and the supernatant was applied to further analyses.

3.2.18 Mass spectrometry analyses

Mass spectrometry analyses were performed either to analyze the oligomeric state behavior of the protein of interest or to investigate the protein sequence of fragments observed during synthesis and purification.

The laser-induced liquid bead ion desorption (LILBID) mass spectrometry (MS) was performed by Oliver Peetz in cooperation with the group of Dr. Nina Morgner (institute of physical and theoretical chemistry, Goethe University Frankfurt). All instrument settings and experimental set-ups were described in previous papers and our publication (Morgner *et al.*, 2006; Henrich *et al.*, 2017a). In brief, LILBID-MS samples were concentrated in 0.5 ml Amicon centrifugal filter units (MWCO 10 kDa), centrifuged (16,100xg, 10 min, 4 °C) and buffer exchanged using Zeba micro spin desalting columns (MWCO 7 kDa) into 50 mM ammonium acetate buffer pH 6.8. Droplets of the samples were produced, transferred into high vacuum, and irradiated with laser pulse energies between 18 and 23 mJ that finally led to their explosion. Released, accelerated ions were analyzed by a reflectron-time-of-flight (TOF) set-up, detected, processed, and normalized using the software Massign and OriginPro2016 (Morgner & Robinson, 2012). A new strategy was invented to discriminate the molecular weight patterns of reconstituted VSDs and the molecular weight of the MSP. To this end, the VSDs were labeled with heavy isotopes to increase their overall mass (Table 15) (3.1.9).

Table 15: Molecular weights (MW) of labeled VSD constructs and detergent micelles applied to mass spectrometry analyses.

Construct	Labeling pattern	MW [kDa]
His-hH$_V$1-VSD-Strep	^{15}N,^{2}H	22.22
His-DrVSD-Strep	^{15}N,^{2}H	19.91
His-DrVSD-Strep	^{15}N,^{2}H, ^{15}N-^{13}C6-Ile, ^{13}C-methyl-Met	19.80
His-DrVSD1	^{15}N,^{2}H	18.41
DPC micelle	-	19
Fos14 micelle	-	41

Matrix-assisted laser desorption/ionization (MALDI) analyses using a MALDI-LTQ Orbitrap XL (Thermo Scientific) system were carried on behalf of the group of Prof. Dr. Karas (institute of pharmaceutical chemistry, Goethe University Frankfurt). To this end, a SDS-PAGE with the protein of interest was performed and fragments were cut out after the staining procedure (3.2.1). These gel fragments were applied to an In-gel digest by trypsin and analyzed by peptide mass fingerprinting. Results were sent to me in a PowerPoint format.

3.2.19 CD spectroscopy

CD measurements were performed for analyzing the protein secondary structure contents and protein stability. First, an appropriate buffer system was chosen, which shows nearly no absorbance in the wavelength range of 190 to 300 nm. Samples were prepared as described previously (3.2.9, 3.2.15, 3.2.17). Purified samples were either buffer-exchanged using a desalting column (3.2.5) or were precipitated and afterwards resuspended in the CD buffer. 300 µl of 0.3 mg/ml samples were transferred into a 100-QS 1 mm thickness 350 µl cuvette and measured on a Jasco system. Secondary structure analysis was performed using the following settings: standard sensitivity, 0.2 nm data interval, 551 data points, linear data array *3, a temperature of 20 °C, a band width of 1 nm, scanning speed of 50 nm/min, with baseline correction (buffer only), shutter control auto and three accumulations. The calculated data of ellipticity, Θ in mdeg, were transformed into the molar ellipticity [Θ] in deg*cm^2*dmol^{-1} using the following equation to ensure an easy comparison of different proteins with different molecular weights (Equation 5).

$$[\Theta] = \frac{100 \cdot \Theta_{obs} \cdot MW}{c' \cdot d} \qquad \text{Equation 5}$$

Whereby, Θ_{obs} means the observed ellipticity in deg, MW the molecular weight of the protein of interest, C' the mass concentration in g/l of the protein of interest and d the path length in cm. Data was analyzed using the Jasco software package, in detail Yang's reference.

The stability screen was performed without any blank measurements, starting at a temperature of 20 °C, measuring 426 data points, with a temperature interval of 5 °C, a ramp rate of 1 °C/min and an end temperature of 110 °C. After an increase of 5 °C, a spectrum from 300 to 190 nm was recorded to differentiate between detected unfolding and precipitation events. For evaluation purposes of transition temperatures measured data points at 222 nm were transformed into mean residue weight ellipticity values $[\Theta]_{MRW}$ in deg*cm^2*dmol^{-1}. To this end, the molecular weight in Equation 5 was replaced by the middle molecular weight of one residue (MW/number of residues). The first derivative of the $[\Theta]_{MRW}$ ($\Delta[\Theta]_{MRW}/\Delta T$) was plotted against the temperature to define transition temperatures whereby the maxima correspond to the specific midpoints.

3.2.20 Transmission electron microscopy (TEM)

The transmission electron microscopy (TEM) data were recorded by Simone Prinz (MPI of Biophysics, Frankfurt). First, the coated carbon grids were discharged to allow hydrophilic buffer solutions to stick to them. Next, 2 µl sample were applied on the grid and incubated for 5 min. The grids were washed 5x with a drop of water before 2 µl of a prepared uranyl acetate solution were added and incubated for another 5 min. Afterwards the grids were washed again 5x with a drop of water whereby the last step was performed with 5 min incubation. The water was completely removed by the help of the absorbing effect of filter paper and electron microscopy pictures were recorded on a FEI Biotwin instrument equipped with a CCD camera.

3.2.21 Fluorescence-based activity assay of VSDs

A compartmentalization is necessary for the determination of the activity of an ion channel. Consequently, proteins under investigation had to be reconstituted into liposomes (3.2.13). The fluorescence-based activity assay was previously described (Zhang *et al.*, 1994; Lee *et al.*, 2009) and transferred to my project to determine the activity of the VSDs. In brief, proteoliposomes were formed in the presence of a high potassium concentration. A 20-fold

dilution of proteoliposomes into flux buffer with a lower concentration generated a potassium gradient across the membrane. After a defined incubation period that enable recordings of a stable baseline (100 % value, F_{max}), the VSDs were activated by the addition of 1 µl valinomycin (final concentration of 20 nM). Valinomycin, as a potassium-selective ionophore, induced a potassium efflux from the liposomal lumen, which generated a membrane depolarization and therewith activated voltage-gated proton channels (-60 mV inside for a 10x potassium gradient) (Lee *et al.*, 2009). The channel opened and caused an influx of protons (directional to the chemical gradient). The decreased pH in the liposomal lumen protonated the fluorescence dye ACMA leading to a quench of its fluorescence, which could be measured directly. Protonated ACMA molecules cannot pass the liposomal membrane anymore. Consequently, the fluorescence decreased exponentially over time. Finally, after a defined incubation time, 0.5 µl CCCP (final concentration of 2 µM), as a proton-selective ionophore, were added. CCCP addition led to an influx of protons into all liposomes even those in which no or differently-oriented VSDs were incorporated. The obtained value could now be equated with the 0 % fluorescence value (F_{min}) and allowed the evaluations of all measurements based on the relative fluorescence. Data evaluation was performed by normalizing the measured fluorescence $(F_{obs}-F_{min})/(F_{max}-F_{min})$, whereby F_{obs} represents the measured signal at each time point, F_{max} is the average value of the maximum baseline prior to valinomycin addition and F_{min} is the average value of the minimum baseline after CCCP addition. Mistakenly, the initial measurements were performed with 2 mM CCCP addition as it was described in the thesis of J.A. Letts, 2014, co-author of the referenced paper. This caused a complete precipitation of the sample. Consequently, the data evaluation revealed less prominent fluorescence signal changes when working with the relative fluorescence values.

The inhibitory effect of 2GBI was tested. To this end, a stock solution of 4 mM 2GBI in flux buffer was prepared. The inhibitor was added to a final concentration of 200 µM and incubated with the proteoliposomes for at least 1 min prior to the measurement. Measurements were performed as mentioned before.

A Cary Eclipse Varian fluorescence spectrophotometer and 1 ml or 160 µl fluorescence cuvettes were used for the experimental set-up. Measurements were repeated minimal three times (n is always indicated). Instrument settings were listed in the following table.

Table 16: The instrument settings for the Varian Eclipse spectrophotometer for performing the flux assay are listed.

Setting	Value
data mode	fluorescence
excitation wavelength	410 nm
emission wavelength	480 nm
excitation slit	5 nm
emission slit	10 nm
average time	0.05 s

Setting	Value
cycle time	30 s
stop time	810 s
emission filter	auto
excitation filter	auto
PMT voltage (V)	medium

As a control, empty liposomes were prepared and measured in parallel. Furthermore, different potassium gradients were applied by dilution of the proteoliposomes in flux buffer containing different potassium concentrations. Another control experiment was performed by reconstituting a non-conductive protein (MraY) into the liposomes. To this end, MraY and in parallel hH_V1-VSD were P-CF-expressed, solubilized in 1 % DPC, 1:1 diluted in equilibration buffer, and IMAC purified as aforementioned (3.2.3). The protein-containing elution fractions in 0.1 % DPC were combined, concentrated, and the protein concentration was determined at the NanoDrop instrument prior to the reconstitution procedure. Afterwards, the flux assay was performed as previously described.

3.2.22 NMR experiments

Dr. Frank Löhr (Institute of biophysical chemistry, Goethe University Frankfurt) performed all NMR experiments. 2D ^{15}N-^{1}H correlations were either of the BEST-TROSY or HMQC type (Pervushin *et al.*, 1997; Schanda *et al.*, 2006; Farjon *et al.*, 2009). “Proton-carbon correlations of methyl groups employed a gradient-selected version of the [^{13}C,^{1}H]-SOFAST-HMQC (band-selective optimized flip-angle short-transient heteronuclear multiple-quantum coherence) pulse sequence (Schanda *et al.*, 2005)” (Laguerre *et al.*, 2016). Experimental settings like temperature, number of scans (NS), delay time (TD1), used NMR buffer, field strength and recorded spectra types are always indicated in the figure legend. One-dimensional ^{31}P spectra were recorded at a sample temperature of 318 K on a Bruker DRX500 spectrometer equipped with a broadband inverse probe. The recycle delay was set

to 3 s and the acquisition period to 1 s. These spectra were used for the q-ratio determination during a detergent titration.

NMR samples were prepared as previously described (3.1.9, 3.2.9). In brief, labeled amino acids were added directly to the cell-free expression set-up. A fully $^{15}N,^{2}H$-labeled sample was obtained using the cell-free amino acid mix from CIL (2.5.5). The algal amino acid mix contained 16 $^{15}N,^{2}H$- or ^{2}H-labeled amino acid (deuterated at non-exchangeable positions). The residual amino acids were added as 1.5 mg/ml to the set-up as ^{15}N-labeled asparagine, ^{15}N-labeled tryptophan, ^{15}N-labeled glutamine and non-labeled cysteine (VSDs contain only one cysteine residue) for a fully ^{15}N-labeled sample or in a non-labeled form when selective labeling strategies were applied. Selective ^{13}C-labeling of isoleucine and the methyl-group of methionine was achieved by adding finally 3 mg/ml of the labeled amino acids in combination with 1.5 mg/ml of the $^{15}N,^{2}H$-labeled algal amino acid mix supplemented with the missing ^{15}N-labeled amino acids as previously mentioned. Selective ^{15}N-Ala and ^{15}N-Gly labeling was obtained by adding 1.5 mg/ml of the ^{2}H-labeled algal amino acid mix supplemented with non-labeled missing amino acids and 4.5 mg/ml of selectively labeled alanine and glycine. The addition of scrambling inhibitors during the cell-free expression is always indicated in the specific experiments whereby the amount of each inhibitor was added as a powder to feeding and reaction mix. Final protein concentrations in the NMR experiments ranged between 10 to 300 µM. The software TopSpin was used for data acquisition, processing, and spectra analysis. Sparky was used for peak size distribution analyses.

3.2.23 Malvern experiments – analysis of protein aggregation

The Malvern Instruments Company is specified on material characterization including protein aggregation in pharmaceutical relevant therapeutics. During a SFB-organized workshop, the students had the possibility to get their samples analyzed by different techniques. To this end, His-DrVSD1 and His-hH_V1-VSD were produced by P-CF expression, solubilized and purified in Fos14-containing buffers, buffer exchanged to 50 mM K_2HPO_4 pH 7.0, 0.08 % DPC via a PD Midi Trap G-25 desalting column and ultracentrifuged at 300,000xg for 30 min at 4 °C. The supernatant was concentrated in Amicon centrifugal filter units (MWCO 30 kDa) to 400 µl followed by another centrifugation step (30,000xg, 30 min,

4 °C). Samples were shock frozen in liquid nitrogen and stored for 3 d at -80°C. After rapid defrosting, the VSD samples (hH_V1-VSD 151 µM and DrVSD1 180 µM) were centrifuged again and used for the different experiments.

Dynamic light scattering (DLS) measurements and data evaluation were performed by Dr. Tartsch (Malvern Instruments Limited) on a Zetasizer Nano ZS. The measurements were recorded in triplicates. 50 µl samples were transferred in a disposable plastic cuvette and the measurements were started using system-defined parameters. Afterwards, the software algorithm converted measured intensity fluctuations into a correlation function into a particle size. The determination of the molecular weight relates to globular proteins and is therefore an approximation. However, using the peak maximum value of the intensity plots enabled the calculation of the molecular weight by the following Equation 6 whereby MW represents the molecular weight, **K** a value of 3.3883 and **a** a value of 2.338 (determined for globular proteins) and r the maximum measured radii.

$$MW = K \cdot r^a \qquad \text{Equation 6}$$

Nanoparticle tracking analysis (NTA) measurements and data evaluation were also performed by Dr. Tartsch (Malvern Instruments Limited) with a NanoSight NS3000. A laser beam hit a liquid sample stream under a microscope whereby the scattering light and movement of each particle in solution were detected and converted into a particle size. The system requires a particle concentration between 10^8-10^9 particles/ml in minimum 500 µl.

Resonant mass measurements (RMM) and data evaluation were performed by Dr. Epe (Malvern Instruments Limited) with an Archimedes instrument. 100 µl sample volume were applied as a pneumatic fluid, continuously passing the sensor whereby always a frequency is measured. Differences in mass will change the measured frequency (shifts above 14 mHz can be detected by the resonator). If the viscosity is known, the system is able to calculate the mass and size of floating particles. As a standard, latex beads were used, which show a monodispersity of 98-99 % in a size of 500 nm.

Dr. Marenchino (Malvern Instruments Limited) performed isothermal titration calorimetry (ITC) measurements on a MicroCal ITC instrument. 300 µl sample and 100 µl 1 mM 2GBI inhibitor solution in 50 mM K_2HPO_4 pH 7.0, 0.08 % DPC were required for one experiment.

Prior to measurements, the VSD concentration was determined using a UV-Vis spectrometer by measuring the absorption at 280 nm and 330 nm (Equation 7) (Pace *et al.*, 1995).

$$A_{280true} = A_{280} - (1.96 \cdot A_{330}) \qquad \text{Equation 7}$$

The runs were performed with pre-defined settings and were evaluated using the system analysis software (done by Dr. Marenchino).

4 Results

The following sections describe the first *in vitro* cell-free synthesis of voltage-sensing domains of voltage-gated proton channels. Screening processes in terms of stability measurements and feasibility tests of NMR applications could be performed and functional studies revealed active cell-free-produced VSDs.

4.1 Cell-free protein synthesis

The cell-free protein production offers numerous advantages (1.4). Hence, this system was chosen for VSD synthesis (3.1.9). As an example, the results of a P-CF expression in continuous-exchange mode are shown for hH_V1-VSD and DrVSD (Figure 9).

Both containers represent a 3 ml preparative-scale expression approach and were incubated for 16 h at 30 °C for VSDs production. The dialysis cassettes contain the precipitated protein (white pellet) in the reaction mix (RM). Hence, the protein synthesis was successful. Rough estimation of the amount of produced protein revealed an increased expression of hH_V1-VSD in comparison with DrVSD. Dealing with new protein constructs in any kind of expression technique implicates an initial screening procedure, to show their complete translation and to achieve maximum protein quality and quantity. Therefore, different conditions and modes in the cell-free expression experiments are routinely examined, which are described in the next sections.

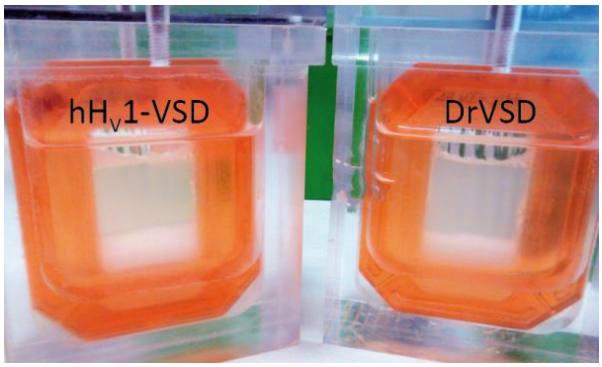

Figure 9: 3 ml P-CF expression after overnight incubation at 30 °C. On the left side and on the right side cell-free dialysis cassettes containing the hH_V1-VSD and DrVSD construct, respectively, are shown. The white fraction at the bottom represents precipitated protein as in P-CF mode no hydrophobic environment for the synthesized membrane protein has been provided.

4.1.1 Different cell-free expression modes for VSD synthesis

Cell-free protein synthesis quantification mainly starts with the expression of different gene constructs in P-CF mode as this procedure benefits from maximum protein yields compared to L-CF expression.

To this end, His-hH$_V$1-VSD and His-DrVSD genes in pET15b vectors were applied to small-scale P-CF reactions (55 µl RM). The obtained protein pellets after 16 h expression at 30 °C were washed twice with the RM-volume of S30 buffer C, afterwards resuspended in SDS sample-loading buffer and analyzed by SDS-PAGE and western blot (3.2.1, 3.2.2) (Figure 10).

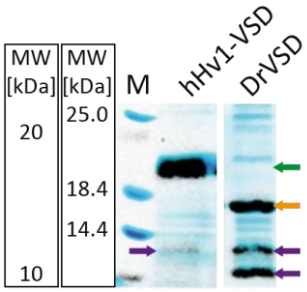

Figure 10: Analysis of P-CF-synthesized voltage-sensing domains. The dissolved pellet fraction in S30 buffer C of each construct was loaded on a 16 % SDS gel and analyzed either by Coomassie-staining or by western blot analysis with an anti-His-antibody. An overlay of gel and blot is shown where M indicates the two different protein markers (left: Roti®-Mark 10-150, right: unstained protein ladder). A green arrow indicates the hH$_V$1-VSD, an orange one the DrVSD construct and purple arrows represent specific low molecular weight signals detected by the anti-His-antibody, too.

Both constructs could be detected after Coomassie-staining and as specific anti-His-antibody recognized bands on a western blot membrane at the expected molecular weights. For DrVSD as well as for hH$_V$1-VSD additional low molecular weight signals could be identified by western blot, which were analyzed in detail in chapter 4.1.2.

Without the supplementation of a hydrophobic environment a purification and further analysis of P-CF-produced membrane proteins is impossible. Here, I first analyzed different detergents concerning their solubilization efficiency. The insoluble protein pellet was treated with standard buffer containing different detergents to a final concentration of 2 % (w/v). After an incubation of 1 h at room temperature and a following centrifugation step (10 min, 16,100xg, 4 °C) 25 µl of the supernatant and of the buffer-resuspended pellet (RM-volume) were mixed with 12.5 µl 4x SDS sample-loading buffer and analyzed by SDS-PAGE (Figure 11 A/B).

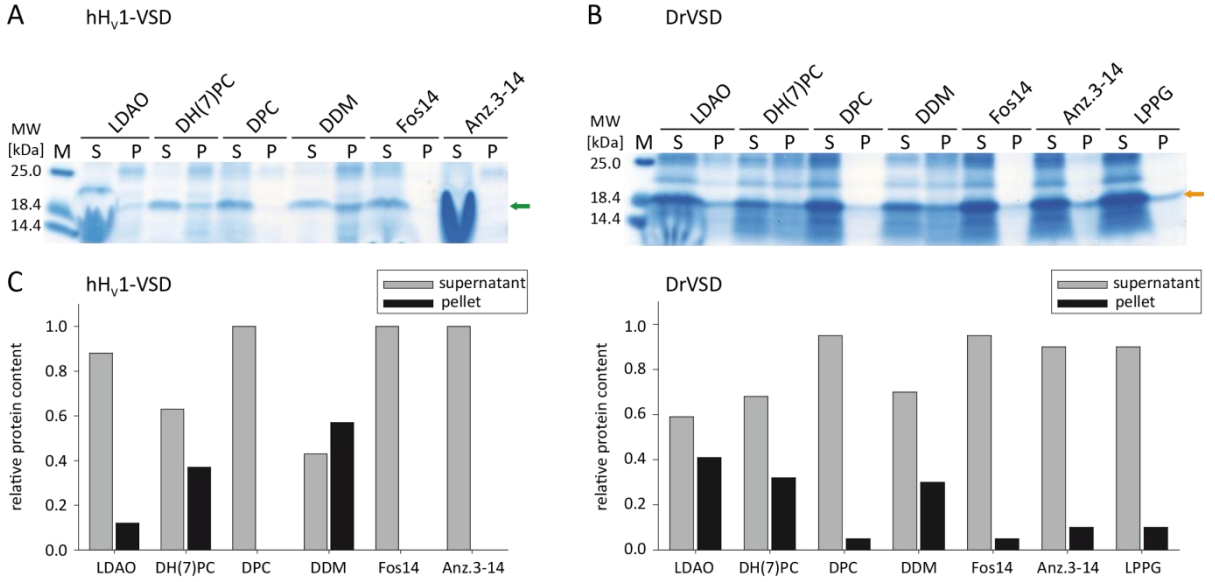

Figure 11: Solubilization screening of hH$_V$1-VSD and DrVSD after synthesis in P-CF mode. The listed detergents were used to 2 % in solubilization buffer and incubated with the protein pellets (His-hH$_V$1-VSD and His-DrVSD-Strep) for 1 h at RT. Separated fractions of supernatant (**S**) and pellet (**P**) after centrifugation were loaded on 4-15 % Tris-glycine gels and stained with Coomassie. **A** The SDS-PAGE analysis of hH$_V$1-VSD (green arrow) resuspended in different detergents is shown. The protein marker is indicated by **M**. **B** The SDS-PAGE analysis of DrVSD (orange arrow) resuspended in different detergents is shown. The protein marker is indicated by **M**. **C** Bar charts represent the relative protein content in the supernatant and pellet fraction of the two constructs in different detergents. The quantification of the relative protein content was done by analyzing the protein gel bands with ImageJ.

The solubility properties were nearly 100 % for DPC-, Fos14-, Anzergent3-14 (Anz.3-14)- and LPPG -treated VSD constructs (Figure 11 C/D). Consequently, these detergents were used for further screening processes including purification strategies and NMR analyses (4.2.1, 4.2.2). LDAO could solubilize the hH$_V$1-VSD to more than 80 %. Unfortunately, the DrVSD construct could be detected to only 60 % in the supernatant after LDAO treatment. DDM and DH(7)PC failed to solubilize the protein pellets efficiently.

Next, I tested the L-CF expression mode whereby lipids as bilayers e.g. in form of nanodiscs (NDs) or liposomes are present during the protein synthesis (1.4, 1.4.1, 3.1.9, 3.2.8, 3.2.13). Hence, VSDs are supposed to be co-translationally-inserted. First, the cell-free reaction was supplied with different NDs (1.4.1). Thereby, the NDs were composed of either DMPG or DMPC as the lipid bilayer content and MSP variants, which differ in size resulting into NDs with a different diameter (3.2.8, 3.1.7, 3.2.7). Pre-formed NDs were added as the last compound of each reaction into the RM of a cell-free VSD synthesis. ND concentrations range from 20 µM to 120 µM. DrVSD and hH$_V$1-VSD were first L-CF-produced in a small-scale volume (55 µl) in the presence of different NDs. After expression, the RM was divided in supernatant and pellet fraction by the usual centrifugation step. The pellet fraction was

resolubilized in RM-volume S30 buffer C and mixed 1:1 with SDS sample-loading buffer (Figure 12). The supernatant had to be applied to a purification process to be analyzed by SDS-PAGE (3.2.9).

In the elution fractions, a signal for the differently-sized MSP variants as well as for the VSDs could be detected (Figure 12, elution). The MSP-variants except for MSP1 were devoid of the His-tag (-). Consequently, column-bound VSDs (with His-tag) that co-elute with MSPs are likely to be inserted or even attached to the nanodiscs. For precise signal identification of MSPs and VSDs, western blot analyses were performed with anti-His-antibody (VSD signal) and anti-ApoAI-antibody (MSP signal) (3.2.2). This clearly identified both proteins in the same elution fraction pointing towards a successful VSD-ND-incorporation (data not shown). All tested differently-sized NDs seemed to be suitable for VSD insertion during L-CF expression. The smallest MSP version available to date, the MSP1D1 ΔH4-6, was not stable at all and started to precipitate during its purification procedure. In addition, the insertion of hH_V1-VSD was only rarely possible (data not shown). The smallest stable VSD-NDs were obtained with MSP1D1 ΔH5, which were used in the upcoming screening processes for NMR measurements.

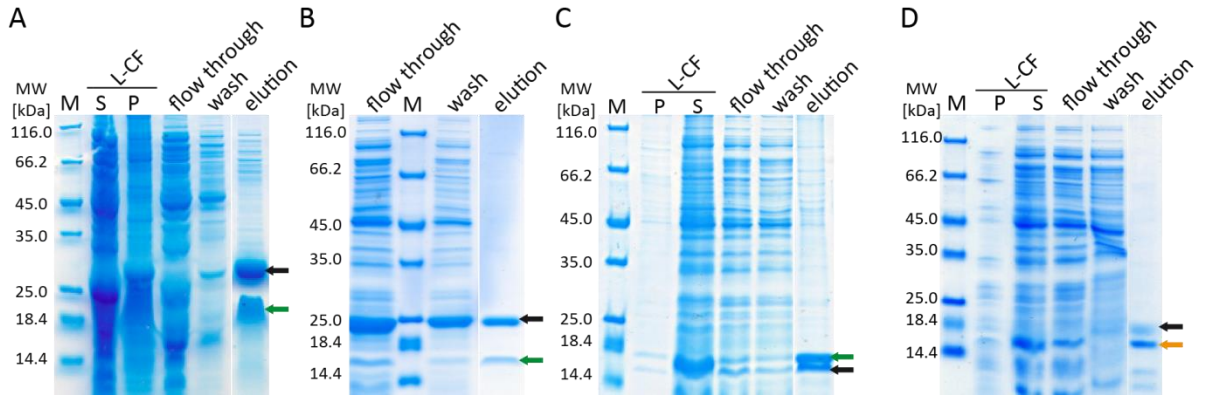

Figure 12: Co-translational insertion of hH_V1-VSD and DrVSD into different NDs. The analysis of the inserted VSDs from L-CF mode expression (**S** – soluble fraction; **P** – pellet fraction) was only possible after purification of the reaction mix by performing a Ni^{2+}-IMAC step. The flow through, wash fractions and the elution fractions are indicated. A green arrow represents the hH_V1-VSD construct, an orange arrow the DrVSD one and a black arrow highlights the different MSP versions. The protein marker is indicated by **M**. **A** The insertion of His-hH_V1-VSD into MSP1E3D1(-)-DMPC-containing NDs is shown (12 % Tris-glycine gel). **B** The insertion of hH_V1-VSD-Strep into MSP1-DMPC-containing NDs is shown (11 % Tricine gel). **C** The insertion of His-hH_V1-VSD into ΔH5(-)-DMPG-containing NDs is shown (11 % Tricine gel). **D** The insertion of His-DrVSD-Strep into ΔH5(-)-DMPG-containing NDs is shown (11 % Tricine gel).

Next, I analyzed the insertion behavior of the VSDs into NDs composed of different lipids. Here, lipid head groups like PC and PG were used to mimic the human and bacterial cell membrane, respectively. Furthermore, the influence of the lipid packing in a ND was tested by using DMPC (saturated) and DOPC (unsaturated) lipids. Large NDs with MSP1E3D1(-) as the scaffold protein were prepared with either DMPC, DMPG or DOPC lipids and applied to L-CF expression of the VSDs (3.1.9, 3.2.8). Afterwards, supernatant and pellet fraction were divided and analyzed via SDS-PAGE and western blot analysis with an anti-His-antibody, as aforementioned. The lanes for the soluble fractions were analyzed with ImageJ based on their content of soluble protein and plotted against the different lipid compositions (Figure 13).

Soluble VSDs can only be detected if they are completely or partially inserted into the bilayer of a ND, which will be claimed from now on as co-translationally-inserted. No soluble DrVSD was detected in DOPC-containing NDs. However, the hH_V1-VSD construct was successfully solubilized using this kind of lipid composition. Furthermore, the co-translational insertion was successful for both constructs in DMPC-containing NDs, but not as efficient as for the DMPG lipid component. DMPG turned out to be the best lipid for obtaining the highest fraction of soluble VSDs. Consequently, for further analysis DMPG-containing NDs were used to maximize the final protein yield.

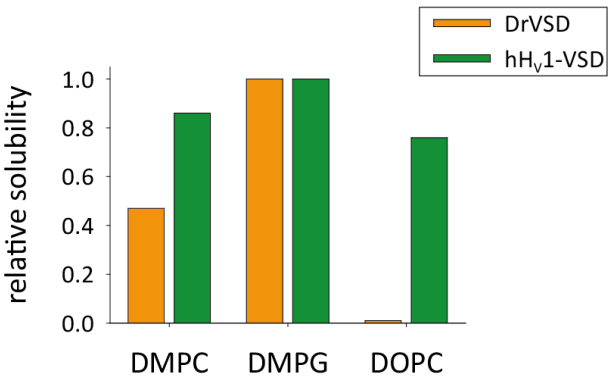

Figure 13: DrVSD and hH_V1-VSD insertion into MSP1E3D1-NDs composed of different lipids. The percentage of soluble protein was analyzed by applying the supernatant of a cell-free reaction to SDS-PAGE and western blot analysis, and calculating ratios by densitometry with ImageJ. The relative solubility of each construct was plotted against the applied lipids. Orange bars represent the DrVSD and green bars the hH_V1-VSD construct.

As mentioned before, the RM in L-CF mode can be supplemented in a similar fashion with pre-formed liposomes (3.2.13). To this end, different lipids were hydrated in liposome buffer and extruded to a uniform size of 200 nm. Again, lipids representing the human cell membrane (DMPC, total brain lipids) and more unsaturated lipids representing a mixture of human and bacterial cell membrane compositions (POPE/POPG) were used. The liposomes were added with a final concentration of 6.4 mg/ml to a 500 µl CF reaction. After cell-free expression, the conventional centrifugation step separated supernatant and pellet fraction. The supernatant was mixed 1:1 with 2x SDS sample-loading buffer and loaded on an 11 % Tricine gel (Figure 14).

The Coomassie-stained gel shows signals for soluble hH_V1-VSD at the expected molecular weight for all supplied liposomes. The overall protein synthesis yield was highest in total brain lipid- and POPE/POPG (3:1)-composed liposomes. In accordance to previously obtained data of VSDs in NDs, DMPC-containing liposomes showed decreased insertion efficiency. In a next step, the hH_V1-VSDs co-translationally-inserted into liposomes were evaluated by activity studies, shown in section 4.3.2 (3.2.21).

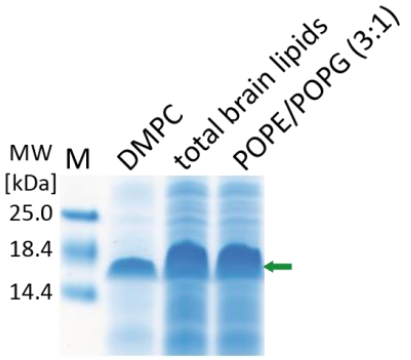

Figure 14: Co-translational insertion of hH_V1-VSD into liposomes composed of different lipids. The soluble fractions after cell-free protein synthesis were applied to gel analysis (Coomassie-stained 11 % Tricine gel). The green arrow highlights the hH_V1-VSD construct. The protein marker is indicated by **M**.

In summary, I demonstrated for the first time that the production of DrVSD and hH_V1-VSD in all tested cell-free modes was successful and first hints for detergent- and lipid-dependencies could be obtained. Nevertheless, especially in DrVSD construct-productions smaller molecular weight fragments in gel and western blot analyses were always detected. The next section will focus on my approach for the exclusive production of the full-length construct.

4.1.2 Codon optimization strategy

The low molecular weight fragments detected for DrVSD and hH_V1-VSD in Figure 10 had to be analyzed in detail. Especially for further studies including NMR screenings and dynamic studies, it is indispensable to get homogenous samples for correct assignments.

First, new purification strategies were designed to get rid of the smaller fragments. In western blot analyses, both VSDs showed low molecular weight signals representing the N-terminal His-tag of the constructs. Consequently, the purification by a Ni^{2+}-IMAC would not have been successful for removing these fragments. Ion exchange chromatography steps would have been useful. Here, a prerequisite is the knowledge of the sequences of the proteins that have to be separated to identify their isoelectric points. In order to obtain this information, the fragments of around 10 kDa and 13 kDa and the full-length DrVSD versions were cut out of a 12 % Tris-glycine gel, digested with trypsin and applied to MALDI-TOF analysis (3.2.18). The protein sequence coverage for the fragments and the full-length DrVSD was 27 % representing the first 40 amino acids. The rest of the protein could not be analyzed due to an extremely high content of hydrophobic patches in the sequence preventing the transfer of these peptides into the gas phase. Further tests done with the LILBID mass spectrometry analysis failed too (3.2.18). In summary, the length of the shorter fragments and therewith their isoelectric points could not be determined, which impeded the use of an ion exchange chromatography step as another purification method.

A second, simpler option would have been the transfer of the N-terminal tag to the C-terminus to allow purification of solely full-length VSDs (3.1.6). Unexpectedly, VSD constructs with a C-terminal His-tag or Strep-tag, tested in different vector systems (pET15b, pET21a), could not be expressed anymore in cell-free. Highly likely, the translation initiation was dysfunctional. The AT-rich sequence of the His-tag was extremely important for VSD synthesis in a cell-free expression background (Haberstock *et al.*, 2012). Providing proof of concept, other VSD constructs were designed that contained an N-terminal His-tag together with a C-terminal Strep-tag in the pET15b vector system (3.1.6). The cell-free production of these constructs was successful, but the purification via a Strep-resin failed in removing the additional protein fragments (3.2.4, 3.2.9). The detergent used for P-CF pellet solubilization was maybe not compatible with the column. L-CF-produced VSDs, co-translationally-inserted

into ND, might be not able to bind to the column due to inaccessibility of the Strep-tag or the short constructs were also purified because they were inserted into the same ND as the full-length protein. Instead of screening now more tag-variations and different purification procedures, which would have cost a lot of time, I focused on another strategy.

The occurrence of low molecular weight fragments could be caused by two factors. First, the VSDs could have been proteolytically cleaved during the incubation process of 16 h at 30 °C as recent proteomic studies revealed the existence of several proteases in our cell-free lysate (Foshag *et al.*, 2018). Due to the addition of high concentrations of protease as well as RNase inhibitor cocktails, a cleavage did not seemed to be very likely. Second, critical steps during the transcription/translation process, like only partially unwinding of RNA elements, the unavailability of tRNAs or otherwise caused translational abortions could have caused premature termination of translation leading to shorter fragments of the VSDs. Usually, this case is prevented by applying codon-optimized constructs with a specifically adjusted codon usage for the protein expression host. Before I started my experiments, I received the information that the His-tagged VSDs in pET15b, which were sent by our cooperation partners, were optimized for the production in *E. coli* cells (1.1, 3.1.4). Hence, it was again not very likely that the fragments were caused by translational stops during cell-free VSD synthesis in *E. coli* lysate. However, I did some tests.

The whole codon-optimization procedure is based on computer algorithms, which can differ from company to company, website to website and even between the same proteins used twice in an optimization process. The DrVSD construct was applied again to a codon-optimization process for *E. coli* by the algorithm from Integrated DNA Technologies (IDT) (3.1.4). The new template, DrVSD1, was obtained. The alignment shows that the codons of DrVSD and DrVSD1 differ over the whole sequence (Figure 15 A).

The new DrVSD1 construct was cloned into the pET15b vector with an N-terminal His-tag and applied to a P-CF reaction in parallel with the N-terminal His-tagged DrVSD construct. The protein pellets were washed once with RM-volume S30 buffer C and afterwards solubilized in 2x SDS sample-loading buffer and analyzed by SDS-PAGE (Figure 15 B). Gel analysis showed no obvious low molecular weight fragments for the crude supernatant of the DrVSD1 sample. The new codon optimization procedure was successful.

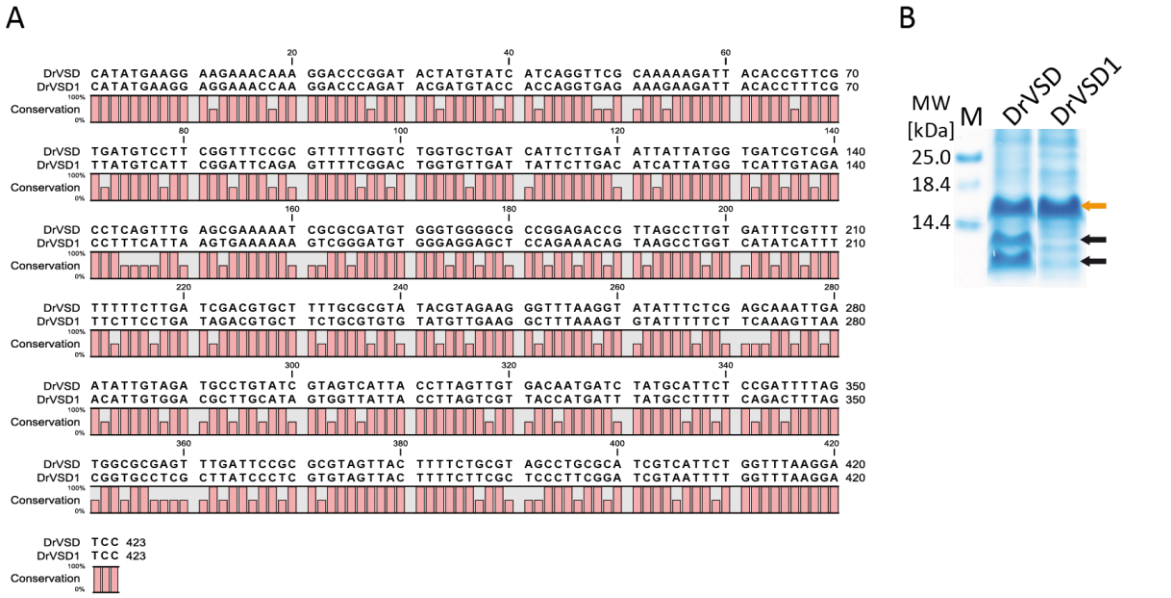

Figure 15: Codon optimization of the DrVSD gene for controlled gene expression. A The codon-optimized DrVSD DNA was used in a second iteration step to further optimize the gene for in-*E. coli* expression. An alignment of the DrVSD DNA with the newly designed DrVSD1 DNA is shown. The full red bars highlight a 100 % sequence coverage and half bars represent differences. **B** P-CF expressions of DrVSD and DrVSD1 were analyzed on a Coomassie-stained 11 % Tricine gel whereby the orange arrow indicates the full-length construct and the black arrows the shorter fragments of the DrVSD, respectively. The protein marker is indicated by **M**.

The optimized sequence was now used for comparison with the initial sequence using the rare codon analysis tool from GenScript. The initial sample had a codon adaption index (CAI) of 0.74, which is out of range of the optimal values (between 0.8 and 1) to ensure high protein synthesis. After the new codon optimization procedure, the CAI was 0.64, even worse. However, the codon optimization was successful in avoiding the presence of shorter VSD fragments after cell-free synthesis. Only the full-length construct could be obtained, which was further used for downstream processing and screenings.

4.2 Screening of protein stability and feasibility of NMR studies

Dynamic or structural investigations of proteins by liquid-state NMR routinely include a previous experimental design process based on a variety of conditions like suitable buffers (pH, ionic strength…), measurement temperatures, and labeling strategies. Within the extensive screening process, the balance between protein folding issues and NMR resolution has to be considered to identify the best conditions (1.4.2). In this thesis, NMR spectra were used as the final read-out to decide whether good conditions for a stable/folded protein, suitable for NMR studies, were found (Figure 16 A/B). A good quality NMR spectrum represents a high peak resolution and a reduced signal overlap (Figure 16 B).

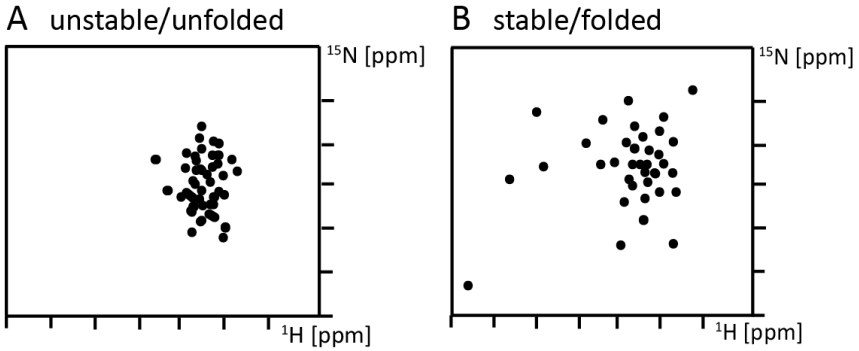

Figure 16: Theoretical [^{15}N,^{1}H]-HSQC spectra of a fictive protein. A The NMR spectrum of an unfolded and/or unstable protein is shown with low resolution and signal overlap. **B** The NMR spectrum of a stable and/or folded protein is shown with high resolution and signal dispersion.

Different conditions for CF-synthesized VSDs were tested and analyzed to enable NMR investigations, which are described in the next sections. Initially, the focus was set to the increase of protein yield for NMR measurements.

4.2.1 Purification strategies and yield analyses

The previously obtained data indicated a successful VSD production *in vitro* using the CF protein synthesis platform. To determine whether the CF-synthesized VSDs exhibit native folds and activity, they had to be analyzed in more detail. First, different purification strategies were tested to obtain the highest possible yield and purity. As described before, constructs with His- and Strep-tag were available, which allowed the use of a tandem purification procedure (3.2.9). The SDS-PAGE analyses of the different purification steps for hH_V1-VSD in DPC and DrVSD in NDs are exemplarily shown whereby all samples were loaded in a volume : volume quantity on gel for comparison (Figure 17, Figure 18). For other tested hydrophobic environments, the purified samples at the final stage are shown.

The purifications showed no protein in the flow through of the IMAC column. The first washing step with 10 mM imidazole removed nearly all impurities as nearly no signals could be detected in the washing step with 30 mM imidazole. In the elution fractions, the VSD samples smeared all over the lane with distinct signals at higher molecular weights than the monomer pointing towards ongoing oligomerization processes (seen by western blot analyses). Protein was lost during the purification process as seen by applying a sample of Ni^{2+}-beads solved in SDS sample-loading buffer to the gel after protein elution. The dialyzed or desalted IMAC-elution fractions were applied to Strep-Tactin beads (excluding the purification in LPPG; only IMAC purification) (3.2.5).

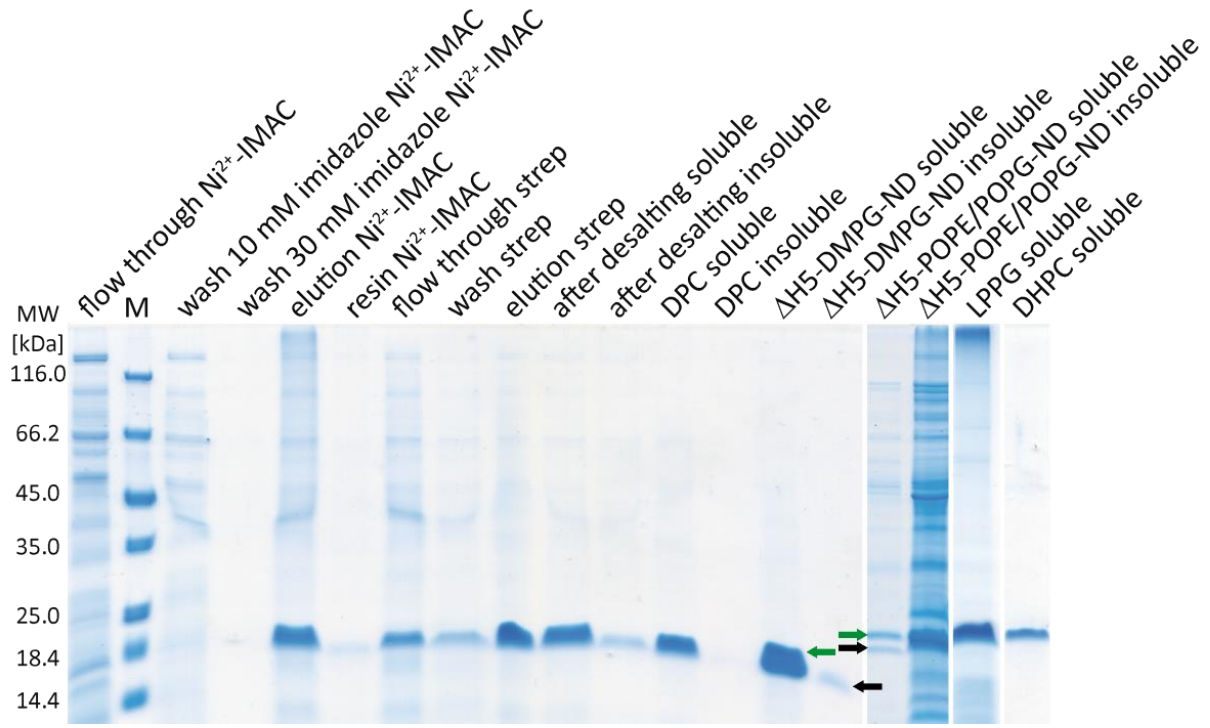

Figure 17: Purification analysis of hH_V1-VSD. The purification is exemplarily shown for hH_V1-VSD in DPC, but was comparable to all other hydrophobic environments used (except of LPPG). After P-CF- or L-CF-expression hH_V1-VSD (green arrow) was purified by an immobilized Ni^{2+}-affinity chromatography step followed by purification via the Strep-tag of the protein using a Strep-tactin matrix. After a desalting step, concentration and centrifugation procedures, the samples were analyzed by NMR spectroscopy. Prior, they were analyzed by a 11 % Tricine PAGE. The last eight lanes show the final stage of purification for different hydrophobic environments whereby the black arrows represent the MSP ΔH5(-).The protein marker is indicated by **M**.

The flow through of the Strep-Tactin column was reloaded more than five times. Afterwards, the column was washed and VSDs were eluted following the customers manual (3.2.4, 3.2.9). The purified proteins were buffer exchanged into the final NMR buffer, concentrated, centrifuged and analyzed by NMR in the listed hydrophobic surroundings (3.2.22, 4.2.2, 4.2.4). In DPC, DH(7)PC, and ΔH5(-)-DMPG-NDs, hH_V1-VSD could be obtained in a pure form without any visible aggregates. Contrary, in LPPG and in NDs with POPE/POPG (3:1) lipids a smear was visible. Although the samples were treated with SDS-urea loading buffer, expecting the complete solvation of oligomers, this smear belongs to the hH_V1-VSD representing higher oligomers or even aggregates (stated by western blot analyses - data not shown). Moreover, hH_V1-VSD was not stable in the POPE/POPG-containing NDs shown by the high amount of insoluble material in the final NMR sample, possibly caused by the general instability of this nanodisc species. The same tandem-purification strategy was applied to the DrVSD construct (Figure 18).

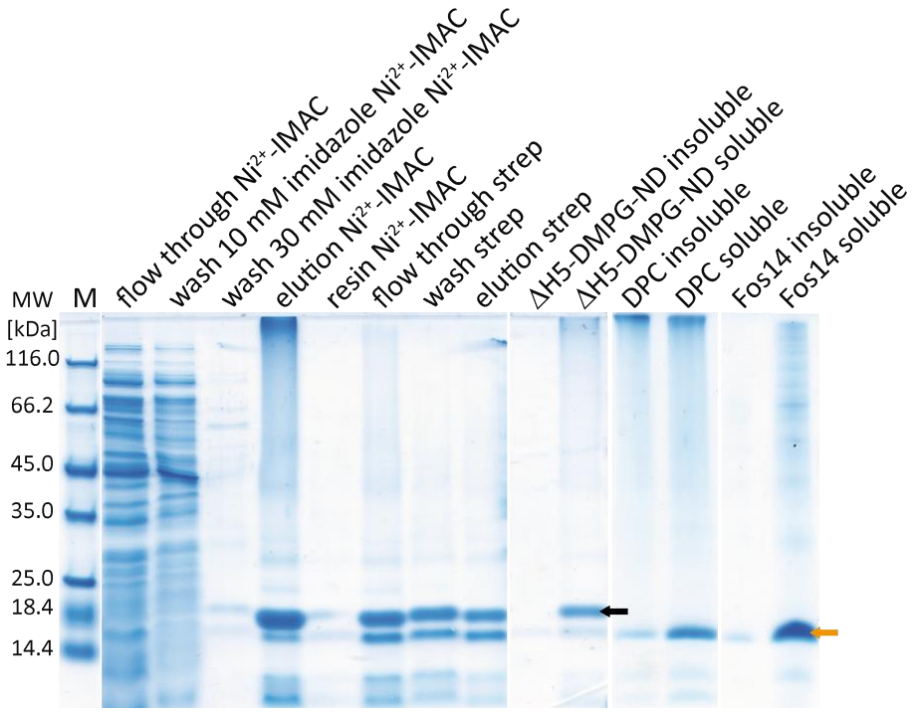

Figure 18: Purification analysis of DrVSD. The purification is exemplarily shown for DrVSD in ΔH5-DMPG-NDs, but was comparable to all other hydrophobic environments used. After P-CF- or L-CF-expression DrVSD (orange arrow) was purified by an immobilized Ni^{2+}-affinity chromatography step followed by purification via the Strep-tag of the protein using a Strep-tactin matrix (excluding the sample in Fos14 – only IMAC purification). After a desalting step, concentration and centrifugation procedures, the samples were analyzed by NMR spectroscopy. Prior, they were analyzed by an 11 % Tricine PAGE. The last six lanes show the final stage of purification for different hydrophobic environments whereby the black arrow represents the MSP ΔH5(-). The protein marker is indicated by **M**.

DrVSD could be successfully purified in ΔH5(-)-DMPG-NDs as well as in DPC and Fos14 detergent micelles. The same trend as for the hH_V1-VSD was observed. Protein got lost during the IMAC purification procedure by sticking to the beads and during the Strep purification set-up. Furthermore, a smear could be detected representing higher oligomers or even aggregates in the final NMR samples.

Taken together, after the first IMAC purification the VSDs were high concentrated and pure. The MSPs had no His-tag anymore. Hence, empty NDs were removed by the initial IMAC purification step. Using the Strep column procedure only caused loss of protein wherefore in future experiments Strep purification was omitted. The increased smear effect of the elution fractions from the IMAC column compared to the final NMR samples could be attributed to a concentration-dependent effect, which will be analyzed in detail in another chapter (4.2.2).

The final protein concentration could either be determined by measuring the absorbance at 280 nm against the buffer blank with a NanoDrop and calculating the concentration by Lambert-Beer's law or by estimation of signal intensities in NMR analyses (3.2.6). For a

single-step purification (IMAC only), pure VSDs in different hydrophobic environments were obtained to 1-3 mg/ml expression of the hH_V1-VSD construct and 0.5-3.2 mg/ml of the DrVSD, respectively. The results indicated that further downstream processing was non-VSD specific. The tandem-purification procedures yielded less protein amounts. However, the final concentrations of this procedure are shown exemplary in Table 17 for different provided hydrophobic environments to ensure comparability between the presented purification results in Figure 17 and Figure 18 and the corresponding measured concentrations.

Highest concentrations for both constructs could be obtained in ΔH5(-)-DMPG-NDs and in LPPG for the purified hH_V1-VSD and in Fos14 for DrVSD. The results of the NMR experiments will be shown in the next sections (4.2.2, 4.2.4).

Table 17: Comparison of yields of cell-free-produced voltage-sensing domain samples for NMR applications.

Hydrophobic environment	hH_V1-VSD concentration	DrVSD concentration
DPC	77 µM (550 µl)	20 µM (580 µl)*
ΔH5-DMPG-ND	100 µM (630 µl)	300 µM (530 µl)*
ΔH5-POPE/POPG-ND	10 µM (500 µl)	-
LPPG	157 µM (380 µl)	-
DH(7)PC	50 µM (350 µl)	-
Fos14	-	308 µM (680 µl)

*Protein obtained from a 6 ml CF expression. Unmarked samples resulted from a 3 ml CF reaction.

In summary, VSDs could be synthesized by cell-free protein production in different hydrophobic environments and purified in quantities sufficient for NMR applications. The next step was the screening of VSDs stability in detergent as well as in NDs (4.2.2, 4.2.4).

4.2.2 Stability screening of VSDs in detergent micelles

Maximizing the protein stability is a key component when working with *in vitro*-produced samples. On the one hand, it is important to obtain information about protein folding characteristics. Does the protein tend to aggregate or is it degraded over time? On the other hand, it is worth knowing the proteins overall stability. Are longer incubation times at for example 45 °C or treatments with low-salt buffer conditions with respect to NMR

applications possible? Initially, the P-CF-produced VSDs solubilized in detergent were under investigation. The quality check started with SEC runs probing the aggregation tendency and oligomerization behavior of the samples, followed by recordings of ^{1}H-^{15}N correlation spectra analyzing the folding and dynamic behaviors. Stability issues were analyzed by CD spectroscopy and LILBID mass spectrometry analysis (3.2.16, 3.2.18, 3.2.19, 3.2.22).

VSDs in contact with a mild detergent

First, the His-hH$_V$1-VSD construct was expressed in P-CF mode, solubilized and purified in DH(7)PC (3.2.9) (Figure 17, DH(7)PC lane). Afterwards an unlabeled, concentrated sample (7 µM) was loaded onto the SEC column and the elution fractions were analyzed by western blot with an anti-His-antibody (Figure 19 A).

The SEC profile showed no aggregated protein in the void volume. Two main peaks were detected at 1.47 ml and 1.65 ml corresponding to a mass of ~75 kDa and ~30.5 kDa, respectively (3.2.16). Calculating the overall mass of hH$_V$1-VSD and a DH(7)PC micelle (Table 10, Table 14), the first peak could represent the dimeric and the second one the monomeric VSD species. Furthermore, this was proven by western blot analysis where signals of hH$_V$1-VSD as monomers and dimers were detected.

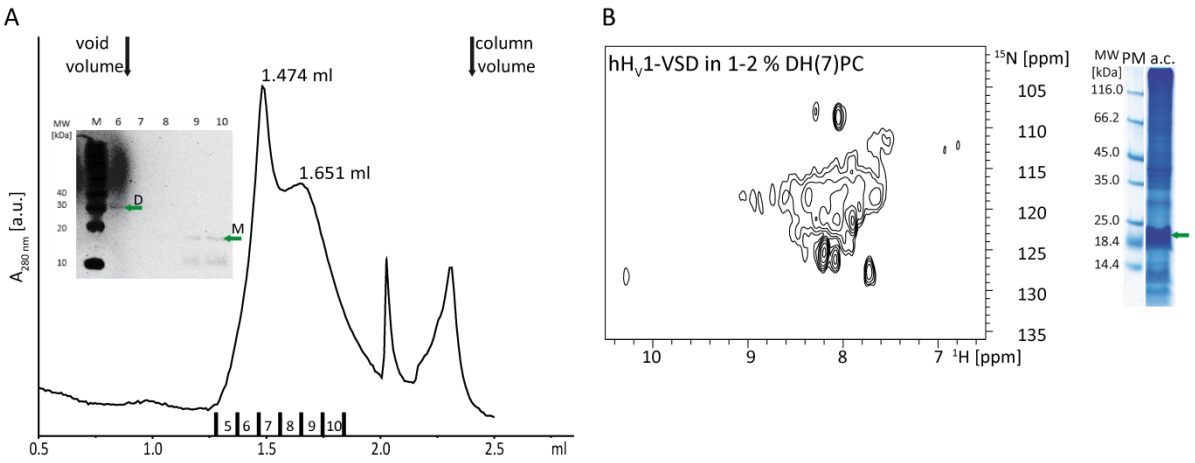

Figure 19: SEC and NMR analysis of hH$_V$1-VSD in DH(7)PC micelles. Green arrows indicate the hH$_V$1-VSD monomer (**M**) and dimer (**D**). **A** The SEC run was performed by injecting 50 µl protein (~7 µM) to an analytical Superdex200 PC 3.2/30 column with a flow rate of 0.05 ml/min at 16 °C in 50 mM sodium acetate pH 5.2 and 0.2 % DH(7)PC as running buffer. Black arrows indicate the void (0.89 ml) and the column volume (2.4 ml). The SEC profile shows two protein peaks whereby the one at 1.474 ml represents higher oligomers and the one at 1.651 ml represents the monomer fraction. No higher aggregates in the void volume could be detected. Fractions were analyzed by an anti-His-antibody-developed western blot. **B** [^{15}N,^{1}H]-BEST-TROSY spectrum recorded at 600 MHz and 318 K (NS = 128, TD1 = 37) in 20 mM HEPES-NaOH pH 7.0, 100 mM NaCl and 0.2 % DH(7)PC of the concentrated ^{15}N,^{2}H-labeled hH$_V$1-VSD sample (50 µM). The VSD was cell-free-expressed in the presence of scrambling inhibitors (20 mM AOA, 9.8 mM D-cycloserine, 2.76 mM D-malic acid). This sample was analyzed on a Coomassie-stained 11 % Tricine gel after concentration and centrifugation (**a.c.**). High aggregates are visible as a smear over the whole lane. The protein marker is indicated by **PM**.

Additional low molecular weight signals represent fragments of the hH_V1-VSD as observed and discussed previously (Figure 10). Moreover, the western blot showed again a smear effect, which could correspond to aggregated protein.

The final protein concentration (10 µM) was very low, which hampered NMR experiments (Appendix, Figure A 1 A). Hence, a new solubilization and purification strategy was applied based on promising results of NMR experiments performed with another membrane protein (Tumulka *et al.*, 2013). Here, the P-CF pellet was first solubilized with the harsh detergent DPC to increase the overall protein yield (Figure 11). During the purification procedure, DPC was slowly exchanged to the milder DH(7)PC in three steps (1. Wash buffer W2 with 0.15 %DPC/0.05 % DH(7)PC, 2. Wash buffer W3 with 0.1 % DPC/0.1 % DH(7)PC and 3. Wash buffer W4 with 0.2 % DH(7)PC). SEC runs were performed, which confirmed previous results (data not shown). Monomeric and dimeric species of hH_V1-VSD in 0.2 % DH(7)PC as well as no signal in the void volume range could be detected. Applying this strategy, the VSD concentration could be increased to 50 µM in a final volume of 350 µl, suitable for NMR experiments (Figure 19 B).

The NMR spectrum showed poor resolution. The peaks were broad and many signals were missing (Figure 19 B). Only some peaks were well-resolved including the Trp signal (above 10 ppm ^{1}H-direction). The analysis of the concentrated, centrifuged hH_V1-VSD fraction in NMR buffer via SDS-PAGE revealed higher oligomeric states (smear) that may indicate the formation of soluble aggregates. High molecular weight complexes would tumble very slow, causing a reduced peak resolution in the NMR spectrum. The data raised the question if this was a specific problem of cell-free-produced VSDs. It was tempting to speculate that the protein solubilized from a pellet fraction was not correctly folded and tended to aggregate leading to a worse NMR spectra quality. To proof this hypothesis, the obtained spectrum was compared with a spectrum of *E. coli*-produced hH_V1-VSD in DH(7)PC micelles (Appendix, Figure A 1 B). The result was obvious: no resolution for both experimental set-ups. This indicated that there is no difference of *in vivo*- or *in vitro*-synthesized VSDs. However, no further conclusion about the folding state and sample behavior of cell-free-expressed VSDs was possible at this experimental stage.

VSDs in contact with a harsh detergent

Next, I decided to test another detergent to prove the feasibility of cell-free-produced VSDs for functional and structural studies. Is it possible to reproduce data from *E. coli*-produced hH_V1-VSD with a higher resolution in NMR applications? To this end, the His-hH_V1-VSD P-CF pellet was solubilized in LPPG. J. Letts did first assignments of *E.coli*-produced hH_V1-VSD in LPPG, but failed because of misfolded protein species clarified by PRE measurements. Nevertheless, the overall spectra resolution, Letts obtained, was promising (Figure 20 D). LPPG was now used trying to reproduce the spectrum quality of *E. coli*-synthesized VSDs in comparison to cell-free protein production (Figure 20).

The SEC profile of His-hH_V1-VSD in LPPG (86 µM) showed one broad peak with a maximum at 1.37 ml corresponding to a molecular weight of 126 kDa (Figure 20 A). A mixture of monomeric and dimeric protein in association with the LPPG micelle (Table 14) might explain the peak width. This was also proven by gel and western blot analysis (overlaid) where the monomeric and dimeric hH_V1-VSD could be detected. Furthermore, SDS-PAGE results revealed higher oligomeric states that may indicate again the formation of soluble aggregates. Inevitably, also, the NMR spectrum was of poor resolution and comparable to the one obtained of His-hH_V1-VSD in DH(7)PC (Figure 20 B, Figure 19 B). The huge signal harboring many overlaid resonances in the middle reminds of an unfolded protein (7.5-8.5 ppm ^{1}H dimension), but additional signals could be detected in regions described for folded protein species (6.8-9 ppm ^{1}H dimension). Furthermore, the Trp signal of the Strep-tag splits, which could be either a hint of ongoing dynamic events or the presence of different species (various folding or oligomeric states). In contrast to the huge signal overlap, this is no indication for an unfolded protein under investigation. The next step was to test whether the purification of the VSD construct is necessary for spectroscopic analyses. A streamlined VSD preparation process would have been beneficial for a time- and cost-saving stability screening procedure. As described in the literature, cell-free-produced proteins can be directly analyzed by NMR based on their exclusively labeling during the synthesis (Klammt *et al.*, 2012). To this end, the P-CF-produced hH_V1-VSD pellet was solved in the same buffer used for the assignments of the *E.coli*-produced hH_V1-VSD in LPPG (Letts, 2014) additionally supplemented with 1 % LPPG for solubilization purposes. The recorded NMR spectrum showed resolved signals in the glycine (around H 8.3 ppm, N 109 ppm), asparagine/glutamine (around H 7 ppm, N 112 ppm) and arginine region (around H 7.8 ppm, N 127 ppm).

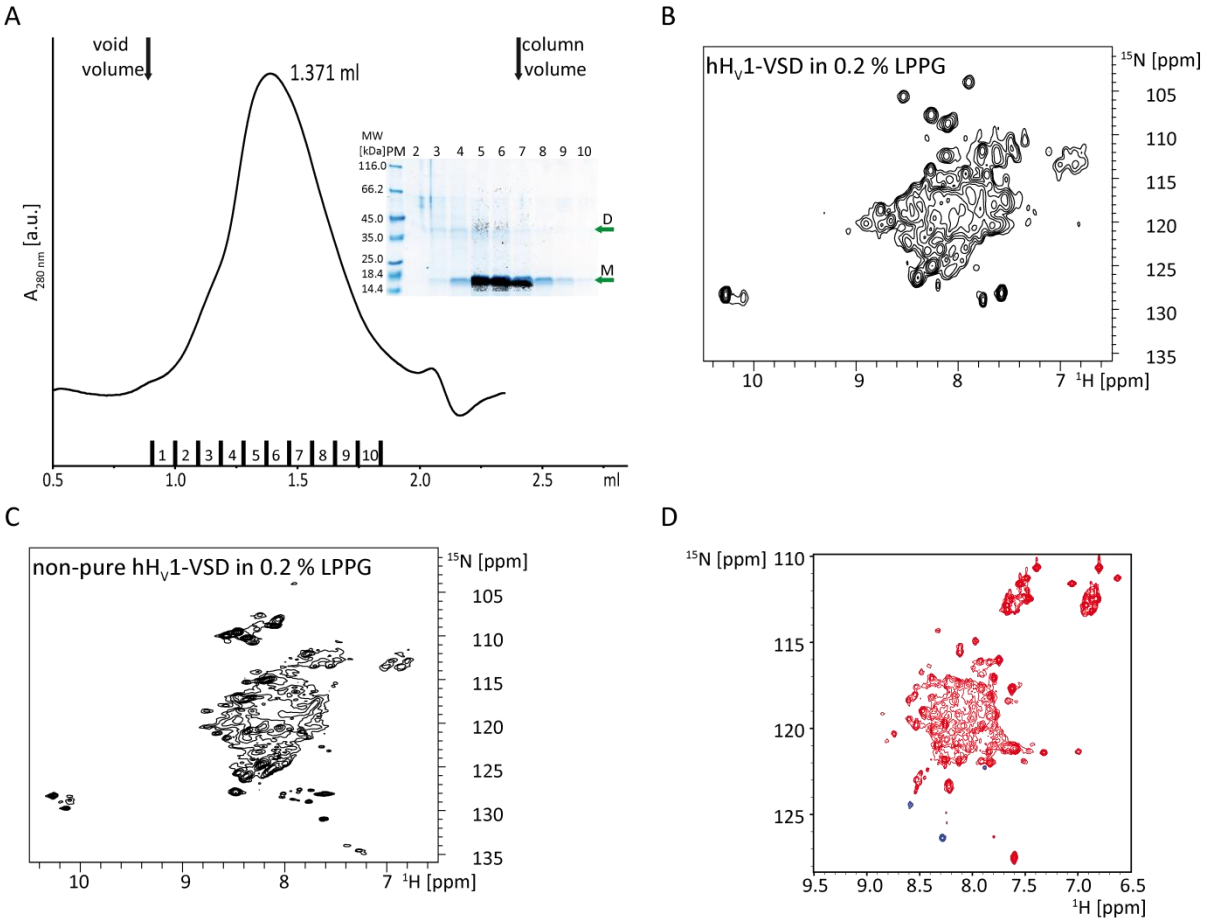

Figure 20: SEC and NMR analysis of hH$_V$1-VSD in LPPG micelles. A The SEC run was performed by injecting 50 µl protein (86 µM) to an analytical Superdex200 PC 3.2/30 column with a flow rate of 0.05 ml/min at 16 °C in 100 mM Tris-HCl pH 8.0 at 4 °C, 150 mM NaCl and 0.2 % LPPG as running buffer. Black arrows indicate the void (0.89 ml) and the column volume (2.4 ml). The SEC profile shows one protein peak at 1.371 ml with little shoulders. No higher aggregates in the void volume could be detected. Fractions were analyzed by a Coomassie-stained 11 % Tricine gel overlaid with an anti-His-antibody-developed western blot. The green arrows indicate the hH$_V$1-VSD monomer (**M**) and dimer (**D**). The protein marker is indicated by **PM**. **B** [^{15}N,^{1}H]-BEST-TROSY spectrum recorded at 599 MHz and 308 K (NS = 192, TD1 = 512) in 100 mM Tris-HCl pH 8.0 at 4 °C, 150 mM NaCl and 0.2 % LPPG of the concentrated ^{15}N,^{2}H-labeled hH$_V$1-VSD sample. Here, the elution fraction after Ni^{2+}-IMAC purification was under investigation. Residual imidazole might be present. The VSD was cell-free-expressed in the presence of scrambling inhibitors (20 mM AOA, 9.8 mM D-cycloserine, 2.76 mM D-malic acid). **C** [^{15}N,^{1}H]-BEST-TROSY spectrum recorded at 599 MHz and 298 K (NS = 256, TD1 = 576) in 10 mM HEPES-NaOH pH 7.0, 50 mM NaCl and 1 % LPPG of directly solubilized P-CF-produced ^{15}N,^{2}H-labeled hH$_V$1-VSD pellet without any prior purification. The construct was expressed in the presence of scrambling inhibitors (20 mM AOA, 9.8 mM D-cycloserine, 2.76 mM D-malic acid). **D** [^{15}N,^{1}H]-HSQC spectrum of *E. coli*-expressed ^{15}N-labeled hH$_V$1-VSD in 10 mM HEPES-NaOH pH 7.0, 50 mM NaCl and 0.1 % LPPG at 298 K (adapted from Letts, 2014).

Again, the Trp side chain signal splits pointing towards different oligomeric states or flexible regions. However, no enhancement of the overall signal dispersion and resolution could be obtained. The spectrum is comparable to the spectrum of the purified VSD and could not be used for further assignment processes.

VSDs in detergents known for efficient membrane protein solubilization

LPPG as a very harsh detergent and DH(7)PC as a milder version could not lead to a satisfying protein- and NMR spectrum-quality. Next, a mixture of DPC/LDAO micelles, which was successfully used to solve the structure of the voltage-dependent potassium channel K_VAP by NMR (Shenkarev *et al.*, 2010b) and DPC micelles alone were tested. Results are shown in Figure 21.

First, the His-hH_V1-VSD was solubilized directly in DPC/LDAO (2:1) after P-CF expression, purified, and analyzed by NMR spectroscopy (done by Christina Helming, practical student in our lab) (Figure 21 A). The NMR spectrum had a bad resolution and was comparable to the ones obtained of His-hH_V1-VSD in DH(7)PC and LPPG (Figure 19 B, Figure 20 B). Next, an hH_V1-VSD pellet from P-CF expression was solubilized in DPC and analyzed by SEC (Figure 21 B) (3.2.22). The SEC profile of the concentrated His-hH_V1-VSD-Strep sample in DPC (151 µM) showed again a very broad peak with maximum at 1.47 ml corresponding to a molecular mass of ~77 kDa (dimeric protein) (Table 10, Table 14, Table 15). Furthermore, a signal in the void volume of the column could be detected, visualizing aggregates. The corresponding SDS-PAGE analysis showed that the VSD was distributed in all fractions of the peak area with more or less detectable higher oligomers. The observed smear effect was more than clearly visible in the concentrated VSD sample after centrifugation (30,000xg, 30 min, 4 °C) prior to SEC loading (Figure 21 B IP). Oppositely, the non-concentrated elution fraction from an IMAC purification (Figure 17) showed no significant smear. Hence, there was evidence that VSDs in high concentrations tend to form aggregates in a concentration-dependent manner. These aggregates cannot be removed by a centrifugation step.

The NMR spectrum of His-hH_V1-VSD (330 µM) in DPC looked different to the one obtained with the mixture of DPC/LDAO, but still the resolution and signal dispersion, necessary for assignment purposes, was missing (Figure 21 C). The DPC concentration during purification was set to 0.08 %. While concentrating the protein sample in Amicon centrifugal filter units (30 kDa MWCO), the detergent was concentrated too. The final amount was estimated by analyzing the DPC peak in a 1D ^{31}P-NMR spectrum to around 2 %. The step-wise addition of LDAO (pH 8.0) to the sample did not change the quality of dispersion or resolution drastically (Figure 21 D). The observable minor changes could be due to an increased pH instead of being a result of the creation of more stable proteo-mixed micelles.

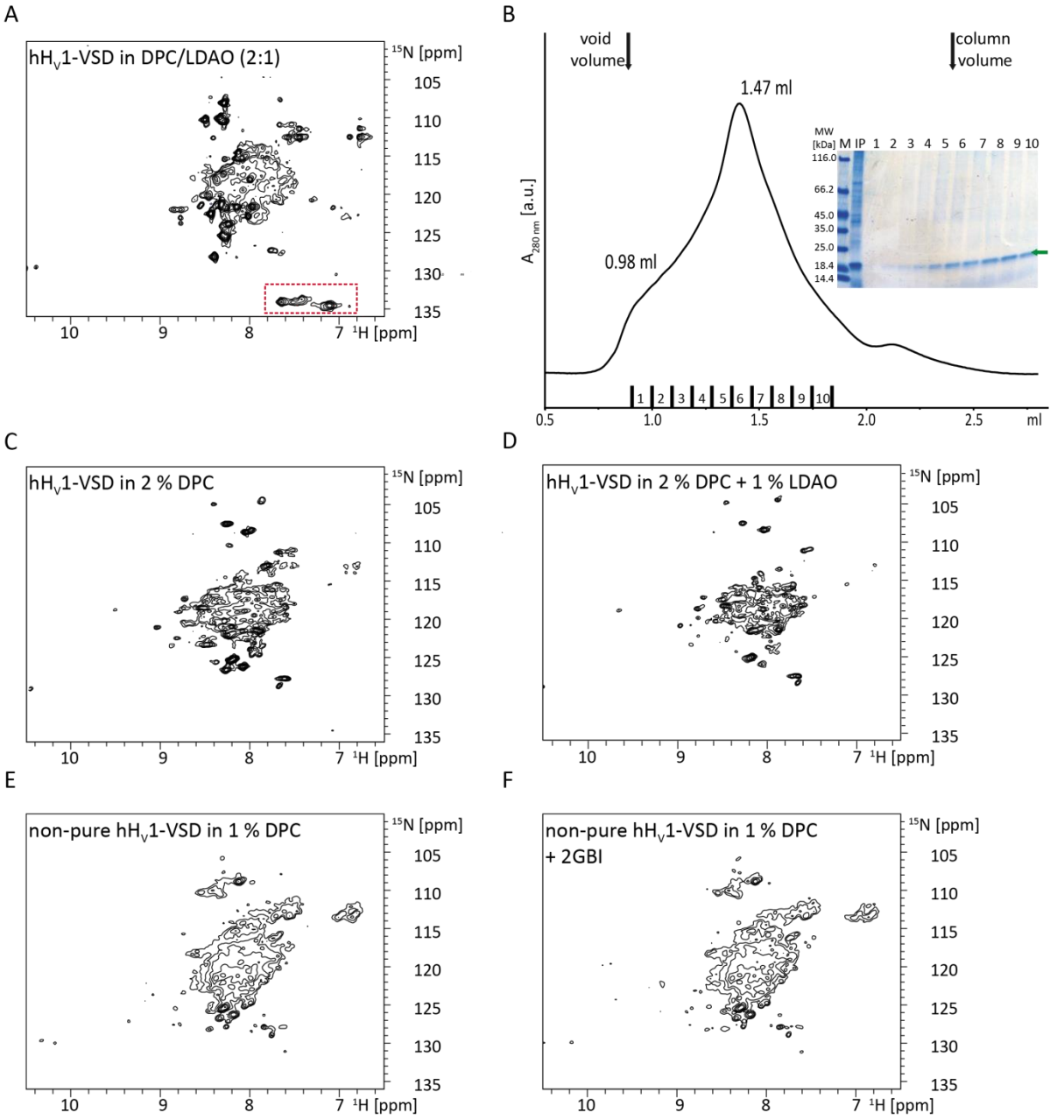

Figure 21: SEC and NMR analysis of hH$_V$1-VSD in DPC/LDAO (2:1) and DPC micelles. [^{15}N,^{1}H]-BEST-TROSY spectra were recorded under the stated conditions. **A** The spectrum of cell-free-expressed, purified ^{15}N,^{2}H-labeled hH$_V$1-VSD was recorded at 313 K, 800 MHz in 20 mM sodium acetate buffer pH 4.7 and DPC/LDAO (w/w 2:1) (NS = 64 , TD1 = 256) (done by Christina Helmling, practical student). The red box represents enfolded arginine side chains. **B** The SEC run of hH$_V$1-VSD in DPC micelles was performed by injecting 50 µl protein (151 µM) to an analytical Superdex200 PC 3.2/30 column with a flow rate of 0.05 ml/min at 16 °C in 50 mM K_2HPO_4 pH 7.0, 200 mM NaCl and 0.08 % DPC as running buffer. Black arrows indicate the void (0.89 ml) and the column volume (2.4 ml). The SEC profile shows one protein peak at 1.47 ml with a huge shoulder with a maximum at around 0.98 ml. Higher aggregates in the void volume could be detected. Fractions were analyzed by a Coomassie-stained 4-15 % Tris-glycine gel (**IP** – sample prior to SEC loading after ultracentrifugation). The green arrow indicates the hH$_V$1-VSD signal. The protein marker is indicated by **M**. **C** The spectrum of cell-free-expressed, purified, and concentrated ^{15}N,^{2}H-labeled hH$_V$1-VSD was recorded at 318 K, 800 MHz in 20 mM HEPES-NaOH pH 7.0, 20 mM NaCl and 2 % DPC (NS = 104 , TD1 = 384). **D** The figure shows the NMR spectrum of ^{15}N,^{2}H-labeled hH$_V$1-VSD recorded under the same conditions as described in C with up to 1 % step-wise addition of LDAO (NS = 104, TD1 = 374). **E-F** The pictures show NMR spectra of cell-free-expressed ^{15}N,^{2}H-labeled hH$_V$1-VSD without any prior purification step. The pellets were directly solved in 10 mM HEPES-NaOH pH 7.0, 50 mM NaCl and 1 % DPC (**E**) and additional 100 µM 2GBI (**F**) (308 K, 599 MHz, NS = 320, TD1 = 256).

In a next step, His-hH$_V$1-VSD was analyzed by NMR in a non-pure state directly after solubilization of the P-CF pellet in 1 % DPC (Figure 21 E), comparable to the experiment done with LPPG micelles (Figure 20 C). We expected to detect the same NMR spectrum as for the purified sample in DPC. However, the [^{15}N,^{1}H]-BEST-TROSY spectrum showed a comparable dispersion but nearly no signal resolution. This could be due to a higher protein and/or salt concentration in the NMR sample causing the formation of higher oligomers, thereby reducing the tumbling rate and therewith decreasing spectra resolution. I further tested whether the addition of the inhibitor 2GBI (1.2.3) might either stabilize flexible regions or support the overall folding of the VSD as it was described for other membrane proteins (Schwaiger *et al.*, 1998; Ozawa *et al.*, 2005; Laguerre *et al.*, 2016) (1.2.3, Figure 5). Here, 100 µM of the inhibitor were directly applied to the solubilization buffer. The NMR spectrum looked similar to the one without 2GBI (Figure 21 E/F). The inhibitor had no influence on spectra quality for the non-purified hH$_V$1-VSD construct.

In summary, the best results for NMR spectra quality and SEC running behavior were obtained for hH$_V$1-VSD in DPC micelles and not in the DPC/LDAO mixture, which has been demonstrated in literature to be successful for other voltage-gated channels (Shenkarev *et al.*, 2010b). Consequently, the His-DrVSD-Strep P-CF-produced pellet was solubilized in DPC too, purified via an IMAC column, concentrated, and analyzed by NMR (Appendix, Figure A 2). Although only around 50 % of expected signals could be detected, the overall spectra resolution and dispersion looked promising.

Taken together, in all three tested detergents the VSDs seemed to be unstable at high concentrations and at higher temperatures. However, DPC was the most promising detergent candidate as both VSDs could be purified in a high quality and quantity when analyzing the results of the SDS-PAGEs and SEC runs (Figure 17, Figure 18, Figure 21). Furthermore, the NMR results exhibited characteristics of folded protein structures. Detailed folding properties of cell-free-produced VSDs of voltage-gated proton channels in detergent are the focus of the next sections.

Secondary structure analysis of VSDs in detergent micelles

To investigate the stability and folding behavior in more detail, CD measurements were performed with the VSDs in DPC (3.2.19). His-DrVSD-Strep and His-hH$_V$1-VSD-Strep were P-CF-expressed, solubilized in Fos14, purified and buffer exchanged to the CD buffer containing 0.08 % DPC using Bio-Spin® 6 columns (3.2.5). Afterwards the samples were filtered through a 200 nm syringe filter and the concentration was determined (hH$_V$1-VSD 15 µM in 300 µl, DrVSD 19 µM in 500 µl) (3.2.6). CD spectra were recorded and analyzed with respect of the VSD fold using Yang's reference (Figure 22 A).

In addition, hH$_V$1-VSD in DPC was analyzed by recording CD spectra in a temperature gradient from 20 to 110 °C in 5 °C steps to determine the melting points of the protein as a measure of its stability (Figure 22 B). Both VSDs showed a typical spectrum for an α-helical protein with a specific maximum of the molar ellipticity ([Θ]) at 192 nm and two minima at 209 nm and 222 nm (Quadrifoglio & Urry, 1968).

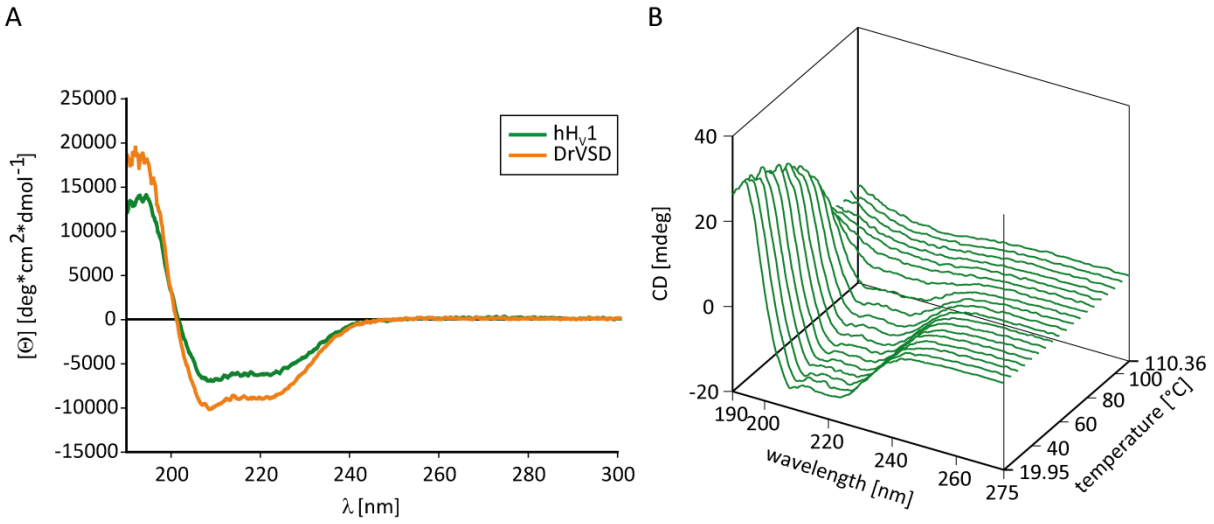

Figure 22: CD spectroscopy analyses of the VSDs in DPC micelles. Samples with a concentration of 0.3 mg/ml were recorded in CD buffer containing 10 mM K_2HPO_4 pH 7.0 and 0.08 % DPC. The orange line represents the DrVSD construct and green lines the hH$_V$1-VSD. **A** Shown is the secondary structure analyses of hH$_V$1-VSD and DrVSD in DPC micelles at 20 °C. By analyzing the data with Yang's reference hH$_V$1 has an α-helical content of 40.5 % (sheet: 37 %, random: 22.5 %) and DrVSD of 37 % (sheet: 37.1 %, random: 25.9 %). Raw data were transferred to molar ellipticity values. **B** The figure shows a plot of the measured CD signal in mdeg of hH$_V$1-VSD in DPC micelles against wavelength and temperature (20-110 °C). With increasing temperatures (1 °C/min) the CD signal decreases. Detailed analysis can be found in the appendix (**Figure A 3**).

The contents of calculated secondary structural elements were listed and compared with the secondary structure prediction, done with the PredictProtein server (Table 18) (Rost *et al.*, 2004).

Table 18: Comparison of calculated contents of secondary structural elements in cell-free-expressed VSDs between measured CD data at 20 °C and results of a structure prediction.

Structural element	hH_V1-VSD PredictProtein	hH_V1-VSD CD	DrVSD PredictProtein	DrVSD CD
α-helix	79.33	40.5	56.20	37.0
β-strand	0.0	37.0	16.79	37.1
loop	20.67	0.0	27.01	0.0
random	-	22.5	-	25.9

Interpreting the CD spectra obtained at 20 °C, the VSDs showed the expected behavior of α-helical proteins. The reference of the CD measurement calculated high percentages of β-strands and no loop structures conversely to the predicted proportions. To exclude a drastically influence of the experimental parameters on the outcome I performed further experiments. The analysis of the high-tension voltage (HT) values revealed that they were in the working range of the detector (<600 V), meaning not saturated, whereas the absorbance values were out of range between 190 and 210 nm (>2). This would result in a decrease of the light intensity at the detector leading to the receipt of unreliable information about secondary structural elements in this region (Appendix, Figure A 3). However, it was concluded that the proteins were somehow folded and did not exist as random coil motifs in DPC.

In addition, I tried to focus on stability parameters by recording a temperature-dependent CD profile. The full spectra were recorded to distinguish between a loss of CD signal at a defined wavelength based on loss of structure or based on ongoing protein aggregation/precipitation. It could be clearly shown that the loss of signal corresponds to protein precipitation. The ellipticity was reduced by increasing wavelengths and a white precipitate was detected in the cuvette after measurements. However, the temperature-dependent mean residue weight ellipticity values at 222 nm were plotted against temperature to analyze potential folding transitions prior to aggregation events. In more detail, their first deviation helped analyzing the melting temperatures (T_M) (Appendix, Figure A 3 B/C). The mean inflection point could be detected at 75 °C, which could correspond either to an unfolding of α-helical structures or to complete protein precipitation. Additional transition states could be assumed at 30 °C and 55 °C. A discussion of these values was omitted, as there was no evidence for a detected “real” unfolding event. In accordance with

this notion, the analysis of secondary structures using Yang's reference revealed an increase of the α-helical content at 45 °C (NMR measurement temperature) for hH_V1-VSD to 46.9 % and for DrVSD to 40.5 % while the β-strand content was reduced, which cannot be interpreted as an unfolding event for a predicted mainly α-helical protein.

In summary, these results showed that the VSDs in DPC display folded structures, but a melting temperature could not be determined. Finally, an accurate conclusion from the obtained results by SEC runs, NMR and CD spectroscopy about VSDs stability and correct folding in detergent micelles was not possible. To investigate further stability issues of the VSDs in detergent micelles, SEC runs were performed with samples incubated at different temperatures.

Temperature-dependent stability of VSDs

The analysis of cell-free-produced VSDs by NMR requires certain stability at temperatures up to 45 °C for a longer period. CD experiments showed possible transition states of the VSDs at around 30 and 50 °C pointing towards instabilities in this temperature range. The upcoming experiments should help evaluating the VSDs stability in detergent micelles at higher temperatures to obtain a final answer about the feasibility of NMR studies.

To this end, His-hH_V1-VSD and His-DrVSD1 were P-CF-expressed, solubilized in buffer containing 1 % Fos14, purified by Ni^{2+}-affinity chromatography, buffer exchanged to 50 mM K_2HPO_4 pH 7.0 and 0.08 % DPC, ultracentrifuged at 300,000xg for 1 h and concentrated in Amicon centrifugal filter units (MWCO 30 kDa). Additionally, the samples were centrifuged for 30 min at 30,000xg prior to loading onto the SEC column. First, different concentrations of the same samples were loaded whereby the initial sample in the highest concentration, hH_V1-VSD to 2.95 mg/ml (151 µM) and DrVSD1 to 3.17 mg/ml (181 µM), was diluted 1:3 and 1:17 in SEC running buffer (50 mM K_2HPO_4 pH 7.0, 200 mM NaCl and 0.08 % DPC). The elution profiles were compared and showed no difference (data not shown). This implied that the initial protein concentration seemed to be not the solely triggering factor for the observed aggregation during NMR measurements. Next, the highest possible initial VSD concentration (hH_V1-VSD 2.95 mg/ml and DrVSD1 3.17 mg/ml) was used for an overnight incubation of the same samples at different temperatures (Figure 23) (3.2.16). On the next day, the samples were centrifuged (30,000xg, 30 min, 4 °C) and reapplied to the SEC column. The elution profiles changed drastically (Figure 23 A/B).

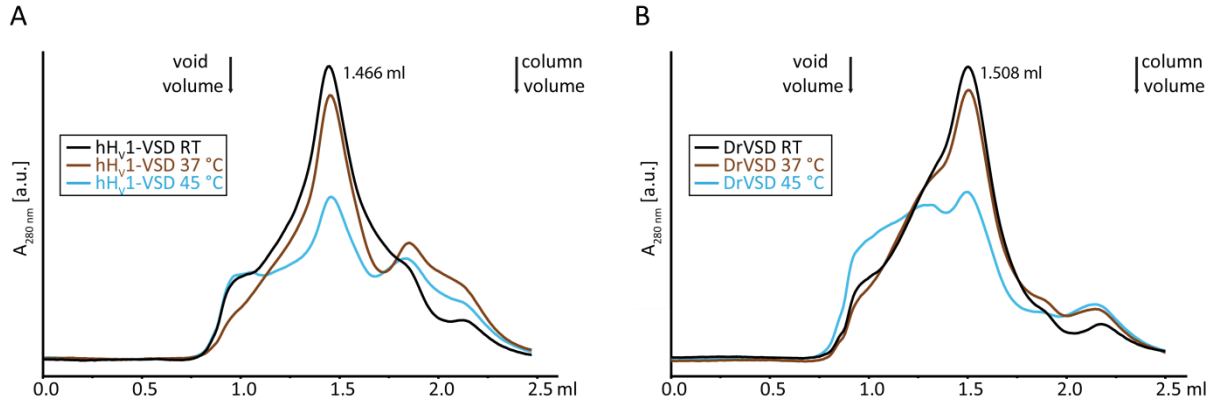

Figure 23: Temperature screens of different VSDs in DPC by SEC analysis. SEC runs were performed by injecting 50 µl of centrifuged protein to an analytical Superdex200 PC 3.2/30 column with a flow rate of 0.05 ml/min at 16 °C in 50 mM K_2HPO_4 pH 7.0, 200 mM NaCl and 0.08 % DPC as running buffer. Black arrows indicate the void (0.89 ml) and the column volume (2.4 ml). Black lines represent the SEC profile of a sample incubated at RT, the brown line represent a sample incubated at 37 °C and the blue line a sample incubated at 45 °C. **A** The SEC profile of 151 µM hH_V1-VSD at the indicated temperatures shows one protein peak at 1.466 ml (~78 kDa) with a shoulder at lower elution volumes whose proportion increased over time. **B** The SEC profile of 181 µM DrVSD at the indicated temperatures shows one protein peak at 1.508 ml (~63 kDa) with a shoulder at lower elution volumes whose proportion increased over time. Higher aggregates in the void volume could be detected, which increased by raising the temperature up to 45 °C.

For both VSDs, the signal intensities of the main peak decreased with increasing incubation temperatures and the SEC profile shifted completely to smaller elution volumes. Comparisons of samples incubated at RT and 37 °C, respectively, revealed only a slight decrease in signal intensity at 280 nm. However, the overnight incubation at 45 °C caused peak shifts to smaller elution volumes indicating the formation of higher oligomeric species. The data suggested that the interplay between a high protein concentration, necessary for performing NMR experiments, and the incubation at high temperatures over prolonged periods during NMR measurements caused the origination of soluble aggregates. These aggregates could not be removed by tested centrifugation steps, sample filtrations or by ultracentrifugations. Examination of more detergents as stable environments for the VSDs with the described procedures would have been expensive and time-consuming. To streamline the screening procedure I tested if it is possible to recycle a cell-free produced sample for a variety of experiments with different detergents.

Simplified VSD sample preparation in different detergent environments

The method of detergent exchange of a membrane protein sample by TCA precipitation was described (Shenkarev *et al.*, 2010b) and transferred to my experimental set-up (3.2.17). Therefore, the P-CF-produced His-VSD-Strep pellets were solved in the “best suited” detergent know so far (DPC or Fos14), purified and the IMAC elution fractions were applied

to TCA precipitation. The resulting protein pellet was resolubilized in buffer containing the next desired detergent and/or a different composition to be tested. For the evaluation of this method, a DPC/LDAO (molar ratio and v/v ratio of 2:1) sample was processed. The comparison of the resulting NMR spectrum with one of an untreated sample yielded no difference. Thus, I assumed that the initial sample is unaltered after TCA precipitation (Figure 21 D; Appendix, Figure A 4 A). Consequently, I included this treatment to the sample preparation, which enables a fast and money-saving screening procedure for the identification of suitable conditions for VSDs in detergent micelles. The comparable spectra obtained for hH_V1-VSD in DPC/LDAO mixed micelles were still of poor resolution. Hence, the TCA precipitation procedure was applied to test different additives and their influence on VSDs behavior in detergent environments. To this end, the aforementioned mixed micelles were treated with lipids (POPE/POPG 3:1 w/w), the inhibitor Zn^{2+} was added to 400 µM ($ZnCl_2$), the pH was changed to 6.0, salt titrations were performed up to 400 mM NaCl and DrVSD was analyzed in DH(7)PC micelles (Appendix, Figure A 4). However, none of the tested conditions could improve spectra quality with respect to possible assignment processes or dynamic analyses.

Both VSDs may have a tendency to form soluble aggregates, which made them inaccessible for analysis by solution-state NMR in a detergent environment. The characteristics of these aggregates were not known at this experimental stage, but were under investigation in the next paragraph.

4.2.3 Oligomeric state of cell-free-produced VSDs in detergent micelles

Laser-induced liquid bead ion desorption (LILBID) mass spectrometry analysis was applied to define oligomeric states of the VSDs. The elution fraction of hH_V1-VSD in Fos14 after IMAC purification was either directly concentrated in 0.5-Amicon centrifugal filter units (MWCO 10 kDa), comparable to the His-DrVSD-Strep sample in Fos14, or buffer exchanged via Bio-Spin® 6 columns to 10 mM K_2HPO_4 pH 7.0 and 0.08 % DPC. Here, the hH_V1-VSD sample was then filtered through a 0.2 µm syringe filter and concentrated, too. The His-DrVSD1 sample in 50 mM arginine, 50 mM glutamine, 20 mM HEPES-NaOH pH 7.0 and 1.4 % DPC after TCA precipitation was concentrated. The residual 74 µl-sized samples of all constructs were centrifuged (30,000xg, 30 min, 4 °C) and buffer exchanged to LILBID buffer containing the desired detergent via Zeba micro spin desalting columns (3.2.18). LILBID measurements were done applying 3 µl sample (110 -170 µM) and a laser power of 23 mJ (Figure 24).

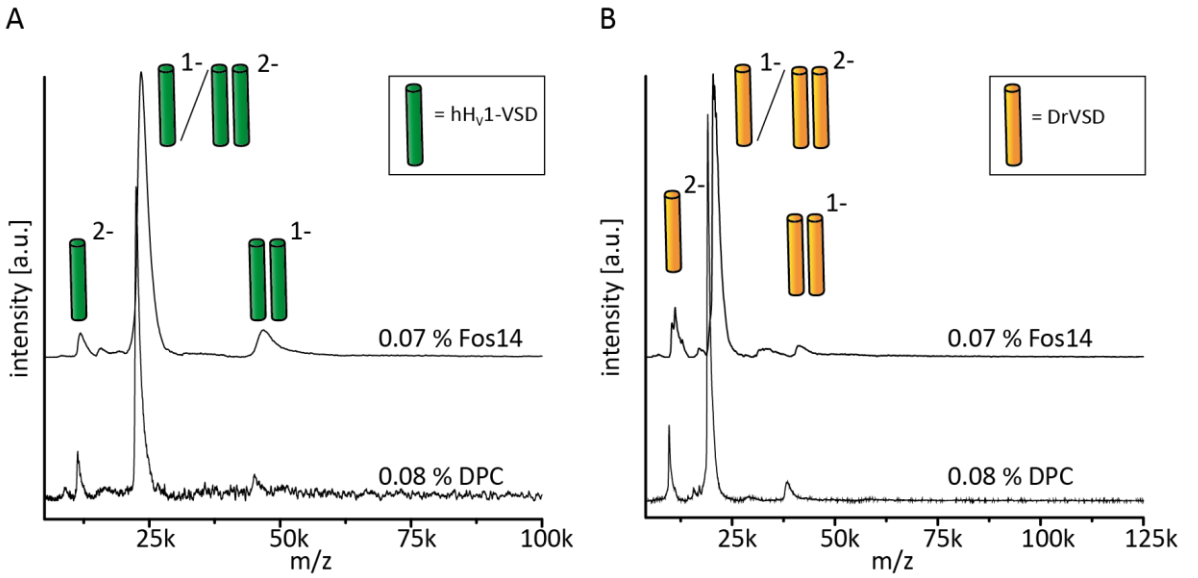

Figure 24: LILBID-MS analyses of VSDs in different detergents. Samples were measured in 50 mM ammonium acetate buffer pH 6.5 with a laser power of 23 mJ. Different complex states of the measured signals are highlighted by the pictograms above whereby one cylinder indicates a VSD monomer (green: hH_V1-VSD, orange: DrVSD). Superscripts represent the different charges of the monomers or dimers in mass spectrometry analysis. **A** $^{15}N,^{2}H$-labeled His-hH_V1-VSD-Strep was analyzed in Fos14 and DPC micelles. Monomeric and dimeric species could be detected. **B** $^{15}N,^{2}H$-labeled His-DrVSD-Strep was analyzed in Fos14. The DPC mass spectrum represents a $^{15}N,^{2}H$-labeled His-DrVSD1 sample (after TCA precipitation). Monomeric and dimeric species could be detected.

DrVSD and hH_V1-VSD could be detected as dimeric and monomeric species in Fos14 as well as in DPC. The size shift in DrVSD analyses corresponds to the different constructs used (3.2.18). The absence of higher oligomers possibly symbolizing aggregates could be due to the high laser power applied during the experiment, which could have destroyed higher molecular weight complexes. On the other hand, aggregates may not have entered the gas phase resulting in no net detection at the LILBID detector. However, LILBID-MS analysis was successful to evaluate the literature-described dimeric state for CF-produced VSDs (1.2).

Another strategy was applied, which focused directly on the determination of high molecular weight complexes in a protein sample (3.2.23). First, the VSDs were analyzed concerning their size by dynamic light scattering. The evaluation was based on the distribution either by intensity or by volume. This separation was necessary to visualize on the one hand the complete data set of size distributions and to obtain on the other hand information about the frequency distribution of each size in the sample. In detail, 10 times bigger particles scatter 100,000 times more light, which would drastically increase the measured signal intensity although these particles might be less represented compared to smaller ones. The DPC-containing buffer as a reference showed a well-defined peak at around 2 nm ± 0.4 nm

corresponding to an empty micelle with a molecular weight of ~20 kDa (Figure 25 A/B). The size distribution plot by intensity showed an additional peak at 230 nm for the buffer sample, which could not be detected in the evaluation pattern by volume and was not detected in each of the triplicate measurements (Figure 25 A/B). Hence, this size seemed to represent dust particles rather than buffer components. The VSD-containing sample showed a size shift compared to the DPC-containing buffer to a size of ~5 nm (± 2 nm) for the main peak (micelle with protein) with a shoulder attached (maximum at 22 nm). The analysis by volume revealed a more narrow size distribution to 3.4 nm ± 1.5 nm without a shoulder. The sizes correspond to a molecular weight distribution between 60-140 kDa. A precise molecular weight determination was complicated because suitable control proteins were missing. The overall protein shape has to be identical. Nevertheless, the size distribution coincides with results from SEC analyses, pointing towards monomers and dimers of the VSDs in a detergent micelle (Figure 23). Additionally, this experiment highlights the presence of expected higher molecular weight particles (>6 nm corresponding to >200 kDa). These findings raised the question if these high molecular weight particles belong to higher oligomers or soluble aggregates. Further experiments, like the NTA and RMM from the Malvern instrument company should help to answer this question (3.2.23).

A liquid stream of 0.31 mg/ml hH_V1-VSD sample was applied to the nanoparticle tracking analysis (Figure 25 C) (3.2.23). Although the sample concentration was with 9.6×10^{15} VSDs per ml way too high (max 10^{10}), particles between 50-300 nm could be identified with an average size of 92 nm. Taken together, these results showed that at 25 °C many soluble aggregates instead of only higher oligomers were present in the VSD sample. Moreover, the RMM determined their size to 387 nm and their concentration to 2.5×10^7 aggregates/ml (Figure 25 D). Nothing below a size of 200 nm could be detected with this set-up due to limits of detection in the resonator. For detailed analysis of size distribution, a repetition would have been necessary because only 255 aggregates were analyzed, which is far too less to draw valid conclusions. However, the concluding results of the Malvern experiments provided the hypothesis of the presence of soluble aggregates in the detergent-containing VSD samples, which could not be removed by applied ultracentrifugation or filtration steps.

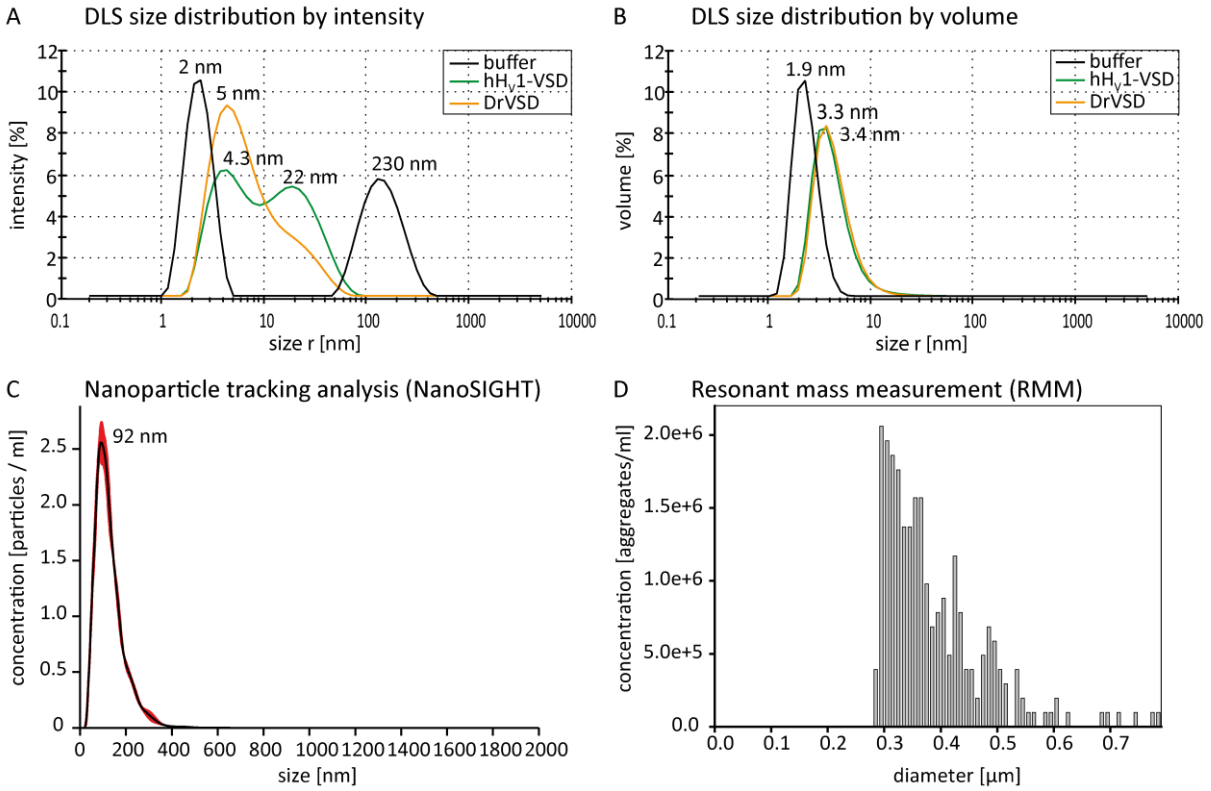

Figure 25: Analyses of VSDs aggregation using DLS, NTA and RMM. Experiments were performed with His-hH$_V$1-VSD and His-DrVSD1 in 50 mM K_2HPO_4 pH 7.0 and 0.08 % DPC. **A** DLS measurements were performed by Dr. Tartsch (Malvern Instruments Limited) on a Zetasizer Nano ZS. DLS analyses of the different VSDs (1.3 mg/ml) and buffer by intensity revealed the presence of higher oligomeric species (>6 nm). Black lines represent the DLS-profile of buffer, green lines the profile of hH$_V$1-VSD and orange lines the ones of DrVSD. **B** DLS analyses by volume showed that the fraction of higher-sized oligomers in the sample is negligible. Both VSDs have a size of 3.3-3.4 nm, which is nearly double to the size of an empty micelle (1.9 nm). Black lines represent the DLS-profile of buffer, green lines the profile of hH$_V$1-VSD and orange lines the one of DrVSD. **C** The NTA calculated the particle size of a 0.31 mg/ml hH$_V$1-VSD sample under a microscope to 50-300 nm. Thereby the size limitation is 10 nm (protein monomers or dimers cannot be detected). The red line demonstrates an average of three individual measurements with a mode value of the merged data of 92 nm. Measurements were done by Dr. Tartsch (Malvern Instruments Limited) with a NanoSight NS3000. **D** RMM, performed by Dr. Epe (Malvern Instruments Limited) with an Archimedes instrument, of hH$_V$1-VSD revealed a mean diameter of aggregates to 387 nm and a concentration of $2.5*10^7$ aggregates/ml. The detectable size limit is 200 nm. Soluble proteins and dust particles are not detected.

I speculate that these soluble higher oligomers act as an aggregation nucleus leading finally to protein instability and formation of aggregates during NMR measurements at high temperatures and high VSD concentrations. Despite that, cell-free-synthesized VSDs should be analyzed concerning their channeling mechanism by solution-state NMR. Hence, different strategies had to be developed.

Referring to possible L-CF production and purification of VSDs (Figure 12, Figure 17, Figure 18), their stability in a more native bilayer environment (lipids present) was now under investigation.

4.2.4 Stability screening of VSDs in nanodiscs

The VSDs could successfully be produced and purified in different NDs (Figure 12, Figure 17, Figure 18). POPE/POPG-containing NDs (conventional liposome mixture) exhibit poor stability. The insertion efficiency was highest in DMPG-composed systems (Figure 13). Hence, DMPG-containing NDs were initially applied for VSD insertion and NMR compatibility tests. Furthermore, different MSP variants were screened in NMR measurements concerning their experimental compatibility and overall stability. Spectra analysis revealed very low dispersed signals and instabilities for hH_V1-VSD in all tested NDs except ΔH5(-)-DMPG-NDs (Appendix, Figure A 5). Accordingly, the following stability screens were done with purified VSDs co-translationally-inserted into ΔH5(-)-DMPG-NDs. First, the efficiency of co-translational insertion was under investigation to ensure the final NMR analysis of homogenous samples in high concentration.

In more detail, the VSD molecules could have been only attached to the lipid surface of the NDs instead of being inserted. To rule out that the VSDs were completely embedded in the lipid bilayer His-DrVSD-Strep-NDs were treated with sodium carbonate buffer (3.2.12). 25 µl of NDs were incubated for 30 min at 4 °C with 25 µl sodium carbonate buffer pH 11.5. Subsequently, the samples were centrifuged and divided in pellet and supernatant fractions, which were analyzed by SDS-PAGE (Figure 26).

The co-translational insertion efficiency seemed to be 100 % as the same percentage of precipitated protein in the pellet fraction could be detected for a treated (+) and a non-treated (-) sample. Unfortunately, a control was missing, which could have shown the behavior of a sample with non-inserted membrane proteins treated with sodium carbonate. Consequently, I tried to include more experiments to confirm the statement of 100 % VSD-insertion into NDs.

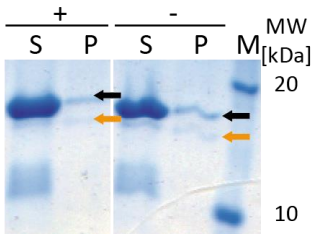

Figure 26: Test of co-translational insertion efficiency of DrVSD in NDs. DrVSD (orange arrow) was L-CF-expressed into ΔH5(-)-DMPG-NDs (black arrow) and treated with sodium carbonate to remove only partially bound protein after its purification. After a centrifugation step, supernatant (**S**) and pellet (**P**) fractions of treated (**+**) and non-treated (**-**) samples were analyzed on a Coomassie-stained 11 % Tricine gel. The protein marker is indicated by **M**.

The incorporation efficiency is not only important for the correct calculation of the VSD concentration, but also even more interesting for interpreting possible aggregation propensities. The more VSDs are only attached to the NDs the more hydrophobic parts are available for hydrophobic interactions of nearby non-inserted VSDs leading to the formation of aggregates.

In conclusion, the insertion was analyzed in more detail as a next step. The statement of a full integration into the lipid bilayer can be supported by protease cleavage assays (3.2.12). Defined cleavage sites are either accessible, and could be cleaved, or not pointing towards incorporated and therefore shielded protein regions or partially inserted species, respectively. The ExPASy PeptideCutter tool determined two thrombin cleavage sites for the His-DrVSD-Strep construct. Here, one was located directly after the His-tag in the soluble part and the second one should be located in the fourth transmembrane domain of the protein. I hypothesized that the first cleavage site would be available for thrombin cleavage, but the second one not when the VSD is completely incorporated in the ND. The cleavage was successful for the N-terminal located position (behind the His-tag), which could be validated by mass spectrometry and western blot analysis (data not shown). As no further cleavage products could be detected, the proposed cleavage site within the fourth helix was unaltered, possibly due to the burial within the bilayer. Another explanation could be that the predicted site Leu-Ile-Pro-Arg*-Val-Val deviates slightly from the conventional/consensus sequence, Leu-Val-Pro-Arg*-Gly-Ser, of a thrombin site and was therefore unaltered. Thought as control, the digestion of DrVSD by thrombin in detergent failed. No cleavage products could be detected. Either the detergent inactivates thrombin or the cleavage sites are shielded by detergent molecules. In conclusion, a positive control for the determination of the second cleavage site in the fourth transmembrane helix was missing so far not allowing for pertinent conclusions.

Consequently, I tested another method based on protein cleavage. A digestion with trypsin or another typical used protease was omitted due to parallel digestion of the NDs-surrounding MSPs, which would have hampered the analysis of cleavage patterns. Therefore, NTCB, a chemical hydrolyzing the peptide bond directly behind cysteine residues (3.2.12), was considered. MSP does not contain any cysteines. DrVSD and hH_V1 contain one cysteine residue predicted to be localized in the third or the first transmembrane segment, respectively. After the NTCB treatment, samples of DrVSD and hH_V1-VSD in NDs were

analyzed by SDS-PAGE revealing no cleavage products by comparing gel patterns with and without treatment (data not shown), pointing towards fully inserted VSDs. In addition, the cleavage of VSDs in detergent micelles was tested. No cleavage products could be detected. Either the detergents inactivate NTCB, the cleavage sites are shielded by detergent molecules or the NTCB is not active under the tested conditions. Again, a positive control was missing. However, different experimental set-ups gave the same results. VSDs seemed to be fully incorporated into the NDs.

Homogeneity screenings of VSDs embedded in a Nanodisc

Combining all information, DrVSD as well as hH_V1-VSD seemed to be fully inserted into NDs after co-translational expression in L-CF mode. In a next step, the stability and feasibility of dynamic measurements by NMR were evaluated by SEC and EM analyses. His-DrVSD-Strep and His-hH_V1-VSD-Strep were purified in a tandem purification procedure (3.2.9). The Strep-column elution fractions were dialyzed for 4 h against 2 l, against 1 l overnight and another 1 h against 1 l of the NMR buffer with 20 mM HEPES-NaOH pH 7.0 and 150 mM NaCl (DrVSD) or 20 mM NaCl (hH_V1-VSD) at 4 °C. The final samples were ultracentrifuged at 150,000xg for 45 min and analyzed by SDS-PAGE (Figure 28 F). Initial stability screenings were performed by applying the protein-NDs to the SEC column and analyzing the elution profiles (Figure 27).

DrVSD as well as hH_V1-VSD co-translationally-inserted into NDs showed nearly the same elution profiles. It was renounced to calculate the molecular weights by using the calibration data, because of the different running buffers used. However, the main peak could be detected at around 1.34 ml, which was slightly shifted towards lower elution volumes compared to the elution profile of empty NDs. Meaning that the ND-size increased due to the VSD insertion. This size-shift could also be detected in SDS-PAGE analysis when comparing the control signal (empty NDs) with the IP signal (hH_V1-VSD-NDs). I had to mention that the elution profiles of empty NDs differ in both figures due to different SEC running buffers and different ND batches used. However, the same ND preparations, which were used for the individual L-CF expressions, were always analyzed as the reference for each sample under the same conditions as the VSD-containing-ND. The ND batch for the hH_V1-VSD-production was thawed after storage at -80 °C, which could explain the broader peak in comparison to the elution profile of the batch of empty NDs used for DrVSD analysis.

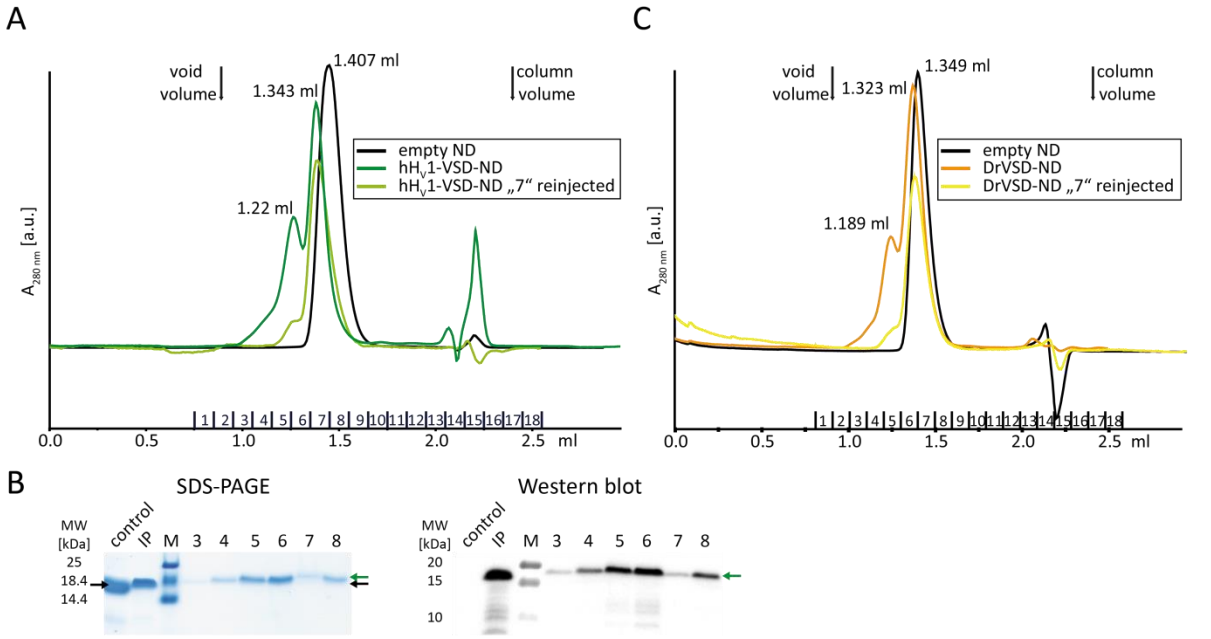

Figure 27: SEC analyses of VSDs co-translationally-inserted into NDs. The runs were performed by injecting 50 µl protein to an analytical Superdex200 PC 3.2/30 increase column with a flow rate of 0.075 ml/min at 16 °C. Black arrows indicate the void (0.93 ml) and the column volume (2.4 ml). Black lines represent the SEC profiles of empty NDs, green lines the profiles of hH_V1-VSD and orange lines the ones of DrVSD. **A** The profile for hH_V1-VSD in ΔH5(-)-DMPG-NDs is shown in comparison with empty NDs and fraction 7 reinjected. The running buffer was composed of 10 mM Tris pH 8.0 at 4 °C and 100 mM NaCl. **B** Fractions of the SEC run (**3-8**) of hH_V1-VSD-ND were analyzed by SDS-PAGE and western blot with an anti-His-antibody. The **control** represents empty NDs that show no signal in western blot analysis, as they contain no His-tag. The hH_V1-VSD (green arrow) could be detected in all analyzed elution fractions. Due to the small difference in size, a distinction between the MSP (black arrow) and VSD molecules in the SDS –PAGE was almost impossible. **IP** represents the hH_V1-VSD-ND sample prior to SEC-loading (input). The protein marker is indicated by **M**. **C** The profile for DrVSD in ΔH5(-)-DMPG-NDs is shown in comparison with empty NDs and fraction 7 reinjected. The running buffer was composed of 20 mM Tris pH 8.0 at 4 °C and 200 mM NaCl.

Both VSDs showed no aggregation peak in the void volume but a shoulder at lower elution volumes. Reinjection of elution fraction 7 successfully diminished the proportion of higher oligomers in the ND samples resulting in a well-defined elution peak. Furthermore, in SDS-PAGE and western blot analysis no higher oligomers for hH_V1-VSD could be detected. In comparison to the samples in detergents (Figure 19, Figure 20, Figure 21), there is already an improvement in the sample quality, most probably caused by the presence of lipids.

Next, the long-term stability of the whole sample was checked by storage for one month at 4 °C, centrifugation (30,000xg, 30 min) and reapplication to the SEC column (Appendix, Figure A 6). The elution profile of the one month-old DrVSD-NDs was identical with the fresh-prepared sample. The peak shoulder did not increase, meaning no presence of an aggregation nucleus. The samples seemed to be stable. Taken together, the elution profiles

of VSDs in NDs looked quite promising compared to the results in detergent micelles and the samples were stable at 4 °C for at least one month in a high concentration (100 µM).

In cooperation with Simone Prinz from the Max-Planck-Institute of Biophysics (Department of Prof. Dr. Kühlbrandt) in Frankfurt, TEM pictures of negative-stained ND samples were collected to further investigate the overall sample homogeneity and stability (Figure 28). Empty NDs, which were stored for two weeks at -80 °C, were diluted 1:10 (34 µM) in NMR buffer (20 mM HEPES-NaOH pH 7.0, 20 mM NaCl). His-hH_V1-VSD-Strep and His-DrVSD-Strep were L-CF-expressed in ΔH5(-)-DMPG-ND (same batch for both), purified using the tandem purification strategy, dialyzed against the NMR buffer, centrifuged, concentrated in Amicon centrifugal filter units (MWCO 10 kDa) and centrifuged again (16,100xg, 10 min, 4 °C). In addition, an ultracentrifugation step was performed for selected samples at 100,000xg for 30 min at 4 °C (Figure 28 C/D/E). The initial VSD-ND samples were diluted 1:1000 (hH_V1-VSD) or 1:100 (DrVSD) in NMR buffer for EM analyses and negatively-stained with uranyl acetate (3.2.20). Parts of the samples used for the grid preparation were applied to SDS-PAGE analysis (Figure 28 F).

Although the ND grid was overloaded, empty ΔH5(-)-NDs showed the expected size of 8-9 nm (Figure 28 A). Some kind of aggregates were visible (red arrow), which were not detected in previous SEC analyses. Two explanations were plausible. On the one hand, the aggregates could have been artefacts of the negative staining procedure or on the other hand it could have been no aggregates but stacks, which are described in the literature for NDs in TEM analysis (Bayburt & Sligar, 2003; Hopper *et al.*, 2013; Bibow *et al.*, 2017). However, when analyzing the hH_V1-VSD in NDs the aggregation problem was even more prominent (Figure 28 B). Large, oligomeric structures could be detected, which could be reduced to a minimum by an ultracentrifugation step, but were present again after sample incubation for 2 d at 4 °C (Figure 28 C/D). Interestingly, the pictures for the DrVSD construct in NDs after ultracentrifugation looked more promising (Figure 28 E). Although some small aggregates/stacks were visible, the overall particle distribution was homogenous. The size for both VSD-NDs could be determined to be between 11-12 nm, which was consistent with the results obtained by SEC runs where the elution volume of protein-NDs was shifted to smaller elution volumes compared to empty NDs (Figure 27).

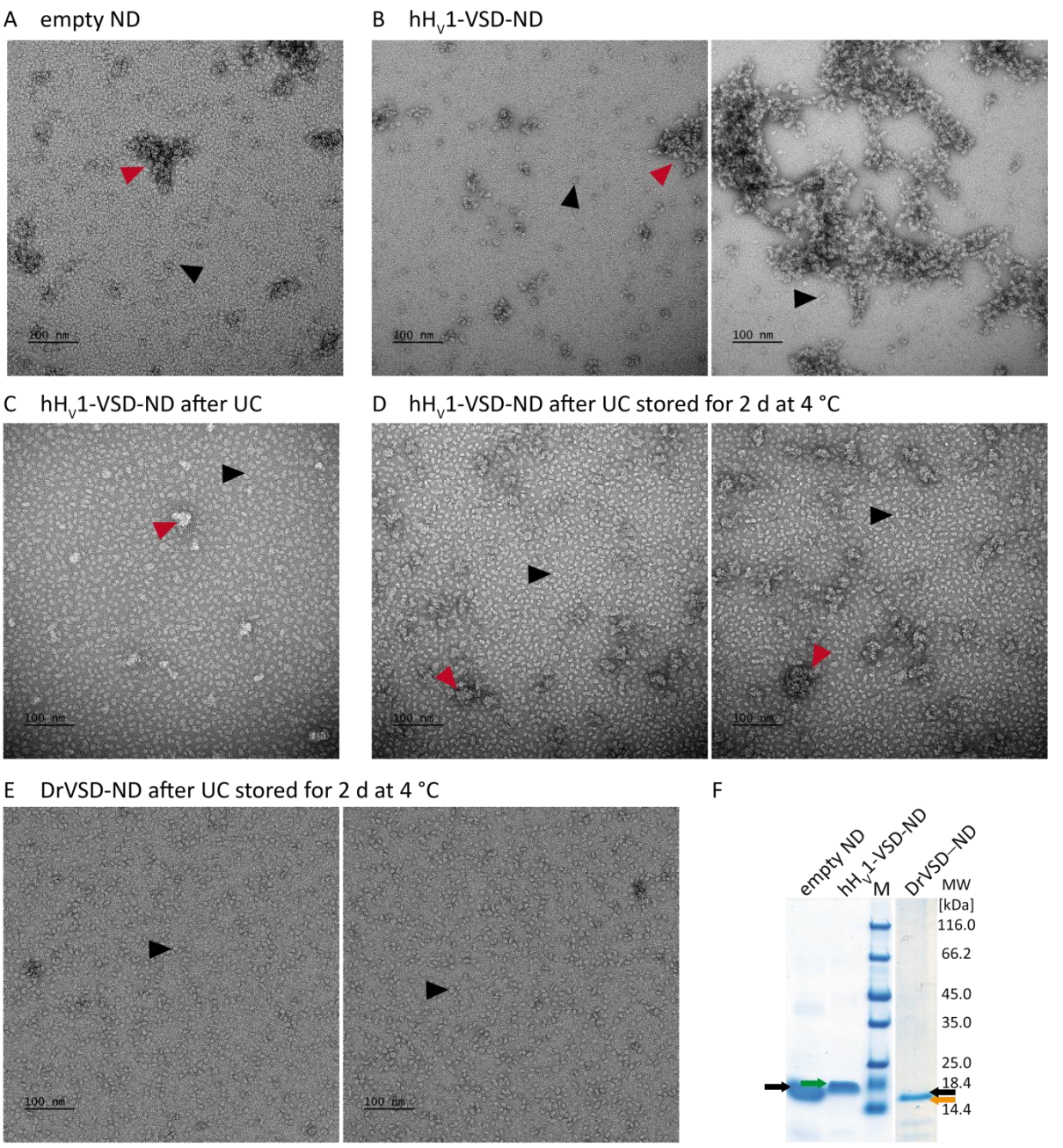

Figure 28: TEM observations of VSDs co-translationally-inserted into NDs. The samples were negatively-stained with uranyl acetate and analyzed on different copper grids by Simone Prinz (Department of Prof. Dr. Kühlbrandt MPI of Biophysics Frankfurt). Red and black arrows indicate aggregated or stacked NDs and single ND particles, respectively. Two pictures below the same heading represent two different spots on the same grid. **A** The picture shows an overloaded grid of empty NDs. A discoidal shape and size between 8-9 nm was detected. **B-D** The pictures show hH_V1-VSD-NDs differently treated as indicated (UC – ultracentrifugation). A size between 11-12 nm could be determined. **E** DrVSD-NDs are shown after 2 d incubation at 4 °C with a size between 11-12 nm. **F** A Coomassie-stained Tricine gel analysis of empty ΔH5(-)-DMPG-NDs (black arrow), ultracentrifuged hH_V1-VSD- (green arrow) and DrVSD-ΔH5(-)-DMPG-NDs (orange arrow) used in SEC, TEM and LILBID studies is shown. The protein marker is indicated by **M**.

Taken together, these results showed that the ultracentrifugation step after sample purification was essential and that the DrVSD-NDs seemed to be more stable than the ones of the hH_V1-VSD construct. TEM and SEC measurements allowed answering questions about

homogeneity and stability issues of VSDs incorporated in NDs. However, no statement about the oligomeric state of the VSDs in NDs is possible using these kinds of methods. The VSDs are too small to be detected in TEM analysis. The knowledge of the oligomeric state will help drawing conclusion about the native protein fold and the overall VSD stability in a lipid bilayer system. Whether aggregates could be detected will be the focus of the next section.

4.2.5 Oligomeric state of cell-free-produced VSDs in nanodiscs

LILBID-MS measurements facilitated the analysis of the native dimeric state of the VSDs in detergent (4.2.3) (Figure 24). Now, this technique was applied to analyze the oligomeric state of the VSDs in NDs (Figure 29).

The analysis of hH_V1-VSD-NDs (red curve) revealed a set of peaks representing the VSD only, the VSD attached to a MSP molecule and two VSD molecules only or attached to MSP (Figure 29 A). The hH_V1-VSD and the ND-surrounding MSP have nearly identical molecular weights. Hence, a conclusion by only analyzing the molecular weights whether the peak represents the VSD or MSP is not trivial. Here, the peak distribution helps to differentiate. However, the question was how to better distinguish two identical masses of two different proteins?

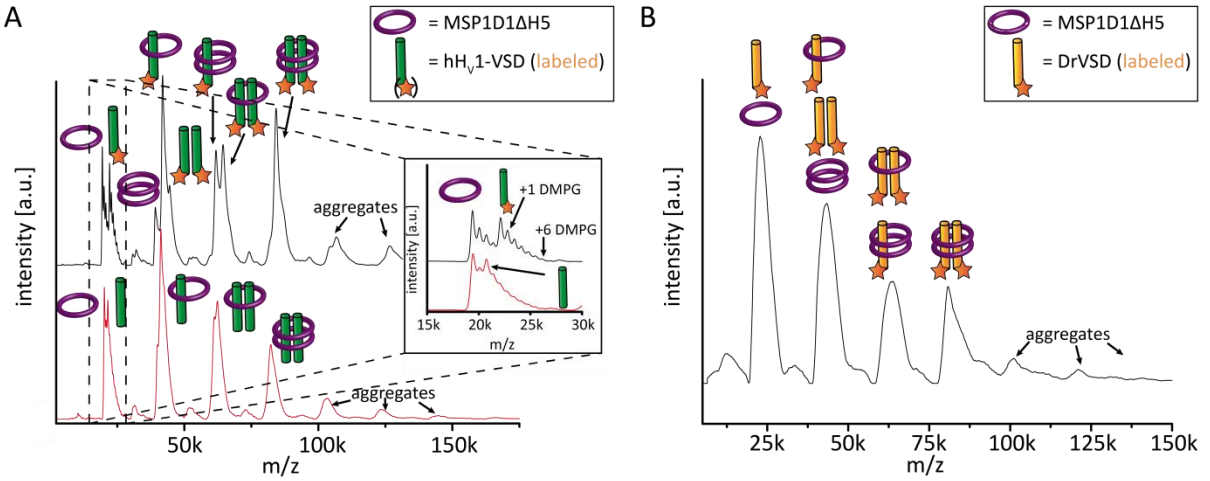

Figure 29: LILBID-MS analyses of hH_V1-VSD- and DrVSD-ND complexes. Samples were measured in 50 mM ammonium acetate buffer pH 6.8 and a laser power of 18 mJ. Different complex states of the measured signals are highlighted by the pictograms above, whereby green cylinders represent the hH_V1-VSD and orange cylinders the DrVSD construct. The purple ring represents the MSP molecule. The asterisk highlights heavy isotopically-labeled proteins (^{15}N,^{2}H-labeled His-hH_V1-VSD-Strep and ^{15}N,^{2}H,^{13}C-Ile/^{13}C-Met-labeled His-DrVSD-Strep). **A** Labeled (black line) and unlabeled (red line) proteins were compared. Due to isotopic labeling, the size-difference between the scaffold protein (19.5 kDa) and hH_V1-VSD (20.8 kDa) could be increased by 1.4 kDa, which resulted in an enhanced spectra resolution highlighted by the inset (Henrich *et al.*, 2017a). Furthermore, this inset showed attached lipid molecules (DMPG) to the VSD construct. **B** Isotopically-labeled DrVSD (19.80 kDa) in NDs showed the same signal pattern as observed for the hH_V1-VSD-NDs. It is mostly detected as a dimer.

The combination of cell-free protein production and immediate heavy isotope labeling of the protein of interest was the key feature (Henrich *et al.*, 2017a). Heavy isotope labeling ensured the increase of the overall mass of the VSD construct thereby creating a size-difference of minimum 1 kDa, which enabled a peak splitting and therewith the opportunity of analyzing signals in more detail (3.2.18). Importantly, the labeling strategy showed an opposite effect for the DrVSD-NDs. The peak splitting was not present anymore (Figure 29 B). Here, the labeling of DrVSD increased its mass resulting in the identical molecular weight of MSP and DrVSD. However, both VSDs in NDs could be detected as monomers and dimers. Furthermore, the attachment of DMPG molecules to the hH_V1-VSD could be addressed pointing towards intact NDs under investigation after co-translational protein insertion and towards important lipid-protein-interactions. There was no evidence for the presence of higher oligomeric states of VSD-NDs when analyzing peak distribution and molecular weights of the signal patterns. Nevertheless, additional high-molecular weight signals were detected that point towards present aggregates in the ND-VSD samples.

In sum, for both VSDs in NDs the native dimeric state could be stated pointing towards stable and folded protein species. Hence, the proteo-NDs were applied to NMR experiments.

NMR analysis of VSD-ND complexes

Although the aggregation propensity could be shown for the ND samples by EM and LILBID-MS analyses, NMR studies were performed to investigate whether the higher oligomers would have the same unfavorable influence on spectra quality as it could be observed previously for VSDs in detergent micelles (4.2.2, 3.2.22). The samples used for the NMR measurements were L-CF-expressed in ΔH5(-)-DMPG-ND. Finally, purified and ultracentrifuged samples were analyzed by SDS-PAGE (Figure 28 F). TROSY spectra were recorded, which revealed a low resolution and peak dispersion comparable to the VSDs in detergent micelles (Figure 30 A/B left picture). Although the smallest, stable version of MSP was used, the overall VSD-ND-sizes seemed to be too big to enable reasonable molecule tumbling rates.

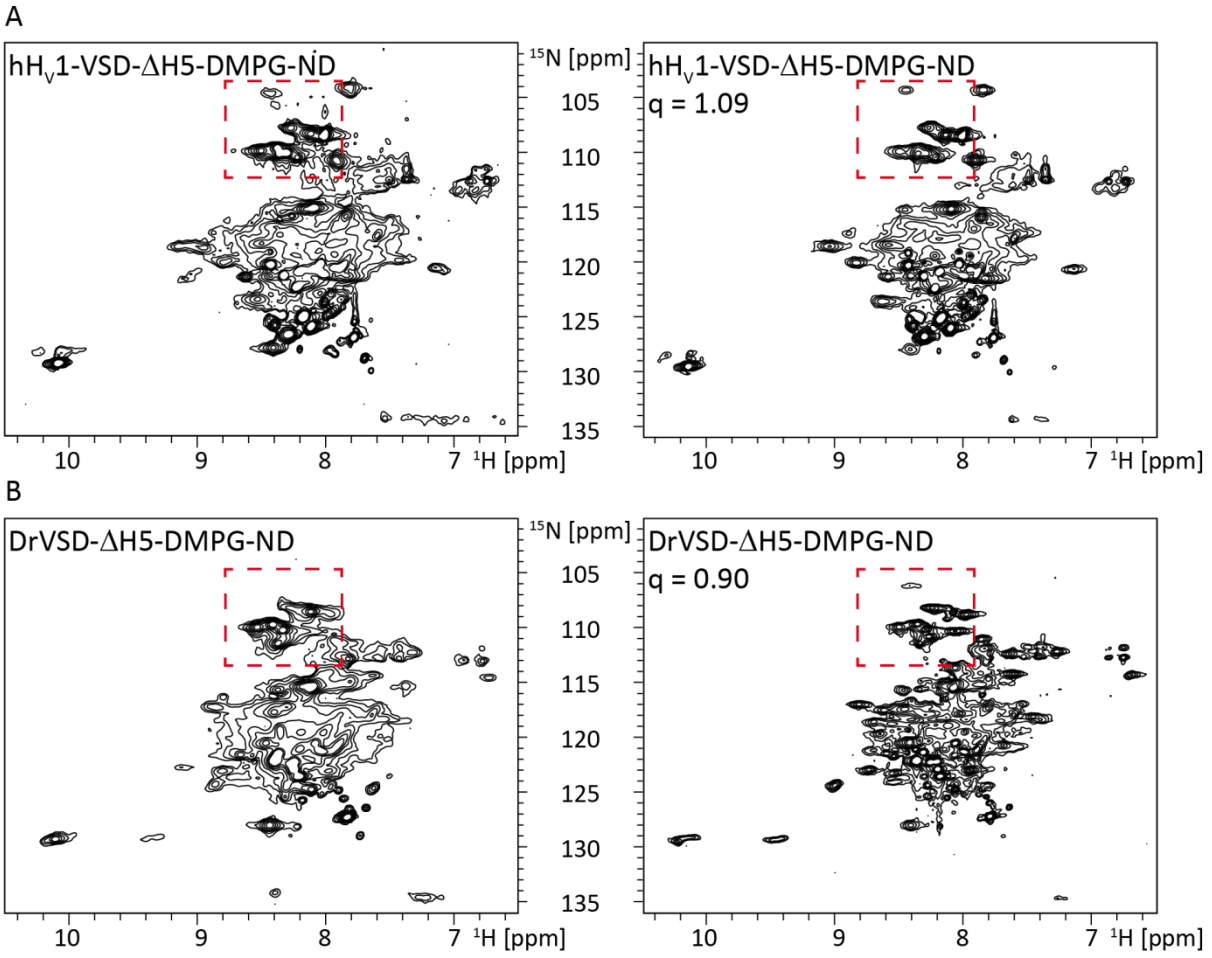

Figure 30: Effects of DPC titration on VSD-NDs. [^{15}N,^{1}H]-BEST-TROSYs were measured of samples in 20 mM HEPES-NaOH pH 7.0 and 20 mM NaCl. The red-dotted line shows the spectra region where mainly glycine signals are detected. As a representative, this region highlights the influence of DPC addition concerning signal resolution. **A** Spectra of ^{15}N,^{2}H-labeled hH$_V$1-VSD in ΔH5(-)-DMPG-NDs were recorded without (left) and with the addition of 0.2 % DPC (right) at 700 MHz and 318 K (NS = 384, TD1 = 256). The q-ratio of 1.09 was determined by recording 1D ^{31}P-NMR spectra (DPC/DMPG ratio). **B** Spectra of ^{15}N,^{2}H-labeled DrVSD in ΔH5(-)-DMPG-NDs were recorded without (left, 599 MHz, 313 K, NS = 512, TD1 = 256) and with the addition of 0.2 % DPC (right, 800 MHz, 318 K, NS = 432, TD1 = 352). The q-ratio of 0.90 was determined by recording 1D ^{31}P-NMR spectra (DPC/DMPG ratio).

A new strategy for membrane protein analysis in NDs by liquid-state NMR was invented in our lab (Laguerre *et al.*, 2016). Thereby, a detergent titration to membrane protein-embedded NDs peeled the protein away from the discs while keeping lipids attached and reducing the overall size, which improved spectra intensities and resolution. Some kind of bicelle-like structure is created. I transferred the described procedure to NMR studies of my VSD-ND samples (Figure 30 A/B right picture). Unfortunately, the DPC titration failed in gaining a reasonable enhancement in spectra resolution and dispersion, which would have been indispensable for further structural studies. However, some additional peaks appeared in the detergent-treated samples (especially in the glycine region, highlighted by the red-dotted lines) and the signals above 8.5 ppm and below 7 ppm in the ^{1}H-dimension

indicated folded protein structures. Furthermore, the Trp signal of both constructs was under examination. It should have shown two peaks for the hH_V1-VSD and one signal for the DrVSD construct. However, the signal was very broad and no defined peak number could be determined. This could have been a result of the increased flexibility of the attached Strep-tag (containing one Trp residue) or a result of different protein conformations present in the sample under investigation. However, the presence of the Trp signal indicated the analyses of full-length proteins as the Strep-tag was localized at the very C-terminus. Nevertheless, the information of full-length, partially-folded VSDs under investigation was not enough to ensure any dynamic or structural analysis. Neither in NDs nor in detergent micelles a spectrum could be generated that showed high resolution and dispersion. Instead, massive signal overlap and low peak dispersion were always detected. Another strategy, based on the selective labeling of amino acid side chains might have helped to gain some structural and dynamic information. Results are shown in the next paragraph.

Selective labeling of VSDs in NDs

Especially dynamic investigations do not necessarily need the analysis of the fully labeled protein. Protein parts, which are known to be involved in dynamic processes, can be analyzed in detail by selective labeling of specific residues. These parts can be deeply investigated by performing pH-, substrate-, or inhibitor-titrations. Selective labeling reduces spectra overlap and increases spectra resolution.

DrVSD spectra looked more promising than the ones of hH_V1-VSD. Consequently, this construct in NDs was initially applied to the selective labeling strategy. First, the NMR-sensitive nuclei, ^{13}C, was used in form of fully ^{13}C-labeled isoleucine and methyl-^{13}C-labeled methionine to obtain information about the protein fold, method feasibility and success rate of the invented detergent titration strategy for the VSD constructs in NDs. His-DrVSD-Strep was L-CF-produced in ΔH5(-)-DMPG-NDs and exclusively $^{13}C_6$,^{15}N-Ile and methyl-^{13}C-Met labeled. The remaining residues were fully deuterated, except of Cys, Gln, Glu and Trp, which were added in an unlabeled form to ensure a better sensitivity and therewith a higher resolution (2.5.5, 3.1.9). The downstream process was identical to the one described for the SEC-sample preparation (4.2.4) extended by a concentration step in Amicon centrifugal filter units (MWCO 30 kDa) followed by another ultracentrifugation step (150,000xg, 45 min, 4 °C). The final VSD concentration was calculated to be around 100 µM. [^{13}C,^{1}H]-SOFAST-HMQC spectra of labeled DrVSD were recorded (Figure 31 A).

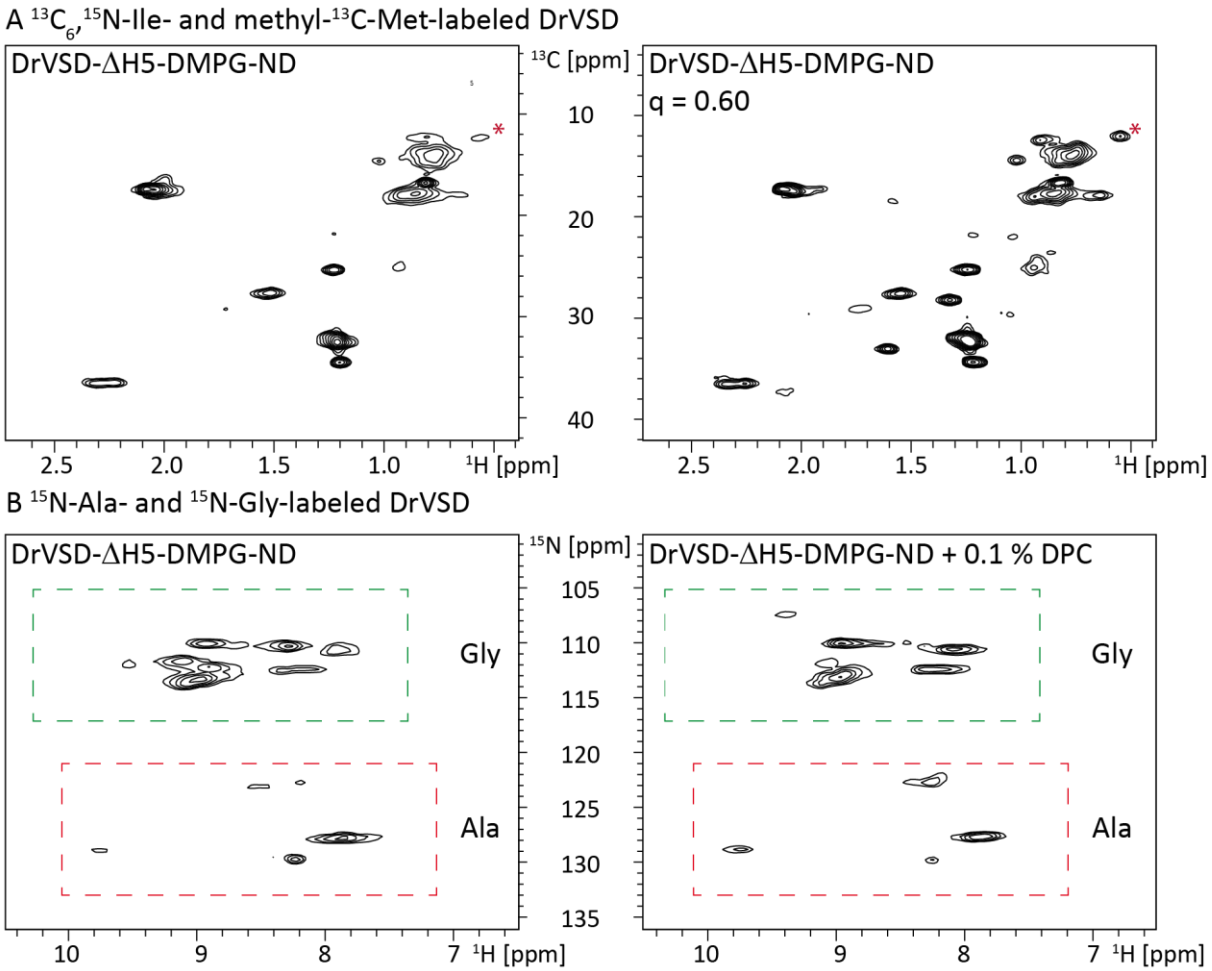

Figure 31: Detailed investigation of DPC titration effects on DrVSD-NDs. DrVSD was selectively labeled in L-CF expression and analyzed in 20 mM HEPES-NaOH pH 7.0, 150 mM NaCl (318 K, 800 MHz). Remaining residues were fully deuterated, except of Cys, Gln, Glu and Trp, which were added in an unlabeled form. **A** [^{13}C,^{1}H]-SOFAST-HMQC spectra of $^{13}C_6$,^{15}N-Ile- and methyl-^{13}C-Met-labeled DrVSD in NDs without (left) and with (right) the addition of 0.15 % DPC are shown (NS = 192, TD1 = 160) (Laguerre *et al.*, 2016). The red asterisk highlights a peak whose linewidths were analyzed to 119.7 Hz (left) and 166 Hz (right), respectively. The q-ratio of 0.60 was determined by recording 1D ^{31}P-NMR spectra (DPC/DMPG ratio). **B** [^{15}N,^{1}H]-BEST-TROSY spectra of ^{15}N-Ala- and ^{15}N-Gly-labeled DrVSD in NDs without (left, NS = 768, TD1 = 186) and with (right, NS = 560, TD1 = 128) the addition of 0.1 % DPC are shown. Regions for alanine (Ala) and glycine (Gly) signals were highlighted by the areas indicated by the dashed lines in red and green, respectively.

Shifts for the methyl-group of methionine were expected at around 1.72±1.89 ppm (^{1}H) and 17.24±4.42 ppm (^{13}C). Unexpectedly, only one pronounced broad peak could be detected instead of six peaks for the six methionine residues in the primary sequence (Figure 4). The other visible peaks belonged to the different chemical shifts of the isoleucine residues. For example, shifts for the isoleucine carbon CD1 were expected at 13.50±3.59 ppm (^{13}C) and 0.67±0.35 ppm (^{1}H). A broad signal met those criteria, but no resolution of 15 individual peaks representing the 15 isoleucine residues could be detected. Nevertheless, DPC titration increased the resolution highlighted by a red asterisk where the peak linewidth was analyzed to be increased to 166 Hz compared to 119.7 Hz without DPC addition (Laguerre *et al.*,

2016). Furthermore, additional peaks appeared caused by a faster overall tumbling rate due to softening of the protein-ND-particles. In sum, the selective labeling of specific residues in the VSDs using cell-free protein synthesis was successful and the new method of detergent titration to ND samples increased the spectra resolution. However, a statement about whether the full-length protein only was analyzed or not was not feasible due to insufficient peak dispersion. In detail, it could have been that only shorter fragments (Figure 10) of the constructs have been given signals in the NMR experiments while the full-length VSDs have been shown reduced signal intensities due to their size concerning their degree of aggregation. Another selective labeling procedure was implemented to address this question. Here, alanine and glycine residues were analyzed. To this end, the DrVSD construct was selectively labeled with $^{15}N,^{2}H$-Ala and $^{15}N,^{2}H$-Gly whereby the remaining residues were fully deuterated, except of Cys, Gln, Glu and Trp, which were added in an unlabeled form. The downstream procedure was the same as described before except that the ultracentrifugation procedure after sample concentration was replaced by the usual centrifugation step (30,000xg, 30 min, 4 °C). [$^{15}N,^{1}H$]-BEST-TROSY spectra were recorded with and without the addition of DPC and peaks were counted and compared to expected peak patterns (Figure 31 B). DPC titration increased the peak resolution. In addition, peaks were shifted especially in the glycine region, which might be due to environmental changes of loop regions when detergent molecules were present. The expected peak number of 11 glycine residues could not be counted due to peak overlap and missing resolution. Contrary, the four expected alanine peaks were present after DPC titration pointing towards the full-length VSD under investigation. However, the strategy of analyzing dynamic events by selective labeling of specific residues failed so far due to continuing loss of information in the tested samples (incorrect peak number, missing dispersion, and resolution). A conclusion whether peak absence/presence or shift events were caused by dynamic processes or even by low resolution or ongoing sample aggregation was not possible.

Next, many different conditions like lower pH, different detergents for the titration procedure or different salt concentrations were tested to increase the NMR spectra quality for the VSDs in NDs, but failed (Appendix, Figure A 7 and Figure A 8). Hence, I studied literature data to develop new strategies for increasing the NMR spectra quality. I found good quality NMR spectra of OmpX and bacteriorhodopsin inserted into ΔH5-NDs (Hagn *et*

al., 2013). Despite the fact that we are talking about model proteins under investigation the authors used a different protein-ND-insertion strategy. Here, the proteins were post-translationally reconstituted into NDs. To exclude co-translational insertion-induced problems the described strategy was tested for P-CF-produced, LPPG-solubilized and purified His-hH$_V$1-VSD (3.2.10). The protein insertion seemed to be successful as His-tag-cleaved-MSP and VSD co-eluted from an IMAC column (data not shown). However, the loss of protein during this procedure was more than 70 %. Consequently, this method was rated as uneconomically for NMR sample preparations from cell-free protein productions (inefficient, cost-intense). Thus, the strategy was avoided for VSD analyses.

In summary, the VSDs assembled in their native oligomeric state in NDs. Co-translationally inserted VSDs exist as monomers and dimers. Furthermore, data could be collected, which supported the full insertion in a co-translational manner of the proteins into the NDs. NMR spectra analyses revealed the presence of folded protein species. However, the overall quality was insufficient for further assignment processes or dynamic studies. Both the signal overlap and missing resolution pointed towards different conformational states of the VSDs in NDs or towards the presence of soluble aggregates causing an increased overall tumbling rate. Aggregates could be identified by EM and LILBID-MS analyses for high concentrated samples. These data were in agreement with the results obtained for cell-free-produced VSDs in detergent. In conclusion, VSD-NDs were not suited so far for investigations by NMR spectroscopy although the VSDs were embedded in a more native environment expecting a higher overall protein stability. These findings raised the question if the *in vitro* synthesis by cell-free expression caused a misfolding of the VSDs inducing an increased aggregation propensity. To answer the question, activity studies of cell-free-produced VSDs were performed and compared with literature results for *in vivo*-synthesized VSDs as only correctly folded proteins can show their specific activity.

4.3 Functional studies of cell-free-produced VSDs

Cell-free-synthesized VSDs are not described so far. Any new production procedure requires the proof of correct protein folding in form of verified activity studies. The proton channeling process for heterologous-expressed VSDs was adequately described by patch-clamp recordings (1.3.1). However, patch-clamp recordings were not directly possible with

cell-free-synthesized VSDs. Other strategies had to be followed to test for active cell-free-produced DrVSD and hH_V1-VSD. First, ITC experiments were performed to reveal the specific binding of the inhibitor 2GBI of CF-produced VSDs (3.2.23) (Figure 32). To this end, His-hH_V1-VSD and His-DrVSD1 were P-CF-expressed, solubilized in 1 % Fos14, purified via a Ni^{2+}-IMAC column, concentrated, buffer exchanged to degassed 50 mM K_2HPO_4 pH 7.0, 0.08 % DPC buffer and ultracentrifuged (300,000xg, 30 min, 4 °C). The concentrations were determined using an UV-VIS spectrometer in triplicate measurements to 64 µM for hH_V1-VSD and 73.6 µM for DrVSD1 (3.2.23). 1 mM 2GBI was dissolved in the same buffer with DPC for 2 h at 42 °C. The pH of the solution was controlled and compared to the pH of the sample buffer. The difference was less than 0.05 units. As a control, 2GBI was titrated into the sample buffer only to exclude any dilution artefacts, which could be misleadingly interpreted as a binding event. Only minor changes in the heat capacity could be observed (Figure 32 control).

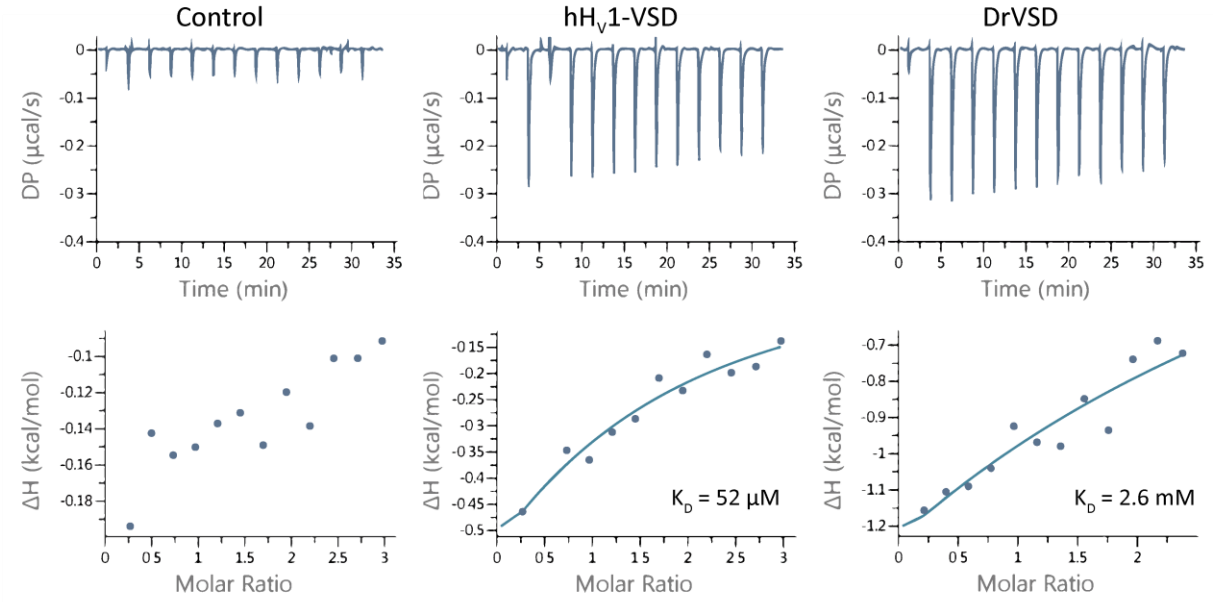

construct	VSD [µM]	N [sites]	ΔH° [kcal/mol]	TΔS° [kcal/mol]	ΔG° [kcal/mol]	K_D [µM]
hH_V1-VSD	64.0	1.30±0.320	-0.655±0.244	5.19	-5.85	51.9±30.2
DrVSD	73.6	1.00 (fixed)	-55.5±24.6	-52.0	-5.53	2600±1240

Figure 32: ITC analysis of VSDs titrated with the inhibitor 2GBI. ITC measurements were done on a MicroCal PEAQ-ITC system from Malvern instruments by Dr. Marenchino (Malvern Instruments Limited) at 298 K in 50 mM K_2HPO_4 buffer pH 7.0 and 0.08 % DPC. The 2GBI concentration was always set to 1 mM. As a control, 2GBI was titrated into buffer to exclude dilution effects in heat capacity changes. The evaluation was done with the instrument software and K_D values were determined to 52 µM for hH_V1-VSD and 1-2 mM for DrVSD1.

The analysis of hH_V1-VSD binding to 2GBI revealed a specific binding event with a K_D value of 52 µM±30 µM (Figure 32 hH_V1-VSD). The number of binding sites was determined to one. Both results were in direct agreement with published data (Hong *et al.*, 2013). Inhibitor binding studies with DrVSD have not been described so far. The K_D value of cell-free-produced DrVSD1 in DPC could be determined in the ITC experiments to 2.6 mM±1.24 mM by setting the N-value to one (Figure 32 DrVSD). Due to the solubility limitations of 2GBI in water, it was impossible to measure 10 times above its K_D value, which hampered a precise determination of thermodynamic parameters for the DrVSD construct. Further measurements would have been necessary. However, the data revealed inhibitor-binding events for both VSDs in detergent micelles. Defining the binding parameters of specific inhibitors gives valuable indications for the active fold of the channel, but does not completely reveal its translocation activity. Here, the gold standards are translocation assays, whereby a specific assay was invented for *in vitro*-synthesized voltage-gated proton channel VSDs by MacKinnon and co-workers (Lee *et al.*, 2009; Letts, 2014). The strategy is based on the reconstitution of VSDs into defined liposomes (3.2.13).

4.3.1 Reconstitution of cell-free-produced proteins

The reconstitution of cell-free-produced VSDs was the first step for performing activity assays. Liposomes with different lipid composition were prepared (3.2.13). The VSDs and the control protein MraY were P-CF-expressed, solubilized in LPPG, DPC or Fos14 and purified (3.1.9, 3.2.3, 3.2.5, 3.2.9). The pure proteins were used for the reconstitution approaches (3.2.13). Finally, an ultracentrifugation step was performed (300,000xg, 1 h, 20 °C) whereby proteoliposomes as well as non-embedded VSDs were present in the pellet fraction. Afterwards the pellet was resolubilized in liposome buffer and used for the fluorescence-based activity studies (4.3.2).

To test whether the reconstitutions of the VSDs were successful, analytical ultracentrifugations were performed for 1 h at 300,000xg and 20 °C (3.2.14). Afterwards, the centrifuge tubes were photographed to highlight the liposome-containing fractions in the sucrose density gradient (Figure 33 A/C/E). In addition, the different fractions were collected, treated with 100 % ice-cooled acetone to precipitate the protein content, centrifuged (30,000xg, 30 min, 4 °C) and washed once with liposome buffer. The resulting pellets were solved in SDS sample-loading buffer and analyzed by SDS-PAGE (Figure 33 B/D/F).

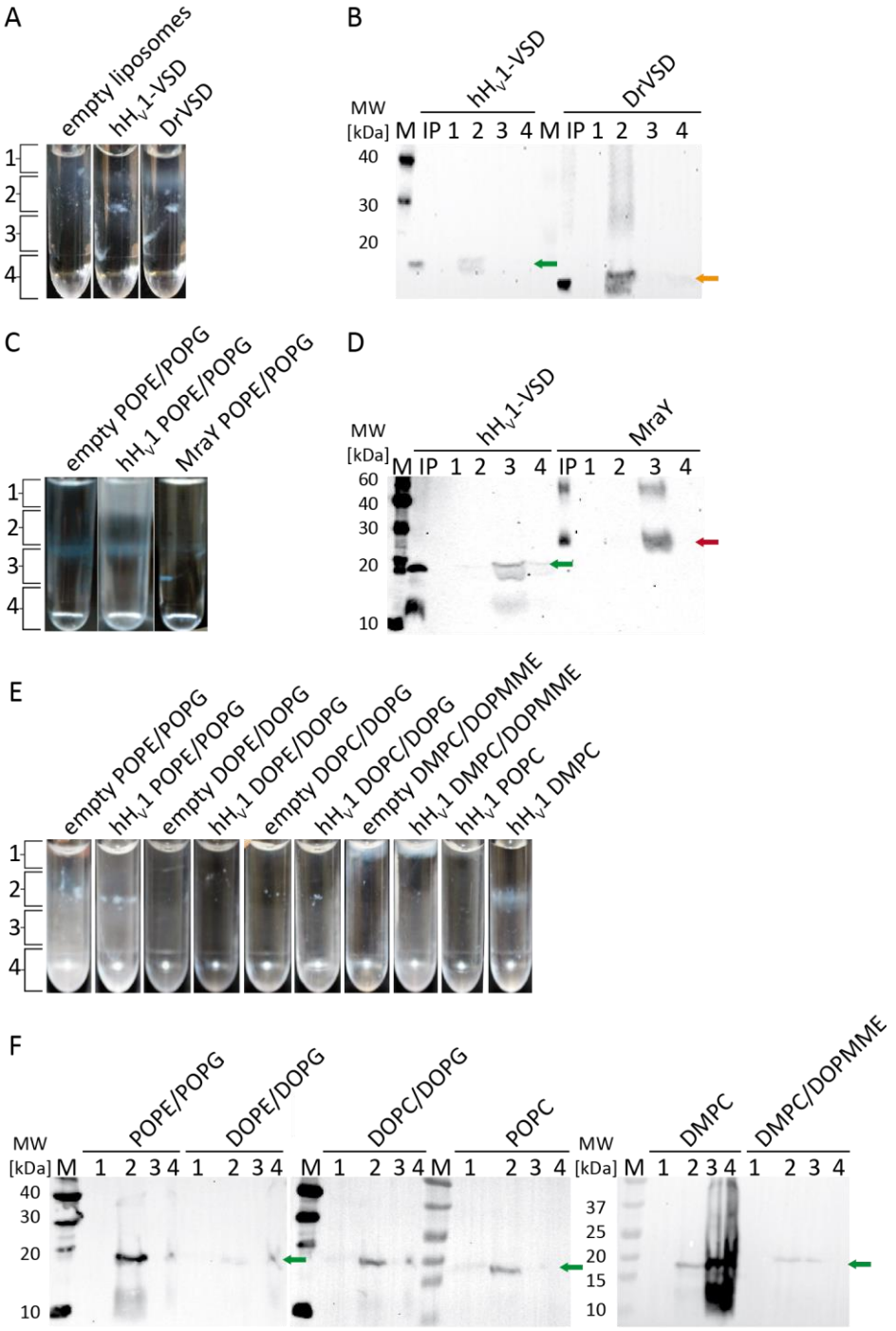

Figure 33: Sucrose gradient centrifugation analyses of reconstituted proteins. Shown are pictures from the centrifuge tubes after density gradient centrifugation (A,C,E) whereby the numbers indicate the different fractions taken out of the centrifuge tube. Here, 1 indicates the liposome buffer fraction, 2 the 5 % sucrose fraction, 3 25 % sucrose and 4 40 % sucrose. The corresponding SDS-PAGE analyses of the different fractions are shown too (B,D,F) (**M** – protein marker, **IP** – input; sample prior to reconstitution). **A,B** A comparison of reconstituted hH_V1-VSD (green arrow) and DrVSD (orange arrow) in POPE/POPG (3:1 w/w) liposomes showed the main presence of the proteins in the second fraction where also empty liposomes are located. **C,D** A comparison of reconstituted hH_V1-VSD (green arrow) and MraY (red arrow) in POPE/POPG (3:1 w/w) liposomes showed the main presence of the proteins in the third fraction where also empty liposomes are located. **E,F** A comparison of reconstituted hH_V1-VSD (green arrow) in different lipid-composed liposomes showed the main presence of the protein in the second fraction. Only for DMPC-containing liposomes hH_V1-VSD could be detected mainly in the third and fourth fraction.

The evidence for a successful protein reconstitution was indicated when the VSDs in SDS-PAGE/western blot analysis were present in the same fraction where liposomes were located (photo of the centrifuge tubes).

The reconstitution seemed to be successful for nearly all tested proteins and lipids. Comparable reconstitution efficiencies could be observed for the hH_V1-VSD and DrVSD constructs in POPE/POPG-containing liposomes (Figure 33 A/B). Nearly no protein could be detected in fraction four (precipitated protein). Moreover, also the protein MraY from *Bacillus subtilis* (Henrich *et al.*, 2016), which was later used as a negative control in the fluorescence-based activity assay, could be successfully reconstituted into POPE/POPG-composed liposomes (Figure 33 C/D). In addition, the successful reconstitution of hH_V1-VSD into different lipid-composed liposomes was demonstrated (Figure 33 F). Similarly to POPE/POPG-containing liposomes, here, hH_V1-VSD was detected in fraction 2, which represents the liposome-carrying fraction, although in some cases no liposomes were visible by eye after the analytical ultracentrifugation step (Figure 33 E). Only the insertion in DMPC-composed liposomes was inefficient. Here, only a small amount of the hH_V1-VSD could be detected in the second fraction. Most of the protein was precipitated (fraction 3/4). The same result was observed previously for the co-translational insertion of VSDs into DMPC-containing NDs (Figure 13). A detailed analysis of reconstitution efficiencies was not possible due to sticking of some protein fractions to the tube wall, which hampered the differentiation between the different fractions three and four. However, the performance of an analytical ultracentrifugation prior to the activity tests was necessary to validate the presence of proteoliposomes and thus, the differentiation between inactive protein and just not incorporated protein when interpreting results of the activity assay.

4.3.2 Activity test of cell-free-produced VSDs

After the successful reconstitution of the VSDs into liposomes, the fluorescence-based activity assay was performed (3.2.21). In brief, proteoliposomes were diluted 1:20 into flux buffer. After reaching a stable baseline, 20 nM valinomycin were added to induce a membrane gradient change causing an opening of voltage-gated channels (-60 mV inside). Proton influx led to a measurable fluorescence quench of the molecule ACMA inside the liposomal lumen due to its protonation. Finally, CCCP was added to open empty liposomes for estimating the overall channel activity. Unfortunately, the concentration of CCCP was set

to 2 mM in the first activity assays, as described in the PhD thesis of J. A. Letts, 2014. This caused a full sample precipitation and thereby impeded the correct evaluation of obtained results. Only the usage of the correct concentration of 2 µM CCCP led finally to comparable results of the performed activity assays with literature data (Lee *et al.*, 2009). However, that was the reason why I first started to validate this assay by using different potassium gradients, analyzing the negative control MraY (Figure 33) and testing the influence of nigericin as a proton ionophor instead of CCCP (Appendix, Figure A 9). As expected, increasing potassium gradients caused an increased fluorescence quench effect by stepwise raising the difference in membrane potential (Appendix, Figure A 9 A). The negative control MraY, as a membrane protein without any known proton channeling function, had no influence on the level of the fluorescence signal after valinomycin addition (Appendix, Figure A 9 B). Moreover, the addition of nigericin, known to disrupt the membrane potential, led to an influx of potassium ions and an efflux of protons from the liposomal lumen whereby ACMA got deprotonated, which recovered its fluorescence (Appendix, Figure A 9 C). Consequently, I could reveal the robustness of this assay, which now was used for activity measurements of hH_V1-VSD and DrVSD reconstituted in POPE/POPG (3:1 w/w) liposomes using the correct concentration of 2 µM CCCP (Figure 34).

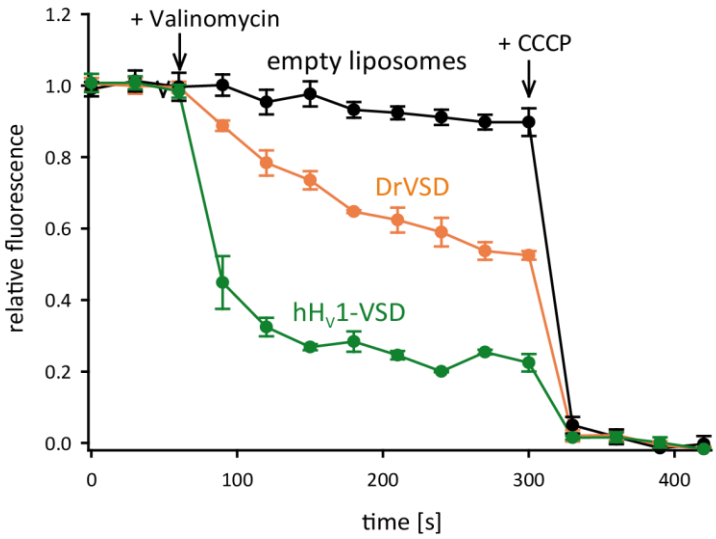

Figure 34: Flux assay analyses of DrVSD and hH_V1-VSD reconstituted in POPE/POPG-(3:1 w/w)-containing liposomes. The VSDs were TCA-precipitated after purification in Fos14 and resolubilized in DPC/LDAO (molar ratio of 2:1). Afterwards they were reconstituted in 200 nm liposomes in a protein to lipid ratio of 1:100. The flux assay was performed by diluting the proteoliposomes 1:20 into flux buffer. After 90 s incubation 20 nM valinomycin were added. After a further incubation of 210 s, CCCP was added to a final concentration of 2 µM. The fluorescence intensity was recorded at 480 nm (emission: 410 nm) and normalized by $(F_{obs}-F_{min})/(F_{max}-F_{min})$ whereby F_{max} is the average value of the maximum baseline prior to valinomycin addition and F_{min} is the average value of the minimum baseline after CCCP addition (n = 3). The different plots are indicated by different colors and labeled on top of each.

As a next step, the influence of the inhibitor 2GBI in the fluorescence-based activity assay was tested. Prior to activity measurements, 2GBI was dissolved to 4 mM in flux buffer and proteoliposomes were added in a 1:20 dilution. The fluorescence intensity values 210 s after valinomycin addition were plotted for the different liposomes under investigation in a reciprocal form to highlight the inhibitor influence. Furthermore, the significance of each event was calculated using the t-test (Figure 35).

As expected, no reduction in the fluorescence signal after valinomycin addition could be observed for empty liposomes. The addition of valinomycin to DrVSD-composed liposomes showed a fluorescence reduction of ~50 % without any inhibitor present, as observed before. Contrary, the fluorescence reduction under supplementation of the inhibitor 2GBI was negligible and approximately on the level of non-treated empty liposomes. This indicated that nearly no protons were channeled. Hence, the ACMA fluorescence signal was still present. The initial fluorescence reduction after the membrane depolarization step was 85 % for the hH_V1-liposomes. The inhibitory effect of 2GBI for the reconstituted DrVSD and hH_V1-VSD construct was significant.

Figure 35: Inhibitory effect of 2GBI on reconstituted VSDs. DrVSD and hH_V1-VSD in DPC/LDAO (molar ratio of 2:1) after TCA precipitation were reconstituted in POPE/POPG-(3:1 w/w)-containing liposomes, diluted 1:20 into flux buffer containing 4 mM 2GBI (**with inhibitor**) or not (**without inhibitor**) and incubated for 1 min. The fluorescence was detected at 480 nm and was recorded 210 s after the addition of 20 nM valinomycin. The plot shows the reciprocal value of the normalized fluorescence to better indicate inhibitor activity (n = 3). Additionally, the p-values (t-test) report the significance of the observed differences whereby empty liposomes showed no significant (**n.s.**) difference (p = 0.25). On the other hand, the inhibitory effect of 2GBI for DrVSD (p = 0.0079) and hH_V1-VSD (p = 0.046) is valid.

In summary, cell-free-produced hH_V1-VSD and DrVSD in POPE/POPG-containing liposomes are correctly folded, demonstrated by the specific proton translocation activity as well as the inhibitory effect of 2GBI. Moreover, the different K_D values determined by ITC and the different results in the inhibition studies in the flux assay experiments suggested different inhibitory mechanisms for both VSDs. Unfortunately the inhibitor binding did not increase the protein stability or NMR spectra quality (Figure 21 F; Appendix, Figure A 7 D and Figure A 8 D). Based on the K_D values for 2GBI, this was not surprising as high values indicate low affinity and therefore no strong interaction that would have been necessary for a stability-increasing influence.

The fluorescence-based activity assay provides a straightforward screening procedure of lipid-dependent VSD folding properties compared to the tedious initial screenings performed with NMR measurements (4.2). To this end, hH_V1-VSD was exemplarily reconstituted into liposomes composed of different lipids (3.2.13). The fluorescence intensities 210 s after valinomycin addition were plotted against the different lipid compositions (Figure 36). Empty liposomes were always present as a negative control where no fluorescence quench effect was expected.

As expected, the results showed no channel activity of hH_V1-VSD reconstituted in DMPC liposomes. Here, it was shown before that the reconstitution procedure was not efficient (Figure 33 E/F). In contrast, the successful embedding of hH_V1-VSD in POPC- and DMPC/DOPMME (1.5:1 w/w)-containing liposomes did not result in active protein samples. This implies a lipid-dependent activity of hH_V1-VSD. Interestingly, in lipid mixtures where PC and PG head groups were present (e.g. DOPC/DOPG), the hH_V1-VSD showed activity. Nevertheless, empty DOPC/DOPG liposomes were leaky, which hampered a detailed analysis of the exact activity of hH_V1-VSD in these liposomes. The highest quench effect of ACMA molecules was observed for hH_V1-VSD reconstituted in DOPE/DOPG-composed liposomes. Two explanations were possible. Either the amount of reconstituted protein was higher or the activity was enhanced by the influence of general bilayer characteristics. The reconstitution efficiencies were comparable for hH_V1-VSD in POPE/POPG, DOPE/DOPG and DOPC/DOPG liposomes (reconstituted protein located in fraction 2 and precipitated VSDs detected in fraction 4) (Figure 33 E/F). Hence, the activity seemed to be modulated by specific lipid contacts or differences in the lateral pressure or fluidity of the formed bilayer.

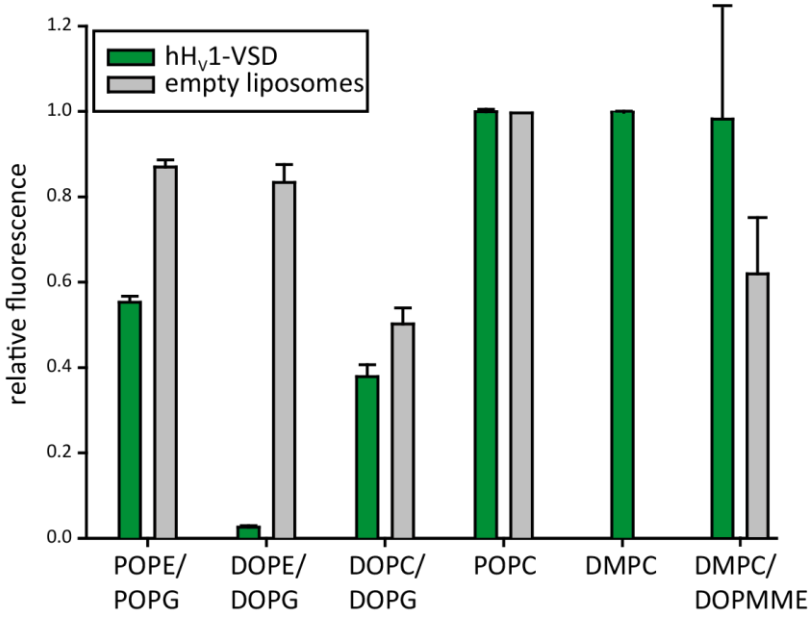

Figure 36: Lipid-dependent activity of hH_V1-VSD reconstituted in liposomes. The activity of hH_V1-VSD reconstituted in different lipid-composed liposomes was examined by the flux assay (n = 3). Therefore the proteoliposomes were diluted 1:20 in flux buffer and the fluorescence intensity was measured at 480 nm every 30 s before and after addition of 20 nM valinomycin. The measured values at 210 s after valinomycin addition were normalized by $(F_{obs}-F_{min})/(F_{max}-F_{min})$ whereby F_{max} is the average value of the maximum baseline prior to valinomycin addition and F_{min} is the average value of the minimum baseline after CCCP addition. Comparison of empty (grey bars) and proteoliposomes (green bars) revealed that the lipid composition with the highest quench effect observed was hH_V1-VSD reconstituted in DOPE/DOPG (3:1 w/w) liposomes. Empty DOPC/DOPG (3:1 w/w) liposomes showed a quench effect too, meaning they are leaky and not useful for further investigations. The control of empty DMPC liposomes is missing.

In summary, the results showed the successful reconstitution of detergent-solubilized VSDs gained by different preparation procedures. VSDs preserved their activity for more than 10 d storage at room temperature indicating a stable protein fold in liposomes (Warinner, 2015). Furthermore, their activity was demonstrated to be lipid-dependent. This raised the question whether VSDs in a liposome environment could be sufficiently stabilized to be analyzed in NMR experiments. Advantages of VSDs reconstituted into liposomes in comparison with previously described NDs are the presence of curvature in a native-like environment, the direct proof of protein activity/fold and the lack of MSP, which might interfere with the VSDs themselves or the lipid-protein contacts. Unfortunately, proteoliposomes are too large to be investigated by solution-state NMR. Hence, a compromise had to be found that would allow reconstitution of the VSDs in liposomes to ensure optimal protein-lipid contacts and a combined size-reduction to ensure liquid-state NMR measurements. A “new” refolding strategy for cell-free-produced proteins was invented (Focke *et al.*, 2016), which was based on the theory that membrane proteins solubilized in a harsh detergent obtain their native fold after reconstitution in liposomes.

Moreover, the membrane proteins were shown to preserve their native fold after resolubilization from liposomes by treatments with milder detergents. Afterwards proteins are in a micelle state with previous contact to lipids and have a reduced overall size suitable for solution-state NMR studies. For that reason, this strategy should be transferred to VSD preparations for improving finally sample as well as NMR spectra quality.

4.3.3 The refolding strategy

Previous screenings of the VSDs in detergent or NDs revealed a high aggregation propensity and allowed for speculations about misfolded protein samples. However, the activity of cell-free-produced VSDs in liposomes could be verified (4.3.2). A strategy was needed to combine a reconstitution step into liposomes and a post-treatment procedure allowing liquid-state NMR measurement. The refolding strategy was first invented by Dr. Valiyaveetil for the *in vitro*-synthesized K^+ channel KcsA and later transferred to cell-free-produced proteins in a cooperation with our group (Valiyaveetil *et al.*, 2002a; Valiyaveetil *et al.*, 2002b; Focke *et al.*, 2016). First, the described method had to be established in our lab (3.2.15). To this end, cell-free-produced KcsA was refolded and analyzed by SDS-PAGE (Figure 37). After refolding into liposomes, KcsA could be detected as an SDS-stable tetramer, which was in agreement with published data (Focke *et al.*, 2016). Hence, the refolding procedure worked. Next, the P-CF-produced VSDs were analyzed (Figure 37, P-CF pellet). His-DrVSD and His-hH_V1-VSD were solubilized in 1 % SDS and reconstituted into asolectin-containing liposomes without any purification step (Figure 37, refolding). Afterwards the proteoliposomes were treated with 1 % Fos14, incubated for 2 h at room temperature, and centrifuged at 30,000xg for 15 min and 4 °C to separate pellet and supernatant fraction (Figure 37, insoluble Fos14 and soluble Fos14).

The same migration pattern as described for the KcsA could be detected for the refolded VSDs. VSDs existed as monomers in the P-CF pellet fraction. After the refolding into asolectin liposomes, a size shift to higher molecular weights could be detected for the monomer fraction, which was due to SDS-stable lipid attachments at the protein. A second signal arose, which corresponds to a dimeric VSD species. The obtained native oligomeric state stayed intact after treatment of the proteoliposomes with Fos14. Moreover, 100 % of the protein could be recovered after liposome solubilization. Taken together, the refolding procedure for the VSDs was successful and led to the formation of SDS-stable native dimers.

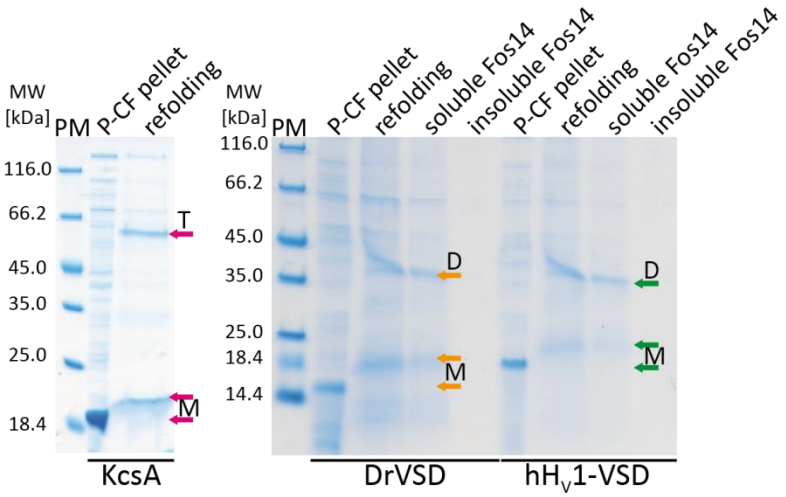

Figure 37: Refolding of KcsA and VSDs. The proteins under investigation are indicated below the SDS-PAGE figures. All proteins showed an overexpression signal in the pellet fraction from P-CF expression (**P-CF pellet**). The protein pellet was solubilized in 1 % SDS and reconstituted into asolectin liposomes (**refolding**). Additional attached lipids might explain the size shift in gel migration pattern for the monomeric (**M**) protein. Furthermore, a tetrameric (**T**) species for KcsA (pink arrow) and dimeric (**D**) species for DrVSD (orange arrow) and hH_V1-VSD (green arrow) could be detected in the proteoliposome fraction ("refolding"). The VSDs in liposomes were resolubilized with 1 % Fos14, followed by a centrifugation step at 30,000xg. In the soluble fraction, the tetrameric/dimeric states as well as the lipid attachment were still observable (**soluble Fos14**). No protein could be detected in the insoluble fraction after Fos14 treatment (**insoluble Fos14**). The protein marker is indicated by **PM** and molecular weights are listed on the left.

Subsequently, the activity of refolded VSDs was tested (3.2.21). The refolded, Fos14-solubilized VSDs were purified in Fos14 performing a Ni^{2+}-IMAC purification step. The elution fractions were collected, concentrated in Amicon centrifugal filter units (MWCO 10 kDa), centrifuged (16,100xg, 10 min, 4 °C) and the concentration was determined with a NanoDrop instrument. Afterwards, the VSDs were reconstituted 1:100 into POPE/POPG (3:1 w/w) liposomes and the fluorescence-based activity assay was performed. Both VSDs were functional (data not shown).

Next, the stability of refolded VSDs resolubilized in detergent was under investigation. Concentrated samples in Fos14 were loaded onto a SEC column (Figure 38 A). Additionally, the refolding was repeated with His-hH_V1-VSD-Strep whereby the liposome solubilization step was performed with DPC and the final sample was loaded onto the SEC column too. Fos14 was used as the primary detergent because it was described in the literature to be favored for the hH_V1-VSD stability (Li *et al.*, 2015). However, its micelle size of 41 kDa could have possibly hindered liquid-state NMR measurements as it would have drastically increased the overall molecule size and therewith the tumbling rate. Contrary, DPC micelles with a size of 19 kDa are more suited for NMR studies with membrane proteins. For that reason, hH_V1-VSD in DPC was additionally analyzed. Compared to previous obtained elution

profiles of the VSDs in DPC (Figure 23), the ones after refolding in Fos14 and DPC looked quite promising (Figure 38 A). Although a little shoulder for each peak could be detected, representing higher oligomeric species, the main peak was well-defined with an elution volume matching perfectly for dimeric hH_V1-VSD in Fos14 and dimeric hH_V1-VSD in DPC. The elution volume of the main peak of DrVSD referred to a monomeric protein species in Fos14 micelles. Additional small peaks at 2.05 ml (Fos14) and 2.15 ml (DPC) belonged to detergent molecules due to a higher detergent concentration in the samples compared to the running buffer caused by the beforehand performed concentration procedure of the VSDs.

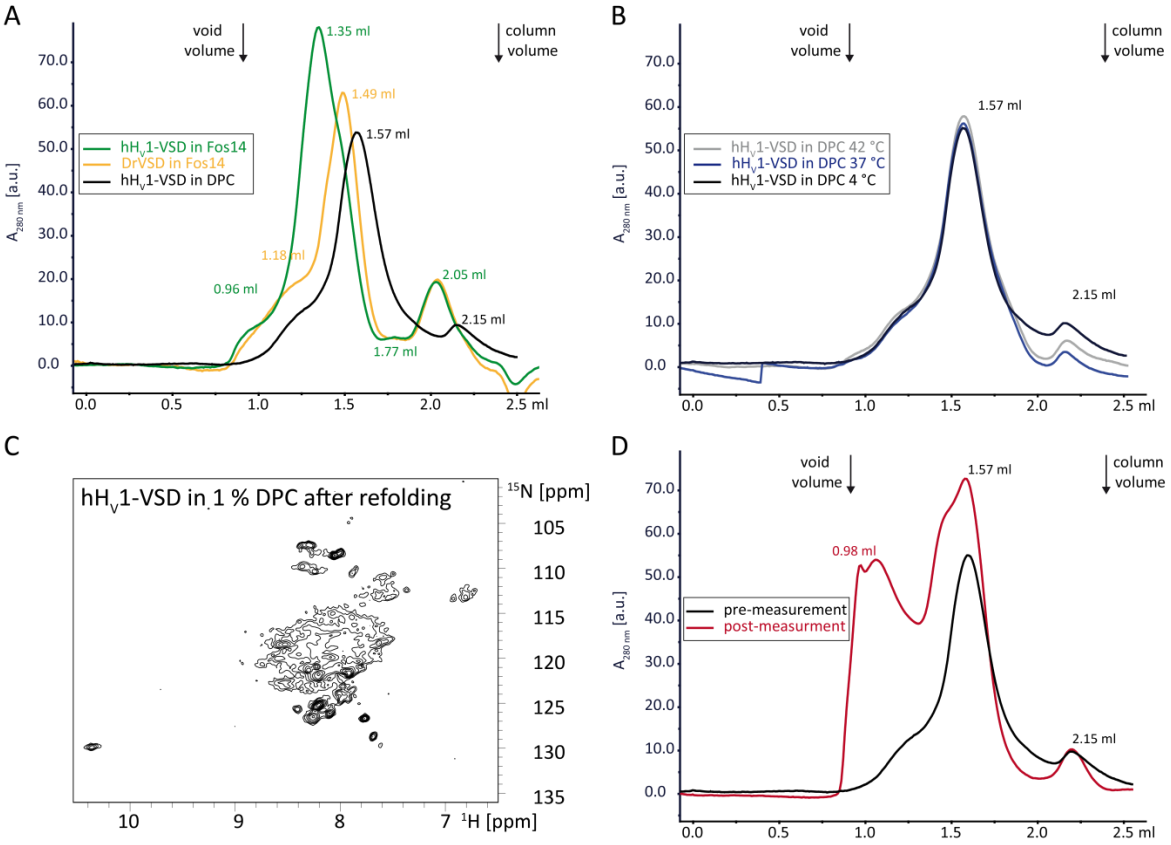

Figure 38: Stability screening of refolded VSDs by SEC and NMR analyses. The SEC runs were performed by injecting 50 µl protein to an analytical Superdex200 PC 3.2/30 column with a flow rate of 0.05 ml/min at 16 °C with either 20 mM Tris-HCl pH 8.0 @ 4 °C, 150 mM NaCl and 0.07 % Fos14 or 20 mM HEPES-NaOH pH 7.0, 200 mM NaCl and 0.1 % DPC as running buffer. Black arrows indicate the void (0.89 ml) and the column volume (2.4 ml). Prior to loading, the samples were centrifuged at 18,000xg for 15 min. **A** The quality screen of VSDs refolded, solubilized and purified in Fos14 and DPC showed evaluated peak maxima for hH_V1-VSD in Fos14 (green line) at around 140 kDa (1.35 ml), for DrVSD in Fos14 (orange line) at around 70 kDa (1.49 ml) and for $^{15}N,^{2}H$-labeled hH_V1-VSD in DPC (black line) at around 46 kDa (1.57 ml). **B** The sample of 33 µM $^{15}N,^{2}H$-labeled hH_V1-VSD in DPC was separated into three individual samples. They were incubated over night at the indicated temperatures and analyzed the next day by SEC runs. The profiles were identical. **C** The [$^{15}N,^{1}H$]-BEST-TROSY spectrum of $^{15}N,^{2}H$-labeled hH_V1-VSD was measured in 20 mM HEPES-NaOH pH 7.0, 20 mM NaCl and 0.1 % DPC and recorded at 318 K and 800 MHz (NS = 512, TD1 = 288). **D** A $^{15}N,^{2}H$- labeled hH_V1-VSD sample of around 76 µM in DPC was analyzed by NMR, centrifuged and loaded again onto the column (**post-measurement**) and compared with the sample of 33 µM (B) stored at 4 °C (**pre-measurement**). Shifts to smaller elution volumes could be detected indicating the presence of aggregates.

Next, the stability of the refolded hH_V1-VSD in DPC micelles (33 µM) was tested by incubation of the same sample at different temperatures overnight and reapplication to the SEC column as described previously (Figure 23, Figure 38 B). No changes in the elution profiles could be observed for any tested temperature even at 42 °C. Refolded VSDs seemed to be more stable than VSDs without any prior lipid contact. Finally, a NMR sample of refolded His-hH_V1-VSD-Strep in DPC was prepared to a concentration of 76 µM. No gain in resolution and dispersion could be observed for the refolded VSD construct (Figure 38 C). The data were in agreement with all other tested conditions. The spectrum from 7.5 to 8.8 ppm in the ^{1}H-dimension pointed towards an unfolded or even a very large protein sample. Only a few signals could be observed above 8.5 ppm or below 7 ppm that would have suggested folded protein structures. To test whether the results support the theory of an aggregation-induced effect, the NMR sample was centrifuged (30,000xg, 30 min, 4 °C) after the measurements were finished. The supernatant was analyzed again by SEC (Figure 38 D). The complete elution profile was shifted to lower elution volumes. A large peak could be recognized at 0.98 ml corresponding to high molecular weight compounds. The incubation at 45 °C for a longer time than 16 h and in a higher sample concentration caused the formation of soluble aggregates of refolded VSDs. In conclusion, the refolding procedure was successful, but failed for studying dynamics of VSDs by liquid-state NMR due to the same reasons as observed before. High sample concentrations and high incubation temperatures induced aggregation of the cell-free-produced, reconstituted VSDs.

5 Discussion

In the next chapter, the obtained results will be discussed and compared with current literature data.

5.1 Cell-free synthesis of VSDs

VSDs of different channel types have been extensively studied *in vivo* as well as *in vitro* to obtain a deeper understanding of their function and regulation. As mentioned previously, the cell-free system offers enormous advantages compared to the more common in-cell protein production (1.4). Successful cell-free synthesis could be described for other voltage-gated proteins like VDAC and K_VAP. In batch mode, pure protein, ranging from 20-300 µg/ml, could be obtained (Kovácsová *et al.*, 2015; Deniaud *et al.*, 2010; Renauld *et al.*, 2017). In comparison, here, I presented for the first time, the cell-free synthesis of active VSDs of human voltage-gated proton channels and zebrafish voltage-sensing phosphatases (4.1). DrVSD and hH_V1-VSD could be successfully produced in all tested modes up to 3.2 mg/ml expression (P-CF and L-CF mode). The D-CF mode was skipped due to intensive necessary screening procedures, high costs of specific detergents and low protein yields compared to P–CF and L-CF expressions (Genji *et al.*, 2010; Lyukmanova *et al.*, 2012). As an additional fact, harsh detergents like LPPG or milder detergents, as DDM, n-octyl-β-D-glucoside (β-OG) and DPC (known to solubilize best the VSDs [Figure 11]), in high concentrations are known to incapacitate the CF machinery (Proverbio *et al.*, 2014). However, if the initial contact of the VSDs with amphiphilic structures became necessary, amphipol molecules would provide an alternative way. Compared to detergents, they stick to the protein, caused by a very low cmc, resulting in avoidance of their addition to all used buffers during the VSDs purification procedure, making the process more cost-effective (Popot *et al.*, 2011).

The choice of the defined cell-free expression mode represents just a little step on the way to produce active proteins finally. Another important fact is the construct design, including expression vectors, tags, and codon-related properties (Haberstock *et al.*, 2012). First, I could figure out that less AT-rich sequences at the 3' end of the DNA lead to low or even no expression of the VSD constructs. As the His-tag is encoded by an AT-rich part of the DNA, it was extremely important to define it as the N-terminal protein tag (4.1.1, 4.1.2). Additional tags at the C-terminal end of the construct could be included without any problems.

Next, I focused more on the origin of the shorter VSD fragments that were detected after cell-free synthesis. Their presence could be due to translational stops during expression caused by e.g. RNA instabilities, different codon usage bias or hindered ribosomal contacts. Consequently, a codon-optimization process is mandatory. Our cooperation partners initially performed it. However, the procedure was repeated based on an algorithm, which is taking care of exclusively the rare codon optimization. Every new iteration results in a "new" optimized construct DNA sequence, which makes comparisons between different constructs considerably more difficult. In future, the initial codon optimization should be based on another tool e.g. from ThermoFisher, as it includes information of the folding and stability of the created mRNA as well as the expression host codon usage, creating finally only one optimized product. Nevertheless, the applied optimizations were successful and allowed further studies of the "full-length" construct only (Figure 15).

The different CF expression modes used in this thesis are discussed in the next sections in more detail.

5.1.1 VSDs produced in the P-CF mode

DrVSD and hH_V1-VSD could be successfully synthesized in CF without any supplementation of a hydrophobic environment (P-CF mode). Hereby, the proteins precipitated (Figure 9, Figure 10). This does not automatically implied unfolded VSDs. Other membrane proteins produced in P-CF and directly solubilized in detergent showed folded structures that could be revealed by NMR spectroscopy (Maslennikov *et al.*, 2010). Hence, I started screening different detergents to obtain suitable hydrophobic environments that enable high yields, correct folding and high stability of the VSD (Figure 11). The choice of the detergent is extremely important. Harsh amphiphilic molecules are good for solubilization purposes but may hinder folding issues, as it was shown for the hH_V1-VSD produced in *E. coli* cells and solubilized in LPPG (Letts, 2014) or for K_VAP solubilized in LPPG or 1-myristoyl-2-hydroxy-sn-glycero-3-phospho-(1'-rac-glycerol) (LMPG) micelles (Shenkarev *et al.*, 2010a). Interestingly, there are also examples were a harsh detergent e.g. LMPG results in folded protein species (Trbovic *et al.*, 2005; Klammt *et al.*, 2006; Maslennikov *et al.*, 2010; Klammt *et al.*, 2012). This means that it is difficult to transfer knowledge of detergent properties between different proteins under investigation. Milder detergents may result in folded

protein species, but the protein yield is drastically reduced e.g. for the VSDs when treated with DH(7)PC (Table 17). Yields can be increased by using harsh detergents for solubilization and stepwise exchange them by milder ones (Tumulka *et al.*, 2013). I could demonstrate an increased yield of around 300 % of the hH_V1-VSD solubilized in DPC and exchanged to DH(7)PC (4.2.2).

Most promising detergent surroundings for VSD solubilization were Fos14, Anzergent3-14, LDAO, DPC/LDAO (2:1) mixed micelles and DM or DDM. Fos14 and Anzergent3-14 were used for the analysis of in-*E. coli*-membranes-produced hH_V1-VSD (Li *et al.*, 2015), DDM for extraction and later exchange to DM for the functional analysis of hH_V1-VSD (Lee *et al.*, 2009), Anzergent3-14 for the functional (Li *et al.*, 2012) and LDAO for the structural analyses of CiVSP (Li *et al.*, 2014) and DPC/LDAO (2:1) for the structure determination of K_VAP by NMR (Shenkarev *et al.*, 2010b). The solubilization efforts as well as the functional tests with all these detergents for the VSDs under investigation in this thesis were more or less successful (Figure 11, Figure 34).

In NMR analysis, the peak resolution and distribution for His-DrVSD-Strep in DPC looked promising (Figure 39 A). However, when comparing this result with a spectrum obtained with the "new" His-DrVSD1 (after a 2^{nd} round of codon optimization), resolution was significantly worse, although stabilizing agents that support protein folding like glutamine and arginine were present in the sample buffer (Figure 39 B/C). Unfortunately, our data were in agreement with the notion that the dispersed and well-resolved peaks belonged to the previously observed shorter fragments of DrVSD and not to the full-length construct. Hence, construct fragments showed a tremendous influence on spectra quality. In conclusion, their occurrence necessarily had to be prevented. However, the NMR spectrum of the new codon-optimized DrVSD1 in DPC showed poor resolution, meaning that the overall VSD-detergent sample was of bad quality for NMR spectroscopy analyses. All chosen detergent environments failed in obtaining good quality NMR spectra for structural investigations (Figure 19; Figure 20; Figure 21; Appendix, Figure A 1 and Figure A 2).

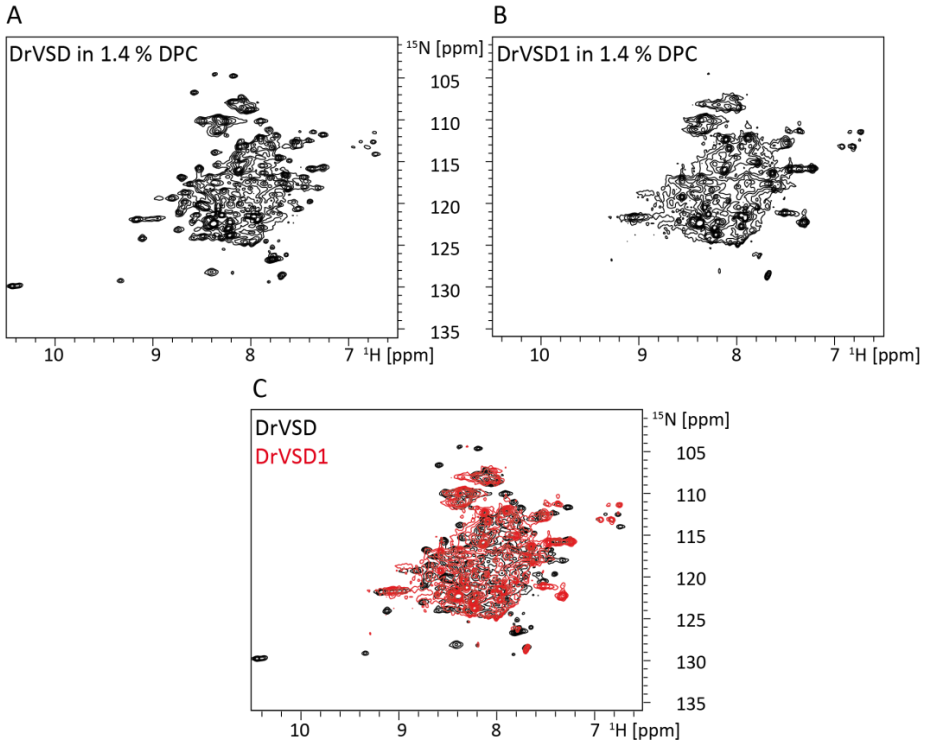

Figure 39: NMR spectra comparison of DrVSD with the new codon-optimized DrVSD1 construct. [^{15}N,^{1}H]-BEST-TROSY were measured of samples in 20 mM HEPES-NaOH pH 7.0, 50 mM arginine, 50 mM glutamine and 1.4 % DPC at 318 K. **A** The NMR spectrum of 120 µM (2.26 mg/ml) His-DrVSD-Strep is shown (NS = 256, TD1 = 352, 700 MHz). **B** The NMR spectrum of 170 µM (3 mg/ml) His-DrVSD1 is shown (NS = 256, TD1 = 315, 800 MHz). **C** The figure shows an overlay of the two spectra A and B to visualize the loss in peak signals, dispersion, and intensity. The color code is indicated in the legend.

Many more detergent screens are possible to increase the NMR sample quality by varying the head groups and tail lengths of the amphiphilic molecules. Another possibility would be the addition of styrene malic acid co-polymer lipid particles (SMALPs) (Knowles *et al.*, 2009; Postis *et al.*, 2015) to P-CF-produced VSD pellets. Thereby the SMA polymer can be used for direct solubilization to form disc particles without any detergent contact (Long *et al.*, 2013; Lee *et al.*, 2016), as it is not clear yet if the detergents might prevent VSD folding, thereby causing aggregation, finally leading to the loss of well-dispersed peaks in NMR analysis.

A comparable strategy, applied in this thesis was the production of VSDs of proton channels in a more native-like environment by the addition of lipid molecules to prevent detergent contact. The L-CF mode production is discussed in the next chapter.

5.1.2 VSDs synthesized in the L-CF mode

The P-CF mode can be described as a harsh method for protein production because the membrane proteins precipitate directly after synthesis and are solubilized afterwards in detergent. Folding properties, as discussed, might be hindered or even avoided. As the

sample quality for NMR investigations of P-CF-produced VSD samples was poor, I tested the L-CF expression. First, I could show a successful, lipid-dependent co-translational insertion of the active hH_V1-VSD into liposomes (Figure 14; Appendix, Figure A 10). Nevertheless, pre-formed liposomes in a CF expression set-up tend to fuse with each other (mainly caused by PEG) and tend to precipitate causing sample heterogeneity, which might hinder further analyses (Kalmbach *et al.*, 2007; Guilvout *et al.*, 2008; Berrier *et al.*, 2011; Roos *et al.*, 2013). Furthermore, liposomes are difficult to handle starting points for the analysis of protein dynamics by solution-state NMR.

A more common and useful tool are NDs for structural investigations of membrane proteins. Successful incorporation and structural analyses could be shown for *E. coli*-produced channels like KcsA and K_VAP (Shenkarev *et al.*, 2009; Shenkarev *et al.*, 2010a). However, in CF a structure determination was only feasible for the P-CF-produced, detergent-solubilized and in ND-reconstituted KcsA (Shenkarev *et al.*, 2013). Attempts for co-translational insertion with VSD from K_VAP and KcsA were not successful yet (Lyukmanova *et al.*, 2012; Paramonov *et al.*, 2017). Here, I demonstrated for the first time the successful co-translational insertion of VSDs in NDs (Figure 12, Figure 17, Figure 18) like it was shown for a variety of other membrane proteins (Roos *et al.*, 2012; Roos *et al.*, 2013; Roos *et al.*, 2014; Henrich *et al.*, 2016; Rues *et al.*, 2016; Henrich *et al.*, 2017b; Henrich *et al.*, 2017a; Rues *et al.*, 2018). The efficient L-CF production of VSDs in NDs offers numerous advantages in future. In more detail, it might be possible to fine tune the system with respect to oligomer insertion by adding different concentrations of pre-formed NDs and possibly observe additional lipid kick-out processes during protein insertion, which was not tested so far (Peetz *et al.*, 2017). This might enable to study the oligomerization behavior, lipid dependencies, and lipid contacts of proton channel VSDs in more detail. However, a test of functionality in NDs is strikingly difficult as two individual compartments are missing that are necessary for a change in the membrane potential to record voltage-gated channeling of protons. Attempts were made to record channel function in solid-supported lipid membrane experimental set-ups (Henrich *et al.*, 2017b), but has not been done so far for in ND-embedded VSDs of voltage-gated proton channels. Information whether the proteins in NDs are correctly folded had to be obtained elsewhere for example by NMR spectra recordings and peak analysis. Unfortunately, no measured NMR spectra of VSDs in NDs showed any well-dispersed peaks.

Always a massive peak overlap and low signal intensity was observed (Figure 30; Figure 31; Appendix, Figure A 5, Figure A 7 and Figure A 8). One could have argued that this is a result of the high flexibility described for VSDs of voltage-gated proton channels (DeCoursey & Cherny, 1998; Kuno *et al.*, 2009; Fujiwara *et al.*, 2012). But SEC and TEM results showed a different picture. The peak overlap and missing resolution seemed to be caused by an increased overall ND size. A significant size shift of loaded discs from 8-9 nm to 11-12 nm was observed in SEC and TEM analyses (Figure 27, Figure 28). In SEC analysis, usually increased hydrodynamic radii explain the size shift after membrane protein insertion, but here the VSDs have no large N- and C-terminal parts, which could have explained the increased diameter. In TEM pictures, the classical ND structure could be shown with an enlargement of the disc width after VSD insertion (Figure 28). Same observations were made by Lambert and co-workers who introduced the 50 kDa channel OprM post-translationally into MSP1D1-POPC-NDs (Daury *et al.*, 2017). Here, EM pictures of empty and loaded discs showed the highest swelling of the NDs when OprM was inserted as a trimer. In their study, the incorporation could be easily observed as OprM contains a large soluble domain that can be seen in TEM pictures. The VSDs under investigation lack such large recognition sites, which made the interpretation of the cause of the disc swelling difficult. Soluble proteins of known structure and stability used as a VSD tag might help in analyzing the VSD-NDs in TEM in more detail. Nevertheless, the enlargement of the ND after protein insertion was a first hint for a real insertion relative to an attachment only. Further tests were done to check for VSD-ND incorporation. First, I tested a $NaCO_3$-treatment procedure. This method is usually used for the removal of peripheral membrane proteins in liposome reconstitution experiments (Covino *et al.*, 2016). No precipitated VSDs were visible after centrifugation pointing towards completely inserted proteins (Figure 26). However, the procedure is solely described for soluble, peripheral-attached proteins and not for half-inserted proteins as it would be probably the case for hydrophobic VSDs. Additionally, as described for liposomes (Deniaud *et al.*, 2010), I tested the successful VSD insertion in NDs by protease treatment. Common proteases like trypsin or chymotrypsin cannot be used because the resulting SDS ladder would be far too complicated to be analyzed due to additionally digested MSP molecules coming from the ND preparations. Consequently, I decided to switch to proteases or chemical compounds, which are directed against the VSDs only e.g. thrombin and NTCB. Initial results looked promising, but the lack of convincing positive and/or negative controls

hindered concrete statements of VSDs insertion into NDs to be made. An alternative would be the use of atomic force microscopy (AFM) to test for efficient protein insertion into NDs as it could be successfully shown for other reconstituted membrane proteins (Klyszejko *et al.*, 2008; Blanchette *et al.*, 2009; Roos *et al.*, 2012; Zocher *et al.*, 2012).

In sum, many experimental results pointed towards successful co-translationally-inserted VSDs. Nevertheless, the simultaneously observed aggregate formation, seen in SDS-PAGE, SEC, and TEM analyses (Figure 17, Figure 18, Figure 27, Figure 28, Figure 29), raised additional questions. Are the VSDs not inserted into the lipid double layer as it was assumed based on experimentally obtained results, but are only attached to it? Do the hydrophobic patches of the non-embedded proteins consequently represent a kind of aggregation nucleus? Alternatively, is the aggregation caused by misfolded and therewith unstable VSDs?

As the first and second questions were answered with “maybe but unlikely”, the misfolding of the VSDs should be under investigation in the further discussion. Incorrect secondary, tertiary, and quaternary structure can be caused by incorrect lipid compositions or size of the NDs. Here, two scenarios are possible. The lipid composition and size are either critical for the embedded protein or for the stability of the whole ND.

Related to the first scenario, in L-CF mode with added NDs, a lipid-dependent rate of soluble-synthesized VSDs could be observed. Neutral charged phosphocholine (PC) head groups seemed to hinder the insertion. Oppositely, increased soluble VSD amounts were obtained when phosphoglycerol (PG) head groups, negatively charged, were present (Figure 13). Such a lipid-dependent post-translational and co-translational insertion could also be shown for other membrane proteins (Long *et al.*, 2012; Shenkarev *et al.*, 2013; Vaish *et al.*, 2018). In future, the insertion rate might be even more enhanced by the addition of cardiolipin during the ND formation as it could have been demonstrated for a carrier protein production in L-CF mode with pre-formed liposomes (Long *et al.*, 2012).

Concerning the stability of the whole ND, one might think about the usage of bigger MSP molecules for ND formation. The larger the MSP variants the more stable are the produced NDs and therewith maybe the embedded proteins too (Hong *et al.*, 2013). Nevertheless, liquid-state NMR studies are hindered with large protein-NDs. Here, solid-state NMR or cryo-EM studies, same as discussed for the L-CF-produced proteoliposomes, can be used for

structural investigations. Cryo-EM analysis would be especially important for the full-length DrVSP as it contains a large soluble C-terminal domain that could be structurally modeled based on known structures of related voltage-gated phosphatases (Matsuda *et al.*, 2011). Here, oligomeric as well as different gating states might be analyzed. However, in both experimental set-ups the analysis of dynamic processes will be hindered due to cryogenic samples with limited movement possibilities.

To sum up, maybe it would be the best to avoid external stimuli during cell free expression in form of added pre-formed NDs with a defined size and lipid composition, but better embed the VSDs in a specially chosen hydrophobic environment. This means that residual lipids of the cell-free extract could be attached to the membrane protein while at the same time it would be surrounded by a special hydrophobic material. Thus, one can prevent that lipids, maybe important for membrane protein folding, might be removed prior to insertion into pre-formed NDs or that the ND swells causing an instability of the whole complex during the co-translational insertion of the VSDs (Peetz *et al.*, 2017; Daury *et al.*, 2017). To this end, it was tested in our group to add a second plasmid containing the MSP expression cassette to the CF set-up. It was thought that residual *E. coli* lipids and the synthesized MSPs would form a ND-like structure thereby enabling the soluble production of membrane proteins. Unfortunately, the experiments failed although they also tested adding additional lipid molecules to the cell-free expression set-up. I focused on a related strategy. I tried to create a fusion construct of the VSDs and MSP (MSP-linker-TEV-hH_V1-VSD). Residual lipids could get into contact with the VSDs and would then be surrounded by the tagged amphiphilic helices of the MSP, which in turn creates again a ND-like structure that keeps the VSDs soluble. Unfortunately, these attempts failed so far. However, more intense screenings especially for lengths and amino acid compositions of the linker between the VSD and the MSP molecule, and screenings of MSP copy numbers following the VSD are necessary and might help to be finally successful. Later, an article was published were they described the same basic idea (Figure 40 A). Here, they fused N-terminally an MBP-tag and C-terminally a truncated version of the ApoA1 molecule to different membrane proteins, which resulted in their soluble production *in vivo* (Mizrachi *et al.*, 2015).

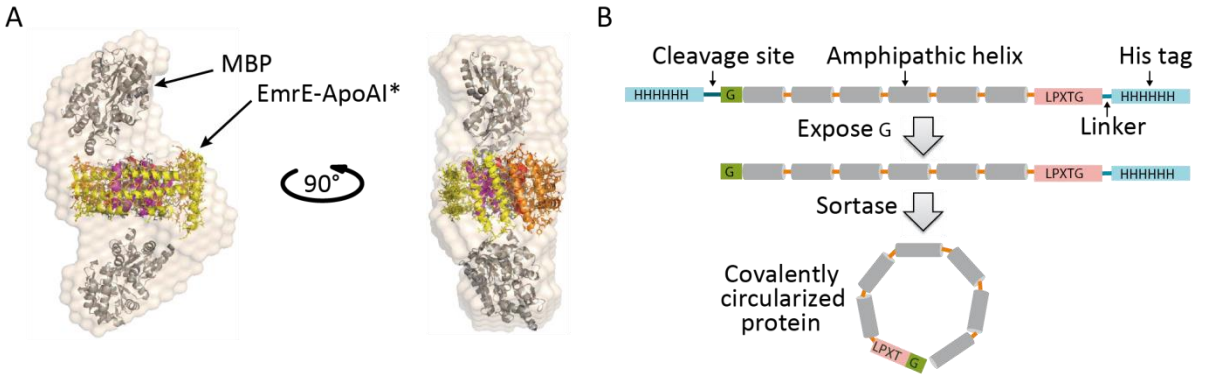

Figure 40: Upgrades in the nanodisc technology field. A Different side views of the fusion construct MBP-EmrE-ApoA1 are shown. The structure was constructed using obtained small-angle X-ray scattering (SAXS) data and the crystal structures of the individual components. The image was reprinted with permission from Mizrachi *et al.*, 2015. **B** A general strategy for the production of circularized ND of a defined size is illustrated. The sortase recognizes the glycine (G) and LPXTG motif at the N- and C-termini of the linear MSP-like protein inducing a final linkage to a circularized product (reprinted with permission from Nasr *et al.*, 2017).

Another strategy based on the idea of avoiding the deformation of pre-formed NDs has been launched recently, the sortase technology (Figure 40 B). Here, an MSP is modified to bind sortase. The MSP is circulated by the sortase treatment, which enables a creation of a ND with a defined size (Nasr *et al.*, 2017). This size cannot be changed by protein insertion processes as the MSP ring is covalently linked. In contrast to the post-translational ND insertion procedure, the ND size can be controlled and adapted to any new protein of interest while considering their special needs. Using this technology, the NMR spectra quality of VDAC could be drastically enhanced compared to spectra in usual ΔH5-ND (Nasr *et al.*, 2017). This strategy should be transferred to the cell-free production of VSDs. On the one hand, they could be produced in P-CF mode, solubilized in detergent, and afterwards incubated with lipids, the defined MSP, and the sortase. On the other hand, the enzyme could be added directly to the cell-free set-up in L-CF mode with the MSP in form of a second transcribed and translated plasmid to ensure direct VSD-MSP contact during protein synthesis. This might help to enhance NMR spectra quality of the VSDs under investigation and should be tested in future experiments.

In sum, L-CF-produced VSDs were soluble and functional pointing towards a real ND insertion and a correct protein fold. However, good quality NMR spectra are missing. The reasons for that are so varied that special screening procedures are necessary to solve the problem in a time- and money-saving manner.

5.1.3 Design of experiments

In this thesis, P-CF and L-CF expression were used for the successful synthesis of VSDs of human voltage-gated proton channels and zebrafish voltage-sensing phosphatases. As discussed in the last sections, many parameters before, during and after the cell-free expression can be varied. Such variations enable the fine-tuning of the system to obtain finally increased protein yields with higher quality. As described already, the added liposomes and NDs in L-CF mode can be varied in their lipid composition and size beforehand. During the CF expression, hundreds of parameters can be changed including for example magnesium and potassium, plasmid, polymerase and extract concentrations. Figure 41 shows exemplarily a cell-free sheet used for the VSD production where modifiable components of feeding (FM) and reaction mix (RM) are listed. Traditional screenings of all listed components without any robotics and strategy in hand would fail due to massive sample productions and analyses.

Units	Concentration stock solution	RM components	Addition to RM [µl]	Added end concentration	Mg^{2+} amount [mM]	K^+ amount [mM]
mg/ml	20	Lipids	**0.0**	0.00		
x	1	S30-extract	**1050.0**	0.35	**4.9**	**21**
mg/ml	0.542	Plasmid	**83.0**	0.015		
U/µl	40	RNasin	**22.50**	0.30		
U/µl	6.5	T7-RNA pol.	**32.31**	0.070		
mg/ml	40	tRNA *E.coli*	**37.50**	0.50		
mg/ml	10	Pyruvat kinas	**12.00**	0.04		
%	15	detergent	*0.0*	0.00		
mM	25.00	RCWMDE	*120.0*	1.00		
mM	25.0	AA-Mix	*66.0*	**0.55**		
mM	1000	AcP	*60.0*	20.00		**22**
mM	1000	PEP	*60.0*	20.00		**67**
x	75	NTP	*40.0*	1.0		
mM	500	DTT	*12.0*	2.0		
mg/ml	10	Folinic acid	*30.0*	0.10		
x	50	Complete	*60.0*	1		
x	24	Buffer (H+E)	*110.0*	1.0		**50**
mM	1000	$Mg(OAc)_2$	*45.3*	15.1	**15.1**	
mM	10000	KOAc	*39.0*	130.0		**130.0**
%	40	PEG8000	*150.0*	2		
%	10	NaN_3	*15.0*	0.05		
		H_2O	**955.4**			
			2044.6		20.0	
		MIX I Vol.	*3000.0*			
		Volume RM	*3000*	TOTAL	**20**	**290.0**
		out of RM/FM	**807.3**		mM Mg^{2+}	mM K^+
					(+/- 2mM)	+/- 20mM)

ist 0,283

End concentration	FM components	Addition to RM/FM [µl]	additional supply to FM [µl]
	S30-buffer		17850
			1411
			383
			549
			638
			204
	detergent	**0.0**	
	RCWMDE	**2160.0**	
0.5	AA-Mix	**1188.0**	1020
	AcP	**1080.0**	
	PEP	**1080.0**	
	NTP	**720.0**	
	DTT	**216.0**	
	Folinic acid	**540.0**	
	Complete	**1080.0**	
	Buffer (H+E)	**1980.0**	
	$Mg(OAc)_2$	**815.4**	
	KOAc	**702.0**	
	PEG8000	**2700.0**	
	NaN_3	**270.0**	
	H_2O	*17196.6*	18406
		36803	*32594*
		14531	51000
	Vol RM+FM	54000	**51000**
		14531	**Volume**
	for RM	***-807.3***	**FM**
	for FM	13724.1	

Figure 41: Cell-free sheet of a P-CF expression. The tables include important components necessary for setting up a cell-free protein production. Here, added end concentrations as well as magnesium and potassium amounts can be varied.

Here, it would be best to focus on the strategy of design of experiments (Fisher, 1935; Vincentelli *et al.*, 2004; Willis *et al.*, 2005; Anselment *et al.*, 2010). To this end, software creates a matrix including all parameters, which should be screened at once. Results can be analyzed and contextualized. Hence, statements about what influences what and what is finally the best expression set-up can be made easily and in a time- and cost-saving manner.

This kind of strategy can be applied for the VSD production in different ways. If only the protein yield is important, fusion constructs of the VSDs with e.g. fluorescence tags/molecules would represent a fast and easy read-out system for analyses (Schwarz *et al.*, 2010; Proverbio *et al.*, 2013; Rues *et al.*, 2016). However, for my studies the correct folding of the produced VSDs was the remaining question and not the yield. Unfortunately a specifically read-out system was missing so far, which prevented the usage of the design of experiments strategy. In future, one might think of C-terminally attached protein-based folding reporters like fluorescent proteins or specific enzymes, which show their fluorescence or activity, respectively, only when the coupled protein of interest is correctly folded. If available, conformational specific antibodies would be a perfect verification tool of folded VSDs species after cell-free expression. The best would be a primary read-out system based on the VSDs activity to ensure correct statements of the VSD folding where no secondary reporters are necessary. In sum, the design of experiments strategy would be a fantastic tool for future studies with cell-free-produced membrane proteins in particular of voltage-gated proton channel VSDs.

5.2 Cell-free-produced VSDs: Properties and applications

The production of active VSDs in a cell-free system is favored over the traditional in-cell expression (1.4). Especially for subsequent applications like NMR studies, or mass spectrometry analyses fast and easy sample preparations and labeling using a CF platform are attractive. However, how do cell-free-synthesized VSD samples behave?

5.2.1 Optimization of purification strategies

First, purification strategies were planned and applied to voltage-gated proton channel VSDs. Initially, the synthesized VSD constructs, either solubilized in detergent or embedded in a ND, were applied to an IMAC column (Figure 17, Figure 18). Yields to an average of

2.5 mg per ml CF expression were obtained. A following Strep-purification procedure failed so far. In future, it can be used for increasing the final protein purity. Here, optimization in terms of buffer composition, protein loading (amount, contact time, temperature, and so on), and construct design e.g. the linker length between the VSD and C-terminally attached StrepII-tag could be applied. However, 100 % sample purity was and is not necessary to perform dynamic and functional studies using cell-free-produced proteins in solution-state NMR applications. In more detail, as the VSD sample produced in CF is solely labeled with heavy nuclei, the RM can be used directly in NMR experiments without any prior purification steps (Klammt *et al.*, 2004; Maslennikov *et al.*, 2010; Hoffmann *et al.*, 2018). In sum, I could show the successful purification of both constructs under investigation to more than 80 % purity.

Nevertheless, no matter which purification strategy was applied, always SDS-stable oligomers/aggregates appeared in SDS-PAGE and western blot analysis. Such SDS-PAGE ladders were described also for other reconstituted VSDs (Paramonov *et al.*, 2017). Not even the sample treatment with a urea buffer could avoid the presence of these artefacts. Incubation of the VSD samples at 95 °C prior the gel loading was omitted, as a membrane protein precipitation should be prevented (Schägger, 2006). Further experiments defined those higher oligomeric signals as real aggregates and not just artefacts caused by sample treatment with gel loading buffer or SDS-PAGE probabilities. Higher oligomers or aggregates can be of different origin. Hence, many parameters have to be screened related to the purification process. Stabilizing agents in the buffer, like arginine and glutamine, known to stabilize folding intermediates, different buffer exchange procedures (dialysis, desalting columns), and the implementation of ultracentrifugation steps failed in preventing aggregate formation. In future, other buffer systems can be tested (using the design of experiments approach 5.1.3) and the ultracentrifugation steps can be optimized by increasing time and speed to reduce the VSDs probability to form higher oligomers.

In summary, CF-produced VSDs of voltage-gated proton channels could be successfully purified in an one-step IMAC purification procedure with high yields, but showed a tendency for aggregation. Consequently, the question arose whether CF-synthesized VSDs are stable at all.

5.2.2 Stability of cell-free-synthesized VSDs

The protein stability can be determined in many different ways. Here, I used experimental strategies ranging from SEC to TEM to RMM analyses.

Stability of cell-free-produced VSDs in detergent micelles

First, I tried to determine the stability of hH_V1-VSD and DrVSD by recording CD spectra in a temperature-dependent manner (Figure 22). Detergent-solubilized samples only were under investigation, as the MSP in NDs would have shown an additional unfolding event during the experiment, which could not have been simply subtracted from the VSD signal. The transition temperature (T_m) for the constructs in DPC was determined to 75 °C. Such a high value is unrealistic, as for example, the T_m for lysozyme, known as a very stable, soluble protein, was determined to 70 °C (Kohlstaedt *et al.*, 2015). The individual recorded CD traces over the whole wavelength scale of the VSDs showed a reduction of the CD signal with increasing temperatures (Figure 22). This indicates an ongoing aggregation of the sample rather than representing an unfolding event. Additionally, I clearly observed a precipitation of my sample in the cuvette after the measurements. In sum, this would explain the lack of any CD signal at 222 nm at higher temperatures and resulted in wrong calculations of high transition temperature values. The T_m of a mutated mouse H_V1 in CYMAL-5 was determined to 71° C in a 7-diethylamino-3-(4'-maleimidylphenyl)-4-methylcoumarin (CPM) assay (Takeshita *et al.*, 2014). Thermodynamically stabilized or not, but these high values do not show the real protein unfolding events. I argue that this represents exclusively the unfolding of the SDS-stable transmembrane α-helices, which are known to lose their secondary structure at around 80 °C (Powl *et al.*, 2012). Additionally, in their described assay, the CPM is known to have a minimal interaction with detergent molecules, but needs to interact with the free cysteines for obtaining any signals in this kind of experiment. Detergent molecules shield cysteine residues in a membrane protein preparation. Hence, they can only get in contact with the CPM after the membrane proteins denaturation (Kohlstaedt *et al.*, 2015). This supports the statement of wrongly assumed high stability of the mouse H_V1 construct.

I also tried to test the unfolding of the VSDs in detergent and NDs with thermal shift experiments using the nanoDSF instrument from NanoTemper (data not shown). This assay is based on recording changes in the Trp fluorescence of a protein during an unfolding

process induced by heat. Measurements were only feasible with the hH_V1-VSD construct, containing at least one Trp residue. The DrVSD construct has no Trp at all. The transition temperature of hH_V1-VSD was determined to 80 °C. This represented again the unfolding of α-helices or even just protein precipitation. Another thermal shift assay I tried was based on the binding of chemical substances to unfolded parts of a protein resulting in an increased or either decreased fluorescence signal, e.g. of SYPRO orange (data not shown). Unfortunately, most substances bind to detergent molecules preventing the measurement of unfolding events with membrane proteins reconstituted in a detergent environment (Kohlstaedt *et al.*, 2015). In future, chemicals that bind directly to the folded protein and change their properties upon protein unfolding like 8-anilinonaphthalene-1-sulfonic acid (ANS) should be tested in thermofluor assays for stability determinations (Kohlstaedt *et al.*, 2015). To my knowledge, no further literature data of voltage-gated proton channel stability is available so far.

Because CD spectroscopy and other thermofluor assays could not provide satisfying results, it has now been tried to determine the VSDs stability by SEC analysis. As a result, I could show that VSDs of voltage-gated proton channels under investigation in my thesis were mostly unstable in detergent. Always high intense signals in the void volume region of the column appeared (Figure 19, Figure 20, Figure 21). Especially in temperature screens the fraction of higher oligomeric species raised (Figure 23). Comparable SEC screenings have been performed with an H_V1 chimera fused to EGFP. Here, they detected raising aggregates in time-dependent experiments in DM, LDAO and β-OG too (Agharkar *et al.*, 2014).

Furthermore, DLS, RMM, and NTA were applied to cell-free-produced VSD samples for stability determination. Here, again higher oligomeric structures in pure protein samples solubilized in detergent micelles were identified (Figure 25). Other reports about P-CF-synthesized VSDs showed a stable solubilization in Fos-detergents, but an insufficient NMR spectra quality for structural studies (Paramonov *et al.*, 2017). Their stability could be increased by lowering the pH to 4, but longer incubation times at 45 °C induced again aggregation (Paramonov *et al.*, 2017). Here, long-term stability could be shown in NMR analysis only for VSDs reconstituted in LPPG and LMPG, but information about distance restraints were missing what prevents concluding remarks about correct protein folding in these cases. J. Letts argued that his hH_V1 construct was stable in LPPG micelles as the HMQC

spectra showed a peak distribution of a folded protein. However, later he recognized that the side chain contacts point towards a misfolded protein species (Letts, 2014).

I could successfully demonstrate that refolding helped to stabilize the detergent-solubilized VSDs when comparing the temperature profiles of the SEC runs before and after treatment (Figure 23, Figure 38). The lipid contact during the reconstitution procedure in asolectin liposomes (one-step in the refolding protocol) seems to enhance solubility and little decreases the aggregation propensity. Nevertheless, the recorded NMR spectra at 45 °C showed no change in the peak distribution pointing again towards aggregates or even unfolded VSD species when incubated at high temperatures for a longer time than 16 h. Because of the enhanced stability of VSDs in detergent after refolding, close existing contacts with lipid molecules let hope for a higher stability of VSDs in NDs and liposomes.

Stability of cell-free-produced VSDs in NDs and liposomes

DrVSD-NDs stored for one month at 4 °C showed the same SEC elution profile when loading a 100 µM sample before and after the storage period (Appendix, Figure A 6). Initially, it seemed that VSD-NDs are substantial more stable than VSDs surrounded by detergent micelles. However, TEM recordings revealed nearly the same instabilities for both VSD-NDs.

Reconstituted samples in liposomes were also analyzed concerning their stability using the activity assay. A bachelor student under my supervision described the procedure in more detail in her bachelor thesis where she could figure out that the in-liposomes-reconstituted VSDs were stable for more than 10 days stored at room temperature (Warinner, 2015).

In summary, CF-produced VSDs in detergent micelles and NDs are not stable. Their stability could be enhanced by lipid contact, but was insufficient for structural investigations by solution-state NMR. An increased stability of CF-produced proteins might be achieved by direct PEGylation (Wilding *et al.*, 2018). Moreover, stabilizing agents like inhibitors (Laguerre *et al.*, 2016) or co-factors can simply be added in a cell-free expression approach to increase proteins stability. Attempts were made by supplementing the inhibitor 2GBI to VSD preparations (Figure 35; Figure 32; Appendix, Figure A 7 and Figure A 8). Determined K_D values for 2GBI indicated low affinity binding and therefore no strong interaction. In conclusion, this inhibitor was not suited for increasing the VSDs stability. In future, more

inhibitors and other possible binding partners should be screened, mainly by applying the design of experiments approach (5.1.3).

Next, I focused on the overall VSD folding and how it relates to the results of the stability experiments.

5.2.3 Folding properties of cell-free-produced VSDs

The protein structure is determined by its amino acid sequence (Anfinsen, 1973). However, the encoding is still a remarkable question. The influence of the environment, chaperones, trafficking sequences, folding catalysts and quality controls (e.g. the unfolded protein response) is complex and especially in *in vitro* experiments difficult to implement (Dobson, 2004). In our cell-free set-up, folding is supported by different chaperones and triggering factors present in the extract itself (Foshag *et al.*, 2018).

Using the CF system without any additional supplementation, I was able to produce pure, more or less stable, and active VSDs of voltage-gated proton channels and voltage-sensing phosphatases. Here, active VSDs indicated folded protein structures (5.2.5). Analyzing different NMR spectra, peaks in defined regions were detected that also point towards folded protein species (6.5-9 ppm in H^1-dimension). Nevertheless, the overall spectra quality was not sufficient for any structure or dynamic calculation. Hence, the question was why the NMR experiments failed although folded VSD species were present.

The analysis of literature data should help answering that question. NMR spectra of different membrane proteins in LPPG and DPC revealed the presence of α-helices (Poget & Girvin, 2007; Dehez *et al.*, 2017; Kurauskas *et al.*, 2018). Hence, they concluded that the proteins were correctly folded. However, finally they were not active. Cell-free-produced VSDs in DPC also revealed the presence of α-helices in CD spectroscopy analysis and peaks for folded proteins appeared in NMR measurements (Figure 22, Figure 19, Figure 20, Figure 21). Transferring the knowledge of the aforementioned literature data, this would mean that the proteins were somehow folded but maybe not completely and/or incorrect. However, I could show activity for my constructs. The drawback for these activity studies with the hH_V1 and DrVSP channel VSDs was that an activity assay in micelles was not feasible. Meaning, they had to be incorporated into the lipid bilayer of liposomes to enable the separation into

two compartments for studying channeling processes from one compartment to the other. Hence, it cannot be ruled out that the folding has not changed under lipid contacts in comparison to the detergent-treated samples. Furthermore, the incubation at 45 °C for a prolonged time during the NMR measurements might destroy initially folded structures. Lower temperatures down to 25 °C were tested but had no influence on the overall spectra quality (data not shown). Hence, it was not possible to conclude whether the proteins were actually correctly folded before reconstitution into liposomes for activity assay evaluations or not.

As mentioned beforehand, the folding parameters for every protein differ. Just because a membrane protein was folded in one defined detergent, does not automatically mean, that a second protein or even the same protein in another detergent behave the same. For example, the structure of K_VAP was solved in DHPC micelles by solution-state NMR (Butterwick & MacKinnon, 2010). On the other hand, K_VAP-VSD soluble-produced in the L-CF mode in NDs was unfolded (Lyukmanova *et al.*, 2012). Only when the P-CF-produced pellet of K_VAP-VSD was solubilized first in SDS/urea buffer and stepwise refolded by an on-column exchange against DPC, folded protein was obtained (Lyukmanova *et al.*, 2012). I started a comparable approach by resuspending the P-CF pellets in SDS buffer, reconstituting them in asolectin-composed liposomes, and extracting the VSDs by detergent treatment (DPC, Fos14) (4.3.3) (Focke *et al.*, 2016). As previously mentioned, the VSDs were much more stable but again the NMR spectra represented only parts of a folded protein but showed nearly no peak dispersion (Figure 38). This example highlights again the complexity of membrane protein folding and shows that the CF expression of voltage-gated channels like K_VAP in *E. coli* extracts can lead to folded protein species, but requires intense screening processes to obtain finally structural or dynamic information about the protein of interest.

The previously mentioned facts about CF-produced VSD folding were all based on obtained results from CD and NMR experiments. Additionally, the ability of a protein to show native oligomeric behavior is a sign for folded protein species under investigation. LILBID measurements of the VSDs in detergent micelles and NDs (Figure 24, Figure 29) revealed the oligomeric state of the hH_V1-VSD, which was identical to literature described data (Koch *et al.*, 2008; Lee *et al.*, 2008b; Li *et al.*, 2010b; Fujiwara *et al.*, 2012; Smith & DeCoursey, 2013; Fujiwara *et al.*, 2013; Fujiwara *et al.*, 2014; Li *et al.*, 2015; Boonamnaj & Sompornpisut, 2018).

Here, mainly dimeric species could be detected (Henrich *et al.*, 2017a). Perozo and co-workers stated a concentration-dependent dimeric behavior of the hH_V1-VSD, determined by SEC-multiangle light scattering (SEC-MALS) (Li *et al.*, 2015). I tested different initial VSD concentrations ranging from 10 to 180 µM in SEC analysis and never observed any differences in the elution profiles (data present in lab book number 4, 11-16-16). Hence, I doubt the concentration dependency. Additionally, in their paper it was inexplicable that first the dimer eluted at 14.5 ml on a preparative column and later at 2.085 ml on an analytical one (Fig. 1 and Fig. S6; Li *et al.*, 2015). Such an elution volume usually represents free detergent molecules on this kind of column and not the protein-micelles. They also stated their idea by reconstituting different protein amounts in liposomes, but they missed a calculation of reconstitution efficiencies what makes the evidence for a concentration-dependent dimerization difficult. In sum, I could not find any hints for a concentration-dependent dimerization when analyzing the results of my performed experiments.

The DrVSD reconstituted in either detergent or NDs existed as monomers and dimers (Figure 19, Figure 20, Figure 21, Figure 24, Figure 25, Figure 29). It was somehow surprising as DrVSP was expected to be monomeric (Okamura *et al.*, 2009). The type of cells chosen for the VSD expression, the overall expression level, membrane composition, construct length and many more might influence the oligomeric state of the voltage-sensing phosphatase domain. However, for other related phosphatases like Mtmr2 and recently for CiVSP also a dimeric behavior was described (Berger *et al.*, 2003; Rayaprolu *et al.*, 2018).

In addition, SDS-PAGE and western blot result interpretation of different samples showed SDS-stable dimeric fractions of the VSDs (Figure 20, Figure 21, Figure 37). Supporting the theory of lipid-based VSD folding, results of the refolding studies showed no dimers in SDS solubilization buffer (Figure 37), but after refolding in liposomes as well as after the following detergent extraction procedure. Such SDS-stable dimeric states were also observed for other VSDs in SDS-PAGE analysis (Lyukmanova *et al.*, 2012). Additional methods like AFM, stepwise photobleaching (Anderluh *et al.*, 2014) or native mass spectrometry based on electron spray ionization (ESI) (Laganowsky *et al.*, 2013) can be used to determine the oligomeric state of the VSDs in more detail. However, the formation of dimers of cell-free-produced hH_V1-VSD and DrVSD could be demonstrated by a variety of different techniques, which was an additional hint for working with folded proteins.

Beyond the secondary structure – What about non-folding?

Although I collected many experimental results, which indicated folded VSDs in detergent micelles and NDs, I cannot exclude a wrong fold of them, as a primary read-out system based on a measurable VSDs activity was not available for all tested hydrophobic environments. Additional parameters like the construct length and lipid contacts can influence the overall protein fold. Because there is no structure available of the hH_V1, most VSD predictions are based on homology models. For model building purposes, I used the crystal structure of the CiVSD as it was claimed to be the best fitting model so far (Li *et al.*, 2015). However, comparison of my structural model and another one revealed differences. The S4 helix in my model is predicted to end at position A210 whereby my VSD construct ends at position R223. Hence, some residues are left that are not involved in α-helix formation, which might finally support folding. In contrast, the end of the S4 helix in the other model is claimed to be at position I218 (DeCoursey *et al.*, 2016), only five amino acids apart from the end of my construct, which might hinder folding processes in this case. This less distance might be responsible for incorrect overall protein folding. Even in my model the S4 helix is not completely structured, but instead ends up in a loop region rather than in an α-helical structure (Figure 2). In conclusion, different construct lengths should be tested to exclude influences in folding issues.

Another influence on VSDs fold might be the contact to surrounding lipid molecules. The lipid dependency for VSDs insertion and activity was demonstrated (Figure 13, Figure 14, Figure 36). The lipid properties determine finally the protein-lipid contact, the membrane fluidity, and thickness, which are important parameters for correct protein folding. The more saturated lipids are present, the higher dense they are packed. Often plasma membranes are enriched in sphingolipids and sterols to make them more fluid, but anyhow also robust against external stress. The membrane is in-between a solid and fluid state whereby an α-helical protein prefers the liquid phase (van Meer *et al.*, 2008). Hence, saturated lipids are good for liposome or ND stability, but worse for protein insertion tendency and overall stability. Especially for the regulation of transporter and channel activity, bilayer thickness dependency was described (Andersen & Koeppe, 2007; Yuan *et al.*, 2004). The thickness will be changed, e.g. when PE lipids are present that can induce curvature (Andersen & Koeppe, 2007). Figure 42 illustrates different membrane spanning regions for the modeled hH_V1-VSD

and DrVSD. Although both structures are based on the same template model, the thicknesses of the hydrophobic parts as well as their angle orientations in the membrane seemed to be different. This could mean different lipid dependencies for both constructs. Furthermore, the VSDs show more positively charged amino acid residues in the cytoplasm and more negatively charged ones on the extracellular site. This might influence lipid interactions too. Despite all these differences, comparing the human and zebrafish lipidome, researchers figured out that they are very similar (Fraher *et al.*, 2016). Screening of thousands of different lipid compositions by the design of experiment approach or using some kind of robotics might help here to support correct folding of the VSDs.

When talking about the support and analysis of the direct folding of the nascent amino acid chain of the VSDs, the cell-free system can help supporting folding properties. For example, heat-shock extracts can be used where additional chaperones and proteases were upregulated or newly synthesized, which are known to assist folding and are known to remove aggregates, respectively (Foshag *et al.*, 2018). Additionally, hundreds of folding supporters could be supplied to the CF reaction if necessary. Again, a design of experiment strategy would be helpful for screening purposes (5.1.3).

In sum, all recorded data with different kinds of experiments point towards folded VSDs, but have always detected higher oligomers, later defined as real aggregates. I could not figure out so far if the VSDs were either initially not correctly folded, which caused aggregation or just were not stable in the tested environments leading to their oligomerization.

5.2.4 A question of aggregation

When I started this project, I observed signals for higher oligomers in different kinds of experiments like SEC, LILBID and SDS-PAGE/western blot analysis. Their proportion was always negligible. For example, I never detected an intense void volume peak in SEC analyses and the sometimes-occurring smear effect in SDS-PAGE experiments could be explained by standard membrane protein behavior in SDS sample-loading buffer. Nevertheless, I was not able to record any good quality NMR spectra in all tested hydrophobic environments. How can this be explained?

As we know so far, the line broadening and peak overlap was caused by the presence of huge VSD aggregates. Were these aggregates present directly after protein production and purification? If yes, were they too big and stuck to the filter in SEC experiments or were they underestimated and were therefore not visible? For answering these questions, first I controlled the pressure change during sample-loading in SEC experiments. Always a low increase in the overall pressure was detectable but not as large as it would have been expected if proteins had clogged the filter of the column. Second, I used the instruments of the Malvern company to find further evidence for the theory of aggregate formation (Figure 25). The presence of aggregates could be proven. Here, I determined their size between 92 and 387 nm and their concentration to $2.5*10^7$/ml. The initial concentration of hH_V1-VSD in 100 µl was 1.88 mg/ml meaning $9.033*10^{16}$ particles per ml. The percentage of the aggregates in the sample was vanishingly low (0.000000027 %), which would explain why they were not detected in SEC runs. Nevertheless, their initial presence was proven. Accordingly, there was an explanation for the decreased sample stability (5.2.2). Especially, in NMR recordings with higher temperatures up to 45 °C the presence of an aggregate fraction will finally result in the formation of higher VSD oligomers and their clumping. In conclusion, these initial aggregates had to be removed.

First, I tested stabilizing agents in the solubilization buffer like arginine and glutamine to avoid aggregate formation during protein folding events. No difference in the final NMR spectrum could be observed. In a second step, I performed ultracentrifugation runs to remove aggregates efficiently, as it was described for other cell-free-produced channels (Deniaud *et al.*, 2010). However, the attempts failed. The missing precipitation of the aggregates during the ultracentrifugation steps pointed towards soluble aggregates. In future, the speed as well as the centrifugation time of ultracentrifugation runs should be increased (5.2.1). Furthermore, additional buffers with other stabilizing agents could be tested. The incubation times of the CF expression could be reduced to less than 16 h at 30 °C and different filters varying in their pore size could be tested for efficient aggregate removal.

Aggregation was also observed for other membrane proteins reconstituted in NDs (Nikolaev *et al.*, 2017). Nevertheless, here protein crystals could be grown under high salt concentrations (1-2.8 M) although the membrane proteins showed an aggregation tendency. Crystals were of good quality and finally scattered light. Usually high salt concentrations

increase hydrophobic interactions (salting-out) leading to protein precipitation. However, high salt concentrations in membrane protein preparations decrease solvation. Hydrophobic areas become exposed and might be more accessible for detergent or lipid molecules. This theory was also tested for the VSD preparations. Unfortunately, high salt concentrations in VSD-ND samples did not result in increased NMR spectra quality (Appendix, Figure A 4 and Figure A 8). Again, intense screening processes might help to figure out the influence of higher salt concentrations in VSDs folding behavior.

It seemed that the detection as well as the elimination of protein aggregates in the sample was not trivial. Hence, the best solution would have been to prevent the oligomerization behavior initially. However, what are the triggering factors for VSDs aggregation? As already discussed, the VSDs synthesized in L-CF mode might not be inserted and just stick to the membrane causing their aggregation. Furthermore, the complete shielding of hydrophobic parts of detergent-solubilized VSDs might be hindered due to false detergent properties for these kinds of proteins. Here, again intensive screenings would be necessary to figure out the "correct" environment. For example, one could test mixed micelles and mixed lipid compositions in NDs to ensure native thickness and curvature of the lipid double layer (5.1.2). Additionally, the temperature in CF expression and following downstream processes can have a big influence. Hot and cold aggregation, in addition to concentration-dependent aggregation, was described (Rosa *et al.*, 2017). Unfortunately, the determination of T_m for DrVSD and hH_V1-VSD failed so far (5.2.2), preventing the evaluation of suitable purification and storage conditions. Another influence of the temperature could be detected when focusing on the lipids used for ND preparations. The lipids could be based on different temperature behaviors than a CF-synthesized protein. Often, the lipid phase transition temperature is higher than 25 °C (Table 12). Consequently, the lipids are present in a gel phase below that temperature, which might hinder VSDs co-translational insertion and/or their correct fold. A strong temperature-dependent gating behavior for VSDs in cells is described (DeCoursey & Cherny, 1998; Kuno *et al.*, 2009; Fujiwara *et al.*, 2012), which might be even more critical in *in vitro* applications. Here, the high flexibility of the VSDs can lead to the formation of aggregates too. As speculated by other groups, the full-length protein might be necessary to protect VSDs from aggregation, as they will stabilize the whole

protein. They showed high fluctuations and dynamics in the VSD of a voltage-gated sodium channel making it too flexible to be studied (Paramonov *et al.*, 2017).

In addition, posttranslational modifications may influence protein folding behavior and stability, thus influencing aggregation. Their presence in the CF-synthesized VSDs had to be proven in future experiments. For example, the full-length construct of hH_V1 contains two known phosphorylation sites, Thr29 and S97 (Musset *et al.*, 2010a). In leukocytes, Thr29 is described to activate hH_V1, but Thr29 is not present any more in my construct. Nothing is known about its influence on the overall channel structure and folding behavior. However, its loss might cause increased aggregation because of missing overall stability. The problem of aggregation might explain why no structure of the human hH_V1 is reported so far. The available structures are from CiVSP and mouse hH_V1, whereby the homology to hH_V1-VSD is low, and the represented structure is not native as they exchanged half of the protein (Takeshita *et al.*, 2014), respectively. The construct used in the doctoral thesis of J. Letts was not described in detail, but as previously mentioned, it was stable in DHPC and LPPG micelles (Letts, 2014). In comparison, his construct had a size of 138 residues and mine of 149, which might influence the final stability and aggregation tendency. However, finally his construct was stable, but not correctly folded. He also tried to crystallize the hH_V1 channel under a variety of different conditions, but failed too.

In sum, VSDs under investigation tend to aggregate. The initial aggregate concentration is low, but strikingly influences further experiments, especially NMR applications. Unfortunately, this ongoing process could not be suppressed or even prevented so far. Nevertheless, active VSDs could be obtained using the CF expression system as discussed in the next section, pointing again towards folded protein species under investigation.

5.2.5 Activity studies of VSDs

The activity of cell-free-produced hH_V1-VSD and DrVSD could be successfully shown by ITC measurements and using the fluorescence-based activity assay (FbAA) (Zhang *et al.*, 1994; Lee *et al.*, 2009) (4.3.2). Recently, also successful electrophysiology measurements with CF-produced, in liposomes-reconstituted membrane proteins could be demonstrated, which could be of future interest. Using this kind of technology would enable easier sample comparisons between CF-synthesized and in-cell-analyzed VSDs (Deniaud *et al.*, 2010;

Kovácsová *et al.*, 2015). However, in this thesis the VSDs showed proton-channeling activity in the FbAA when they were reconstituted in POPE/POPG-containing liposomes after P-CF synthesis (Figure 32, Figure 34), after treatment with TCA, after a refolding step (Figure 35, Figure 36) and after co-translational insertion in liposomes in L-CF mode (Appendix, Figure A 10). Referring to the refolding approach, the proteoliposomes composed of asolectin lipids were not directly used in the FbAA, as asolectin is a lipid mixture from the soybean, which differs in its composition from batch to batch. To this end, it would have been difficult to control all parameters in the assay and compare results with each other. The refolded VSDs in asolectin liposomes were solubilized in detergent and subsequently reconstituted in POPE/POPG-containing liposomes. In sum, the overall activity of cell-free-produced VSDs was comparable to published data (Lee *et al.*, 2009; Li *et al.*, 2015).

MacKinnon and co-workers described the reduction of fluorescence intensity in the FbAA after CCCP addition as an illustration of the amount of empty vesicles in the sample (Lee *et al.*, 2009; Letts, 2014). CCCP, as a proton-ionophor, destroys the proton gradient established in VSD-containing liposomes. Now, protons enter the lumen of all vesicles either with or without VSDs incorporated. Hence, an increased ACMA protonation occurs, leading to a massive reduction in the fluorescence signal. In accordance with this notion it would suggest a higher reconstitution efficiency for hH_V1-VSD (15 % empty liposomes) as for DrVSD (~50 % empty liposomes) in my studies (Figure 34). Using the CCCP interpretation of reconstitution efficiencies, one can determine the amount of VSDs that can be activated by the induced membrane depolarization. However, this amount only represents VSDs that showed the correct insertion direction in the liposomal membrane to passively channel protons. The overall reconstitution efficiency might be higher but cannot be detected in this case. Other techniques had to be applied for their determination. For example, the analyses of the sucrose density gradient centrifugations revealed similar reconstitution efficiencies for both VSDs (Figure 33 A/B). Furthermore, a bachelor student in our group determined the VSDs reconstitution efficiency in POPE/POPG-containing liposomes to 25-30 %. To this end, she analyzed reconstituted VSD samples by SDS-PAGE and extrapolated obtained signals with ImageJ in comparison with a reference sample. This sample represented the initially present amount of VSDs (in detergent) prior to reconstitution, equivalent to the 100 % input (Warinner, 2015). Here, the SDS present in the sample-loading buffer should have been

sufficient in proteoliposome solubilization and therewith sufficient in detection of the whole VSD western blot signal. A comparable study was done for K_V1.1 and 1.3 channels reconstituted in liposomes (Renauld *et al.*, 2017). They treated their proteoliposomes with triton instead of SDS prior to western blot analysis. Thus, the His-tag got solvent-exposed when assumed that the N-terminal part with the His-tag of the embedded protein was also located inside the liposomes. Doing so, the western-blot signals of their dot blots were increased compared to non-treated samples resulting in determinations of overall reconstitution efficiencies independent of the direction of protein incorporation. This strategy can be tested for the VSD-liposomes too, to validate the reconstitution efficiency calculations.

Referring back to the result interpretation of MacKinnon and co-workers in the last paragraph (Lee *et al.*, 2009), the results of the DrVSD activity assay looked similar to the curves obtained with different potassium gradients rather than being a result of less reconstitution efficiencies (Appendix, Figure A 9 A). It suggests that the DrVSD opens at a different membrane potential and was not fully active at the investigated 1:20 dilution. Nevertheless, the slope of the DrVSD fluorescence curve was identical to one described in the literature for another phosphatase-coupled VSD from *ciona intestinalis*, CiVSD (Li *et al.*, 2015). They claimed that the proton conduction is slower compared to hH_V1-VSD without defining a reason. For the voltage-sensing phosphatases, as DrVSP, a conformational change in the phosphatase domain is described that influences movements in the VSD (Hossain *et al.*, 2008). This missing domain might be responsible for the slower gating kinetics of DrVSD observed in the FbAA. Additionally the lipid composition may play an import role in DrVSD response to membrane potential changes, as naturally phosphoinosites were changed in charge distribution and size by dephosphorylation when the phosphatase domain gets activated. Taken together, it remains unclear why the DrVSD showed a different behavior in the fluorescence-based activity studies than hH_V1-VSD. This phenomenon should be addressed in future experiments.

In sum, the same results for the activity assays were obtained with P-CF-produced, solubilized, purified, and reconstituted VSD samples and with non-purified L-CF-produced VSDs in liposomes. Now, the lipid-dependent activity of VSDs will be discussed. As mentioned previously, different lipids influence activity (London & Feigenson, 1981a, b; Caffrey & Feigenson, 1981a, b; Soubias *et al.*, 2006) shown for hH_V1-VSD in Figure 36. No

activity was observed in POPC-containing liposomes. Interestingly, hH_V1-VSD was active in a POPC/POPG mixture (Li *et al.*, 2015) and in DOPC/DOPG-, DOPE/DOPG- and POPE/POPG-composed liposomes. These results suggest an important role for PG head groups in VSD activity that could be further enhanced by PE head group addition. PE is described to induce membrane curvature (Marsh, 2007), which might enhance the insertion efficiency and/or head group interactions that support channeling activity by inducing conformational changes. Additionally, polyunsaturated fatty acids as lipid tails enhance the gating as well (DO instead of PO). Unsaturated lipids are less tightly packed, which might enable the adaption of another pH of the direct membrane surrounding of the VSD than in bulk solution, necessary for increased activity (Kawanabe & Okamura, 2016). Such lipid-dependent activities could also be shown for other membrane proteins co-translationally-inserted in CF protein production (Ma *et al.*, 2011; Roos *et al.*, 2012; Henrich *et al.*, 2016). As represented for other membrane proteins different protein conformations depend on interactions with the lipid head group or fatty acid chain (Koshy *et al.*, 2013; Bechara & Robinson, 2015). For example, the proposed Grotthus-type mechanism in simulations for hH_V1 channels revealed salt bridge interactions of active protein side chains like R205 with either D119 or a neighboring lipid head group (van Keulen *et al.*, 2017). Hence, many more lipid composition might be screened for increasing the VSDs overall activity. Again, the design of experiments strategy would be helpful (5.1.3).

Additionally, I tested liposomes composed of DMPC lipids, which failed in successful reconstitutions, comparable to results obtained with co-translationally-inserted VSDs into NDs (5.1.2). DMPC lipids seemed to hinder the VSD insertion. Furthermore, I tested DMPC/DOPMME-containing liposomes. This lipid composition was chosen, because a specific phospholipid methyltransferase (Opi3) was available that changes PMME head groups to PC ones, which could have helped to detect in real-time lipid-dependent gating events. The idea was that active channels were observed in DOPMME-containing liposomes. After transferase treatment of the sample, the activity should have been lost. However, the successfully reconstituted VSDs showed no activity in this kind of liposomes. Nevertheless, I hope that such theories can be applied in future experiments to study lipid-dependent protein behavior.

As mentioned, many more lipids can be screened for improving proton-channeling activity. Mixed lipids should always be preferred to ensure optimal protein behavior. I looked for requirements in the native cell membranes of eukaryotes that are mostly composed of phospholipids with PC-, PE-, PS-, PI-, and PA-head groups. For example, PI head groups should be present in DrVSD reconstitution experiments as DrVSP has its enzymatic activity here. In particular, the knowledge of a zebrafish and e.g. human granulocyte membrane lipid composition might be helpful. MacKinnon and co-workers tested successfully a lipid composition of a human neutrophil plasma membrane in their FbAA with hH_V1-VSD (6:6:3:3:1 POPC:POPE:POPS:SM:PI) (Lee *et al.*, 2009). However, in less complicated mixtures like POPE:POPG and POPC/POPG 3:1 a comparable activity could have been observed (Letts, 2014; Li *et al.*, 2015). Thus, the presence of such complex lipid mixtures for being more native-like was skipped in this thesis as activity could be shown in some two-lipid mixtures as well. Nevertheless, lipid-screening procedures are always important and might help increasing NMR spectra quality finally.

As already mentioned, the tests of proton channeling activity are so far based on proteoliposomes. Here, two compartments are available to allow recognition of membrane polarization and pH changes. Dynamic studies using solution-state NMR are only feasible with detergent- or ND-reconstituted samples. Therefore, another technique is required to determine the activity of VSDs in detergents or NDs to ensure working with folded protein species ultimately. Recently, it was shown for another membrane protein that also NDs could be applied to solid-supported membrane measurements determining channel activity, which might be a method of choice for future investigations (Henrich *et al.*, 2017b).

Inhibition of cell-free produced VSDs

An additional test for clearly demonstrating the cell-free production of active voltage-gated proton channels was to analyze their ability to be blocked. First, this was tested by the addition of the inhibitor 2GBI to proteoliposomes in the FbAA. An inhibitory effect was detected for both VSDs (Figure 35). The inhibition rate was more pronounced for the DrVSD construct. Analyzing the electrostatic surface of the activated DrVSD model, the increased inhibition can be explained by an increased access of 2GBI (Figure 42 B). The access in the hH_V1-VSD seemed to be more blocked, which would hamper protein-inhibitor interactions (Figure 42 A).

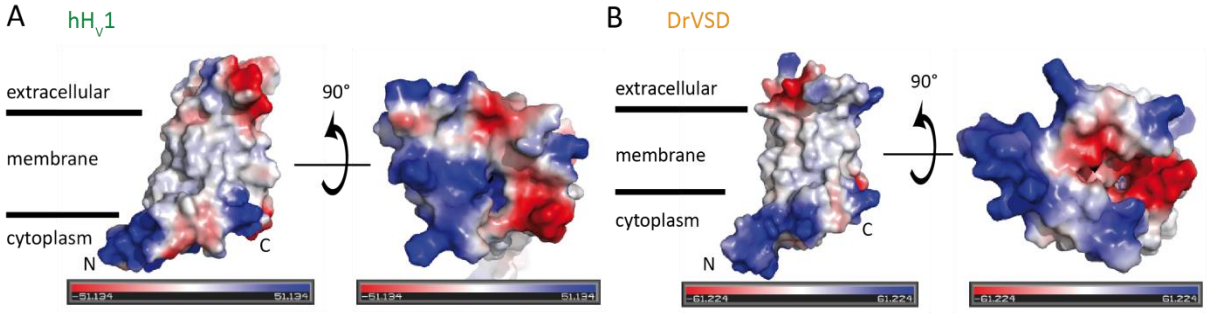

Figure 42: Surface presentations of PyMOL-based 2GBI docking in modeled VSD structures. The surface was created using PyMOL and the initially applied models of the VSDs used in this thesis based on the CiVSP crystal structure (Figure 2, Figure 4). Neutral charged residues are shown in white, positively charged ones in blue and the red color represents negatively charged residues. The electrostatic surface of modeled hH$_V$1-VSD (**A**) and DrVSD (**B**) are shown. The N- and C-termini of each construct are highlighted by capitals N and C, respectively. A 90 ° flip of the models enabled a detailed view from the intracellular site. Here, 2GBI, represented as ribbons, could be detected in a hole of the DrVSD model, which was not visible in the hH$_V$1-VSD structure.

Inhibitor addition of 2GBI was claimed to have IC_{50} values of 38 µM for the human and 52 µM for the voltage-gated proton channel of *ciona intestinalis* (Hong *et al.*, 2013). I analyzed the inhibition rate of 2GBI in more detail by ITC measurements (4.3, Figure 32). Here, the K_D for hH$_V$1-VSD was determined to 52 µM ± 30 µM that is in complete agreement with literature data. For the very first time, the K_D of DrVSD was determined to 2.6 mM ± 1.2 mM. No literature data for this kind of protein was available so far. The initial VSD concentrations, used for calculation processes, might have been wrong caused by present aggregates in the VSD samples solubilized in DPC. This may explain high deviations in the final K_D values. The increased K_D value for the DrVSD construct in comparison to hH$_V$1-VSD is in good agreement with the presented model structures. Here, DrVSD shows a higher accessibility for 2GBI. Hence, the overall exchange rate is expected to be more pronounced when the side chain interactions are weakened. The inhibitor binds less tightly. In the interpretation of the ITC test results in general, it should be noted that the change in heat capacity during the experiments with the addition of 2GBI was low, especially for the DrVSD construct. Hence, data should be interpreted with some caution. Two options are possible to strengthen the obtained results. Either the 2GBI concentration could be increased or the initial VSD concentration could be decreased. Both set-ups were not tested so far. High 2GBI concentrations could ultimately lead to solubility problems and low initial VSD amounts might cause too much loss of signal in ITC experiments. However, most important for obtaining valid ITC results is reaching saturation as it explains real binding events. Here, I could demonstrate that buffer addition to the VSD sample (negative control)

did not induced heat capacity changes pointing towards real binding events under investigation.

In addition to the inhibition by 2GBI, the inhibition of cell-free produced proton channel VSDs by Zn^{2+}-binding should have been shown. This would have additionally supported the finding of active VSDs produced by applying the cell-free expression technology. Unfortunately, although the same concentration of Zn^{2+} was used as in electrophysiology recordings whereby a 100 % inhibition could be addressed (Ramsey *et al.*, 2006), the addition of $ZnCl_2$ led to complete sample precipitation induced by drastic local pH changes. In future, the zinc buffer solution has to be changed and better controlled to address the phenomenon of polyvalent cation binding to cell-free-produced voltage-gated proton channels.

To sum up, active DrVSD and hH_V1-VSD could be obtained using the cell-free protein synthesis platform. Unfortunately, the samples were instable, causing the formation of higher oligomeric structures up to aggregates. Due to increased sample size, mechanistically studies of the channeling process of protons by solution-state NMR were impossible so far. One could think of using VSD-incorporated liposomes for performing solid-state NMR measurements. Here, the method is almost independent of sample size. However, it is based on cryogenic samples, which makes the investigation of dynamic processes difficult. Another suitable method is the recently invented technology of introducing unnatural amino acids in proteins to study movements and changes in defined positions by solution-state NMR also for higher-molecular-weight molecules (Jackson *et al.*, 2007; Elvington *et al.*, 2009). Background information, first results, and critical discussions about this topic can be found in the next section.

5.3 Unnatural amino acids in cell-free synthesis

A variety of different techniques for protein labeling exists e.g. site-specific labeling via lysine or cysteine side chains. Labels facilitate for example the analysis of transport/channeling processes, conformational changes, or ligand binding events in proteins (1.3.1, 1.3.2, 1.3.3). Furthermore, they can be used to increase the protein stability by e.g. introducing artificial post-translational modifications usually missing in the expression host system. Nevertheless, the common labeling strategies are based on the post-translational labeling of the protein of

interest, which can influence protein folding, function, and stability. Another possibility is to introduce the label directly during the proteins translation process using unnatural amino acids.

Schultz and co-workers developed this method of site-specifically protein labeling (Noren *et al.*, 1989). Here, unnatural amino acids (aa) were introduced into a defined position of the protein by exchanging one codon in its DNA sequence against a non-sense codon e.g. the *amber* TAG codon (Figure 43). Usually, translation would stop here, as no anti-codon tRNA is available (mRNA codon: UAG). To overcome these difficulties, a specific aminoacyl-tRNA/synthetase pair has to be provided. The aminoacyl-tRNA-synthetase is designed to transfer the label of interest to the tRNA holding the AUC anti-codon. Often the knowledge of the crystal structure might help designing synthetases aminoacylating tRNAs with a specific unnatural aa (Kavran *et al.*, 2007; Nozawa *et al.*, 2009; Yanagisawa *et al.*, 2008a, b; Flügel *et al.*, 2014). In a second step, the loaded aminoacyl-tRNA competes with the release factor about the binding site in the ribosome-mRNA-complex.

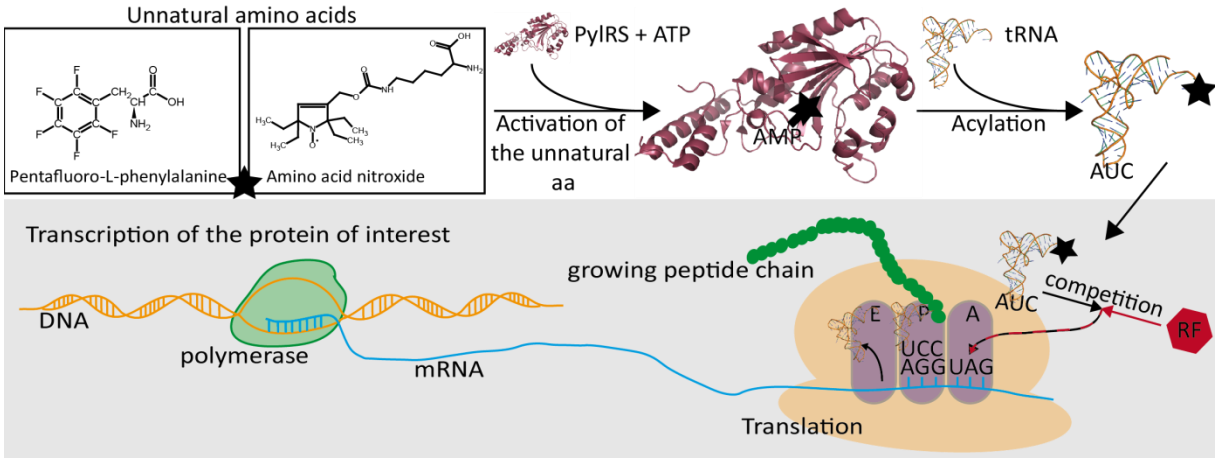

Figure 43: Incorporation of unnatural amino acids into a protein of interest. The scheme illustrates the different steps necessary for unnatural amino acid introduction into a growing polypeptide chain. First, an aminoacyl-tRNA-synthetase (e.g. PylRS) responsible for the transfer of defined unnatural aa (black star) has to be designed. In the presented scheme, the unnatural compounds represent possible substrates introduced by the PylRS system. After their activation by ATP leading to an adenosine-5'-monophosphate (AMP) product, they were loaded onto the corresponding tRNA comprising the AUC anti-*amber*-codon. After transcribing the DNA by a polymerase, the ribosomal subunits bind the mRNA and start the translation process. Here, aminoacyl-tRNAs in complex with elongation factors (EF) bind their corresponding codon in the aminoacyl-site (A) of the ribosome. Afterwards a peptide bond between the growing protein chain and the following aa is formed in the peptidyl-site (P). The deacylated tRNA from the P-site is directed to the exit-site (E) and leaves the ribosome with simultaneous movement of the mRNA by one codon finally. Once the *amber* codon position in the mRNA is reached, unnatural-aa-loaded tRNA and release factors (RF) compete against the A binding site. Once the star-loaded tRNA binds, the unnatural aa is introduced into the growing polypeptide chain in the P-site.

Third, once the loaded tRNA is bound, the loaded label is connected with the previous amino acid of the growing polypeptide chain. Mainly, the *methanococcus jannaschii* derived aminoacyl-tRNA/synthetase pair is used to introduce unnatural amino acids (Wang *et al.*, 2001; Wang *et al.*, 2003; Ryu & Schultz, 2006; Jackson *et al.*, 2006; Goerke & Swartz, 2009; Bundy & Swartz, 2010; Albayrak & Swartz, 2013a; Gan *et al.*, 2017). Substrates of these synthetases are tyrosine or serine analogues. Synthetases that are supposed to introduce unnatural amino acids in VSDs in the future, were derived from *methanosarcina barkeri* (*M. barkeri*) to incorporate pentafluoro-L-phenylalanine (5FP) for ^{19}F-NMR experiments or from *methanosarcina mazei* (*M. mazei*) to introduce a radical for PRE or EPR studies (Figure 43) (Schmidt *et al.*, 2014a). In nature, both pairs drive the incorporation of pyrrolysine, the 22nd aa in archaea (Polycarpo *et al.*, 2004; Kavran *et al.*, 2007). Hence, the pair is also referred to as pyrrolysyl-tRNA and pyrrolysyl-tRNA-synthetase (PylRS).

In acid-sensing ion channels the incorporation of unnatural aa lead to the elucidation of their selectivity filters (Lynagh *et al.*, 2017). In voltage-gated sodium channels, expressed in oocytes, unnatural aa enabled the determination of drug interaction properties (Pless *et al.*, 2011). Shielded protein regions, usually inaccessible for any kind of labels, e.g. side chains deep inside the pore of H_V1 channels, are target structures for this kind of technology. This might be especially important for voltage-clamp fluorometry studies to analyze the mechanism of proton transfer in future (1.3.1) (Kalstrup & Blunck, 2017, 2018). Furthermore, dynamic and ligand binding studies are possible by the incorporation of Förster resonance energy transfer- (FRET) pairs (Mitchell *et al.*, 2017) or o-tert-butyltyrosine (Chen *et al.*, 2015; Jabar *et al.*, 2017) enabling the determination of short- and long-range distance restraints. For example, in mechanistic studies of H_V1 channels it could be important to label solely one of the three arginines in the voltage-sensor of the VSD either with heavy nuclei for NMR experiments, with paramagnetic chemicals for EPR and NMR studies or with fluorophores for fluorescence-based methods. In detail, the introduction of a NMR-sensitive nucleus by 5FP incorporation, could enable studying conformational changes during channeling events, even for highly dynamic or large protein complexes like it was shown for the chloride channel ClC-ec1 (molecular weight of 50 kDa) (Jackson *et al.*, 2007; Elvington *et al.*, 2009). This makes the system especially attractive for the investigation of the cell-free-synthesized VSDs described in this thesis that showed a high overall flexibility and an increased size when

surrounded by detergent molecules, and lipid bilayers in form of NDs or liposomes. Additionally, in-cell NMR studies with ^{19}F-labeled proteins are possible to study channeling processes in a native environment (Li *et al.*, 2010a). The introduction of a radical in defined positions would enable gaining information about the overall distance changes (Jiang *et al.*, 2017).

In cooperation with the Membrane Structural Dynamics Consortium specific synthetases, tRNA sequences and substrates for the introduction of unnatural aa in voltage-gated proton channel VSDs were chosen and were tested in our lab (1.1, 7.1).

First, a model protein, GFP Y151* (stop codon at position 151) was analyzed in view of specific substrate integration and product yield. The GFP Y151* was produced in cell-free approaches where all necessary components were added (3.1.9). For example, the tRNA was produced in a high copy number as double stranded DNA with a T7 promotor region and a 5'end Hammerhead ribozyme sequence in a PCR reaction and added in a purified form to the cell-free set-up (3.1.6). It was also tested to add a plasmid containing the PylRS and the tRNA, but full-length GFP expression failed. Adding a number of different plasmids to the cell-free reaction would decrease the expression yield drastically as precursors, amino acids and energy sources were consumed faster and unequally distributed. To reduce the amount of added DNA to a minimum, the synthetases were tried to be produced beforehand and added in a purified, active form. To this end, both synthetases in a pBH4 vector were synthesized in *E .coli* using an auto-induction medium overnight at 37 °C (3.1.6, 3.1.10). Afterwards a subfractionation step was performed to separate soluble proteins from insoluble expressed ones (3.1.11) (Figure 44 A).

Unfortunately, most of the synthetases could be detected in the insoluble fraction. Reducing the expression temperature to 20 °C overnight did not increase the yield of soluble PylRS (data not shown). Next, the synthetases were fused to an ubiquitin-tag (pET39(+)_Ub19) to increase the overall solubility (3.1.6). The procedure was equally unsuccessful in the preparation of soluble synthetases. Another solubility tag, an N-terminal fusion of a maltose-binding protein (MBP) in a pMAL vector system, was successful in producing soluble fusion proteins (3.1.6, 3.1.10, 3.2.11). Synthetases fused to MBP could be purified and stored at -80 °C (Figure 44 B). Furthermore, the direct expression of the PylRS genes in a cell-free reaction was tested. Samples were taken after 2 h and 16 h incubation at 30 °C (Figure 44 C).

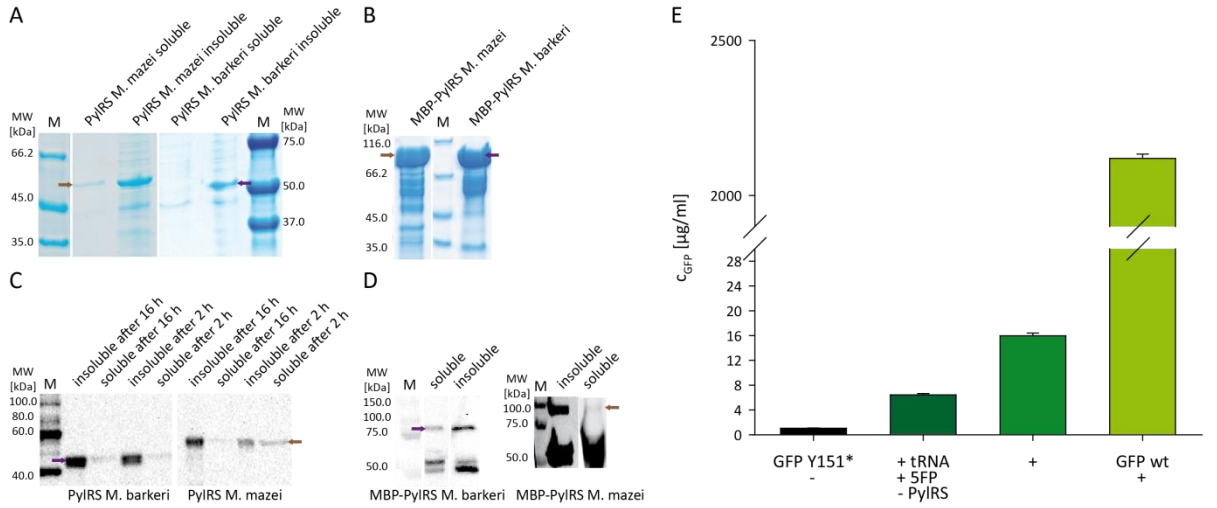

Figure 44: Incorporation of unnatural amino acids in GFP Y151* using the CF technology. The synthetase from *M. barkeri* is always labeled with a purple arrow and the one from *M. mazei* with a brown arrow. The protein marker is indicated by **M**. **A** The 11 % Tricine gel analysis of *E. coli*-synthesized synthetases in auto-induction media (overnight @ 37 °C) shows separated soluble and insoluble fractions (Coomassie-stained). Most of the protein was produced insoluble and could not be purified from *E. coli* cell production. **B** The 11 % Tricine gel analysis of IMAC-purified synthetases fused to MBP is shown (Coomassie-stained). Both synthetases could be purified and stored as a fusion construct. **C** Western blot analysis with anti-His antibody of the cell-free-expressed synthetases showed mostly insoluble protein independent from different incubation times at 30 °C. **D** Western blot analysis with anti-MBP-antibody (PylRS *M. barkeri*) and anti-His-antibody (PylRS *M. mazei*) of purified MBP-fusion constructs added to a cell-free reaction showed mostly insoluble protein. This was comparable to the cell-free expression of the synthetases without any solubility tag when they were added directly as plasmid (C). **E** The bar charts represent the amount of GFP in µg/ml synthesized in a cell-free reaction under different conditions (indicated on the x-axis). The fluorescence of GFP was measured and the concentration calculated using a standard curve (3.2.6). GFP Y151* or GFP wild-type (wt) were either expressed in the presence of all components necessary for the introduction of the unnatural amino acid pentafluoro-L-phenylalanine (5FP) (**+**), of all components except the tRNA synthetase (**+tRNA, +5FP, -PylRS**) or in the absence of each component (**-**). The addition of substrate, synthetase and specific tRNA led to an increased synthesis of GFP Y151*, but it was more than 100 times less compared to wild-type GFP production.

Supernatant and pellet fraction were separated by centrifugation (16,100xg, 10 min, 4 °C). The majority of each synthetase was located in the insoluble fraction independent of incubation durations in the cell-free set-up.

To conclude, these results indicate that the synthetases could only be obtained in a soluble form as an MBP-fusion construct from *E. coli* expressions. In the following analyses, the purified MBP-PylRS-fusions were added to a cell-free reaction to test their solubility under these conditions (Figure 44 D). Unfortunately, after 16 h incubation at 30 °C the PylRS was located nearly completely in the insoluble fraction. All tested methods for gaining a mostly soluble synthetase failed. Nevertheless, it was tried to use the tiny amount of soluble MBP-PylRS in a cell-free reaction to incorporate the different substrates into the stop-codon GFP construct (Figure 44 E). Here, many cell-free set-ups were tested to receive the full-length GFP Y151* including for example the plasmid expression of PylRS. Furthermore,

the T7 polymerase concentration was increased from 0.04 U/µl to 0.16 U/µl. The initial substrate concentration was changed from 0.55 mM to 1 mM (Chemla *et al.*, 2015). The tRNA concentration was increased from 2-5 ng/µl to 20 ng/µl (Albayrak & Swartz, 2013a used 200 ng/µl) and the solvation of the substrate in different solvents was tested (100 % and 60 % ethanol, 1 M NaOH). However, the full-length GFP Y151* synthesis in detectable amounts was only feasible when the purified MBP-PylRS fusion construct (*M. barkeri*) was added. In this case, 5FP was solved in 1 M NaOH and added to 1 mM final concentration. The T7 polymerase concentration was set to 0.10 U/µl. Under these conditions, a fluorescence signal was detectable (3.2.6). Using a standard calibration curve the GFP concentration was determined to be ~17 µg/ml. This concentration was below the limit of detectable signals in western blot analysis with the anti-His-antibody, which prevented full-length GFP detection in standard SDS-PAGE analysis. Compared to the wild-type GFP production (2.1 mg/ml), in the same experiment, the expression of the stop-codon construct was less than 1 %. Even worse, a background expression of the GFP Y151* without any synthetase present could be detected to 30 % compared to the set-up where all necessary components were available. Either the stop-codon position was read through and another amino acid was incorporated at this position, or the special tRNA was loaded with the substrate in an unknown manner. However, a test of successful insertion of 5FP was omitted because the protein amount was too low to perform any control assays.

In summary, the strategy of incorporating these specific unnatural amino acids into GFP failed so far. The reasons for this can be so varied that a detailed discussion would go beyond the scope of this work. Briefly, there can be competition problems of unnatural amino acid-loaded tRNAs and release factors (Guo *et al.*, 2009; Johnson *et al.*, 2011; Heinemann *et al.*, 2012; Lajoie *et al.*, 2013; Hong *et al.*, 2014c; Lee *et al.*, 2017). Bacterial strains were designed that are release-factor-1-deficient (Δ*prfA*) thereby preventing competition events (Heinemann *et al.*, 2012; Lajoie *et al.*, 2013; Hong *et al.*, 2014c; Chemla *et al.*, 2015; Ozer *et al.*, 2017; Martin *et al.*, 2018), which might be used in future as the cell extract source. Furthermore, strategies were developed to remove the release factor from cell-free extract preparations (Shimizu *et al.*, 2001; Peuker *et al.*, 2016). Another problem could have been that the designed synthetases could fail in binding the substrates under cell-free reaction conditions and/or were not properly folded. Hence, screenings of new

production and purification strategies are necessary and could be based on previously performed experiments (Kavran *et al.*, 2007; Yanagisawa *et al.*, 2008a; Lee *et al.*, 2008a; Nozawa *et al.*, 2009; Flügel *et al.*, 2014; Schmidt *et al.*, 2014b). Additionally, one might consider loading the tRNA with the unnatural amino acid before adding it to the cell-free reaction (Lynagh *et al.*, 2017). Furthermore, the elected GFP-stop-codon position, GFP Y151*, could have hindered unnatural aa incorporations. Usually, most of the literature data are based on working with GFP Y39*, which should be tried next (Miyake-Stoner *et al.*, 2010; Plass *et al.*, 2011; Schmidt & Summerer, 2013; Albayrak & Swartz, 2013a; Schmidt *et al.*, 2014a; Chemla *et al.*, 2017; Kucher *et al.*, 2017; Ozer *et al.*, 2017). As mentioned before many other parameters can have an influence on unnatural amino acid incorporation into the protein of interest. Nevertheless, other strategies and methods of introducing unnatural amino acids into proteins can be invented, and tested to overcome specific problems and ultimately transfer knowledge to investigate VSDs. Here again, a design of experiments strategy would enable faster and more successful screening procedures (5.1.3).

5.4 Future perspective

The question asked at the beginning tried to answer the dynamics behind the channeling of protons via voltage-gated proton channels. So far, most information about involved residues and influence of protein movements were obtained from *in vivo* data and computational analyses of channeling events (DeCoursey, 2018b). Tries of synthesizing large VSD amounts using *E. coli* as a host organism for solution-state NMR analyses and crystallization failed (Letts, 2014). In this thesis, I could demonstrate that changing the production strategy to a cell-free approach was successful in gaining active dimeric hH_V1-VSD and DrVSD in high yields up to 3.2 mg/ml. The cell-free synthesis is easy, cheap and time-saving compared to the more common in-*E. coli*-protein synthesis. Furthermore, any desired parameter can be adjusted to ensure ideal conditions for protein folding and activity. Samples for solution-state NMR can be easily prepared using this kind of production strategy as labels can be integrated directly and exclusively during protein synthesis in the protein of interest. In comparison, J. Letts prepared more than 12 individual samples to assign 82 % of the backbone amides. Using a combinatorial labeling approach in cell-free expression, not more than four samples are necessary to obtain all the information (Hein *et al.*, 2017; Hoffmann *et al.*, 2018). Unfortunately, the application of this procedure on voltage-gated proton channels

failed due to their tendency of aggregation. This hindered any kind of dynamic measurements so far. Consequently, opening and closing probabilities remain unclear. Here, different aspects are important for future considerations.

First, working with shortened and mutated constructs is always problematic. Synthesized mutants were shown to be functional. Especially, often-used chimeric constructs show activity comparable to the native protein under investigation. Does it mean, however, that the protein is folded exactly like the wild-type? Moreover, does it behave similar concerning oligomerization tendencies, lipid preferences and so on? Clear answer is No! Rather "it is easier to impair function than to explain it" (DeCoursey, 2018b). Results obtained with mutated or fragmented proteins of interest should always be treated with caution. It would be best to work with the full-length, non-mutated constructs of hH_V1 and DrVSP. For sure, at the moment solution-state NMR investigations are almost impossible with construct sizes larger than 80 kDa (Tugarinov *et al.*, 2005). However, in the near future there will be further developments that make analyses of larger proteins imaginable. First steps were done by selective protein labeling (Liang *et al.*, 2006; Jackson *et al.*, 2007; Elvington *et al.*, 2009; Chen *et al.*, 2015; Yang *et al.*, 2015; Löhr *et al.*, 2015; Nitsche & Otting, 2017; Hein *et al.*, 2017; Lazarova *et al.*, 2018) and by ongoing developments of better and more sensitive NMR instruments (Schwalbe, 2017). To this end, as a next step, the cell-free synthesis of the full-length proteins should be carried out, testing all the different modes and conclusively clarifying the stability and functionality of the produced proteins to be ready when the NMR instrument settings are available for measurements.

Second, more attention should be focused on the extract source used for cell-free expressions. In native environment, protein translation/transcription as well as folding processes are tightly controlled by a variety of different mechanisms. In order to be as close as possible to nature while taking full advantage of cell-free protein production, the source of the extract should be adapted to the organism, in the best case to the cell from which the protein of interest is derived. For example, the hH_V1 channel should be produced in a cell extract derived from human cells. Recently, leukocyte cell extract preparations from human blood cells were successfully used in cell-free synthesis of three model proteins (Burgenson *et al.*, 2018). Implementations of new extracts in our standardized cell-free expression system are not trivial, as many parameters need to be changed and/or adjusted to ensure

high yields of folded protein species ultimately. In future, such cell-free platforms will be available where components can be easily replaced and manipulated concerning the proteins properties. The proteins synthesized in this way can then be studied by any experimental methodology to answer various questions, such as channeling mechanisms in voltage-gated proton channels. Nevertheless, the analysis of the dynamics in voltage-gated proton channels will remain a very demanding task in the future.

6 References

Abdine, A., Verhoeven, M. A. and Warschawski, D. E. 2011. Cell-free expression and labeling strategies for a new decade in solid-state NMR. ***N Biotechnol***, 28(3): 272-276.

Agharkar, A., Rzadkowolski, J., McBroom, M. and Gonzales, E. B. 2014. Detergent screening of the human voltage-gated proton channel using fluorescence-detection size-exclusion chromatography. ***Protein Sci***, 23(8): 1136-1147.

Agmon, N. 1995. The Grotthuss mechanism. ***Chemical Physics Letters***, 244(5-6): 456-462.

Albayrak, C. and Swartz, J. R. 2013a. Cell-free co-production of an orthogonal transfer RNA activates efficient site-specific non-natural amino acid incorporation. ***Nucleic Acids Res***, 41(11): 5949-5963.

Albayrak, C. and Swartz, J. R. 2013b. Using *E. coli*-based cell-free protein synthesis to evaluate the kinetic performance of an orthogonal tRNA and aminoacyl-tRNA synthetase pair. ***Biochem Biophys Res Commun***, 431(2): 291-295.

Anderluh, A., Klotzsch, E., Reismann, A. W., Brameshuber, M., Kudlacek, O., Newman, A. H., Sitte, H. H. and Schütz, G. J. 2014. Single molecule analysis reveals coexistence of stable serotonin transporter monomers and oligomers in the live cell plasma membrane. ***J Biol Chem***, 289(7): 4387-4394.

Andersen, O. S. and Koeppe, R. E., 2nd. 2007. Bilayer thickness and membrane protein function: An energetic perspective. ***Annu Rev Biophys Biomol Struct***, 36: 107-130.

Ando, M., Akiyama, M., Okuno, D., Hirano, M., Ide, T., Sawada, S., Sasaki, Y. and Akiyoshi, K. 2016. Liposome chaperon in cell-free membrane protein synthesis: One-step preparation of KcsA-integrated liposomes and electrophysiological analysis by the planar bilayer method. ***Biomater Sci***, 4(2): 258-264.

Anfinsen, C. B. 1973. Principles that govern the folding of protein chains. ***Science***, 181(4096): 223-230.

Anselment, B., Baerend, D., Mey, E., Buchner, J., Weuster-Botz, D. and Haslbeck, M. 2010. Experimental optimization of protein refolding with a genetic algorithm. ***Protein Sci***, 19(11): 2085-2095.

Armstrong, C. M. and Bezanilla, F. 1973. Currents related to movement of the gating particles of the sodium channels. ***Nature***, 242(5398): 459-461.

Arnold, K., Bordoli, L., Kopp, J. and Schwede, T. 2006. The SWISS-MODEL workspace: a web-based environment for protein structure homology modelling. ***Bioinformatics***, 22(2): 195-201.

Babcock, D. F. and Pfeiffer, D. R. 1987. Independent elevation of cytosolic [Ca^{2+}] and pH of mammalian sperm by voltage-dependent and pH-sensitive mechanisms. ***J Biol Chem***, 262(31): 15041-15047.

Bach, L. T., Mackinder, L. C., Schulz, K. G., Wheeler, G., Schroeder, D. C., Brownlee, C. and Riebesell, U. 2013. Dissecting the impact of CO_2 and pH on the mechanisms of photosynthesis and calcification in the coccolithophore *Emiliania huxleyi*. ***New Phytol***, 199(1): 121-134.

Bayburt, T. H., Carlson, J. W. and Sligar, S. G. 1998. Reconstitution and imaging of a membrane protein in a nanometer-size phospholipid bilayer. ***J Struct Biol***, 123(1): 37-44.

Bayburt, T. H., Grinkova, Y. V. and Sligar, S. G. 2002. Self-assembly of discoidal phospholipid bilayer nanoparticles with membrane scaffold proteins. ***Nano Letters***, 2(8): 853-856.

Bayburt, T. H. and Sligar, S. G. 2003. Self-assembly of single integral membrane proteins into soluble nanoscale phospholipid bilayers. ***Protein Sci***, 12(11): 2476-2481.

Bazzacco, P., Billon-Denis, E., Sharma, K. S., Catoire, L. J., Mary, S., Le Bon, C., Point, E., Banères, J. L., Durand, G., Zito, F., Pucci, B. and Popot, J. L. 2012. Nonionic homopolymeric amphipols: application to membrane protein folding, cell-free synthesis, and solution nuclear magnetic resonance. ***Biochemistry***, 51(7): 1416-1430.

Bechara, C. and Robinson, C. V. 2015. Different modes of lipid binding to membrane proteins probed by mass spectrometry. ***J Am Chem Soc***, 137(16): 5240-5247.

Benkert, P., Biasini, M. and Schwede, T. 2011. Toward the estimation of the absolute quality of individual protein structure models. ***Bioinformatics***, 27(3): 343-350.

Bennett, A. L. and Ramsey, I. S. 2017. CrossTalk opposing view: proton transfer in Hv1 utilizes a water wire, and does not require transient protonation of a conserved aspartate in the S1 transmembrane helix. ***J Physiol***, 595(22): 6797-6799.

Berger, P., Schaffitzel, C., Berger, I., Ban, N. and Suter, U. 2003. Membrane association of myotubularin-related protein 2 is mediated by a pleckstrin homology-GRAM domain and a coiled-coil dimerization module. ***Proc Natl Acad Sci U S A***, 100(21): 12177-12182.

Berger, T. K. and Isacoff, E. Y. 2011. The pore of the voltage-gated proton channel. ***Neuron***, 72(6): 991-1000.

Berger, T. K., Fußhöller, D. M., Goodwin, N., Bönigk, W., Müller, A., Dokani Khesroshahi, N., Brenker, C., Wachten, D., Krause, E., Kaupp, U. B. and Strünker, T. 2017. Post-translational cleavage of Hv1 in human sperm tunes pH- and voltage-dependent gating. ***J Physiol***, 595(5): 1533-1546.

Berman, H. M., Westbrook, J., Feng, Z., Gilliland, G., Bhat, T. N., Weissig, H., Shindyalov, I. N. and Bourne, P. E. 2000. The Protein Data Bank. ***Nucleic Acids Res***, 28(1): 235-242.

Berrier, C., Guilvout, I., Bayan, N., Park, K. H., Mesneau, A., Chami, M., Pugsley, A. P. and Ghazi, A. 2011. Coupled cell-free synthesis and lipid vesicle insertion of a functional oligomeric channel MscL. MscL does not need the insertase YidC for insertion *in vitro*. ***Biochim Biophys Acta***, 1808(1): 41-46.

Bezanilla, F. 2008. How membrane proteins sense voltage. ***Nat Rev Mol Cell Biol***, 9(4): 323-332.

Biasini, M., Bienert, S., Waterhouse, A., Arnold, K., Studer, G., Schmidt, T., Kiefer, F., Gallo Cassarino, T., Bertoni, M., Bordoli, L. and Schwede, T. 2014. SWISS-MODEL: modelling protein tertiary and quaternary structure using evolutionary information. ***Nucleic Acids Res***, 42(Web Server issue): W252-258.

Bibow, S., Polyhach, Y., Eichmann, C., Chi, C. N., Kowal, J., Albiez, S., McLeod, R. A., Stahlberg, H., Jeschke, G., Güntert, P. and Riek, R. 2017. Solution structure of discoidal high-density lipoprotein particles with a shortened apolipoprotein A-I. ***Nat Struct Mol Biol***, 24(2): 187-193.

Blanchette, C. D., Cappuccio, J. A., Kuhn, E. A., Segelke, B. W., Benner, W. H., Chromy, B. A., Coleman, M. A., Bench, G., Hoeprich, P. D. and Sulchek, T. A. 2009. Atomic force microscopy differentiates discrete size distributions between membrane protein containing and empty nanolipoprotein particles. ***Biochim Biophys Acta***, 1788(3): 724-731.

Bloch, F., Hansen, W. W. and Packard, M. 1946. The nuclear induction experiment. ***Physical Review***, 70(7-8): 474-485.

Boggs, J. M. 1987. Lipid intermolecular hydrogen bonding: Influence on structural organization and membrane function. ***Biochim Biophys Acta***, 906(3): 353-404.

Boland, C., Li, D., Shah, S. T. A., Haberstock, S., Dötsch, V., Bernhard, F. and Caffrey, M. 2014. Cell-free expression and *in meso* crystallisation of an integral membrane kinase for structure determination. ***Cell Mol Life Sci***, 71(24): 4895-4910.

Boonamnaj, P. and Sompornpisut, P. 2018. Insight into the role of the Hv1 C-terminal domain in dimer stabilization. ***J Phys Chem B***, 122(3): 1037-1048.

Boron, W. F. 1983. Transport of H^+ and of ionic weak acids and bases. ***J Membr Biol***, 72(1-2): 1-16.

Boron, W. F. and Boulpaep, E. L. 2012. Medical Physiology, 2nd ed.: 1352: Elsevier Health Sciences.

Bundy, B. C. and Swartz, J. R. 2010. Site-specific incorporation of *p*-propargyloxyphenylalanine in a cell-free environment for direct protein-protein click conjugation. ***Bioconjug Chem***, 21(2): 255-263.

Buntru, M., Vogel, S., Spiegel, H. and Schillberg, S. 2014. Tobacco BY-2 cell-free lysate: an alternative and highly-productive plant-based in vitro translation system. ***BMC Biotechnol***, 14: 37.

Burgenson, D., Gurramkonda, C., Pilli, M., Ge, X., Andar, A., Kostov, Y., Tolosa, L. and Rao, G. 2018. Rapid recombinant protein expression in cell-free extracts from human blood. ***Sci Rep***, 8(1): 9569.

Butterwick, J. A. and MacKinnon, R. 2010. Solution structure and phospholipid interactions of the isolated voltage-sensor domain from KvAP. ***J Mol Biol***, 403(4): 591-606.

Caffrey, M. and Feigenson, G. W. 1981a. Fluorescence quenching in model membranes. 3. Relationship between calcium adenosinetriphosphatase enzyme activity and the affinity of the protein for phosphatidylcholines with different acyl chain characteristics. ***Biochemistry***, 20(7): 1949-1961.

Caffrey, M. and Feigenson, G. W. 1981b. Fatty-acyl-chain characteristics of phosphatidylcholines affect Ca^{2+}-dependent ATPase enzymic activity but not the affinity of the protein for these different lipid species. ***Biochem Soc Trans***, 9(1): 155-156.

Capasso, M., Bhamrah, M. K., Henley, T., Boyd, R. S., Langlais, C., Cain, K., Dinsdale, D., Pulford, K., Khan, M., Musset, B., Cherny, V. V., Morgan, D., Gascoyne, R. D., Vigorito, E., DeCoursey, T. E., MacLennan, I. C. and Dyer, M. J. 2010. HVCN1 modulates BCR signal strength via regulation of BCR-dependent generation of reactive oxygen species. ***Nat Immunol***, 11(3): 265-272.

Carlson, J. W., Jonas, A. and Sligar, S. G. 1997. Imaging and manipulation of high-density lipoproteins. ***Biophys J***, 73(3): 1184-1189.

Carmona, E. M., Larsson, H. P., Neely, A., Alvarez, O., Latorre, R. and Gonzalez, C. 2018. Gating charge displacement in a monomeric voltage-gated proton (H_V1) channel. ***Proc Natl Acad Sci U S A***, 115(37): 9240-9245.

Chamberlin, A., Qiu, F., Rebolledo, S., Wang, Y., Noskov, S. Y. and Larsson, H. P. 2014. Hydrophobic plug functions as a gate in voltage-gated proton channels. ***Proc Natl Acad Sci U S A***, 111(2): E273-282.

Chamberlin, A., Qiu, F., Wang, Y., Noskov, S. Y. and Larsson, H. P. 2015. Mapping the gating and permeation pathways in the voltage-gated proton channel Hv1. ***J Mol Biol***, 427(1): 131-145.

Chaves, G., Derst, C., Franzen, A., Mashimo, Y., Machida, R. and Musset, B. 2016. Identification of an H_V1 voltage-gated proton channel in insects. ***FEBS J***, 283(8): 1453-1464.

Chemla, Y., Ozer, E., Schlesinger, O., Noireaux, V. and Alfonta, L. 2015. Genetically expanded cell-free protein synthesis using endogenous pyrrolysyl orthogonal translation system. ***Biotechnol Bioeng***, 112(8): 1663-1672.

Chemla, Y., Friedman, M., Heltberg, M., Bakhrat, A., Nagar, E., Schwarz, R., Jensen, M. H. and Alfonta, L. 2017. Expanding the Genetic Code of a Photoautotrophic Organism. ***Biochemistry***, 56(16): 2161-2165.

Chen, W. N., Kuppan, K. V., Lee, M. D., Jaudzems, K., Huber, T. and Otting, G. 2015. O-tert-Butyltyrosine, an NMR tag for high-molecular-weight systems and measurements of submicromolar ligand binding affinities. ***J Am Chem Soc***, 137(13): 4581-4586.

Cherny, V. V. and DeCoursey, T. E. 1999. pH-dependent inhibition of voltage-gated H^+ currents in rat alveolar epithelial cells by Zn^{2+} and other divalent cations. ***J Gen Physiol***, 114(6): 819-838.

Cherny, V. V., Morgan, D., Musset, B., Chaves, G., Smith, S. M. and DeCoursey, T. E. 2015. Tryptophan 207 is crucial to the unique properties of the human voltage-gated proton channel, hH_V1. ***J Gen Physiol***, 146(5): 343-356.

Conese, M., Castellani, S., Lepore, S., Palumbo, O., Manca, A., Santostasi, T., Polizzi, A. M., Copetti, M., Di Gioia, S., Casavola, V., Guerra, L., Diana, A., Montemurro, P., Mariggiò, M. A., Gallo, C., Maffione, A. B. and Carella, M. 2014. Evaluation of genome-wide expression profiles of blood and sputum neutrophils in cystic fibrosis patients before and after antibiotic therapy. ***PLoS One***, 9(8): e104080.

Consortium, T. U. 2017. UniProt: the universal protein knowledgebase. ***Nucleic Acids Res***, 45(D1): D158-D169.

Covino, R., Ballweg, S., Stordeur, C., Michaelis, J. B., Puth, K., Wernig, F., Bahrami, A., Ernst, A. M., Hummer, G. and Ernst, R. 2016. A eukaryotic sensor for membrane lipid saturation. ***Mol Cell***, 63(1): 49-59.

Cybulski, L. E. and de Mendoza, D. 2011. Bilayer hydrophobic thickness and integral membrane protein function. ***Curr Protein Pept Sci***, 12(8): 760-766.

Daury, L., Taveau, J. C., Salvador, D., Glavier, M. and Lambert, O. 2017. Reconstitution of membrane proteins into Nanodiscs for single-particle electron microscopy. ***Methods Mol Biol***, 1635: 317-327.

DeCoursey, T. E. 1991. Hydrogen ion currents in rat alveolar epithelial cells. ***Biophys J***, 60(5): 1243-1253.

DeCoursey, T. E. and Cherny, V. V. 1993. Potential, pH, and arachidonate gate hydrogen ion currents in human neutrophils. ***Biophys J***, 65(4): 1590-1598.

DeCoursey, T. E. and Cherny, V. V. 1994. Voltage-activated hydrogen ion currents. ***J Membr Biol***, 141(3): 203-223.

DeCoursey, T. E. and Cherny, V. V. 1997. Deuterium isotope effects on permeation and gating of proton channels in rat alveolar epithelium. ***J Gen Physiol***, 109(4): 415-434.

DeCoursey, T. E. 1998. Four varieties of voltage-gated proton channels. ***Front Biosci***, 3: d477-482.

DeCoursey, T. E. and Cherny, V. V. 1998. Temperature dependence of voltage-gated H^+ currents in human neutrophils, rat alveolar epithelial cells, and mammalian phagocytes. ***J Gen Physiol***, 112(4): 503-522.

DeCoursey, T. E. 2003. Voltage-gated proton channels and other proton transfer pathways. ***Physiol Rev***, 83(2): 475-579.

DeCoursey, T. E. 2013. Voltage-gated proton channels: molecular biology, physiology, and pathophysiology of the H_V family. ***Physiol Rev***, 93(2): 599-652.

DeCoursey, T. E. 2015. The voltage-gated proton channel: A riddle, wrapped in a mystery, inside an enigma. ***Biochemistry***, 54(21): 3250-3268.

DeCoursey, T. E., Morgan, D., Musset, B. and Cherny, V. V. 2016. Insights into the structure and function of H_V1 from a meta-analysis of mutation studies. ***J Gen Physiol***, 148(2): 97-118.

DeCoursey, T. E. 2017. CrossTalk proposal: Proton permeation through H_V1 requires transient protonation of a conserved aspartate in the S1 transmembrane helix. ***J Physiol***, 595(22): 6793-6795.

DeCoursey, T. E. 2018a. Gating currents indicate complex gating of voltage-gated proton channels. ***Proc Natl Acad Sci U S A***, 115(37): 9057-9059.

DeCoursey, T. E. 2018b. Voltage and pH sensing by the voltage-gated proton channel, HV1. ***J R Soc Interface***, 15(141).

Dehez, F., Schanda, P., King, M. S., Kunji, E. R. S. and Chipot, C. 2017. Mitochondrial ADP/ATP carrier in dodecylphosphocholine binds cardiolipins with non-native affinity. ***Biophys J***, 113(11): 2311-2315.

Demaurex, N., Grinstein, S., Jaconi, M., Schlegel, W., Lew, D. P. and Krause, K. H. 1993. Proton currents in human granulocytes: regulation by membrane potential and intracellular pH. ***J Physiol***, 466: 329-344.

Deng, N. N., Yelleswarapu, M. and Huck, W. T. 2016. Monodisperse uni- and multicompartment liposomes. ***J Am Chem Soc***, 138(24): 7584-7591.

Deniaud, A., Liguori, L., Blesneac, I., Lenormand, J. L. and Pebay-Peyroula, E. 2010. Crystallization of the membrane protein hVDAC1 produced in cell-free system. ***Biochim Biophys Acta***, 1798(8): 1540-1546.

Denisov, I. G., Grinkova, Y. V., Lazarides, A. A. and Sligar, S. G. 2004. Directed self-assembly of monodisperse phospholipid bilayer Nanodiscs with controlled size. ***J Am Chem Soc***, 126(11): 3477-3487.

Denisov, I. G., McLean, M. A., Shaw, A. W., Grinkova, Y. V. and Sligar, S. G. 2005. Thermotropic phase transition in soluble nanoscale lipid bilayers. ***J Phys Chem B***, 109(32): 15580-15588.

Dobson, C. M. 2004. Experimental investigation of protein folding and misfolding. ***Methods***, 34(1): 4-14.

Dudev, T., Musset, B., Morgan, D., Cherny, V. V., Smith, S. M., Mazmanian, K., DeCoursey, T. E. and Lim, C. 2015. Selectivity mechanism of the voltage-gated proton channel, H_V1. ***Sci Rep***, 5: 10320.

Eder, C. and DeCoursey, T. E. 2001. Voltage-gated proton channels in microglia. ***Prog Neurobiol***, 64(3): 277-305.

Elter, S., Raschle, T., Arens, S., Viegas, A., Gelev, V., Etzkorn, M. and Wagner, G. 2014. The use of amphipols for NMR structural characterization of 7-TM proteins. ***J Membr Biol***, 247(9-10): 957-964.

Elvington, S. M., Liu, C. W. and Maduke, M. C. 2009. Substrate-driven conformational changes in ClC-ec1 observed by fluorine NMR. ***EMBO J***, 28(20): 3090-3102.

Farjon, J., Boisbouvier, J., Schanda, P., Pardi, A., Simorre, J. P. and Brutscher, B. 2009. Longitudinal-relaxation-enhanced NMR experiments for the study of nucleic acids in solution. ***J Am Chem Soc***, 131(24): 8571-8577.

Fisher, R. A. 1935. ***The design of experiments***. Oxford, England: Oliver & Boyd.

Flügel, V., Vrabel, M. and Schneider, S. 2014. Structural basis for the site-specific incorporation of lysine derivatives into proteins. ***PLoS One***, 9(4): e96198.

Focke, P. J., Hein, C., Hoffmann, B., Matulef, K., Bernhard, F., Dötsch, V. and Valiyaveetil, F. I. 2016. Combining *in vitro* folding with cell-free protein synthesis for membrane protein expression. ***Biochemistry***, 55(30): 4212-4219.

Fogel, M. and Hastings, J. W. 1972. Bioluminescence: mechanism and mode of control of scintillon activity. ***Proc Natl Acad Sci U S A***, 69(3): 690-693.

Foshag, D., Henrich, E., Hiller, E., Schäfer, M., Kerger, C., Burger-Kentischer, A., Diaz-Moreno, I., Garcia-Maurino, S. M., Dötsch, V., Rupp, S. and Bernhard, F. 2018. The *E. coli* S30 lysate proteome: A prototype for cell-free protein production. ***N Biotechnol***, 40(Pt B): 245-260.

Fraher, D., Sanigorski, A., Mellett, N. A., Meikle, P. J., Sinclair, A. J. and Gibert, Y. 2016. Zebrafish embryonic lipidomic analysis reveals that the Yolk cell is metabolically active in processing lipid. ***Cell Rep***, 14(6): 1317-1329.

Fujiki, Y., Hubbard, A. L., Fowler, S. and Lazarow, P. B. 1982. Isolation of intracellular membranes by means of sodium carbonate treatment: Application to endoplasmic reticulum. ***J Cell Biol***, 93(1): 97-102.

Fujiwara, K. and Doi, N. 2016. Biochemical preparation of cell extract for cell-free protein synthesis without physical disruption. ***PLoS One***, 11(4): e0154614.

Fujiwara, Y., Kurokawa, T., Takeshita, K., Kobayashi, M., Okochi, Y., Nakagawa, A. and Okamura, Y. 2012. The cytoplasmic coiled-coil mediates cooperative gating temperature sensitivity in the voltage-gated H^+ channel Hv1. ***Nat Commun***, 3: 816.

Fujiwara, Y., Takeshita, K., Nakagawa, A. and Okamura, Y. 2013. Structural characteristics of the redox-sensing coiled coil in the voltage-gated H^+ channel. ***J Biol Chem***, 288(25): 17968-17975.

Fujiwara, Y., Kurokawa, T. and Okamura, Y. 2014. Long α helices projecting from the membrane as the dimer interface in the voltage-gated H^+ channel. ***J Gen Physiol***, 143(3): 377-386.

Gan, R., Perez, J. G., Carlson, E. D., Ntai, I., Isaacs, F. J., Kelleher, N. L. and Jewett, M. C. 2017. Translation system engineering in *Escherichia coli* enhances non-canonical amino acid incorporation into proteins. ***Biotechnol Bioeng***, 114(5): 1074-1086.

Genji, T., Nozawa, A. and Tozawa, Y. 2010. Efficient production and purification of functional bacteriorhodopsin with a wheat-germ cell-free system and a combination of Fos-choline and CHAPS detergents. ***Biochem Biophys Res Commun***, 400(4): 638-642.

Gianti, E., Delemotte, L., Klein, M. L. and Carnevale, V. 2016. On the role of water density fluctuations in the inhibition of a proton channel. ***Proc Natl Acad Sci U S A***, 113(52): E8359-E8368.

Gill, S. C. and von Hippel, P. H. 1989. Calculation of protein extinction coefficients from amino acid sequence data. ***Anal Biochem***, 182(2): 319-326.

Goerke, A. R. and Swartz, J. R. 2008. Development of cell-free protein synthesis platforms for disulfide bonded proteins. ***Biotechnol Bioeng***, 99(2): 351-367.

Goerke, A. R. and Swartz, J. R. 2009. High-level cell-free synthesis yields of proteins containing site-specific non-natural amino acids. ***Biotechnol Bioeng***, 102(2): 400-416.

Gonzalez, C., Koch, H. P., Drum, B. M. and Larsson, H. P. 2010. Strong cooperativity between subunits in voltage-gated proton channels. ***Nat Struct Mol Biol***, 17(1): 51-56.

Grinkova, Y. V., Denisov, I. G. and Sligar, S. G. 2010. Engineering extended membrane scaffold proteins for self-assembly of soluble nanoscale lipid bilayers. ***Protein Eng Des Sel***, 23(11): 843-848.

Guarino, C. and DeLisa, M. P. 2012. A prokaryote-based cell-free translation system that efficiently synthesizes glycoproteins. ***Glycobiology***, 22(5): 596-601.

Guignard, L., Ozawa, K., Pursglove, S. E., Otting, G. and Dixon, N. E. 2002. NMR analysis of in vitro-synthesized proteins without purification: A high-throughput approach. ***FEBS Lett***, 524(1-3): 159-162.

Guilvout, I., Chami, M., Berrier, C., Ghazi, A., Engel, A., Pugsley, A. P. and Bayan, N. 2008. *In vitro* multimerization and membrane insertion of bacterial outer membrane secretin PulD. ***J Mol Biol***, 382(1): 13-23.

Guo, J., Melancon, C. E., 3rd, Lee, H. S., Groff, D. and Schultz, P. G. 2009. Evolution of amber suppressor tRNAs for efficient bacterial production of proteins containing nonnatural amino acids. ***Angew Chem Int Ed Engl***, 48(48): 9148-9151.

Gutknecht, J. 1988. Proton conductance caused by long-chain fatty acids in phospholipid bilayer membranes. ***J Membr Biol***, 106(1): 83-93.

Haberstock, S., Roos, C., Hoevels, Y., Dötsch, V., Schnapp, G., Pautsch, A. and Bernhard, F. 2012. A systematic approach to increase the efficiency of membrane protein production in cell-free expression systems. ***Protein Expr Purif***, 82(2): 308-316.

Haglund, S., Almer, S., Peterson, C. and Söderman, J. 2013. Gene expression and thiopurine metabolite profiling in inflammatory bowel disease - novel clues to drug targets and disease mechanisms? ***PLoS One***, 8(2): e56989.

Hagn, F., Etzkorn, M., Raschle, T. and Wagner, G. 2013. Optimized phospholipid bilayer nanodiscs facilitate high-resolution structure determination of membrane proteins. ***J Am Chem Soc***, 135(5): 1919-1925.

Harbers, M. 2014. Wheat germ systems for cell-free protein expression. ***FEBS Lett***, 588(17): 2762-2773.

Hein, C., Henrich, E., Orbán, E., Dötsch, V. and Bernhard, F. 2014. Hydrophobic supplements in cell-free systems: Designing artificial environments for membrane proteins. ***Engineering in Life Sciences***, 14(4): 365-379.

Hein, C., Löhr, F., Schwarz, D. and Dötsch, V. 2017. Acceleration of protein backbone NMR assignment by combinatorial labeling: Application to a small molecule binding study. ***Biopolymers***, 107(5).

Heinemann, I. U., Rovner, A. J., Aerni, H. R., Rogulina, S., Cheng, L., Olds, W., Fischer, J. T., Söll, D., Isaacs, F. J. and Rinehart, J. 2012. Enhanced phosphoserine insertion during *Escherichia coli* protein synthesis via partial UAG codon reassignment and release factor 1 deletion. ***FEBS Lett***, 586(20): 3716-3722.

Henderson, L. M., Chappell, J. B. and Jones, O. T. 1987. The superoxide-generating NADPH oxidase of human neutrophils is electrogenic and associated with an H^+ channel. ***Biochem J***, 246(2): 325-329.

Henrich, E., Ma, Y., Engels, I., Münch, D., Otten, C., Schneider, T., Henrichfreise, B., Sahl, H. G., Dötsch, V. and Bernhard, F. 2016. Lipid requirements for the enzymatic activity of MraY translocases and *in vitro* reconstitution of the lipid II synthesis pathway. ***J Biol Chem***, 291(5): 2535-2546.

Henrich, E., Peetz, O., Hein, C., Laguerre, A., Hoffmann, B., Hoffmann, J., Dötsch, V., Bernhard, F. and Morgner, N. 2017a. Analyzing native membrane protein assembly in nanodiscs by combined non-covalent mass spectrometry and synthetic biology. ***Elife***, 6.

Henrich, E., Sörmann, J., Eberhardt, P., Peetz, O., Mezhyrova, J., Morgner, N., Fendler, K., Dötsch, V., Wachtveitl, J., Bernhard, F. and Bamann, C. 2017b. From gene to function:

Cell-free electrophysiological and optical analysis of ion pumps in Nanodiscs. ***Biophys J***, 113(6): 1331-1341.

Hille, B. 2001. ***Ion channels of excitable membranes*** (3rd ed.): Sinauer Sunderland, MA.

Hodgman, C. E. and Jewett, M. C. 2013. Optimized extract preparation methods and reaction conditions for improved yeast cell-free protein synthesis. ***Biotechnol Bioeng***, 110(10): 2643-2654.

Hoffmann, B., Löhr, F., Laguerre, A., Bernhard, F. and Dötsch, V. 2018. Protein labeling strategies for liquid-state NMR spectroscopy using cell-free synthesis. ***Prog Nucl Magn Reson Spectrosc***, 105: 1-22.

Hondares, E., Brown, M. A., Musset, B., Morgan, D., Cherny, V. V., Taubert, C., Bhamrah, M. K., Coe, D., Marelli-Berg, F., Gribben, J. G., Dyer, M. J., DeCoursey, T. E. and Capasso, M. 2014. Enhanced activation of an amino-terminally truncated isoform of the voltage-gated proton channel HVCN1 enriched in malignant B cells. ***Proc Natl Acad Sci U S A***, 111(50): 18078-18083.

Hong, L., Pathak, M. M., Kim, I. H., Ta, D. and Tombola, F. 2013. Voltage-sensing domain of voltage-gated proton channel Hv1 shares mechanism of block with pore domains. ***Neuron***, 77(2): 274-287.

Hong, L., Kim, I. H. and Tombola, F. 2014a. Molecular determinants of Hv1 proton channel inhibition by guanidine derivatives. ***Proc Natl Acad Sci U S A***, 111(27): 9971-9976.

Hong, L., Singh, V., Wulff, H. and Tombola, F. 2015. Interrogation of the intersubunit interface of the open Hv1 proton channel with a probe of allosteric coupling. ***Sci Rep***, 5: 14077.

Hong, S. H., Kwon, Y. C. and Jewett, M. C. 2014b. Non-standard amino acid incorporation into proteins using *Escherichia coli* cell-free protein synthesis. ***Front Chem***, 2: 34.

Hong, S. H., Ntai, I., Haimovich, A. D., Kelleher, N. L., Isaacs, F. J. and Jewett, M. C. 2014c. Cell-free protein synthesis from a release factor 1 deficient *Escherichia coli* activates efficient and multiple site-specific nonstandard amino acid incorporation. ***ACS Synth Biol***, 3(6): 398-409.

Hopper, J. T., Yu, Y. T., Li, D., Raymond, A., Bostock, M., Liko, I., Mikhailov, V., Laganowsky, A., Benesch, J. L., Caffrey, M., Nietlispach, D. and Robinson, C. V. 2013. Detergent-free mass spectrometry of membrane protein complexes. ***Nat Methods***, 10(12): 1206-1208.

Hossain, M. I., Iwasaki, H., Okochi, Y., Chahine, M., Higashijima, S., Nagayama, K. and Okamura, Y. 2008. Enzyme domain affects the movement of the voltage sensor in ascidian and zebrafish voltage-sensing phosphatases. ***J Biol Chem***, 283(26): 18248-18259.

Hu, F., Luo, W. and Hong, M. 2010. Mechanisms of proton conduction and gating in influenza M2 proton channels from solid-state NMR. ***Science***, 330(6003): 505-508.

Iwasaki, H., Murata, Y., Kim, Y., Hossain, M. I., Worby, C. A., Dixon, J. E., McCormack, T., Sasaki, T. and Okamura, Y. 2008. A voltage-sensing phosphatase, Ci-VSP, which shares sequence identity with PTEN, dephosphorylates phosphatidylinositol 4,5-bisphosphate. ***Proc Natl Acad Sci U S A***, 105(23): 7970-7975.

Jabar, S., Adams, L. A., Wang, Y., Aurelio, L., Graham, B. and Otting, G. 2017. Chemical tagging with *tert*-butyl and trimethylsilyl groups for measuring intermolecular nuclear overhauser effects in a large protein-ligand complex. ***Chemistry***, 23(53): 13033-13036.

Jackson, J. C., Duffy, S. P., Hess, K. R. and Mehl, R. A. 2006. Improving nature's enzyme active site with genetically encoded unnatural amino acids. ***J Am Chem Soc***, 128(34): 11124-11127.

Jackson, J. C., Hammill, J. T. and Mehl, R. A. 2007. Site-specific incorporation of a ^{19}F-amino acid into proteins as an NMR probe for characterizing protein structure and reactivity. ***J Am Chem Soc***, 129(5): 1160-1166.

Jiang, W. X., Gu, X. H., Dong, X. and Tang, C. 2017. Lanthanoid tagging via an unnatural amino acid for protein structure characterization. ***J Biomol NMR***, 67(4): 273-282.

Johnson, D. B., Xu, J., Shen, Z., Takimoto, J. K., Schultz, M. D., Schmitz, R. J., Xiang, Z., Ecker, J. R., Briggs, S. P. and Wang, L. 2011. RF1 knockout allows ribosomal incorporation of unnatural amino acids at multiple sites. ***Nat Chem Biol***, 7(11): 779-786.

Junge, F., Haberstock, S., Roos, C., Stefer, S., Proverbio, D., Dötsch, V. and Bernhard, F. 2011. Advances in cell-free protein synthesis for the functional and structural analysis of membrane proteins. ***N Biotechnol***, 28(3): 262-271.

Kalmbach, R., Chizhov, I., Schumacher, M. C., Friedrich, T., Bamberg, E. and Engelhard, M. 2007. Functional cell-free synthesis of a seven helix membrane protein: In situ insertion of bacteriorhodopsin into liposomes. ***J Mol Biol***, 371(3): 639-648.

Kalstrup, T. and Blunck, R. 2017. Voltage-clamp fluorometry in xenopus oocytes using fluorescent unnatural amino acids. ***J Vis Exp***(123).

Kalstrup, T. and Blunck, R. 2018. S4-S5 linker movement during activation and inactivation in voltage-gated K^+ channels. ***Proc Natl Acad Sci U S A***, 115(29): E6751-E6759.

Kapus, A., Romanek, R., Qu, A. Y., Rotstein, O. D. and Grinstein, S. 1993. A pH-sensitive and voltage-dependent proton conductance in the plasma membrane of macrophages. ***J Gen Physiol***, 102(4): 729-760.

Kavran, J. M., Gundllapalli, S., O'Donoghue, P., Englert, M., Söll, D. and Steitz, T. A. 2007. Structure of pyrrolysyl-tRNA synthetase, an archaeal enzyme for genetic code innovation. ***Proc Natl Acad Sci U S A***, 104(27): 11268-11273.

Kawanabe, A. and Okamura, Y. 2016. Effects of unsaturated fatty acids on the kinetics of voltage-gated proton channels heterologously expressed in cultured cells. ***J Physiol***, 594(3): 595-610.

Kigawa, T., Muto, Y. and Yokoyama, S. 1995. Cell-free synthesis and amino acid-selective stable isotope labeling of proteins for NMR analysis. ***J Biomol NMR***, 6(2): 129-134.

Kigawa, T., Yabuki, T., Matsuda, N., Matsuda, T., Nakajima, R., Tanaka, A. and Yokoyama, S. 2004. Preparation of *Escherichia coli* cell extract for highly productive cell-free protein expression. ***J Struct Funct Genomics***, 5(1-2): 63-68.

Kigundu, G., Cooper, J. L. and Smith, S. M. E. 2018. H_V1 proton channels in dinoflagellates: Not just for bioluminescence? ***J Eukaryot Microbiol***.

Kim, M. K. and Kang, Y. K. 1999. Positional preference of proline in α-helices. ***Protein Sci***, 8(7): 1492-1499.

Klammt, C., Löhr, F., Schäfer, B., Haase, W., Dötsch, V., Rüterjans, H., Glaubitz, C. and Bernhard, F. 2004. High level cell-free expression and specific labeling of integral membrane proteins. ***Eur J Biochem***, 271(3): 568-580.

Klammt, C., Schwarz, D., Löhr, F., Schneider, B., Dötsch, V. and Bernhard, F. 2006. Cell-free expression as an emerging technique for the large scale production of integral membrane protein. ***FEBS J***, 273(18): 4141-4153.

Klammt, C., Maslennikov, I., Bayrhuber, M., Eichmann, C., Vajpai, N., Chiu, E. J., Blain, K. Y., Esquivies, L., Kwon, J. H., Balana, B., Pieper, U., Sali, A., Slesinger, P. A., Kwiatkowski,

W., Riek, R. and Choe, S. 2012. Facile backbone structure determination of human membrane proteins by NMR spectroscopy. ***Nat Methods***, 9(8): 834-839.

Klyszejko, A. L., Shastri, S., Mari, S. A., Grubmüller, H., Muller, D. J. and Glaubitz, C. 2008. Folding and assembly of proteorhodopsin. ***J Mol Biol***, 376(1): 35-41.

Knapp, K. G., Goerke, A. R. and Swartz, J. R. 2007. Cell-free synthesis of proteins that require disulfide bonds using glucose as an energy source. ***Biotechnol Bioeng***, 97(4): 901-908.

Knowles, T. J., Finka, R., Smith, C., Lin, Y. P., Dafforn, T. and Overduin, M. 2009. Membrane proteins solubilized intact in lipid containing nanoparticles bounded by styrene maleic acid copolymer. ***J Am Chem Soc***, 131(22): 7484-7485.

Koch, H. P., Kurokawa, T., Okochi, Y., Sasaki, M., Okamura, Y. and Larsson, H. P. 2008. Multimeric nature of voltage-gated proton channels. ***Proc Natl Acad Sci U S A***, 105(26): 9111-9116.

Kohlstaedt, M., von der Hocht, I., Hilbers, F., Thielmann, Y. and Michel, H. 2015. Development of a Thermofluor assay for stability determination of membrane proteins using the Na^+/H^+ antiporter NhaA and cytochrome c oxidase. ***Acta Crystallogr D Biol Crystallogr***, 71(Pt 5): 1112-1122.

Kohout, S. C., Ulbrich, M. H., Bell, S. C. and Isacoff, E. Y. 2008. Subunit organization and functional transitions in Ci-VSP. ***Nat Struct Mol Biol***, 15(1): 106-108.

Koshy, C., Schweikhard, E. S., Gärtner, R. M., Perez, C., Yildiz, O. and Ziegler, C. 2013. Structural evidence for functional lipid interactions in the betaine transporter BetP. ***EMBO J***, 32(23): 3096-3105.

Kovácsová, G., Gustavsson, E., Wang, J., Kreir, M., Peuker, S. and Westenhoff, S. 2015. Cell-free expression of a functional pore-only sodium channel. ***Protein Expr Purif***, 111: 42-47.

Kucher, S., Korneev, S., Tyagi, S., Apfelbaum, R., Grohmann, D., Lemke, E. A., Klare, J. P., Steinhoff, H. J. and Klose, D. 2017. Orthogonal spin labeling using click chemistry for *in vitro* and *in vivo* applications. ***J Magn Reson***, 275: 38-45.

Kulleperuma, K., Smith, S. M., Morgan, D., Musset, B., Holyoake, J., Chakrabarti, N., Cherny, V. V., DeCoursey, T. E. and Pomès, R. 2013. Construction and validation of a homology model of the human voltage-gated proton channel hH_V1. ***J Gen Physiol***, 141(4): 445-465.

Kuno, M., Ando, H., Morihata, H., Sakai, H., Mori, H., Sawada, M. and Oiki, S. 2009. Temperature dependence of proton permeation through a voltage-gated proton channel. ***J Gen Physiol***, 134(3): 191-205.

Kurauskas, V., Hessel, A., Ma, P., Lunetti, P., Weinhäupl, K., Imbert, L., Brutscher, B., King, M. S., Sounier, R., Dolce, V., Kunji, E. R. S., Capobianco, L., Chipot, C., Dehez, F., Bersch, B. and Schanda, P. 2018. How detergent impacts membrane proteins: Atomic-level views of mitochondrial carriers in dodecylphosphocholine. ***J Phys Chem Lett***, 9(5): 933-938.

Lacroix, J. J., Hyde, H. C., Campos, F. V. and Bezanilla, F. 2014. Moving gating charges through the gating pore in a Kv channel voltage sensor. ***Proc Natl Acad Sci U S A***, 111(19): E1950-1959.

Laemmli, U. K. 1970. Cleavage of structural proteins during the assembly of the head of bacteriophage T4. ***Nature***, 227(5259): 680-685.

Laganowsky, A., Reading, E., Hopper, J. T. and Robinson, C. V. 2013. Mass spectrometry of intact membrane protein complexes. ***Nat Protoc***, 8(4): 639-651.

Laguerre, A., Löhr, F., Bernhard, F. and Dötsch, V. 2015. Labeling of membrane proteins by cell-free expression, ***Methods in Enzymology***, Vol. 565: 367-388: Elsevier.

Laguerre, A., Löhr, F., Henrich, E., Hoffmann, B., Abdul-Manan, N., Connolly, P. J., Perozo, E., Moore, J. M., Bernhard, F. and Dötsch, V. 2016. From Nanodiscs to isotropic bicelles: A procedure for solution nuclear magnetic resonance studies of detergent-sensitive integral membrane proteins. ***Structure***, 24(10): 1830-1841.

Lajoie, M. J., Rovner, A. J., Goodman, D. B., Aerni, H. R., Haimovich, A. D., Kuznetsov, G., Mercer, J. A., Wang, H. H., Carr, P. A., Mosberg, J. A., Rohland, N., Schultz, P. G., Jacobson, J. M., Rinehart, J., Church, G. M. and Isaacs, F. J. 2013. Genomically recoded organisms expand biological functions. ***Science***, 342(6156): 357-360.

Lazarova, M., Löhr, F., Rues, R. B., Kleebach, R., Dötsch, V. and Bernhard, F. 2018. Precursor-based selective methyl labeling of cell-free synthesized proteins. ***ACS Chem Biol***, 13(8): 2170-2178.

Lee, B. S., Kim, S., Ko, B. J. and Yoo, T. H. 2017. An efficient system for incorporation of unnatural amino acids in response to the four-base codon AGGA in *Escherichia coli*. ***Biochim Biophys Acta Gen Subj***, 1861(11 Pt B): 3016-3023.

Lee, M. M., Jiang, R., Jain, R., Larue, R. C., Krzycki, J. and Chan, M. K. 2008a. Structure of *Desulfitobacterium hafniense* PylSc, a pyrrolysyl-tRNA synthetase. ***Biochem Biophys Res Commun***, 374(3): 470-474.

Lee, S. C., Knowles, T. J., Postis, V. L., Jamshad, M., Parslow, R. A., Lin, Y. P., Goldman, A., Sridhar, P., Overduin, M., Muench, S. P. and Dafforn, T. R. 2016. A method for detergent-free isolation of membrane proteins in their local lipid environment. ***Nat Protoc***, 11(7): 1149-1162.

Lee, S. Y., Letts, J. A. and MacKinnon, R. 2008b. Dimeric subunit stoichiometry of the human voltage-dependent proton channel Hv1. ***Proc Natl Acad Sci U S A***, 105(22): 7692-7695.

Lee, S. Y., Letts, J. A. and MacKinnon, R. 2009. Functional reconstitution of purified human Hv1 H^+ channels. ***J Mol Biol***, 387(5): 1055-1060.

Letts, J. A. 2014. ***Functional and structural studies of the human voltage-gated proton channel***. The Rockefeller University.

Li, C., Wang, G. F., Wang, Y., Creager-Allen, R., Lutz, E. A., Scronce, H., Slade, K. M., Ruf, R. A., Mehl, R. A. and Pielak, G. J. 2010a. Protein ^{19}F NMR in *Escherichia coli*. ***J Am Chem Soc***, 132(1): 321-327.

Li, Q., Jogini, V., Wanderling, S., Cortes, D. M. and Perozo, E. 2012. Expression, purification, and reconstitution of the voltage-sensing domain from Ci-VSP. ***Biochemistry***, 51(41): 8132-8142.

Li, Q., Wanderling, S., Paduch, M., Medovoy, D., Singharoy, A., McGreevy, R., Villalba-Galea, C. A., Hulse, R. E., Roux, B., Schulten, K., Kossiakoff, A. and Perozo, E. 2014. Structural mechanism of voltage-dependent gating in an isolated voltage-sensing domain. ***Nat Struct Mol Biol***, 21(3): 244-252.

Li, Q., Shen, R., Treger, J. S., Wanderling, S. S., Milewski, W., Siwowska, K., Bezanilla, F. and Perozo, E. 2015. Resting state of the human proton channel dimer in a lipid bilayer. ***Proc Natl Acad Sci U S A***, 112(44): E5926-5935.

Li, S. J., Zhao, Q., Zhou, Q., Unno, H., Zhai, Y. and Sun, F. 2010b. The role and structure of the carboxyl-terminal domain of the human voltage-gated proton channel Hv1. ***J Biol Chem***, 285(16): 12047-12054.

Liang, B., Bushweller, J. H. and Tamm, L. K. 2006. Site-directed parallel spin-labeling and paramagnetic relaxation enhancement in structure determination of membrane proteins by solution NMR spectroscopy. ***J Am Chem Soc***, 128(13): 4389-4397.

Lin, T. I. and Schroeder, C. 2001. Definitive assignment of proton selectivity and attoampere unitary current to the M2 ion channel protein of influenza A virus. ***J Virol***, 75(8): 3647-3656.

Lipfert, J., Columbus, L., Chu, V. B., Lesley, S. A. and Doniach, S. 2007. Size and shape of detergent micelles determined by small-angle X-ray scattering. ***J Phys Chem B***, 111(43): 12427-12438.

Lishko, P. V., Botchkina, I. L., Fedorenko, A. and Kirichok, Y. 2010. Acid extrusion from human spermatozoa is mediated by flagellar voltage-gated proton channel. ***Cell***, 140(3): 327-337.

Lishko, P. V. and Kirichok, Y. 2010. The role of Hv1 and CatSper channels in sperm activation. ***J Physiol***, 588(Pt 23): 4667-4672.

Löhr, F., Reckel, S., Karbyshev, M., Connolly, P. J., Abdul-Manan, N., Bernhard, F., Moore, J. M. and Dötsch, V. 2012. Combinatorial triple-selective labeling as a tool to assist membrane protein backbone resonance assignment. ***J Biomol NMR***, 52(3): 197-210.

Löhr, F., Laguerre, A., Bock, C., Reckel, S., Connolly, P. J., Abdul-Manan, N., Tumulka, F., Abele, R., Moore, J. M. and Dötsch, V. 2014. Time-shared experiments for efficient assignment of triple-selectively labeled proteins. ***J Magn Reson***, 248: 81-95.

Löhr, F., Tumulka, F., Bock, C., Abele, R. and Dötsch, V. 2015. An extended combinatorial ^{15}N, $^{13}C^{\alpha}$, and $^{13}C'$ labeling approach to protein backbone resonance assignment. ***J Biomol NMR***, 62(3): 263-279.

Lomize, M. A., Pogozheva, I. D., Joo, H., Mosberg, H. I. and Lomize, A. L. 2012. OPM database and PPM web server: resources for positioning of proteins in membranes. ***Nucleic Acids Res***, 40(Database issue): D370-376.

London, E. and Feigenson, G. W. 1981a. Fluorescence quenching in model membranes. 1. Characterization of quenching caused by a spin-labeled phospholipid. ***Biochemistry***, 20(7): 1932-1938.

London, E. and Feigenson, G. W. 1981b. Fluorescence quenching in model membranes. 2. Determination of local lipid environment of the calcium adenosinetriphosphatase from sarcoplasmic reticulum. ***Biochemistry***, 20(7): 1939-1948.

Long, A. R., O'Brien, C. C. and Alder, N. N. 2012. The cell-free integration of a polytopic mitochondrial membrane protein into liposomes occurs cotranslationally and in a lipid-dependent manner. ***PLoS One***, 7(9): e46332.

Long, A. R., O'Brien, C. C., Malhotra, K., Schwall, C. T., Albert, A. D., Watts, A. and Alder, N. N. 2013. A detergent-free strategy for the reconstitution of active enzyme complexes from native biological membranes into nanoscale discs. ***BMC Biotechnol***, 13: 41.

Long, S. B., Tao, X., Campbell, E. B. and MacKinnon, R. 2007. Atomic structure of a voltage-dependent K^+ channel in a lipid membrane-like environment. ***Nature***, 450(7168): 376-382.

Lynagh, T., Flood, E., Boiteux, C., Wulf, M., Komnatnyy, V. V., Colding, J. M., Allen, T. W. and Pless, S. A. 2017. A selectivity filter at the intracellular end of the acid-sensing ion channel pore. ***Elife***, 6.

Lyukmanova, E. N., Shenkarev, Z. O., Khabibullina, N. F., Kopeina, G. S., Shulepko, M. A., Paramonov, A. S., Mineev, K. S., Tikhonov, R. V., Shingarova, L. N., Petrovskaya, L. E., Dolgikh, D. A., Arseniev, A. S. and Kirpichnikov, M. P. 2012. Lipid-protein nanodiscs

for cell-free production of integral membrane proteins in a soluble and folded state: comparison with detergent micelles, bicelles and liposomes. ***Biochim Biophys Acta***, 1818(3): 349-358.

Ma, Y., Münch, D., Schneider, T., Sahl, H. G., Bouhss, A., Ghoshdastider, U., Wang, J., Dötsch, V., Wang, X. and Bernhard, F. 2011. Preparative scale cell-free production and quality optimization of MraY homologues in different expression modes. ***J Biol Chem***, 286(45): 38844-38853.

Mahaut-Smith, M. P. 1989. The effect of zinc on calcium and hydrogen ion currents in intact snail neurones. ***J Exp Biol***, 145: 455-464.

Marsh, D. 2007. Lateral pressure profile, spontaneous curvature frustration, and the incorporation and conformation of proteins in membranes. ***Biophys J***, 93(11): 3884-3899.

Martin, R. W., Des Soye, B. J., Kwon, Y. C., Kay, J., Davis, R. G., Thomas, P. M., Majewska, N. I., Chen, C. X., Marcum, R. D., Weiss, M. G., Stoddart, A. E., Amiram, M., Ranji Charna, A. K., Patel, J. R., Isaacs, F. J., Kelleher, N. L., Hong, S. H. and Jewett, M. C. 2018. Cell-free protein synthesis from genomically recoded bacteria enables multisite incorporation of noncanonical amino acids. ***Nat Commun***, 9(1): 1203.

Maslennikov, I., Klammt, C., Hwang, E., Kefala, G., Okamura, M., Esquivies, L., Mörs, K., Glaubitz, C., Kwiatkowski, W., Jeon, Y. H. and Choe, S. 2010. Membrane domain structures of three classes of histidine kinase receptors by cell-free expression and rapid NMR analysis. ***Proc Natl Acad Sci U S A***, 107(24): 10902-10907.

Matsuda, M., Takeshita, K., Kurokawa, T., Sakata, S., Suzuki, M., Yamashita, E., Okamura, Y. and Nakagawa, A. 2011. Crystal structure of the cytoplasmic phosphatase and tensin homolog (PTEN)-like region of *Ciona intestinalis* voltage-sensing phosphatase provides insight into substrate specificity and redox regulation of the phosphoinositide phosphatase activity. ***J Biol Chem***, 286(26): 23368-23377.

Matsuda, T., Kigawa, T., Koshiba, S., Inoue, M., Aoki, M., Yamasaki, K., Seki, M., Shinozaki, K. and Yokoyama, S. 2006. Cell-free synthesis of zinc-binding proteins. ***J Struct Funct Genomics***, 7(2): 93-100.

Matthies, D., Haberstock, S., Joos, F., Dötsch, V., Vonck, J., Bernhard, F. and Meier, T. 2011. Cell-free expression and assembly of ATP synthase. ***J Mol Biol***, 413(3): 593-603.

Matz, C. E. and Jonas, A. 1982. Micellar complexes of human apolipoprotein A-I with phosphatidylcholines and cholesterol prepared from cholate-lipid dispersions. ***J Biol Chem***, 257(8): 4535-4540.

Mitchell, A. L., Addy, P. S., Chin, M. A. and Chatterjee, A. 2017. A unique genetically encoded FRET pair in mammalian cells. ***Chembiochem***, 18(6): 511-514.

Miyake-Stoner, S. J., Refakis, C. A., Hammill, J. T., Lusic, H., Hazen, J. L., Deiters, A. and Mehl, R. A. 2010. Generating permissive site-specific unnatural aminoacyl-tRNA synthetases. ***Biochemistry***, 49(8): 1667-1677.

Mizrachi, D., Chen, Y., Liu, J., Peng, H. M., Ke, A., Pollack, L., Turner, R. J., Auchus, R. J. and DeLisa, M. P. 2015. Making water-soluble integral membrane proteins *in vivo* using an amphipathic protein fusion strategy. ***Nat Commun***, 6: 6826.

Mony, L., Berger, T. K. and Isacoff, E. Y. 2015. A specialized molecular motion opens the Hv1 voltage-gated proton channel. ***Nat Struct Mol Biol***, 22(4): 283-290.

Morgan, D., Cherny, V. V., Finnegan, A., Bollinger, J., Gelb, M. H. and DeCoursey, T. E. 2007. Sustained activation of proton channels and NADPH oxidase in human eosinophils

and murine granulocytes requires PKC but not cPLA$_2\alpha$ activity. ***J Physiol***, 579(Pt 2): 327-344.

Morgan, D., Musset, B., Kulleperuma, K., Smith, S. M., Rajan, S., Cherny, V. V., Pomès, R. and DeCoursey, T. E. 2013. Peregrination of the selectivity filter delineates the pore of the human voltage-gated proton channel hH$_V$1. ***J Gen Physiol***, 142(6): 625-640.

Morgan, D., McIntire, P., Cherny, V., Smith, S., Musset, B. and DeCoursey, T. 2015. Proton channels are present in cell membranes of the breast cancer cell line MDA MB 231 and affect recovery from an acid load. ***Biophysical Journal***, 108(2): 587a.

Morgner, N., Barth, H.-D. and Brutschy, B. 2006. A New Way To Detect Noncovalently Bonded Complexes of Biomolecules from Liquid Micro-Droplets by Laser Mass Spectrometry. ***Australian Journal of Chemistry***, 59(2): 109.

Morgner, N. and Robinson, C. V. 2012. Massign: An assignment strategy for maximizing information from the mass spectra of heterogeneous protein assemblies. ***Anal Chem***, 84(6): 2939-2948.

Murata, Y., Iwasaki, H., Sasaki, M., Inaba, K. and Okamura, Y. 2005. Phosphoinositide phosphatase activity coupled to an intrinsic voltage sensor. ***Nature***, 435(7046): 1239-1243.

Musset, B., Morgan, D., Cherny, V. V., MacGlashan, D. W., Jr., Thomas, L. L., Rios, E. and DeCoursey, T. E. 2008. A pH-stabilizing role of voltage-gated proton channels in IgE-mediated activation of human basophils. ***Proc Natl Acad Sci U S A***, 105(31): 11020-11025.

Musset, B., Capasso, M., Cherny, V. V., Morgan, D., Bhamrah, M., Dyer, M. J. and DeCoursey, T. E. 2010a. Identification of Thr^{29} as a critical phosphorylation site that activates the human proton channel *Hvcn1* in leukocytes. ***J Biol Chem***, 285(8): 5117-5121.

Musset, B., Smith, S. M., Rajan, S., Cherny, V. V., Morgan, D. and DeCoursey, T. E. 2010b. Oligomerization of the voltage-gated proton channel. ***Channels (Austin)***, 4(4): 260-265.

Musset, B., Smith, S. M., Rajan, S., Cherny, V. V., Sujai, S., Morgan, D. and DeCoursey, T. E. 2010c. Zinc inhibition of monomeric and dimeric proton channels suggests cooperative gating. ***J Physiol***, 588(Pt 9): 1435-1449.

Musset, B., Smith, S. M., Rajan, S., Morgan, D., Cherny, V. V. and DeCoursey, T. E. 2011. Aspartate 112 is the selectivity filter of the human voltage-gated proton channel. ***Nature***, 480(7376): 273-277.

Myers, V. B. and Haydon, D. A. 1972. Ion transfer across lipid membranes in the presence of gramicidin A. II. The ion selectivity. ***Biochim Biophys Acta***, 274(2): 313-322.

Nagle, J. F. and Morowitz, H. J. 1978. Molecular mechanisms for proton transport in membranes. ***Proc Natl Acad Sci U S A***, 75(1): 298-302.

Nasr, M. L., Baptista, D., Strauss, M., Sun, Z. J., Grigoriu, S., Huser, S., Plückthun, A., Hagn, F., Walz, T., Hogle, J. M. and Wagner, G. 2017. Covalently circularized nanodiscs for studying membrane proteins and viral entry. ***Nat Methods***, 14(1): 49-52.

Nealson, K. H., Eberhard, A. and Hastings, J. W. 1972. Catabolite repression of bacterial bioluminescence: functional implications. ***Proc Natl Acad Sci U S A***, 69(5): 1073-1076.

Neher, E. and Sakmann, B. 1976. Single-channel currents recorded from membrane of denervated frog muscle fibres. ***Nature***, 260(5554): 799-802.

Nernst, W. 1888. Zur Kinetik der in Lösung befindlichen Körper. ***Zeitschrift für physikalische Chemie***, 2(1): 613-637.

Nernst, W. 1889. Die elektromotorische Wirksamkeit der Ionen. ***Zeitschrift für physikalische Chemie***, 4(1): 129-181.

Nikolaev, M., Round, E., Gushchin, I., Polovinkin, V., Balandin, T., Kuzmichev, P., Shevchenko, V., Borshchevskiy, V., Kuklin, A., Round, A., Bernhard, F., Willbold, D., Büldt, G. and Gordeliy, V. 2017. Integral membrane proteins can be crystallized directly from nanodiscs. ***Crystal Growth & Design***, 17(3): 945-948.

Nitsche, C. and Otting, G. 2017. Pseudocontact shifts in biomolecular NMR using paramagnetic metal tags. ***Prog Nucl Magn Reson Spectrosc***, 98-99: 20-49.

Niwa, T., Kanamori, T., Ueda, T. and Taguchi, H. 2012. Global analysis of chaperone effects using a reconstituted cell-free translation system. ***Proc Natl Acad Sci U S A***, 109(23): 8937-8942.

Niwa, T., Sasaki, Y., Uemura, E., Nakamura, S., Akiyama, M., Ando, M., Sawada, S., Mukai, S. A., Ueda, T., Taguchi, H. and Akiyoshi, K. 2015. Comprehensive study of liposome-assisted synthesis of membrane proteins using a reconstituted cell-free translation system. ***Sci Rep***, 5: 18025.

Noren, C. J., Anthony-Cahill, S. J., Griffith, M. C. and Schultz, P. G. 1989. A general method for site-specific incorporation of unnatural amino acids into proteins. ***Science***, 244(4901): 182-188.

Nozawa, K., O'Donoghue, P., Gundllapalli, S., Araiso, Y., Ishitani, R., Umehara, T., Söll, D. and Nureki, O. 2009. Pyrrolysyl-tRNA synthetase-tRNA^{Pyl} structure reveals the molecular basis of orthogonality. ***Nature***, 457(7233): 1163-1167.

Ogawa, A., Namba, Y. and Gakumasawa, M. 2016. Rational optimization of amber suppressor tRNAs toward efficient incorporation of a non-natural amino acid into protein in a eukaryotic wheat germ extract. ***Org Biomol Chem***, 14(9): 2671-2678.

Okamura, Y., Murata, Y. and Iwasaki, H. 2009. Voltage-sensing phosphatase: actions and potentials. ***J Physiol***, 587(3): 513-520.

Okuda, H., Yonezawa, Y., Takano, Y., Okamura, Y. and Fujiwara, Y. 2016. Direct interaction between the voltage sensors produces cooperative sustained deactivation in voltage-gated H^+ channel dimers. ***J Biol Chem***, 291(11): 5935-5947.

Ozawa, K., Dixon, N. E. and Otting, G. 2005. Cell-free synthesis of ^{15}N-labeled proteins for NMR studies. ***IUBMB Life***, 57(9): 615-622.

Ozer, E., Chemla, Y., Schlesinger, O., Aviram, H. Y., Riven, I., Haran, G. and Alfonta, L. 2017. In vitro suppression of two different stop codons. ***Biotechnol Bioeng***, 114(5): 1065-1073.

Pace, C. N., Vajdos, F., Fee, L., Grimsley, G. and Gray, T. 1995. How to measure and predict the molar absorption coefficient of a protein. ***Protein Sci***, 4(11): 2411-2423.

Paramonov, A. S., Lyukmanova, E. N., Myshkin, M. Y., Shulepko, M. A., Kulbatskii, D. S., Petrosian, N. S., Chugunov, A. O., Dolgikh, D. A., Kirpichnikov, M. P., Arseniev, A. S. and Shenkarev, Z. O. 2017. NMR investigation of the isolated second voltage-sensing domain of human Nav1.4 channel. ***Biochim Biophys Acta Biomembr***, 1859(3): 493-506.

Peetz, O., Henrich, E., Laguerre, A., Löhr, F., Hein, C., Dötsch, V., Bernhard, F. and Morgner, N. 2017. Insights into cotranslational membrane protein insertion by combined LILBID-mass spectrometry and NMR spectroscopy. ***Anal Chem***, 89(22): 12314-12318.

Pervushin, K., Riek, R., Wider, G. and Wüthrich, K. 1997. Attenuated T_2 relaxation by mutual cancellation of dipole-dipole coupling and chemical shift anisotropy indicates an

avenue to NMR structures of very large biological macromolecules in solution. ***Proc Natl Acad Sci U S A***, 94(23): 12366-12371.

Peuker, S., Andersson, H., Gustavsson, E., Maiti, K. S., Kania, R., Karim, A., Niebling, S., Pedersen, A., Erdelyi, M. and Westenhoff, S. 2016. Efficient isotope editing of proteins for site-directed vibrational spectroscopy. ***J Am Chem Soc***, 138(7): 2312-2318.

Plass, T., Milles, S., Koehler, C., Schultz, C. and Lemke, E. A. 2011. Genetically encoded copper-free click chemistry. ***Angew Chem Int Ed Engl***, 50(17): 3878-3881.

Pless, S. A., Galpin, J. D., Frankel, A. and Ahern, C. A. 2011. Molecular basis for class Ib anti-arrhythmic inhibition of cardiac sodium channels. ***Nat Commun***, 2: 351.

Poget, S. F. and Girvin, M. E. 2007. Solution NMR of membrane proteins in bilayer mimics: Small is beautiful, but sometimes bigger is better. ***Biochim Biophys Acta***, 1768(12): 3098-3106.

Polycarpo, C., Ambrogelly, A., Bérubé, A., Winbush, S. M., McCloskey, J. A., Crain, P. F., Wood, J. L. and Söll, D. 2004. An aminoacyl-tRNA synthetase that specifically activates pyrrolysine. ***Proc Natl Acad Sci U S A***, 101(34): 12450-12454.

Popot, J. L., Althoff, T., Bagnard, D., Banères, J. L., Bazzacco, P., Billon-Denis, E., Catoire, L. J., Champeil, P., Charvolin, D., Cocco, M. J., Crémel, G., Dahmane, T., de la Maza, L. M., Ebel, C., Gabel, F., Giusti, F., Gohon, Y., Goormaghtigh, E., Guittet, E., Kleinschmidt, J. H., Kühlbrandt, W., Le Bon, C., Martinez, K. L., Picard, M., Pucci, B., Sachs, J. N., Tribet, C., van Heijenoort, C., Wien, F., Zito, F. and Zoonens, M. 2011. Amphipols from A to Z. ***Annu Rev Biophys***, 40: 379-408.

Porath, J. and Olin, B. 1983. Immobilized metal ion affinity adsorption and immobilized metal ion affinity chromatography of biomaterials. Serum protein affinities for gel-immobilized iron and nickel ions. ***Biochemistry***, 22(7): 1621-1630.

Postis, V., Rawson, S., Mitchell, J. K., Lee, S. C., Parslow, R. A., Dafforn, T. R., Baldwin, S. A. and Muench, S. P. 2015. The use of SMALPs as a novel membrane protein scaffold for structure study by negative stain electron microscopy. ***Biochim Biophys Acta***, 1848(2): 496-501.

Powl, A. M., Miles, A. J. and Wallace, B. A. 2012. Transmembrane and extramembrane contributions to membrane protein thermal stability: Studies with the NaChBac sodium channel. ***Biochim Biophys Acta***, 1818(3): 889-895.

Proverbio, D., Roos, C., Beyermann, M., Orbán, E., Dötsch, V. and Bernhard, F. 2013. Functional properties of cell-free expressed human endothelin A and endothelin B receptors in artificial membrane environments. ***Biochim Biophys Acta***, 1828(9): 2182-2192.

Proverbio, D., Henrich, E., Orbán, E., Dötsch, V. and Bernhard, F. 2014. Membrane protein quality control in cell-free expression systems: tools, strategies and case studies. In I. Mus-Veteau (Ed.), ***Membrane Proteins Production for Structural Analysis***: 45-70: Springer, New York, NY.

Pupo, A., Baez-Nieto, D., Martínez, A., Latorre, R. and González, C. 2014. Proton channel models: filling the gap between experimental data and the structural rationale. ***Channels (Austin)***, 8(3): 180-192.

Purcell, E. M., Torrey, H. C. and Pound, R. V. 1946. Resonance absorption by nuclear magnetic moments in a solid. ***Physical review***, 69(1-2): 37.

Qiu, F., Rebolledo, S., Gonzalez, C. and Larsson, H. P. 2013. Subunit interactions during cooperative opening of voltage-gated proton channels. ***Neuron***, 77(2): 288-298.

Qiu, F., Chamberlin, A., Watkins, B. M., Ionescu, A., Perez, M. E., Barro-Soria, R., González, C., Noskov, S. Y. and Larsson, H. P. 2016. Molecular mechanism of Zn^{2+} inhibition of a voltage-gated proton channel. ***Proc Natl Acad Sci U S A***, 113(40): E5962-E5971.

Quadrifoglio, F. and Urry, D. W. 1968. Ultraviolet rotatory properties of polypeptides in solution. I. Helical poly-L-alanine. ***J Am Chem Soc***, 90(11): 2755-2760.

Ramsey, I. S., Moran, M. M., Chong, J. A. and Clapham, D. E. 2006. A voltage-gated proton-selective channel lacking the pore domain. ***Nature***, 440(7088): 1213-1216.

Ramsey, I. S., Ruchti, E., Kaczmarek, J. S. and Clapham, D. E. 2009. Hv1 proton channels are required for high-level NADPH oxidase-dependent superoxide production during the phagocyte respiratory burst. ***Proc Natl Acad Sci U S A***, 106(18): 7642-7647.

Ramsey, I. S., Mokrab, Y., Carvacho, I., Sands, Z. A., Sansom, M. S. P. and Clapham, D. E. 2010. An aqueous H^+ permeation pathway in the voltage-gated proton channel Hv1. ***Nat Struct Mol Biol***, 17(7): 869-875.

Randolph, A. L., Mokrab, Y., Bennett, A. L., Sansom, M. S. and Ramsey, I. S. 2016. Proton currents constrain structural models of voltage sensor activation. ***Elife***, 5.

Rayaprolu, V., Royal, P., Stengel, K., Sandoz, G. and Kohout, S. C. 2018. Dimerization of the voltage-sensing phosphatase controls its voltage-sensing and catalytic activity. ***J Gen Physiol***, 150(5): 683-696.

Reckel, S., Sobhanifar, S., Schneider, B., Junge, F., Schwarz, D., Durst, F., Löhr, F., Güntert, P., Bernhard, F. and Dötsch, V. 2008. Transmembrane segment enhanced labeling as a tool for the backbone assignment of α-helical membrane proteins. ***Proc Natl Acad Sci U S A***, 105(24): 8262-8267.

Reckel, S., Sobhanifar, S., Durst, F., Löhr, F., Shirokov, V. A., Dötsch, V. and Bernhard, F. 2010. Strategies for the cell-free expression of membrane proteins. In Y. Endo, K. Takai, & T. Ueda (Eds.), ***Cell-free protein production. Methods in Molecular Biology (Methods and Protocols)***, Vol. 607: 187-212: Humana Press.

Reckel, S., Gottstein, D., Stehle, J., Löhr, F., Verhoefen, M. K., Takeda, M., Silvers, R., Kainosho, M., Glaubitz, C., Wachtveitl, J., Bernhard, F., Schwalbe, H., Güntert, P. and Dötsch, V. 2011. Solution NMR structure of proteorhodopsin. ***Angew Chem Int Ed Engl***, 50(50): 11942-11946.

Renauld, S., Cortes, S., Bersch, B., Henry, X., De Waard, M. and Schaack, B. 2017. Functional reconstitution of cell-free synthesized purified K_V channels. ***Biochim Biophys Acta Biomembr***, 1859(12): 2373-2380.

Ritchie, T. K., Grinkova, Y. V., Bayburt, T. H., Denisov, I. G., Zolnerciks, J. K., Atkins, W. M. and Sligar, S. G. 2009. Reconstitution of membrane proteins in phospholipid bilayer nanodiscs. In N. Düzgünes (Ed.), ***Methods in Enzymology, Liposomes, Part F***, Vol. 464: 211-231: Elsevier BV.

Roos, C., Zocher, M., Müller, D., Münch, D., Schneider, T., Sahl, H. G., Scholz, F., Wachtveitl, J., Ma, Y., Proverbio, D., Henrich, E., Dötsch, V. and Bernhard, F. 2012. Characterization of co-translationally formed nanodisc complexes with small multidrug transporters, proteorhodopsin and with the *E. coli* MraY translocase. ***Biochim Biophys Acta***, 1818(12): 3098-3106.

Roos, C., Kai, L., Proverbio, D., Ghoshdastider, U., Filipek, S., Dötsch, V. and Bernhard, F. 2013. Co-translational association of cell-free expressed membrane proteins with supplied lipid bilayers. ***Mol Membr Biol***, 30(1): 75-89.

Roos, C., Kai, L., Haberstock, S., Proverbio, D., Ghoshdastider, U., Ma, Y., Filipek, S., Wang, X., Dötsch, V. and Bernhard, F. 2014. High-level cell-free production of membrane

proteins with nanodiscs. In K. Alexandrov, & W. Johnston (Eds.), ***Cell-Free Protein Synthesis. Methods in Molecular Biology (Methods and Protocols)***, Vol. 1118: 109-130: Humana Press, Totowa, NJ.

Rosa, M., Roberts, C. J. and Rodrigues, M. A. 2017. Connecting high-temperature and low-temperature protein stability and aggregation. ***PLoS One***, 12(5): e0176748.

Rost, B., Yachdav, G. and Liu, J. 2004. The PredictProtein server. ***Nucleic Acids Res***, 32(Web Server issue): W321-326.

Rues, R. B., Dötsch, V. and Bernhard, F. 2016. Co-translational formation and pharmacological characterization of beta1-adrenergic receptor/nanodisc complexes with different lipid environments. ***Biochim Biophys Acta***, 1858(6): 1306-1316.

Rues, R. B., Gräwe, A., Henrich, E. and Bernhard, F. 2017. Membrane protein production in *E. coli* lysates in presence of preassembled Nanodiscs. In N. Burgess-Brown (Ed.), ***Heterologous gene expression in E. coli, Methods in Molecular Biology***, Vol. 1586: 291-312: Humana Press, New York, NY.

Rues, R. B., Dong, F., Dötsch, V. and Bernhard, F. 2018. Systematic optimization of cell-free synthesized human endothelin B receptor folding. ***Methods***, 147: 73-83.

Ryabova, L. A., Desplancq, D., Spirin, A. S. and Plückthun, A. 1997. Functional antibody production using cell-free translation: Effects of protein disulfide isomerase and chaperones. ***Nat Biotechnol***, 15(1): 79-84.

Ryu, Y. and Schultz, P. G. 2006. Efficient incorporation of unnatural amino acids into proteins in *Escherichia coli*. ***Nat Methods***, 3(4): 263-265.

Sasaki, M., Takagi, M. and Okamura, Y. 2006. A voltage sensor-domain protein is a voltage-gated proton channel. ***Science***, 312(5773): 589-592.

Schägger, H. and von Jagow, G. 1987. Tricine-sodium dodecyl sulfate-polyacrylamide gel electrophoresis for the separation of proteins in the range from 1 to 100 kDa. ***Anal Biochem***, 166(2): 368-379.

Schägger, H. 2006. Tricine-SDS-PAGE. ***Nat Protoc***, 1(1): 16-22.

Schanda, P., Kupce, E. and Brutscher, B. 2005. SOFAST-HMQC experiments for recording two-dimensional heteronuclear correlation spectra of proteins within a few seconds. ***J Biomol NMR***, 33(4): 199-211.

Schanda, P., Van Melckebeke, H. and Brutscher, B. 2006. Speeding up three-dimensional protein NMR experiments to a few minutes. ***J Am Chem Soc***, 128(28): 9042-9043.

Schmidt, M. J. and Summerer, D. 2013. Red-light-controlled protein-RNA crosslinking with a genetically encoded furan. ***Angew Chem Int Ed Engl***, 52(17): 4690-4693.

Schmidt, M. J., Borbas, J., Drescher, M. and Summerer, D. 2014a. A genetically encoded spin label for electron paramagnetic resonance distance measurements. ***J Am Chem Soc***, 136(4): 1238-1241.

Schmidt, M. J., Weber, A., Pott, M., Welte, W. and Summerer, D. 2014b. Structural basis of furan-amino acid recognition by a polyspecific aminoacyl-tRNA-synthetase and its genetic encoding in human cells. ***Chembiochem***, 15(12): 1755-1760.

Schneider, B., Junge, F., Shirokov, V. A., Durst, F., Schwarz, D., Dötsch, V. and Bernhard, F. 2010. Membrane protein expression in cell-free systems. In I. Mus-Veteau (Ed.), ***Heterologous Expression of Membrane Proteins. Methods in Molecular Biology (Methods and Protocols)***, Vol. 601: 165-186: Humana Press.

Schwaiger, M., Lebendiker, M., Yerushalmi, H., Coles, M., Gröger, A., Schwarz, C., Schuldiner, S. and Kessler, H. 1998. NMR investigation of the multidrug transporter EmrE, an integral membrane protein. ***Eur J Biochem***, 254(3): 610-619.

Schwalbe, H. 2017. Editorial: New 1.2 GHz NMR spectrometers- New horizons? ***Angew Chem Int Ed Engl***, 56(35): 10252-10253.

Schwarz, D., Junge, F., Durst, F., Frölich, N., Schneider, B., Reckel, S., Sobhanifar, S., Dötsch, V. and Bernhard, F. 2007. Preparative scale expression of membrane proteins in *Escherichia coli*-based continuous exchange cell-free systems. ***Nat Protoc***, 2(11): 2945-2957.

Schwarz, D., Dötsch, V. and Bernhard, F. 2008. Production of membrane proteins using cell-free expression systems. ***Proteomics***, 8(19): 3933-3946.

Schwarz, D., Daley, D., Beckhaus, T., Dötsch, V. and Bernhard, F. 2010. Cell-free expression profiling of *E. coli* inner membrane proteins. ***Proteomics***, 10(9): 1762-1779.

Shenkarev, Z. O., Lyukmanova, E. N., Solozhenkin, O. I., Gagnidze, I. E., Nekrasova, O. V., Chupin, V. V., Tagaev, A. A., Yakimenko, Z. A., Ovchinnikova, T. V., Kirpichnikov, M. P. and Arseniev, A. S. 2009. Lipid-protein nanodiscs: Possible application in high-resolution NMR investigations of membrane proteins and membrane-active peptides. ***Biochemistry (Mosc)***, 74(7): 756-765.

Shenkarev, Z. O., Lyukmanova, E. N., Paramonov, A. S., Shingarova, L. N., Chupin, V. V., Kirpichnikov, M. P., Blommers, M. J. and Arseniev, A. S. 2010a. Lipid-protein nanodiscs as reference medium in detergent screening for high-resolution NMR studies of integral membrane proteins. ***J Am Chem Soc***, 132(16): 5628-5629.

Shenkarev, Z. O., Paramonov, A. S., Lyukmanova, E. N., Shingarova, L. N., Yakimov, S. A., Dubinnyi, M. A., Chupin, V. V., Kirpichnikov, M. P., Blommers, M. J. and Arseniev, A. S. 2010b. NMR structural and dynamical investigation of the isolated voltage-sensing domain of the potassium channel KvAP: implications for voltage gating. ***J Am Chem Soc***, 132(16): 5630-5637.

Shenkarev, Z. O., Lyukmanova, E. N., Butenko, I. O., Petrovskaya, L. E., Paramonov, A. S., Shulepko, M. A., Nekrasova, O. V., Kirpichnikov, M. P. and Arseniev, A. S. 2013. Lipid-protein nanodiscs promote *in vitro* folding of transmembrane domains of multi-helical and multimeric membrane proteins. ***Biochim Biophys Acta***, 1828(2): 776-784.

Shimizu, Y., Inoue, A., Tomari, Y., Suzuki, T., Yokogawa, T., Nishikawa, K. and Ueda, T. 2001. Cell-free translation reconstituted with purified components. ***Nat Biotechnol***, 19(8): 751-755.

Shrestha, P., Holland, T. M. and Bundy, B. C. 2012. Streamlined extract preparation for *Escherichia coli*-based cell-free protein synthesis by sonication or bead vortex mixing. ***Biotechniques***, 53(3): 163-174.

Smith, S. M., Morgan, D., Musset, B., Cherny, V. V., Place, A. R., Hastings, J. W. and DeCoursey, T. E. 2011. Voltage-gated proton channel in a dinoflagellate. ***Proc Natl Acad Sci U S A***, 108(44): 18162-18167.

Smith, S. M. and DeCoursey, T. E. 2013. Consequences of dimerization of the voltage-gated proton channel. ***Prog Mol Biol Transl Sci***, 117: 335-360.

Soubias, O., Teague, W. E. and Gawrisch, K. 2006. Evidence for specificity in lipid-rhodopsin interactions. ***J Biol Chem***, 281(44): 33233-33241.

Spirin, A. S. 2004. High-throughput cell-free systems for synthesis of functionally active proteins. ***Trends Biotechnol***, 22(10): 538-545.

Staunton, D., Schlinkert, R., Zanetti, G., Colebrook, S. A. and Campbell, I. D. 2006. Cell-free expression and selective isotope labelling in protein NMR. ***Magn Reson Chem***, 44 Spec No: S2-9.

Stordeur, C. 2007. ***NMR-Spektroskopische Untersuchungen an artifiziellen Proteinen***. Martin-Luther-Universität Halle-Wittenberg.

Studier, F. W. 2005. Protein production by auto-induction in high density shaking cultures. ***Protein Expr Purif***, 41(1): 207-234.

Su, X. C., Loh, C. T., Qi, R. and Otting, G. 2011. Suppression of isotope scrambling in cell-free protein synthesis by broadband inhibition of PLP enymes for selective ^{15}N-labelling and production of perdeuterated proteins in H_2O. ***J Biomol NMR***, 50(1): 35-42.

Suh, B. C. and Hille, B. 2005. Regulation of ion channels by phosphatidylinositol 4,5-bisphosphate. ***Curr Opin Neurobiol***, 15(3): 370-378.

Takeshita, K., Sakata, S., Yamashita, E., Fujiwara, Y., Kawanabe, A., Kurokawa, T., Okochi, Y., Matsuda, M., Narita, H., Okamura, Y. and Nakagawa, A. 2014. X-ray crystal structure of voltage-gated proton channel. ***Nat Struct Mol Biol***, 21(4): 352-357.

Tausk, R. J., van Esch, J., Karmiggelt, J., Voordouw, G. and Overbeek, J. T. 1974. Physical chemical studies of short-chain lecithin homologues. II. Micellar weights of dihexanoyl- and diheptanoyllecithin. ***Biophys Chem***, 1(3): 184-203.

Taylor, A. R., Chrachri, A., Wheeler, G., Goddard, H. and Brownlee, C. 2011. A voltage-gated H^+ channel underlying pH homeostasis in calcifying coccolithophores. ***PLoS Biol***, 9(6): e1001085.

Thomas, R. C. and Meech, R. W. 1982. Hydrogen ion currents and intracellular pH in depolarized voltage-clamped snail neurones. ***Nature***, 299(5886): 826-828.

Tombola, F., Ulbrich, M. H. and Isacoff, E. Y. 2008. The voltage-gated proton channel Hv1 has two pores, each controlled by one voltage sensor. ***Neuron***, 58(4): 546-556.

Tombola, F., Ulbrich, M. H., Kohout, S. C. and Isacoff, E. Y. 2010. The opening of the two pores of the Hv1 voltage-gated proton channel is tuned by cooperativity. ***Nat Struct Mol Biol***, 17(1): 44-50.

Tonelli, M., Singarapu, K. K., Makino, S., Sahu, S. C., Matsubara, Y., Endo, Y., Kainosho, M. and Markley, J. L. 2011. Hydrogen exchange during cell-free incorporation of deuterated amino acids and an approach to its inhibition. ***J Biomol NMR***, 51(4): 467-476.

Trbovic, N., Klammt, C., Koglin, A., Löhr, F., Bernhard, F. and Dötsch, V. 2005. Efficient strategy for the rapid backbone assignment of membrane proteins. ***J Am Chem Soc***, 127(39): 13504-13505.

Tribet, C., Audebert, R. and Popot, J. L. 1996. Amphipols: polymers that keep membrane proteins soluble in aqueous solutions. ***Proc Natl Acad Sci U S A***, 93(26): 15047-15050.

Tugarinov, V., Choy, W. Y., Orekhov, V. Y. and Kay, L. E. 2005. Solution NMR-derived global fold of a monomeric 82-kDa enzyme. ***Proc Natl Acad Sci U S A***, 102(3): 622-627.

Tumulka, F., Roos, C., Löhr, F., Bock, C., Bernhard, F., Dötsch, V. and Abele, R. 2013. Conformational stabilization of the membrane embedded targeting domain of the lysosomal peptide transporter TAPL for solution NMR. ***J Biomol NMR***, 57(2): 141-154.

Uhlemann, E. M., Pierson, H. E., Fillingame, R. H. and Dmitriev, O. Y. 2012. Cell-free synthesis of membrane subunits of ATP synthase in phospholipid bicelles: NMR shows subunit a fold similar to the protein in the cell membrane. ***Protein Sci***, 21(2): 279-288.

Vaish, A., Guo, S., Murray, R. M., Grandsard, P. J. and Chen, Q. 2018. On-chip membrane protein cell-free expression enables development of a direct binding assay: A curious case of potassium channel KcsA-Kv1.3. ***Anal Biochem***, 556: 70-77.

Valiyaveetil, F. I., MacKinnon, R. and Muir, T. W. 2002a. Semisynthesis and folding of the potassium channel KcsA. ***J Am Chem Soc***, 124(31): 9113-9120.

Valiyaveetil, F. I., Zhou, Y. and MacKinnon, R. 2002b. Lipids in the structure, folding, and function of the KcsA K^+ channel. ***Biochemistry***, 41(35): 10771-10777.

van der Does, C., Swaving, J., van Klompenburg, W. and Driessen, A. J. 2000. Non-bilayer lipids stimulate the activity of the reconstituted bacterial protein translocase. ***J Biol Chem***, 275(4): 2472-2478.

van Keulen, S. C., Gianti, E., Carnevale, V., Klein, M. L., Rothlisberger, U. and Delemotte, L. 2017. Does proton conduction in the voltage-gated H^+ channel hHv1 involve Grotthuss-like hopping via acidic residues? ***J Phys Chem B***, 121(15): 3340-3351.

van Meer, G., Voelker, D. R. and Feigenson, G. W. 2008. Membrane lipids: Where they are and how they behave. ***Nat Rev Mol Cell Biol***, 9(2): 112-124.

Vincentelli, R., Canaan, S., Campanacci, V., Valencia, C., Maurin, D., Frassinetti, F., Scappucini-Calvo, L., Bourne, Y., Cambillau, C. and Bignon, C. 2004. High-throughput automated refolding screening of inclusion bodies. ***Protein Sci***, 13(10): 2782-2792.

Waberer, L., Henrich, E., Peetz, O., Morgner, N., Dötsch, V., Bernhard, F. and Volknandt, W. 2017. The synaptic vesicle protein SV31 assembles into a dimer and transports Zn^{2+}. ***J Neurochem***, 140(2): 280-293.

Wada, T., Shimono, K., Kikukawa, T., Hato, M., Shinya, N., Kim, S. Y., Kimura-Someya, T., Shirouzu, M., Tamogami, J., Miyauchi, S., Jung, K. H., Kamo, N. and Yokoyama, S. 2011. Crystal structure of the eukaryotic light-driven proton-pumping rhodopsin, *Acetabularia* rhodopsin II, from marine alga. ***J Mol Biol***, 411(5): 986-998.

Wang, L., Brock, A., Herberich, B. and Schultz, P. G. 2001. Expanding the genetic code of *Escherichia coli*. ***Science***, 292(5516): 498-500.

Wang, L., Zhang, Z., Brock, A. and Schultz, P. G. 2003. Addition of the keto functional group to the genetic code of *Escherichia coli*. ***Proc Natl Acad Sci U S A***, 100(1): 56-61.

Wang, Y., Li, S. J., Pan, J., Che, Y., Yin, J. and Zhao, Q. 2011. Specific expression of the human voltage-gated proton channel Hv1 in highly metastatic breast cancer cells, promotes tumor progression and metastasis. ***Biochem Biophys Res Commun***, 412(2): 353-359.

Wang, Y., Li, S. J., Wu, X., Che, Y. and Li, Q. 2012. Clinicopathological and biological significance of human voltage-gated proton channel Hv1 protein overexpression in breast cancer. ***J Biol Chem***, 287(17): 13877-13888.

Wang, Y., Wu, X., Li, Q., Zhang, S. and Li, S. J. 2013a. Human voltage-gated proton channel Hv1: a new potential biomarker for diagnosis and prognosis of colorectal cancer. ***PLoS One***, 8(8): e70550.

Wang, Y., Zhang, S. and Li, S. J. 2013b. Zn^{2+} induces apoptosis in human highly metastatic SHG-44 glioma cells, through inhibiting activity of the voltage-gated proton channel Hv1. ***Biochem Biophys Res Commun***, 438(2): 312-317.

Warburg, O. 1924. Über den Stoffwechsel der Carcinomzelle. ***Naturwissenschaften***, 12(50): 1131-1137.

Warinner, K. 2015. ***Functional analysis of cell-free produced, reconstituted voltage-sensing domains***. Johann-Wolfgang-Goethe-University Frankfurt a.M.

Wilding, K. M., Smith, A. K., Wilkerson, J. W., Bush, D. B., Knotts, T. A. t. and Bundy, B. C. 2018. The locational impact of site-specific PEGylation: Streamlined screening with cell-free protein expression and coarse-grain simulation. ***ACS Synth Biol***, 7(2): 510-521.

Wilkins, M. R., Gasteiger, E., Bairoch, A., Sanchez, J. C., Williams, K. L., Appel, R. D. and Hochstrasser, D. F. 1999. Protein identification and analysis tools in the ExPASy server. ***Methods Mol Biol***, 112: 531-552.

Willis, M. S., Hogan, J. K., Prabhakar, P., Liu, X., Tsai, K., Wei, Y. and Fox, T. 2005. Investigation of protein refolding using a fractional factorial screen: A study of reagent effects and interactions. ***Protein Sci***, 14(7): 1818-1826.

Wood, M. L., Schow, E. V., Freites, J. A., White, S. H., Tombola, F. and Tobias, D. J. 2012. Water wires in atomistic models of the Hv1 proton channel. ***Biochim Biophys Acta***, 1818(2): 286-293.

Worst, E. G., Exner, M. P., De Simone, A., Schenkelberger, M., Noireaux, V., Budisa, N. and Ott, A. 2016. Residue-specific incorporation of noncanonical amino acids into model proteins using an *Escherichia coli* cell-free transcription-translation system. ***J Vis Exp***(114).

Wulf, M. and Pless, S. A. 2018. High-sensitivity fluorometry to resolve ion channel conformational dynamics. ***Cell Rep***, 22(6): 1615-1626.

Yanagisawa, T., Ishii, R., Fukunaga, R., Kobayashi, T., Sakamoto, K. and Yokoyama, S. 2008a. Crystallographic studies on multiple conformational states of active-site loops in pyrrolysyl-tRNA synthetase. ***J Mol Biol***, 378(3): 634-652.

Yanagisawa, T., Ishii, R., Fukunaga, R., Kobayashi, T., Sakamoto, K. and Yokoyama, S. 2008b. Multistep engineering of pyrrolysyl-tRNA synthetase to genetically encode N^{ε}-(o-azidobenzyloxycarbonyl) lysine for site-specific protein modification. ***Chem Biol***, 15(11): 1187-1197.

Yanagisawa, T., Umehara, T., Sakamoto, K. and Yokoyama, S. 2014. Expanded genetic code technologies for incorporating modified lysine at multiple sites. ***Chembiochem***, 15(15): 2181-2187.

Yang, F., Yu, X., Liu, C., Qu, C. X., Gong, Z., Liu, H. D., Li, F. H., Wang, H. M., He, D. F., Yi, F., Song, C., Tian, C. L., Xiao, K. H., Wang, J. Y. and Sun, J. P. 2015. Phospho-selective mechanisms of arrestin conformations and functions revealed by unnatural amino acid incorporation and ^{19}F-NMR. ***Nat Commun***, 6: 8202.

Yokoyama, J., Matsuda, T., Koshiba, S., Tochio, N. and Kigawa, T. 2011. A practical method for cell-free protein synthesis to avoid stable isotope scrambling and dilution. ***Anal Biochem***, 411(2): 223-229.

Yuan, C., O'Connell, R. J., Feinberg-Zadek, P. L., Johnston, L. J. and Treistman, S. N. 2004. Bilayer thickness modulates the conductance of the BK channel in model membranes. ***Biophys J***, 86(6): 3620-3633.

Zhang, J., Feng, Y. and Forgac, M. 1994. Proton conduction and bafilomycin binding by the V_0 domain of the coated vesicle V-ATPase. ***J Biol Chem***, 269(38): 23518-23523.

Zocher, M., Roos, C., Wegmann, S., Bosshart, P. D., Dötsch, V., Bernhard, F. and Müller, D. J. 2012. Single-molecule force spectroscopy from nanodiscs: An assay to quantify folding, stability, and interactions of native membrane proteins. ***ACS Nano***, 6(1): 961-971.

7 Appendix

7.1 DNA and protein sequences

His-hH$_V$1-VSD in pET15b

DNA	Protein
AAGGAGATATACC**ATG**GGCAGCAGCCATCATCATCATCATCACAGCAGCGGCCTGGTG CCGCGCGGCAGCCAT**ATG**GCGCCGGCCCCGGGCCCGGCTCCGCGTGCTCCCCTGGACT TTCGCGGTATGCTGCGCAAACTGTTTAGCAGCCACCGCTTTCAGGTAATCATTATTTG TCTCGTGGTCCTGGATGCCTTACTGGTGTTGGCCGAGCTGATCCTGGACCTTAAGATC ATCCAGCCTGACAAAAACAATTATGCCGCGATGGTTTTTCATTATATGAGCATCACCA TTCTTGTTTTTTTCATGATGGAGATCATCTTTAAGCTGTTCGTTTTTCGCCTCGAATT CTTTCATCACAAATTCGAAATCCTGGACGCGGTGGTTGTGGTGGTGAGCTTCATTCTT GATATCGTACTGTTATTCCAGGAACATCAATTCGAGGCGTTGGGTCTGCTGATTTTGT TACGCCTGTGGCGTGTCGCGCGCATTATTAACGGCATCATCATTAGCGTGAAGACCCG TTAG	**M**GSSHHHHHHSSGLVPRGSH**M**APAPGPAPRA PLDFRGMLRKLFSSHRFQVIIICLVVLDALL VLAELILDLKIIQPDKNNYAAMVFHYMSITI LVFFMMEIIFKLFVFRLEFFHHKFEILDAVV VVVSFILDIVLLFQEHQFEALGLLILLRLWR VARIINGIIISVKTR

hH$_V$1-VSD-His in pET21a

DNA	Protein
AAGGAGATATACAT**ATG**GCGCCGGCCCCGGGCCCGGCTCCGCGTGCTCCCCTGGACTT TCGCGGTATGCTGCGCAAACTGTTTAGCAGCCACCGCTTTCAGGTAATCATTATTTGT CTCGTGGTCCTGGATGCCTTACTGGTGTTGGCCGAGCTGATCCTGGACCTTAAGATCA TCCAGCCTGACAAAAACAATTATGCCGCGATGGTTTTTCATTATATGAGCATCACCAT TCTTGTTTTTTTCATGATGGAGATCATCTTTAAGCTGTTCGTTTTTCGCCTCGAATTC TTTCATCACAAATTCGAAATCCTGGACGCGGTGGTTGTGGTGGTGAGCTTCATTCTTG ATATCGTACTGTTATTCCAGGAACATCAATTCGAGGCGTTGGGTCTGCTGATTTTGTT ACGCCTGTGGCGTGTCGCGCGCATTATTAACGGCATCATCATTAGCGTGAAGACCCGT GGATCCGGATCAGGACTCGAGCATCATCACCATCACCACCATCACCATCATTAG	**M**APAPGPAPRAPLDFRGMLRKLFSSHRFQVI IICLVVLDALLVLAELILDLKIIQPDKNNYA AMVFHYMSITILVFFMMEIIFKLFVFRLEFF HHKFEILDAVVVVVSFILDIVLLFQEHQFEA LGLLILLRLWRVARIINGIIISVKTRGSGSG LEHHHHHHHHHH

hH$_V$1-VSD-Strep in pET21a

DNA	Protein
AAGGAGATATACAT**ATG**GCGCCGGCCCCGGGCCCGGCTCCGCGTGCTCCCCTGGACTT TCGCGGTATGCTGCGCAAACTGTTTAGCAGCCACCGCTTTCAGGTAATCATTATTTGT CTCGTGGTCCTGGATGCCTTACTGGTGTTGGCCGAGCTGATCCTGGACCTTAAGATCA TCCAGCCTGACAAAAACAATTATGCCGCGATGGTTTTTCATTATATGAGCATCACCAT TCTTGTTTTTTTCATGATGGAGATCATCTTTAAGCTGTTCGTTTTTCGCCTCGAATTC TTTCATCACAAATTCGAAATCCTGGACGCGGTGGTTGTGGTGGTGAGCTTCATTCTTG ATATCGTACTGTTATTCCAGGAACATCAATTCGAGGCGTTGGGTCTGCTGATTTTGTT ACGCCTGTGGCGTGTCGCGCGCATTATTAACGGCATCATCATTAGCGTGAAGACCCGT GGATCCGGATCAGGACTCGAGTGGAGTCACCCTCAGTTTGAAAAGTAG	**M**APAPGPAPRAPLDFRGMLRKLFSSHRFQVI IICLVVLDALLVLAELILDLKIIQPDKNNYA AMVFHYMSITILVFFMMEIIFKLFVFRLEFF HHKFEILDAVVVVVSFILDIVLLFQEHQFEA LGLLILLRLWRVARIINGIIISVKTRGSGSG LEWSHPQFEK

His-hH$_V$1-VSD-Strep in pET15b

DNA	Protein
AAGGAGATATACCATGGGCAGCAGCCATCATCATCATCATCACAGCAGCGGCCTGGTG CCGCGCGGCAGCCATATGGCGCCGGCCCCGGGCCCGGCTCCGCGTGCTCCCCTGGACT TTCGCGGTATGCTGCGCAAACTGTTTAGCAGCCACCGCTTTCAGGTAATCATTATTTG TCTCGTGGTCCTGGATGCCTTACTGGTGTTGGCCGAGCTGATCCTGGACCTTAAGATC ATCCAGCCTGACAAAAACAATTATGCCGCGATGGTTTTTCATTATATGAGCATCACCA TTCTTGTTTTTTTCATGATGGAGATCATCTTTAAGCTGTTCGTTTTTCGCCTCGAATT CTTTCATCACAAATTCGAAATCCTGGACGCGGTGGTTGTGGTGGTGAGCTTCATTCTT GATATCGTACTGTTATTCCAGGAACATCAATTCGAGGCGTTGGGTCTGCTGATTTTGT TACGCCTGTGGCGTGTCGCGCGCATTATTAACGGCATCATCATTAGCGTGAAGACCCG TGGATCAGGATGGAGTCACCCTCAGTTTGAAAAGTAG	**M**GSSHHHHHHSSGLVPRGSH**M**APAPGPAPRA PLDFRGMLRKLFSSHRFQVIIICLVVLDALL VLAELILDLKIIQPDKNNYAAMVFHYMSITI LVFFMMEIIFKLFVFRLEFFHHKFEILDAVV VVVSFILDIVLLFQEHQFEALGLLILLRLWR VARIINGIIISVKTRGSGWSHPQFEK

Strep-hH$_V$1-VSD in pET15b

DNA	Protein
AAGGAGATATACCATGGGCAGCAGCTGGAGTCACCCTCAGTTTGAAAAGAGCAGCGGC CTGGTGCCGCGCGGCAGCCATATGGCGCCGGCCCCGGGCCCGGCTCCGCGTGCTCCCC TGGACTTTCGCGGTATGCTGCGCAAACTGTTTAGCAGCCACCGCTTTCAGGTAATCAT TATTTGTCTCGTGGTCCTGGATGCCTTACTGGTGTTGGCCGAGCTGATCCTGGACCTT AAGATCATCCAGCCTGACAAAAACAATTATGCCGCGATGGTTTTTCATTATATGAGCA TCACCATTCTTGTTTTTTTCATGATGGAGATCATCTTTAAGCTGTTCGTTTTTCGCCT CGAATTCTTTCATCACAAATTCGAAATCCTGGACGCGGTGGTTGTGGTGGTGAGCTTC ATTCTTGATATCGTACTGTTATTCCAGGAACATCAATTCGAGGCGTTGGGTCTGCTGA TTTTGTTACGCCTGTGGCGTGTCGCGCGCATTATTAACGGCATCATCATTAGCGTGAA GACCCGTTAG	**M**GSSWSHPQFEKSSGLVPRGSH**M**APAPGPAP RAPLDFRGMLRKLFSSHRFQVIIICLVVLDA LLVLAELILDLKIIQPDKNNYAAMVFHYMSI TILVFFMMEIIFKLFVFRLEFFHHKFEILDA VVVVVSFILDIVLLFQEHQFEALGLLILLRL WRVARIINGIIISVKTR

His-DrVSD in pET15b

DNA	Protein
AAGGAGATATACCATGGGCAGCAGCCATCATCATCATCACAGCAGCGGCCTGGTG CCGCGCGGCAGCCATATGAAGGAAGAAACAAAGGACCCGGATACTATGTATCATCAGG TTCGCAAAAAGATTACACCGTTCGTGATGTCCTTCGGTTTCCGCGTTTTTGGTCTGGT GCTGATCATTCTTGATATTATTATGGTGATCGTCGACCTCAGTTTGAGCGAAAAATCG CGCGATGTGGGTGGGGCGCCGGAGACCGTTAGCCTTGTGATTTCGTTTTTTTTCTTGA TCGACGTGCTTTTGCGCGTATACGTAGAAGGGTTTAAGGTATATTTCTCGAGCAAATT GAATATTGTAGATGCCTGTATCGTAGTCATTACCTTAGTTGTGACAATGATCTATGCA TTCTCCGATTTTAGTGGCGCGAGTTTGATTCCGCGCGTAGTTACTTTTCTGCGTAGCC TGCGCATCGTCATTCTGGTTTAA	**M**GSSHHHHHHSSGLVPRGSH**M**KEETKDPDTM YHQVRKKITPFVMSFGFRVFGLVLIILDIIM VIVDLSLSEKSRDVGGAPETVSLVISFFFLI DVLLRVYVEGFKVYFSSKLNIVDACIVVITL VVTMIYAFSDFSGASLIPRVVTFLRSLRIVI LV

His-DrVSD-Strep in pET15b

DNA	Protein
AAGGAGATATACC**ATG**GGCAGCAGCCATCATCATCATCACAGCAGCGGCCTGGTG CCGCGCGGCAGCCAT**ATG**AAGGAAGAAACAAAGGACCCGGATACTATGTATCATCAGG TTCGCAAAAAGATTACACCGTTCGTGATGTCCTTCGGTTTCCGCGTTTTTGGTCTGGT GCTGATCATTCTTGATATTATTATGGTGATCGTCGACCTCAGTTTGAGCGAAAAATCG CGCGATGTGGGTGGGGCGCCGGAGACCGTTAGCCTTGTGATTTCGTTTTTTTTCTTGA TCGACGTGCTTTTGCGCGTATACGTAGAAGGGTTTAAGGTATATTTCTCGAGCAAATT GAATATTGTAGATGCCTGTATCGTAGTCATTACCTTAGTTGTGACAATGATCTATGCA TTCTCCGATTTTAGTGGCGCGAGTTTGATTCCGCGCGTAGTTACTTTTCTGCGTAGCC TGCGCATCGTCATTCTGGTTGGATCAGGATGGAGTCACCCTCAGTTTGAAAAGTAG	**M**GSSHHHHHHSSGLVPRGSH**M**KEETKDPDTM YHQVRKKITPFVMSFGFRVFGLVLIILDIIM VIVDLSLSEKSRDVGGAPETVSLVISFFFLI DVLLRVYVEGFKVYFSSKLNIVDACIVVITL VVTMIYAFSDFSGASLIPRVVTFLRSLRIVI LVGSGWSHPQFEK

DrVSD-His in pET21a

DNA	Protein
AAGGAGATATACAT**ATG**AAGGAAGAAACAAAGGACCCGGATACTATGTATCATCAGGT TCGCAAAAAGATTACACCGTTCGTGATGTCCTTCGGTTTCCGCGTTTTTGGTCTGGTG CTGATCATTCTTGATATTATTATGGTGATCGTCGACCTCAGTTTGAGCGAAAAATCGC GCGATGTGGGTGGGGCGCCGGAGACCGTTAGCCTTGTGATTTCGTTTTTTTTCTTGAT CGACGTGCTTTTGCGCGTATACGTAGAAGGGTTTAAGGTATATTTCTCGAGCAAATTG AATATTGTAGATGCCTGTATCGTAGTCATTACCTTAGTTGTGACAATGATCTATGCAT TCTCCGATTTTAGTGGCGCGAGTTTGATTCCGCGCGTAGTTACTTTTCTGCGTAGCCT GCGCATCGTCATTCTGGTTGGATCCGGATCAGGACTCGAGCATCATCACCATCACCAC CATCACCATCATTAG	**M**KEETKDPDTMYHQVRKKITPFVMSFGFRVF GLVLIILDIIMVIVDLSLSEKSRDVGGAPET VSLVISFFFLIDVLLRVYVEGFKVYFSSKLN IVDACIVVITLVVTMIYAFSDFSGASLIPRV VTFLRSLRIVILVGSGSGLEHHHHHHHHHH

DrVSD-Strep in pET21a

DNA	Protein
AAGGAGATATACAT**ATG**AAGGAAGAAACAAAGGACCCGGATACTATGTATCATCAGGT TCGCAAAAAGATTACACCGTTCGTGATGTCCTTCGGTTTCCGCGTTTTTGGTCTGGTG CTGATCATTCTTGATATTATTATGGTGATCGTCGACCTCAGTTTGAGCGAAAAATCGC GCGATGTGGGTGGGGCGCCGGAGACCGTTAGCCTTGTGATTTCGTTTTTTTTCTTGAT CGACGTGCTTTTGCGCGTATACGTAGAAGGGTTTAAGGTATATTTCTCGAGCAAATTG AATATTGTAGATGCCTGTATCGTAGTCATTACCTTAGTTGTGACAATGATCTATGCAT TCTCCGATTTTAGTGGCGCGAGTTTGATTCCGCGCGTAGTTACTTTTCTGCGTAGCCT GCGCATCGTCATTCTGGTTGGATCCGGATCAGGACTCGAGTGGAGTCACCCTCAGTTT GAAAAGTAG	**M**KEETKDPDTMYHQVRKKITPFVMSFGFRVF GLVLIILDIIMVIVDLSLSEKSRDVGGAPET VSLVISFFFLIDVLLRVYVEGFKVYFSSKLN IVDACIVVITLVVTMIYAFSDFSGASLIPRV VTFLRSLRIVILVGSGSGLEWSHPQFEK

His-DrVSD1 in pET15b

DNA	Protein
AAGGAGATATACC**ATG**GGCAGCAGCCATCATCATCATCATCACAGCAGCGGCCTGGTG CCGCGCGGCAGCCAT**ATG**AAGGAGGAAACCAAGGACCCAGATACGATGTACCACCAGG TGAGAAAGAAGATTACACCTTTCGTTATGTCATTCGGATTCAGAGTTTTCGGACTGGT GTTGATTATTCTTGACATCATTATGGTCATTGTAGACCTTTCATTAAGTGAAAAAAGT CGGGATGTGGGAGGAGCTCCAGAAACAGTAAGCCTGGTCATATCATTTTTCTTCCTGA TAGACGTGCTTCTGCGTGTGTATGTTGAAGGCTTTAAAGTGTATTTTTCTTCAAAGTT AAACATTGTGGACGCTTGCATAGTGGTTATTACCTTAGTCGTTACCATGATTTATGCC TTTTCAGACTTTAGCGGTGCCTCGCTTATCCCTCGTGTAGTTACTTTTCTTCGCTCCC TTCGGATCGTAATTTTGGTTTAA	**M**GSSHHHHHHSSGLVPRGSH**M**KEETKDPDTM YHQVRKKITPFVMSFGFRVFGLVLIILDIIM VIVDLSLSEKSRDVGGAPETVSLVISFFFLI DVLLRVYVEGFKVYFSSKLNIVDACIVVITL VVTMIYAFSDFSGASLIPRVVTFLRSLRIVI LV

MSP1E3D1 in pET28a

DNA	Protein
AAGGAGATATACC**ATG**GGCAGCAGCCATCATCATCATCATCATGAAAACCTGTATTTT CAGGGCAGCACCTTTAGCAAACTGCGTGAACAGCTGGGCCCGGTGACCCAGGAATTTT GGGATAACCTGGAAAAAGAAACCGAAGGCCTGCGTCAGGAAATGAGCAAAGATCTGGA AGAGGTGAAAGCGAAAGTGCAGCCGTATCTGGATGACTTTCAGAAAAAATGGCAGGAA GAGATGGAACTGTATCGTCAGAAAGTGGAACCGCTGCGTGCGGAACTGCAGGAAGGCG CGCGTCAGAAACTGCATGAACTGCAGGAAAAACTGAGCCCGCTGGGCGAAGAGATGCG TGATCGTGCGCGTGCGCATGTGGATGCGCTGCGTACCCATCTGGCGCCGTATCTGGAT GACTTTCAGAAAAAATGGCAGGAAGAGATGGAACTGTATCGTCAGAAAGTGGAACCGC TGCGTGCGGAACTGCAGGAAGGCGCGCGTCAGAAACTGCATGAACTGCAGGAAAAACT GAGCCCGCTGGGCGAAGAGATGCGTGATCGTGCGCGTGCGCATGTGGATGCGCTGCGT ACCCATCTGGCGCCGTATAGCGATGAACTGCGTCAGCGTCTGGCGGCCCGTCTGGAAG CGCTGAAAGAAAACGGCGGTGCGCGTCTGGCGGAATATCATGCGAAAGCGACCGAACA TCTGAGCACCCTGAGCGAAAAAGCGAAACCGGCGCTGGAAGATCTGCGTCAGGGCCTG CTGCCGGTGCTGGAAAGCTTTAAAGTGAGCTTTCTGAGCGCGCTGGAAGAGTATACCA AAAAACTGAACACCCAGTAA	**M**GSSHHHHHHENLYFQGSTFSKLREQLGPVT QEFWDNLEKETEGLRQEMSKDLEEVKAKVQP YLDDFQKKWQEEMELYRQKVEPLRAELQEGA RQKLHELQEKLSPLGEEMRDRARAHVDALRT HLAPYLDDFQKKWQEEMELYRQKVEPLRAEL QEGARQKLHELQEKLSPLGEEMRDRARAHVD ALRTHLAPYSDELRQRLAARLEALKENGGAR LAEYHAKATEHLSTLSEKAKPALEDLRQGLL PVLESFKVSFLSALEEYTKKLNTQ

MSP1 in pET28a

DNA	Protein
AAGGAGATATACC**ATG**GGCAGCAGCCATCATCATCATCATCATGAAAACCTGTATTTT CAGGGCCTGAAACTGCTGGATAACTGGGATAGCGTGACCAGCACCTTTAGCAAACTGC GTGAACAGCTGGGCCCGGTGACCCAGGAATTTTGGGATAACCTGGAAAAAGAAACCGA AGGCCTGCGTCAGGAAATGAGCAAAGATCTGGAAGAGGTGAAAGCGAAAGTGCAGCCG TATCTGGATGACTTTCAGAAAAAATGGCAGGAAGAGATGGAACTGTATCGTCAGAAAG TGGAACCGCTGCGTGCGGAACTGCAGGAAGGCGCGCGTCAGAAACTGCATGAACTGCA GGAAAAACTGAGCCCGCTGGGCGAAGAGATGCGTGATCGTGCGCGTGCGCATGTGGAT GCGCTGCGTACCCATCTGGCGCCGTATAGCGATGAACTGCGTCAGCGTCTGGCGGCCC GTCTGGAAGCGCTGAAAGAAAACGGCGGTGCGCGTCTGGCGGAATATCATGCGAAAGC GACCGAACATCTGAGCACCCTGAGCGAAAAAGCGAAACCGGCGCTGGAAGATCTGCGT CAGGGCCTGCTGCCGGTGCTGGAAAGCTTTAAAGTGAGCTTTCTGAGCGCGCTGGAAG AGTATACCAAAAAACTGAACACCCAGTAA	**M**GSSHHHHHHENLYFQGLKLLDNWDSVTSTF SKLREQLGPVTQEFWDNLEKETEGLRQEMSK DLEEVKAKVQPYLDDFQKKWQEEMELYRQKV EPLRAELQEGARQKLHELQEKLSPLGEEMRD RARAHVDALRTHLAPYSDELRQRLAARLEAL KENGGARLAEYHAKATEHLSTLSEKAKPALE DLRQGLLPVLESFKVSFLSALEEYTKKLNTQ

MSP1D1 ΔH4/H5 in pET28a

DNA	Protein
AAGGAGATATACC**ATG**GGCAGCAGCCATCATCATCATCATCATGAAAACCTGTATTTT CAGGGCAGCACCTTTAGCAAACTGCGTGAACAGCTGGGCCCGGTGACCCAGGAATTTT GGGATAACCTGGAAAAAGAAACCGAAGGCCTGCGTCAGGAAATGAGCAAAGATCTGGA AGAGGTGAAAGCGAAAGTGCAGCCGCTGGGCGAAGAGATGCGTGATCGTGCGCGTGCG CATGTGGATGCGCTGCGTACCCATCTGGCGCCGTATAGCGATGAACTGCGTCAGCGTC TGGCGGCCCGTCTGGAAGCGCTGAAAGAAAACGGCGGTGCGCGTCTGGCGGAATATCA TGCGAAAGCGACCGAACATCTGAGCACCCTGAGCGAAAAAGCGAAACCGGCGCTGGAA GATCTGCGTCAGGGCCTGCTGCCGGTGCTGGAAAGCTTTAAAGTGAGCTTTCTGAGCG CGCTGGAAGAGTATACCAAAAAACTGAACACCCAGTAA	**M**GSSHHHHHHENLYFQGSTFSKLREQLGPVT QEFWDNLEKETEGLRQEMSKDLEEVKAKVQP LGEEMRDRARAHVDALRTHLAPYSDELRQRL AARLEALKENGGARLAEYHAKATEHLSTLSE KAKPALEDLRQGLLPVLESFKVSFLSALEEY TKKLNTQ

MSP1D1 ΔH4-H6 in pET28a

DNA	Protein
AAGGAGATATACC**ATG**GGCAGCAGCCATCATCATCATCATCATGAAAACCTGTATTTT CAGGGCAGCACCTTTAGCAAACTGCGTGAACAGCTGGGCCCGGTGACCCAGGAATTTT GGGATAACCTGGAAAAAGAAACCGAAGGCCTGCGTCAGGAAATGAGCAAAGATCTGGA AGAGGTGAAAGCGAAAGTGCAGCCGTATAGCGATGAACTGCGTCAGCGTCTGGCGGCC CGTCTGGAAGCGCTGAAAGAAAACGGCGGTGCGCGTCTGGCGGAATATCATGCGAAAG CGACCGAACATCTGAGCACCCTGAGCGAAAAAGCGAAACCGGCGCTGGAAGATCTGCG TCAGGGCCTGCTGCCGGTGCTGGAAAGCTTTAAAGTGAGCTTTCTGAGCGCGCTGGAA GAGTATACCAAAAAACTGAACACCCAGTAA	**M**GSSHHHHHHENLYFQGSTFSKLREQLGPVT QEFWDNLEKETEGLRQEMSKDLEEVKAKVQP YSDELRQRLAARLEALKENGGARLAEYHAKA TEHLSTLSEKAKPALEDLRQGLLPVLESFKV SFLSALEEYTKKLNTQ

MSP1D1 ΔH5 in pET28a

DNA	Protein
AAGGAGATATACC**ATG**GGCAGCAGCCATCATCATCATCATCATGAAAACCTGTATTTT CAGGGCAGCACCTTTAGCAAACTGCGTGAACAGCTGGGCCCGGTGACCCAGGAATTTT GGGATAACCTGGAAAAAGAAACCGAAGGCCTGCGTCAGGAAATGAGCAAAGATCTGGA AGAGGTGAAAGCGAAAGTGCAGCCGTATCTGGATGACTTTCAGAAAAAATGGCAGGAA GAGATGGAACTGTATCGTCAGAAAGTGGAACCGCTGGGCGAAGAGATGCGTGATCGTG CGCGTGCGCATGTGGATGCGCTGCGTACCCATCTGGCGCCGTATAGCGATGAACTGCG TCAGCGTCTGGCGGCCCGTCTGGAAGCGCTGAAAGAAAACGGCGGTGCGCGTCTGGCG GAATATCATGCGAAAGCGACCGAACATCTGAGCACCCTGAGCGAAAAAGCGAAACCGG CGCTGGAAGATCTGCGTCAGGGCCTGCTGCCGGTGCTGGAAAGCTTTAAAGTGAGCTT TCTGAGCGCGCTGGAAGAGTATACCAAAAAACTGAACACCCAGTAA	**M**GSSHHHHHHENLYFQGSTFSKLREQLGPVT QEFWDNLEKETEGLRQEMSKDLEEVKAKVQP YLDDFQKKWQEEMELYRQKVEPLGEEMRDRA RAHVDALRTHLAPYSDELRQRLAARLEALKE NGGARLAEYHAKATEHLSTLSEKAKPALEDL RQGLLPVLESFKVSFLSALEEYTKKLNTQ

His-KcsA-Strep in pET28a

DNA	Protein
ATGGGCAGCAGCCATCATCATCATCATCACAGCAGCGGCCTGGTGCCGCGCGGCAGCC ATATGGCACCCATGCTGTCCGGTCTTCTGGCCAGATTGGTCAAACTGCTGCTCGGGCG CCACGGCAGTGCGCTGCACTGGAGGGCCGCGGGTGCCGCGACGGTCCTCCTGGTGATC GTCCTCCTCGCGGGCTCGTACTTGGCCGTCCTGGCTGAGCGCGGCGCACCGGGCGCGC AGCTGATCACGTATCCGCGGGCGCTGTGGTGGTCCGTGGAGACCGCGACGACCGTCGG CTACGGCGACCTGTACCCCGTGACTCTGTGGGGCCGGCTCGTGGCCGTGGTGGTGATG GTCGCCGGGATCACCTCCTTCGGTCTGGTGACCGCCGCGCTGGCCACCTGGTTCGTCG GCCGGGAACAAGAGCGCCGGGGCCACTTCGTGCGCCACTCCGAGAAGGCCGCCGAGGA GGCGTACACGCGGACGACCCGGGCGCTGCACGAGCGTTTCGACCGTTTGGAGCGAATG CTCGACGACAACCTGGTTCCGCGTGGATCTAGCGCTTGGAGCCACCCGCAGTTCGAAA AATAA	**M**GSSHHHHHHSSGLVPRGSHMAP**M**LSGLLAR LVKLLLGRHGSALHWRAAGAATVLLVIVLLA GSYLAVLAERGAPGAQLITYPRALWWSVETA TTVGYGDLYPVTLWGRLVAVVVMVAGITSFG LVTAALATWFVGREQERRGHFVRHSEKAAEE AYTRTTRALHERFDRLERMLDDNLVPRGSSA WSHPQFEK

MraY-His in pET28a

DNA	Protein
AAGGAGATATACAT**ATG**CAACAAACTAACCACCAAGGCGGATCCATGCTTGAGCAAGT CATTCTGTTTACAATTTTAATGGGGTTTTTAATTAGTGTTCTGCTCTCTCCGATTCTT ATTCCGTTTTTAAGAAGATTAAAATTCGGCCAGAGTATTAGAGAAGAAGGACCGAAAT CACATCAGAAAAAATCAGGGACACCGACAATGGGCGGGGTCATGATCATACTTTCTAT CATAGTGACAACAATTGTTATGACACAGAAGTTTTCAGAAATAAGCCCCGAAATGGTG CTGCTTCTGTTTGTTACGCTAGGCTACGGTTTGCTTGGCTTTTTAGATGATTACATCA AGGTTGTCATGAAGCGCAATCTTGGATTGACATCAAAGCAAAAGCTGATCGGACAAAT TATTATTGCAGTTGTATTTTACGCCGTGTATCATTACTACAATTTTGCGACGGATATT CGCATTCCTGGTACTGACTTATCATTTGATCTTGGCTGGGCTTACTTTATTCTTGTGC TCTTTATGCTTGTCGGCGGATCAAACGCAGTTAACCTGACTGACGGCCTTGACGGGTT ATTATCCGGTACTGCGGCGATTGCCTTTGGCGCCTTTGCCATTCTGGCATGGAATCAG TCTCAATATGACGTAGCGATTTTCTCAGTTGCCGTTGTCGGTGCAGTTCTGGGCTTCC TTGTATTTAATGCTCATCCGGCCAAAGTTTTTATGGGAGATACGGGATCGCTTGCATT GGGAGGAGCAATCGTTACCATTGCCATTTTAACGAAATTAGAGATCCTGCTGGTTATC ATCGGCGGTGTATTCGTTATCGAGACATTATCTGTTATTTTGCAGGTCATCAGCTTTA AAACGACAGGTAAACGAATCTTTAAAATGAGTCCGCTTCATCACCATTATGAGCTTGT CGGCTGGTCTGAATGGAGAGTAGTCGTGACGTTTTGGGCTGCGGGACTTTTGCTTGCC GTTTTAGGAATTTACATCGAGGTGTGGTTACTCGAGCACCACCACCACCACCACCATC ATCATCATTGA	**M**QQTNHQGGS**M**LEQVILFTILMGFLISVLLS PILIPFLRRLKFGQSIREEGPKSHQKKSGTP TMGGVMIILSIIVTTIVMTQKFSEISPEMVL LLFVTLGYGLLGFLDDYIKVVMKRNLGLTSK QKLIGQIIIAVVFYAVYHYYNFATDIRIPGT DLSFDLGWAYFILVLFMLVGGSNAVNLTDGL DGLLSGTAAIAFGAFAILAWNQSQYDVAIFS VAVVGAVLGFLVFNAHPAKVFMGDTGSLALG GAIVTIAILTKLEILLVIIGGVFVIETLSVI LQVISFKTTGKRIFKMSPLHHHYELVGWSEW RVVVTFWAAGLLLAVLGIYIEVWLLEHHHHH HHHHH

PylRS-tRNA in pUC57

DNA

```
TAATACGACTCACTATAGGGAGACCGGCTGATGAGTCCGTGAGGACGAAACGGTACCC
GGTACCGTCGGAAACCTGATCATGTAGATCGAACGGACTCTAAATCCGTTCAGCCGGG
TTAGATTCCCGGGGTTTCCGCCAGGAAGCTTACATCCGT
```

PylRS *M. barkeri* in pBH4

DNA	Protein
AAGGAGATATACC**ATG**GGCCATCACCATCACCATCACGACTACGACATCCCGACTACC GAAAACCTGTACTTCCAGGGATCCGATAAAAAACCGCTGGACGTTCTGATCTCCGCTA CGGGTCTGTGGATGAGCCGCACGGGTACGCTGCATAAAATTAAACACCACGAAGTGTC ACGTTCGAAAATCTATATCGAAATGGCGTGCGGTGATCATCTGGTGGTTAACAATAGC CGTTCTTGTCGCACCGCGCGTGCCTTTCGCCATCACAAATACCGCAAAACGTGCAAAC GTTGTCGCGTGTCAGGTGAAGACATTAACAATTTCCTGACCCGTAGTACGGAATCCAA AAACTCAGTGAAAGTTCGCGTCGTGAGTGCTCCGAAAGTTAAAAAAGCGATGCCGAAA AGTGTCTCCCGTGCCCCGAAACCGCTGGAAAACTCAGTGTCGGCAAAAGCTTCCACCA ATACGAGCCGCTCTGTTCCGTCGCCGGCAAAAAGCACCCCGTCCAGCTCTGTCCCGGC AAGCGCACCGGCACCGTCTCTGACGCGTAGTCAGCTGGATCGCGTGGAAGCCCTGCTG TCCCCGGAAGACAAAATCTCACTGAATATGGCAAAACCGTTTCGTGAACTGGAACCGG AACTGGTTACCCGTCGCAAAGATGATTTCCAACGTCTGTATACGAATGATCGCGAAGA CTACCTGGGTAAACTGGAACGTGATATCACCAAATTTTTCGTGGACCGCGGCTTTCTG GAAATCAAATCTCCGATTCTGATCCCGGCTGAATATGTTGAACGCATGGGTATTAACA ATGATACCGAACTGAGTAAACAGATTTTTCGTGTGGATAAAAACCTGTGCCTGCGGCC GATGCTGGCACCGACGCTGTATAATTACCTGCGTAAACTGGATCGCATTCTGCCGGGT CCGATTAAAATCTTTGAAGTGGGCCCGTGTTATCGTAAAGAATCGGATGGCAAAGAAC ACCTGGAAGAATTTACCATGGTTGGTTTCTGCCAAATGGGCAGCGGTTGTACGCGCGA AAATCTGGAAGCGCTGATCAAAGAATTCCTGGATTACCTGGAAATCGACTTCGAAATC GTCGGTGATTCTTGCATGGTGTTTGGCGATACCCTGGACATCATGCATGGTGACCTGG AACTGAGTTCCGCTGTTGTCGGTCCGGTCAGCCTGGATCGTGAATGGGGCATTGACAA ACCGTGGATCGGCGCGGGTTTTGGCCTGGAACGCCTGCTGAAAGTTATGCACGGCTTC AAAAACATCAAACGTGCGTCTCGCTCGGAATCGTATTACAACGGCATCTCAACCAATC TGTAA	**M**GHHHHHHDYDIPTTENLYFQGSDKKPLDVL ISATGLWMSRTGTLHKIKHHEVSRSKIYIEM ACGDHLVVNNSRSCRTARAFRHHKYRKTCKR CRVSGEDINNFLTRSTESKNSVKVRVVSAPK VKKAMPKSVSRAPKPLENSVSAKASTNTSRS VPSPAKSTPSSSVPASAPAPSLTRSQLDRVE ALLSPEDKISLNMAKPFRELEPELVTRRKDD FQRLYTNDREDYLGKLERDITKFFVDRGFLE IKSPILIPAEYVERMGINNDTELSKQIFRVD KNLCLRPMLAPTLYNYLRKLDRILPGPIKIF EVGPCYRKESDGKEHLEEFTMVGFCQMGSGC TRENLEALIKEFLDYLEIDFEIVGDSCMVFG DTLDIMHGDLELSSAVVGPVSLDREWGIDKP WIGAGFGLERLLKVMHGFKNIKRASRSESYY NGISTNL

PylRS *M. mazei* in pBH4

DNA	Protein
AAGGAGATATACC**ATG**GGCCATCACCATCACCATCACGACTACGACATCCCGACTACC GAAAACCTGTACTTCCAGGGATCCGATAAAAAACCGCTGAATACCCTGATTAGCGCAA CCGGTCTGTGGATGAGCCGTACCGGCACCATTCATAAAATCAAACATCATGAAGTGAG CCGCAGCAAAATCTATATTGAAATGGCATGTGGTGATCATCTGGTGGTGAATAATAGC CGTAGCAGTCGTACCGCACGTGCACTGCGTCATCACAAATATCGTAAAACCTGTAAAC GTTGCCGTGTTAGTGATGAGGATCTGAACAAATTTCTGACCAAAGCCAATGAAGATCA GACCAGCGTTAAAGTTAAAGTTGTTAGCGCACCGACCCGTACCAAAAAAGCAATGCCG AAAAGCGTTGCCCGTGCACCGAAACCGCTGGAAAATACCGAAGCAGCACAGGCACAGC CGAGCGGTAGCAAATTTTCACCGGCAATTCCGGTTAGCACCCAAGAAAGCGTTAGCGT TCCGGCAAGCGTGAGCACCAGCATTAGCAGCATTTCAACCGGTGCAACCGCAAGCGCA CTGGTTAAAGGTAATACCAATCCGATTACCAGCATGAGCGCACCGGTTCAGGCAAGTG CACCGGCACTGACCAAAAGTCAGACCGATCGTCTGGAAGTTCTGCTGAATCCGAAAGA TGAAATTAGCCTGAATAGCGGTAAACCGTTTCGTGAACTGGAAAGCGAACTGCTGAGC CGTCGTAAAAAAGATCTGCAGCAGATTTATGCCGAAGAACGCGAAAACTATCTGGGTA AACTGGAACGTGAAATCACCCGTTTTTTTGTGGATCGTGGTTTCCTGGAAATCAAAAG CCCGATTCTGATTCCGCTGGAATATATTGAACGTATGGGCATTGATAACGATACCGAA CTGAGCAAACAAATCTTTCGCGTGGATAAAAACTTTTGTCTGCGTCCGATGCTGGCAC CGAATCTGGCAAATTATCTGCGCAAACTGGATCGCGCACTGCCTGATCCGATTAAAAT CTTTGAAATTGGTCCGTGCTACCGCAAAGAAAGTGATGGTAAAGAACACCTGGAAGAA TTCACCATGCTGAACTTTTGCCAAATGGGTAGCGGTTGTACCCGTGAAAATCTGGAAA GCATTATTACCGATTTTCTGAACCATCTGGGCATCGATTTCAAAATTGTTGGTGATAG CTGCATGGTGTTTGGTGATACCCTGGATGTTATGCATGGTGATCTGGAACTGAGTAGC GCAGTTGTTGGTCCGATCCCGCTGGATCGTGAATGGGGTTTGGATAAACCGTGGATTG GTGCAGGTTTTGGTCTGGAACGCCTGCTGAAAGTTAAACACGACTTCAAAAACATTAA ACGTGCAGCACGTAGCGAGAGCTATTACAATGGTATTAGCACCAACCTGTAA	**M**GHHHHHHDYDIPTTENLYFQGSDKKPLNTL ISATGLWMSRTGTIHKIKHHEVSRSKIYIEM ACGDHLVVNNSRSSRTARALRHHKYRKTCKR CRVSDEDLNKFLTKANEDQTSVKVKVVSAPT RTKKAMPKSVARAPKPLENTEAAQAQPSGSK FSPAIPVSTQESVSVPASVSTSISSISTGAT ASALVKGNTNPITSMSAPVQASAPALTKSQT DRLEVLLNPKDEISLNSGKPFRELESELLSR RKKDLQQIYAEERENYLGKLEREITRFFVDR GFLEIKSPILIPLEYIERMGIDNDTELSKQI FRVDKNFCLRPMLAPNLANYLRKLDRALPDP IKIFEIGPCYRKESDGKEHLEEFTMLNFCQM GSGCTRENLESIITDFLNHLGIDFKIVGDSC MVFGDTLDVMHGDLELSSAVVGPIPLDREWG LDKPWIGAGFGLERLLKVKHDFKNIKRAARS ESYYNGISTNL

GFP (Y151*)-His in pET22b(+)

DNA	Protein
ATGAGCAAAGGAGAAGAACTTTTCACTGGAGTTGTCCCAATTCTTGTTGAATTAGATG GTGATGTTAATGGGCACAAATTTTCTGTCAGTGGAGAGGGTGAAGGTGATGCTACATA CGGAAAACTCACCCTTAAATTTATTTGCACTACTGGAAAACTACCTGTTCCATGGCCA ACACTTGTCACTACTCTGACCTATGGTGTTCAATGCTTTTCCCGTTATCCGGATCACA TGAAACGGCATGACTTTTTCAAGAGTGCCATGCCCGAAGGTTATGTACAGGAACGCAC TATATCTTTCAAAGATGACGGGAACTACAAGACGCGTGCTGAAGTCAAGTTTGAAGGT GATACCCTTGTTAATCGTATCGAGTTAAAGGGTATTGATTTTAAAGAAGATGGAAACA TTCTCGGACACAAACTCGAGTACAACTATAACTCACACAATGTATAGATCACGGCAGA CAAACAAAAGAATGGAATCAAAGCTAACTTCAAAATTCGCCACAACATTGAAGATGGT TCCGTTCAACTAGCAGACCATTATCAACAAAATACTCCAATTGGCGATGGCCCTGTCC TTTTACCAGACAACCATTACCTGTCGACACAATCTGCCCTTTCGAAAGATCCCAACGA AAAGCGTGACCACATGGTCCTTCTTGAGTTTGTAACTGCTGCTGGGATTACACATGGC ATGGATGAGCTCTACAAAAAGCTTGCGGCCGCACTCGAGCACCACCACCACCACCACT GA	**M**SKGEELFTGVVPILVELDGDVNGHKFSVSG EGEGDATYGKLTLKFICTTGKLPVPWPTLVT TLTYGVQCFSRYPDHMKRHDFFKSAMPEGYV QERTISFKDDGNYKTRAEVKFEGDTLVNRIE LKGIDFKEDGNILGHKLEYNYNSHNV*ITAD KQKNGIKANFKIRHNIEDGSVQLADHYQQNT PIGDGPVLLPDNHYLSTQSALSKDPNEKRDH MVLLEFVTAAGITHGMDELYKKLAAALEHHH HHH

His-Ubiquitin-PylRS *M. mazei* in pET39_Ub19

DNA	Protein
AAGGAGATATACAT**ATG**CAGATCTTCGTGAAAACACTGACCGGCAAAACCATTACCCT GGAGGTGGAGCCTGGCAGCGCCCATCATCATCACCATCACCATCACCATCATGCTGGT AGCAGCGATACGATCGAAAACGTCAAAGCCAAAATTCAGGACAAAGAGGGCATTCCGC CTGATCAACAACGTCTGATCTTCGCCGGAAAACAGCTGGAGGATGGCCGTACACTGAG TGACTATAACATTCAAGAGAAATCGACACTGGAACTGGTTCTGGAGCTGCAGAATGAA ACCCAGTCAGCAACTTCTGACGCTTCTGGCGGTGAGAATCTGTATTTTCAGGGCGCCA TGGATAAAAAACCGCTGAATACCCTGATTAGCGCAACCGGTCTGTGGATGAGCCGTAC CGGCACCATTCATAAAATCAAACATCATGAAGTGAGCCGCAGCAAAATCTATATTGAA ATGGCATGTGGTGATCATCTGGTGGTGAATAATAGCCGTAGCAGTCGTACCGCACGTG CACTGCGTCATCACAAATATCGTAAAACCTGTAAACGTTGCCGTGTTAGTGATGAGGA TCTGAACAAATTTCTGACCAAAGCCAATGAAGATCAGACCAGCGTTAAAGTTAAAGTT GTTAGCGCACCGACCCGTACCAAAAAAGCAATGCCGAAAAGCGTTGCCCGTGCACCGA AACCGCTGGAAAATACCGAAGCAGCACAGGCACAGCCGAGCGGTAGCAAATTTTCACC GGCAATTCCGGTTAGCACCCAAGAAAGCGTTAGCGTTCCGGCAAGCGTGAGCACCAGC ATTAGCAGCATTTCAACCGGTGCAACCGCAAGCGCACTGGTTAAAGGTAATACCAATC CGATTACCAGCATGAGCGCACCGGTTCAGGCAAGTGCACCGGCACTGACCAAAAGTCA GACCGATCGTCTGGAAGTTCTGCTGAATCCGAAAGATGAAATTAGCCTGAATAGCGGT AAACCGTTTCGTGAACTGGAAAGCGAACTGCTGAGCCGTCGTAAAAAAGATCTGCAGC AGATTTATGCCGAAGAACGCGAAAACTATCTGGGTAAACTGGAACGTGAAATCACCCG TTTTTTTGTGGATCGTGGTTTCCTGGAAATCAAAAGCCCGATTCTGATTCCGCTGGAA TATATTGAACGTATGGGCATTGATAACGATACCGAACTGAGCAAACAAATCTTTCGCG TGGATAAAAACTTTTGTCTGCGTCCGATGCTGGCACCGAATCTGGCAAATTATCTGCG CAAACTGGATCGCGCACTGCCTGATCCGATTAAAATCTTTGAAATTGGTCCGTGCTAC CGCAAAGAAAGTGATGGTAAAGAACACCTGGAAGAATTCACCATGCTGAACTTTTGCC AAATGGGTAGCGGTTGTACCCGTGAAAATCTGGAAAGCATTATTACCGATTTTCTGAA CCATCTGGGCATCGATTTCAAAATTGTTGGTGATAGCTGCATGGTGTTTGGTGATACC CTGGATGTTATGCATGGTGATCTGGAACTGAGTAGCGCAGTTGTTGGTCCGATCCCGC TGGATCGTGAATGGGGTTTGGATAAACCGTGGATTGGTGCAGGTTTTGGTCTGGAACG CCTGCTGAAAGTTAAACACGACTTCAAAAACATTAAACGTGCAGCACGTAGCGAGAGC TATTACAATGGTATTAGCACCAACCTGTAA	**M**QIFVKTLTGKTITLEVEPGSAHHHHHHHHH HAGSSDTIENVKAKIQDKEGIPPDQQRLIFA GKQLEDGRTLSDYNIQEKSTLELVLELQNET QSATSDASGGENLYFQGAMDKKPLNTLISAT GLWMSRTGTIHKIKHHEVSRSKIYIEMACGD HLVVNNSRSSRTARALRHHKYRKTCKRCRVS DEDLNKFLTKANEDQTSVKVKVVSAPTRTKK AMPKSVARAPKPLENTEAAQAQPSGSKFSPA IPVSTQESVSVPASVSTSISSISTGATASAL VKGNTNPITSMSAPVQASAPALTKSQTDRLE VLLNPKDEISLNSGKPFRELESELLSRRKKD LQQIYAEERENYLGKLEREITRFFVDRGFLE IKSPILIPLEYIERMGIDNDTELSKQIFRVD KNFCLRPMLAPNLANYLRKLDRALPDPIKIF EIGPCYRKESDGKEHLEEFTMLNFCQMGSGC TRENLESIITDFLNHLGIDFKIVGDSCMVFG DTLDVMHGDLELSSAVVGPIPLDREWGLDKP WIGAGFGLERLLKVKHDFKNIKRAARSESYY NGISTNL

pET21a* changed multiple cloning site (Primer 1/2, 10xHis-tag)

```
AGATCTCGATCCCGCGAAATTAATACGACTCACTATAGGGGAATTGTGAGCGGATAACAATTCCCCTCTAGAAATAATTTTGTTTAACTTTA
AGAAGGAGATATACATATG…insert sequence….GGATCCGGATCAGGACTCGAGCATCATCACCATCACCACCATCACCATCATTAGT
GAGATCCGGCTGCTAACAAAGCCCGAAAGGAAGCTGAGTTGGCTGCTGCCACCGCTGAGCAATAACTAGCATAACCCCTTGGGGCCTCTAAA
CGGGTCTTGAGGGGTTTTTTGCTGAAAGGAGGAACTATATCCGGAT
```

pET21a* changed multiple cloning site (Primer 1/3, StrepII-tag)

```
AGATCTCGATCCCGCGAAATTAATACGACTCACTATAGGGGAATTGTGAGCGGATAACAATTCCCCTCTAGAAATAATTTTGTTTAACTTTA
AGAAGGAGATATACATATG…insert sequence…GGATCCGGATCAGGACTCGAGTGGAGTCACCCTCAGTTTGAAAAGTAGTGAGATCC
GGCTGCTAACAAAGCCCGAAAGGAAGCTGAGTTGGCTGCTGCCACCGCTGAGCAATAACTAGCATAACCCCTTGGGGCCTCTAAACGGGTCT
TGAGGGGTTTTTTGCTGAAAGGAGGAACTATATCCGGAT
```

pMAL* (cloned by Jan Heering AK Dötsch)

CCGACACCATCGAATGGTGCAAAACCTTTCGCGGTATGGCATGATAGCGCCCGGAAGAGAGTCAATTCAGGGTGGTGAATGTGAAACCAGTA
ACGTTATACGATGTCGCAGAGTATGCCGGTGTCTCTTATCAGACCGTTTCCCGCGTGGTGAACCAGGCCAGCCACGTTTCTGCGAAAACGCG
GGAAAAAGTGGAAGCGGCGATGGCGGAGCTGAATTACATTCCCAACCGCGTGGCACAACAACTGGCGGGCAAACAGTCGTTGCTGATTGGCG
TTGCCACCTCCAGTCTGGCCCTGCACGCGCCGTCGCAAATTGTCGCGGCGATTAAATCTCGCGCCGATCAACTGGGTGCCAGCGTGGTGGTG
TCGATGGTAGAACGAAGCGGCGTCGAAGCCTGTAAAGCGGCGGTGCACAATCTTCTCGCGCAACGCGTCAGTGGGCTGATCATTAACTATCC
GCTGGATGACCAGGATGCCATTGCTGTGGAAGCTGCCTGCACTAATGTTCCGGCGTTATTTCTTGATGTCTCTGACCAGACACCCATCAACA
GTATTATTTTCTCCCATGAAGACGGTACGCGACTGGGCGTGGAGCATCTGGTCGCATTGGGTCACCAGCAAATCGCGCTGTTAGCGGGCCCA
TTAAGTTCTGTCTCGGCGCGTCTGCGTCTGGCTGGCTGGCATAAATATCTCACTCGCAATCAAATTCAGCCGATAGCGGAACGGGAAGGCGA
CTGGAGTGCCATGTCCGGTTTTCAACAAACCATGCAAATGCTGAATGAGGGCATCGTTCCCACTGCGATGCTGGTTGCCAACGATCAGATGG
CGCTGGGCGCAATGCGCGCCATTACCGAGTCCGGGCTGCGCGTTGGTGCGGATATCTCGGTAGTGGGATACGACGATACCGAAGACAGCTCA
TGTTATATCCCGCCGTTAACCACCATCAAACAGGATTTTCGCCTGCTGGGGCAAACCAGCGTGGACCGCTTGCTGCAACTCTCTCAGGGCCA
GGCGGTGAAGGGCAATCAGCTGTTGCCCGTCTCACTGGTGAAAAGAAAAACCACCCTGGCGCCCAATACGCAAACCGCCTCTCCCCGCGCGT
TGGCCGATTCATTAATGCAGCTGGCACGACAGGTTTCCCGACTGGAAAGCGGGCAGTGAGCGCAACGCAATTAATGTAAGTTAGCTCACTCA
TTAGGCACAATTCTCATGTTTGACAGCTTATCATCGACTGCACGGTGCACCAATGCTTCTGGCGTCAGGCAGCCATCGGAAGCTGTGGTATG
GCTGTGCAGGTCGTAAATCACTGCATAATTCGTGTCGCTCAAGGCGCACTCCCGTTCTGGATAATGTTTTTTGCGCCGACATCATAACGGTT
CTGGCAAATATTCTGAAATGAGCTGTTGACAATTAATCATCGGCTCGTATAATGTGTGGAATTGTGAGCGGATAACAATTTCACACAGGAAA
CAGCCAGTCCGTTTAGGTGTTTTCACGAGCACTTCACCAACAAGGACCATAGATTATGAAAACTGAAGAAGGTAAACTGGTAATCTGGATTA
ACGGCGATAAAGGCTATAACGGTCTCGCTGAAGTCGGTAAGAAATTCGAGAAAGATACCGGAATTAAAGTCACCGTTGAGCATCCGGATAAA
CTGGAAGAGAAATTCCCACAGGTTGCGGCAACTGGCGATGGCCCTGACATTATCTTCTGGGCACACGACCGCTTTGGTGGCTACGCTCAATC
TGGCCTGTTGGCTGAAATCACCCCGGACAAAGCGTTCCAGGACAAGCTGTATCCGTTTACCTGGGATGCCGTACGTTACAACGGCAAGCTGA
TTGCTTACCCGATCGCTGTTGAAGCGTTATCGCTGATTTATAACAAAGATCTGCTGCCGAACCCGCCAAAAACCTGGGAAGAGATCCCGGCG
CTGGATAAAGAACTGAAAGCGAAAGGTAAGAGCGCGCTGATGTTCAACCTGCAAGAACCGTACTTCACCTGGCCGCTGATTGCTGCTGACGG
GGGTTATGCGTTCAAGTATGAAAACGGCAAGTACGACATTAAAGACGTGGGCGTGGATAACGCTGGCGCGAAAGCGGGTCTGACCTTCCTGG
TTGACCTGATTAAAAACAAACACATGAATGCAGACACCGATTACTCCATCGCAGAAGCTGCCTTTAATAAAGGCGAAACAGCGATGACCATC
AACGGCCCGTGGGCATGGTCCAACATCGACACCAGCAAAGTGAATTATGGTGTAACGGTACTGCCGACCTTCAAGGGTCAACCATCCAAACC
GTTCGTTGGCGTGCTGAGCGCAGGTATTAACGCCGCCAGTCCGAACAAAGAGCTGGCAAAAGAGTTCCTCGAAAACTATCTGCTGACTGATG
AAGGTCTGGAAGCGGTTAATAAAGACAAACCGCTGGGTGCCGTAGCGCTGAAGTCTTACGAGGAAGAGTTGGCGAAAGATCCACGTATTGCC
GCCACCATGGAAAACGCCCAGAAAGGTGAAATCATGCCGAACATCCCGCAGATGTCCGCTTTCTGGTATGCCGTGCGTACTGCGGTGATCAA
CGCCGCCAGCGGTCGTCAGACTGTCGATGAAGCCCTGAAAGACGCGCAGACTAATTCGAGCTCGAACAACAACAACAATAACAATAACAACA
ACCTCGGGATCGAGGGTACccatcaccatcaccatcaccatcacccgggtaccgaaaacctgtacttccagggatcc...insert seque
nce...ctcgagGTCGACCTGCAGGCAAGCTTGGCACTGGCCGTCGTTTTACAACGTCGTGACTGGGAAAACCCTGGCGTTACCCAACTTAA
TCGCCTTGCAGCACATCCCCCTTTCGCCAGCTGGCGTAATAGCGAAGAGGCCCGCACCGATCGCCCTTCCCAACAGTTGCGCAGCCTGAATG
GCGAATGGCAGCTTGGCTGTTTTGGCGGATGAGATAAGATTTTCAGCCTGATACAGATTAAATCAGAACGCAGAAGCGGTCTGATAAAACAG
AATTTGCCTGGCGGCAGTAGCGCGGTGGTCCCACCTGACCCCATGCCGAACTCAGAAGTGAAACGCCGTAGCGCCGATGGTAGTGTGGGGTC
TCCCCATGCGAGAGTAGGGAACTGCCAGGCATCAAATAAAACGAAAGGCTCAGTCGAAAGACTGGGCCTTTCGTTTTATCTGTTGTTTGTCG
GTGAACGCTCTCCTGAGTAGGACAAATCCGCCGGGAGCGGATTTGAACGTTGCGAAGCAACGGCCCGGAGGGTGGCGGGCAGGACGCCCGCC
ATAAACTGCCAGGCATCAAATTAAGCAGAAGGCCATCCTGACGGATGGCCTTTTTGCGTTTCTACAAACTCTTTTGTTTATTTTTCTAAATA
CATTCAAATATGTATCCGCTCATGAGACAATAACCCTGATAAATGCTTCAATAATATTGAAAAAGGAAGAGTATGAGTATTCAACATTTCCG
TGTCGCCCTTATTCCCTTTTTTGCGGCATTTTGCCTTCCTGTTTTTGCTCACCCAGAAACGCTGGTGAAAGTAAAAGATGCTGAAGATCAGT
TGGGTGCACGAGTGGGTTACATCGAACTGGATCTCAACAGCGGTAAGATCCTTGAGAGTTTTCGCCCCGAAGAACGTTTCCCAATGATGAGC
ACTTTTAAAGTTCTGCTATGTGGCGCGGTATTATCCCGTGTTGACGCCGGGCAAGAGCAACTCGGTCGCCGCATACACTATTCTCAGAATGA
CTTGGTTGAGTACTCACCAGTCACAGAAAAGCATCTTACGGATGGCATGACAGTAAGAGAATTATGCAGTGCTGCCATAACCATGAGTGATA
ACACTGCGGCCAACTTACTTCTGACAACGATCGGAGGACCGAAGGAGCTAACCGCTTTTTTGCACAACATGGGGGATCATGTAACTCGCCTT
GATCGTTGGGAACCGGAGCTGAATGAAGCCATACCAAACGACGAGCGTGACACCACGATGCCTGTAGCAATGGCAACAACGTTGCGCAAACT
ATTAACTGGCGAACTACTTACTCTAGCTTCCCGGCAACAATTAATAGACTGGATGGAGGCGGATAAAGTTGCAGGACCACTTCTGCGCTCGG
CCCTTCCGGCTGGCTGGTTTATTGCTGATAAATCTGGAGCCGGTGAGCGTGGGTCTCGCGGTATCATTGCAGCACTGGGGCCAGATGGTAAG
CCCTCCCGTATCGTAGTTATCTACACGACGGGGAGTCAGGCAACTATGGATGAACGAAATAGACAGATCGCTGAGATAGGTGCCTCACTGAT
TAAGCATTGGTAACTGTCAGACCAAGTTTACTCATATATACTTTAGATTGATTTACCCCGGTTGATAATCAGAAAAGCCCCAAAAACAGGAA
GATTGTATAAGCAAATATTTAAATTGTAAACGTTAATATTTTGTTAAAATTCGCGTTAAATTTTTGTTAAATCAGCTCATTTTTTAACCAAT
AGGCCGAAATCGGCAAAATCCCTTATAAATCAAAAGAATAGCCCGAGATAGGGTTGAGTGTTGTTCCAGTTTGGAACAAGAGTCCACTATTA
AAGAACGTGGACTCCAACGTCAAAGGGCGAAAAACCGTCTATCAGGGCGATGGCCCACTACGTGAACCATCACCCAAATCAAGTTTTTTGGG
GTCGAGGTGCCGTAAAGCACTAAATCGGAACCCTAAAGGGAGCCCCCGATTTAGAGCTTGACGGGGAAAGCCGGCGAACGTGGCGAGAAAGG
AAGGGAAGAAAGCGAAAGGAGCGGGCGCTAGGGCGCTGGCAAGTGTAGCGGTCACGCTGCGCGTAACCACCACACCCGCCGCGCTTAATGCG
CCGCTACAGGGCGCGTAAAAGGATCTAGGTGAAGATCCTTTTTGATAATCTCATGACCAAAATCCCTTAACGTGAGTTTTCGTTCCACTGAG
CGTCAGACCCCGTAGAAAAGATCAAAGGATCTTCTTGAGATCCTTTTTTTCTGCGCGTAATCTGCTGCTTGCAAACAAAAAAACCACCGCTA
CCAGCGGTGGTTTGTTTGCCGGATCAAGAGCTACCAACTCTTTTTCCGAAGGTAACTGGCTTCAGCAGAGCGCAGATACCAAATACTGTCCT
TCTAGTGTAGCCGTAGTTAGGCCACCACTTCAAGAACTCTGTAGCACCGCCTACATACCTCGCTCTGCTAATCCTGTTACCAGTGGCTGCTG
CCAGTGGCGATAAGTCGTGTCTTACCGGGTTGGACTCAAGACGATAGTTACCGGATAAGGCGCAGCGGTCGGGCTGAACGGGGGGTTCGTGC
ACACAGCCCAGCTTGGAGCGAACGACCTACACCGAACTGAGATACCTACAGCGTGAGCTATGAGAAAGCGCCACGCTTCCCGAAGGGAGAAA
GGCGGACAGGTATCCGGTAAGCGGCAGGGTCGGAACAGGAGAGCGCACGAGGGAGCTTCCAGGGGGAAACGCCTGGTATCTTTATAGTCCTG
TCGGGTTTCGCCACCTCTGACTTGAGCGTCGATTTTTGTGATGCTCGTCAGGGGGGCGGAGCCTATGGAAAAACGCCAGCAACGCGGCCTTT
TTACGGTTCCTGGCCTTTTGCTGGCCTTTTGCTCACATGTTCTTTCCTGCGTTATCCCCTGATTCTGTGGATAACCGTATTACCGCCTTTGA
GTGAGCTGATACCGCTCGCCGCAGCCGAACGACCGAGCGCAGCGAGTCAGTGAGCGAGGAAGCGGAAGAGCGCCTGATGCGGTATTTTCTCC
TTACGCATCTGTGCGGTATTTCACACCGCATATATGGTGCACTCTCAGTACAATCTGCTCTGATGCCGCATAGTTAAGCCAGTATACACTCC
GCTATCGCTACGTGACTGGGTCATGGCTGCGCCCCGACACCCGCCAACACCCGCTGACGCGCCCTGACGGGCTTGTCTGCTCCCGGCATCCG
CTTACAGACAAGCTGTGACCGTCTCCGGGAGCTGCATGTGTCAGAGGTTTTCACCGTCATCACCGAAACGCGCGAGGCAGCTGCGGTAAAGC
TCATCAGCGTGGTCGTGCAGCGATTCACAGATGTCTGCCTGTTCATCCGCGTCCAGCTCGTTGAGTTTCTCCAGAAGCGTTAATGTCTGGCT
TCTGATAAAGCGGGCCATGTTAAGGGCGGTTTTTTCCTGTTTGGTCACTGATGCCTCCGTGTAAGGGGGATTTCTGTTCATGGGGGTAATGA
TACCGATGAAACGAGAGAGGATGCTCACGATACGGGTTACTGATGATGAACATGCCCGGTTACTGGAACGTTGTGAGGGTAAACAACTGGCG
GTATGGATGCGGCGGGACCAGAGAAAAATCACTCAGGGTCAATGCCAGCGCTTCGTTAATACAGATGTAGGTGTTCCACAGGGTAGCCAGCA
GCATCCTGCGATGCAGATCCGGAACATAATGGTGCAGGGCGCTGACTTCCGCGTTTCCAGACTTTACGAAACACGGAAACCGAAGACCATTC
ATGTTGTTGCTCAGGTCGCAGACGTTTTGCAGCAGCAGTCGCTTCACGTTCGCTCGCGTATCGGTGATTCATTCTGCTAACCAGTAAGGCAA
CCCCGCCAGCCTAGCCGGGTCCTCAACGACAGGAGCACGATCATGCGCACCCGTGGCCAGGACCCAACGCTGCCCGAAATT

7.2 Stability screening of cell-free-synthesized VSDs

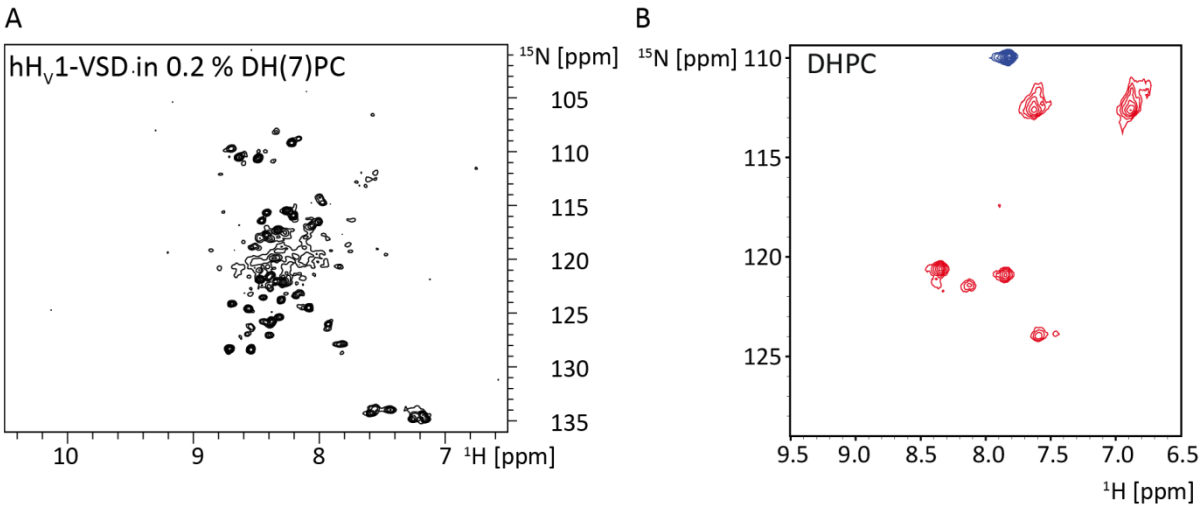

Figure A 1: Spectra of hHV1-VSD in DH(7)PC micelles. A The [^{15}N,^{1}H]-BEST-TROSY spectrum shows cell-free-expressed ^{15}N,^{2}H-labeled hHV1-VSD (10 µM) in 50 mM sodium acetate pH 5.2 at 298 K and 800 MHz. The protein was expressed without the addition of any scrambling inhibitors and directly solubilized and purified in DH(7)PC (NS = 256, TD1 = 304). **B** [^{15}N,^{1}H]-HSQC spectrum of *E. coli*-expressed ^{15}N-labeled hHV1-VSD in DHPC at 298 K (adapted from Letts, 2014).

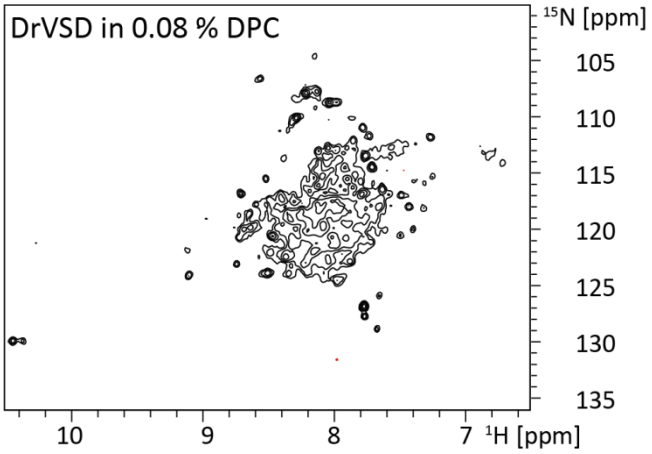

Figure A 2: Spectrum of His-DrVSD-Strep in 0.08 % DPC after IMAC purification. The [^{15}N,^{1}H]-BEST-TROSY spectrum shows cell-free-expressed, purified ^{15}N,^{2}H-labeled DrVSD in 20 mM HEPES-NaOH pH 7.0, 150 mM NaCl, 0.08 % DPC at 318 K and 700 MHz (NS = 352, TD1 = 242).

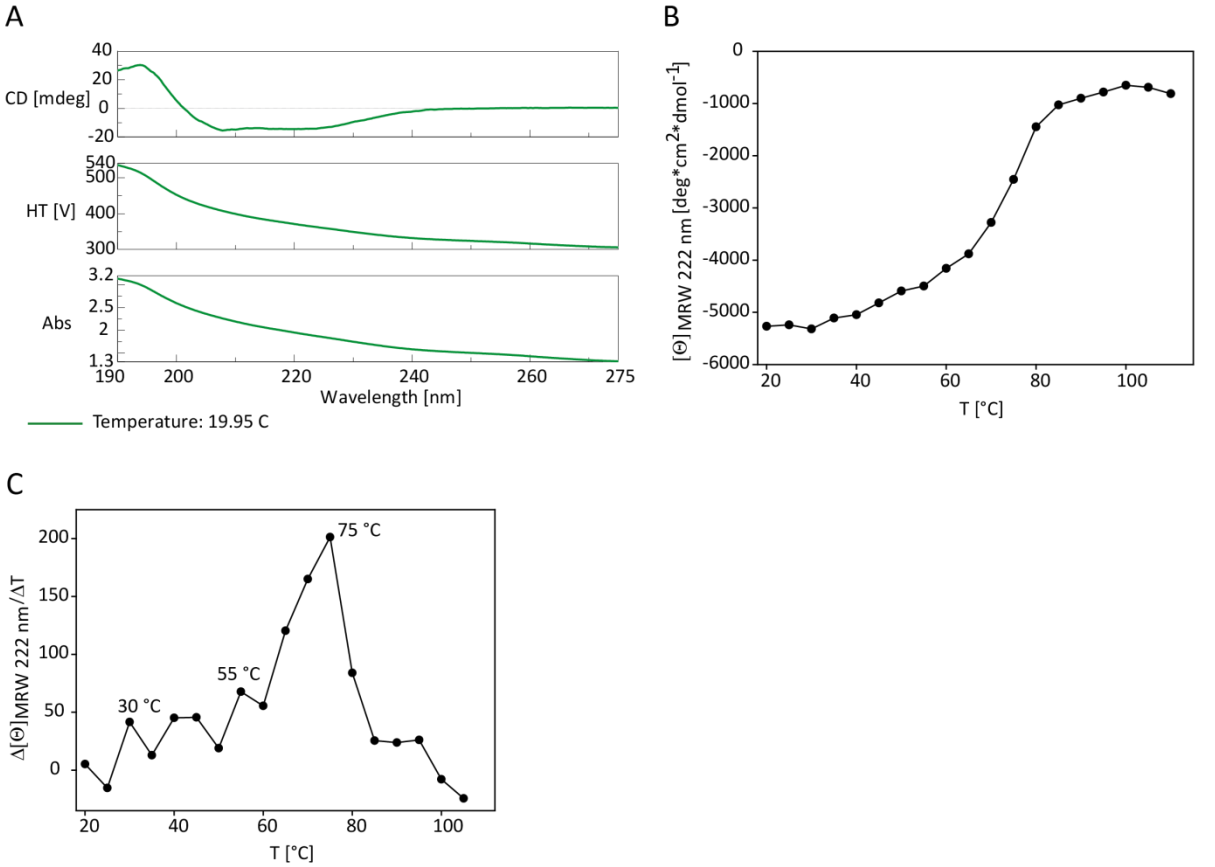

Figure A 3: CD spectroscopy analysis of hH_V1-VSD in DPC micelles. Samples were recorded in CD buffer containing 50 mM K_2HPO_4 and 0.08 % DPC. **A** Plots of the CD signal, HT and absorption (Abs) values are shown for the measured CD signal of hH_V1-VSD at 20 °C. The absorption signal as well as the HT signal increased with decreasing wavelengths. An HT value above 600 V means a saturated detector. The absorption should not be higher than two. **B** Temperature-dependent mean residue weight ellipticity values at 222 nm are plotted to analyze the unfolding of hH_V1-VSD in detergent. **C** The plot shows the first derivative of the mean residue ellipticity values over temperature to determine T_M. Multiple T_M values could be determined at 75 °C, 55 °C and 30 °C. No real unfolding event could be observed. In comparison with the full wavelength scans in **Figure 22** the sample starts to precipitate with increasing temperatures.

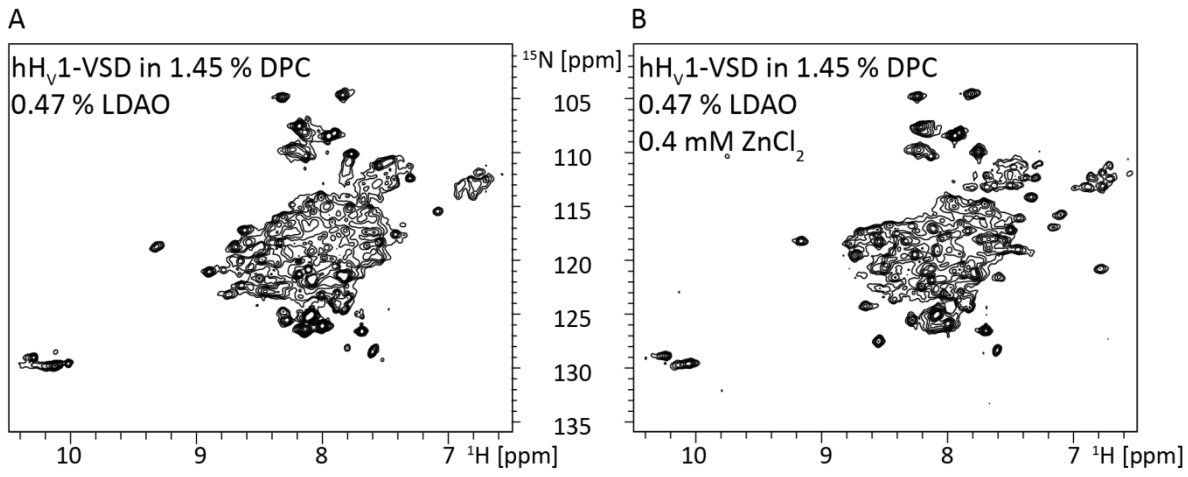

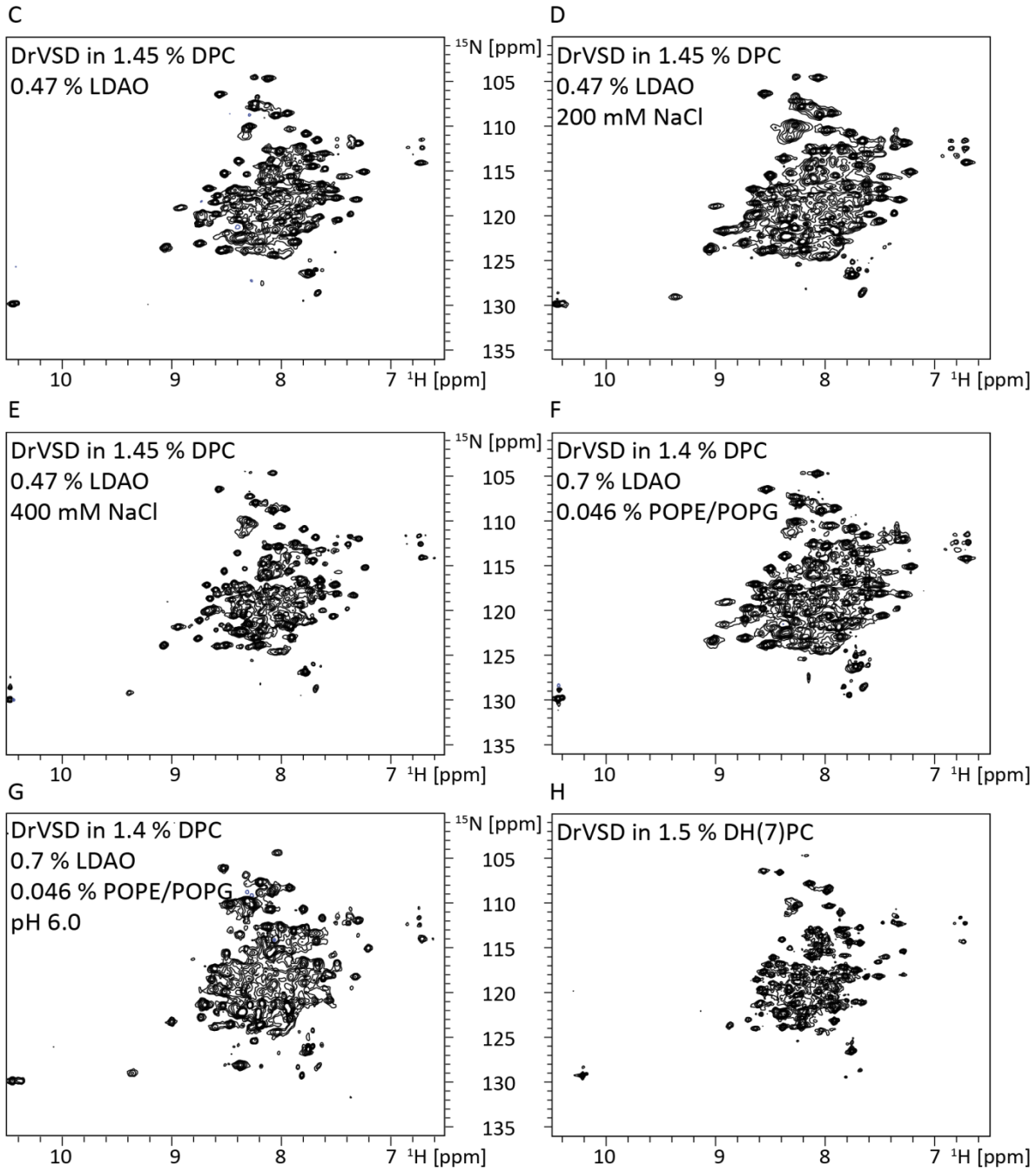

Figure A 4: NMR screening of VSDs in different environments after TCA precipitation. Spectra were recorded at 318 K in 20 mM HEPES-NaOH pH 7.0 with different additives. **A** [^{15}N,^{1}H]-BEST-TROSY spectrum shows resuspended hH_V1-VSD in 1.45 % DPC/0.47 % LDAO (molar ratio of 2:1) buffer (NS = 256, TD1 = 256; 800 MHz). **B** [^{15}N,^{1}H]-BEST-TROSY spectrum shows resuspended hH_V1-VSD in 1.45 % DPC/0.47 %LDAO (molar ratio of 2:1) buffer with additional 400 µM $ZnCl_2$ (NS = 352, TD1 = 256, 700 MHz). **C** [^{15}N,^{1}H]-BEST-TROSY spectrum shows resuspended DrVSD in 1.45 % DPC/0.47 % LDAO (molar ratio of 2:1) buffer (NS = 640, TD1 = 246, 700 MHz). **D** [^{15}N,^{1}H]-BEST-TROSY spectrum shows resuspended DrVSD in 1.45 % DPC/0.47 % LDAO (molar ratio of 2:1) buffer with 200 mM NaCl (NS = 256, TD1 = 320, 700 MHz). **E** [^{15}N,^{1}H]-BEST-TROSY spectrum shows resuspended DrVSD in 1.45 % DPC/0.47 % LDAO (molar ratio of 2:1) buffer with 400 mM NaCl (NS = 200, TD1 = 320, 800 MHz) **F** [^{15}N,^{1}H]-BEST-TROSY spectrum shows resuspended DrVSD in mixed micelles containing 1.4 % DPC/0.7 % LDAO (w/w 2:1) and 0.046 % POPE/POPG (w/w 3:1) (NS = 128, TD1 = 320, 800 MHz). **G** [^{15}N,^{1}H]-BEST-TROSY spectrum shows resuspended DrVSD in mixed micelles containing 1.4 % DPC/0.7 % LDAO (w/w 2:1) and 0.046 % POPE/POPG (w/w 3:1) where the pH was lowered to 6.0 by addition of 28 µl 1 % HCl (NS = 328, TD1 = 168, 800 MHz). **H** [^{15}N,^{1}H]-BEST-TROSY spectrum shows resuspended DrVSD in 1.5 % DH(7)PC buffer (NS = 152, TD1 = 510, 950 MHz).

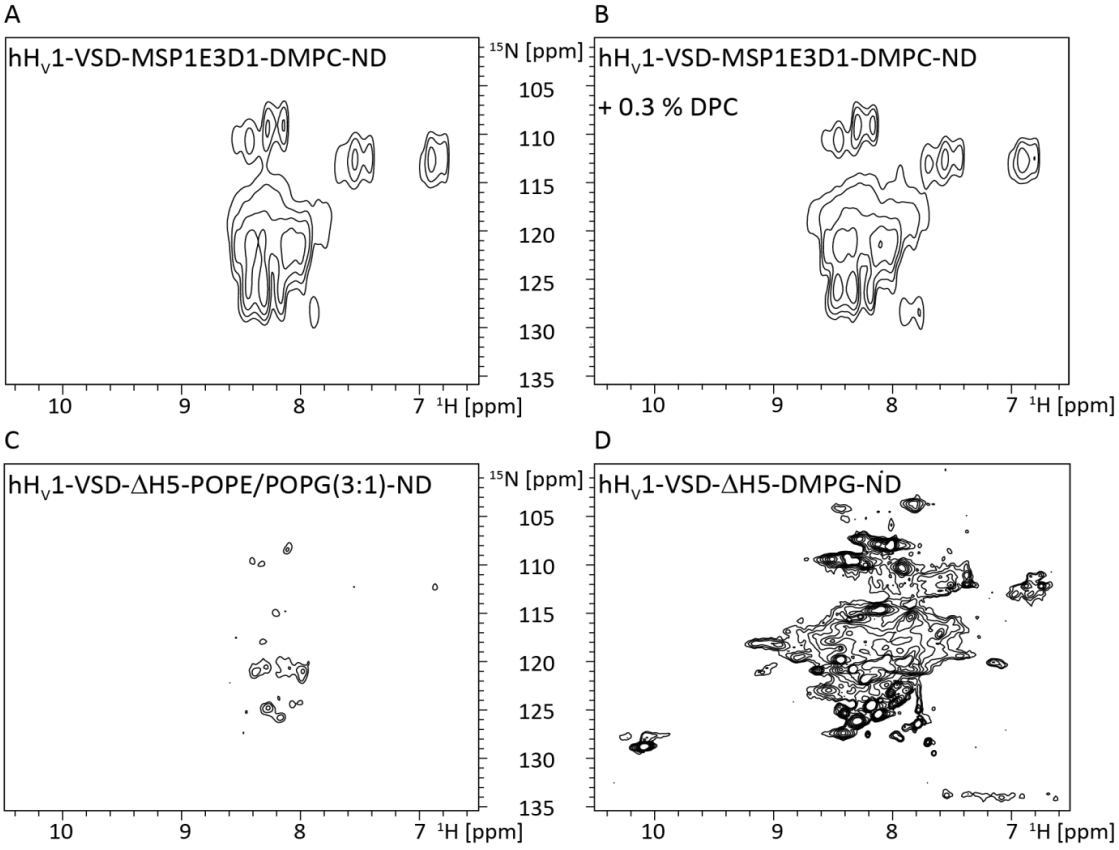

Figure A 5: NMR analyses of $^{15}N,^{2}H$-labeled hH_V1-VSD in different NDs. A The spectrum shows hH_V1-VSD in 11-12 nm NDs containing MSP1E3D1 as scaffold and DMPC as lipid ([$^{15}N,^{1}H$]-SOFAST-HMQC; 599 MHz; 313 K; 50 mM NaP_i pH 7.0, 50 mM NaCl, NS = 128, TD1 = 24). **B** The spectrum shows hH_V1-VSD in 11-12 nm NDs containing MSP1E3D1 as scaffold and DMPC as lipid titrated with 0.3 % DPC to a q-ratio of 1.3 ([$^{15}N,^{1}H$]-SOFAST-HMQC; 599 MHz; 313 K; 50 mM NaP_i pH 7.0, 50 mM NaCl, NS = 128, TD1 = 32). **C** The spectrum shows hH_V1-VSD in 8-9 nm NDs containing MSP1D1ΔH5 as scaffold and POPE/POPG (3:1) as lipids (([$^{15}N,^{1}H$]-SOFAST-HMQC; 800 MHz; 308 K; 20 mM HEPES-NaOH pH 7.0, 100 mM NaCl, NS = 256, TD1 = 150). **D** The spectrum shows hH_V1-VSD in 8-9 nm NDs containing MSP1D1ΔH5 as scaffold and DMPG as lipid ([$^{15}N,^{1}H$]-BEST-TROSY; 700 MHz; 318 K; 20 mM HEPES-NaOH pH 7.0, 20 mM NaCl, NS = 384, TD1 = 256).

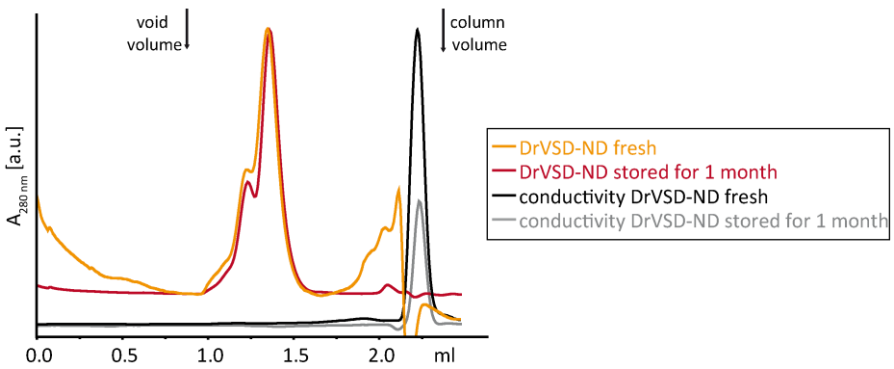

Figure A 6: Stability test of DrVSD inserted into ΔH5(-)-DMPG-NDs. The runs were performed by injecting 50 µl protein to an analytical Superdex200 PC 3.2/30 increase column with a flow rate of 0.075 ml/min at 16 °C. Black arrows indicate the void (0.93 ml) and the column volume (2.4 ml). One fresh prepared sample and one sample stored at 4 °C for 1 month were compared in a 20 mM Tris pH 8.0 at 4 °C and 200 mM NaCl running buffer. For both samples, the conductivity profile is shown to verify the comparability of both runs.

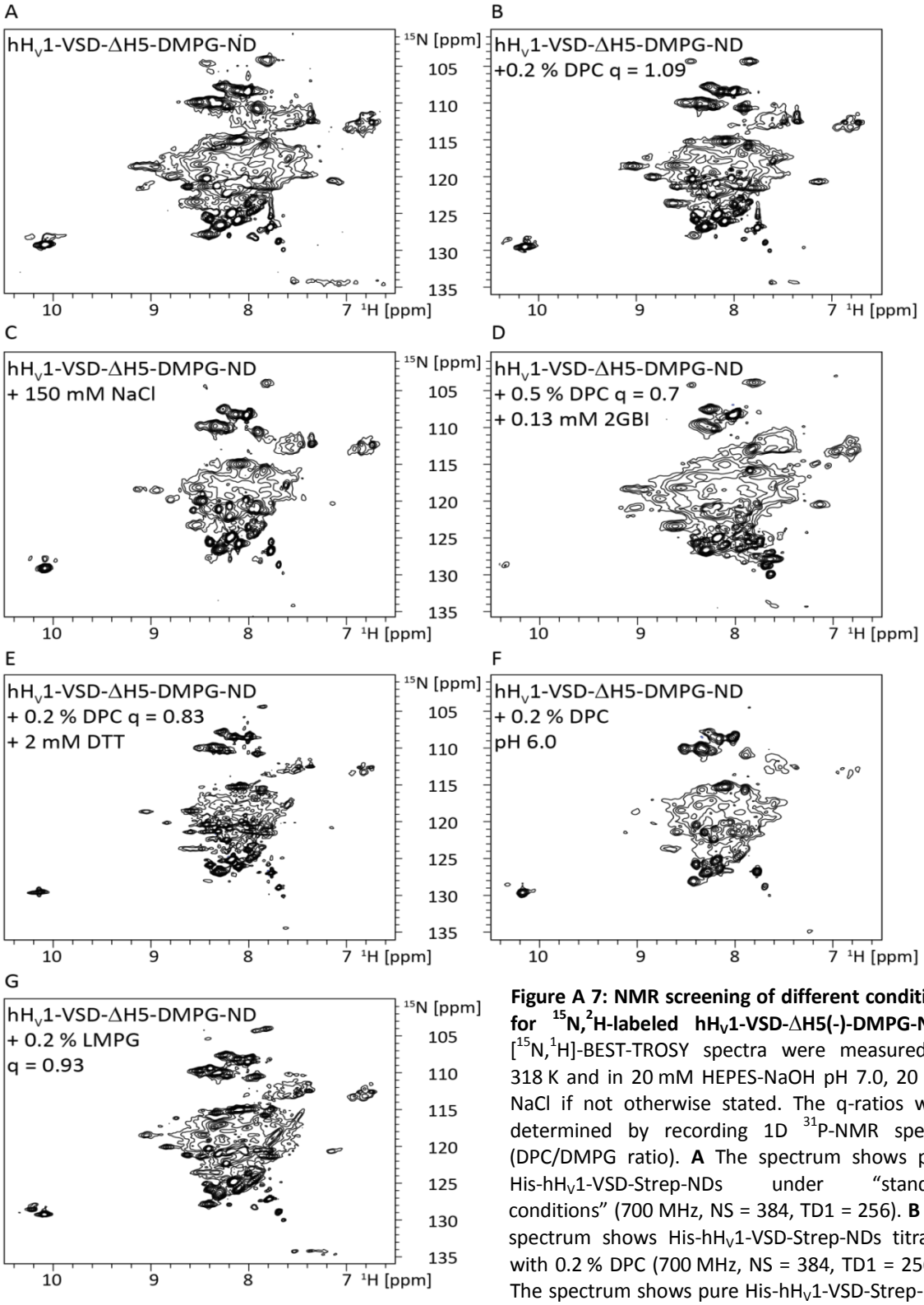

Figure A 7: NMR screening of different conditions for $^{15}N,^{2}H$-labeled hH_V1-VSD-ΔH5(-)-DMPG-NDs. [$^{15}N,^{1}H$]-BEST-TROSY spectra were measured at 318 K and in 20 mM HEPES-NaOH pH 7.0, 20 mM NaCl if not otherwise stated. The q-ratios were determined by recording 1D ^{31}P-NMR spectra (DPC/DMPG ratio). **A** The spectrum shows pure His-hH_V1-VSD-Strep-NDs under "standard conditions" (700 MHz, NS = 384, TD1 = 256). **B** The spectrum shows His-hH_V1-VSD-Strep-NDs titrated with 0.2 % DPC (700 MHz, NS = 384, TD1 = 256) **C** The spectrum shows pure His-hH_V1-VSD-Strep-NDs with additional 150 mM NaCl to increase hydrophobic interactions (800 MHz, NS = 384, TD1 = 184). **D** The spectrum shows His-hH_V1-VSD-NDs titrated with 0.5 % DPC and supplemented with 0.13 mM 2GBI in 100 % DMSO to stabilize the protein complex (600 MHz, NS = 704, TD1 = 288). **E** The spectrum shows His-hH_V1-VSD-Strep-NDs titrated with 0.2 % DPC and supplemented with 2 mM DTT to reduce possible intermolecular disulfide bonds and therewith decreasing the overall complex size (800 MHz, NS = 160, TD1 = 442). **F** The spectrum shows His-hH_V1-VSD-Strep-NDs titrated with 0.2 % DPC in 20 mM Mes pH 6.0, 20 mM NaCl (599 MHz, NS = 1000, TD1 = 214). **G** The spectrum shows His-hH_V1-VSD-Strep-NDs titrated with 0.3 % LMPG to analyze effects induced by different detergents used for the titration procedure (800 MHz, NS = 352, TD1 = 372).

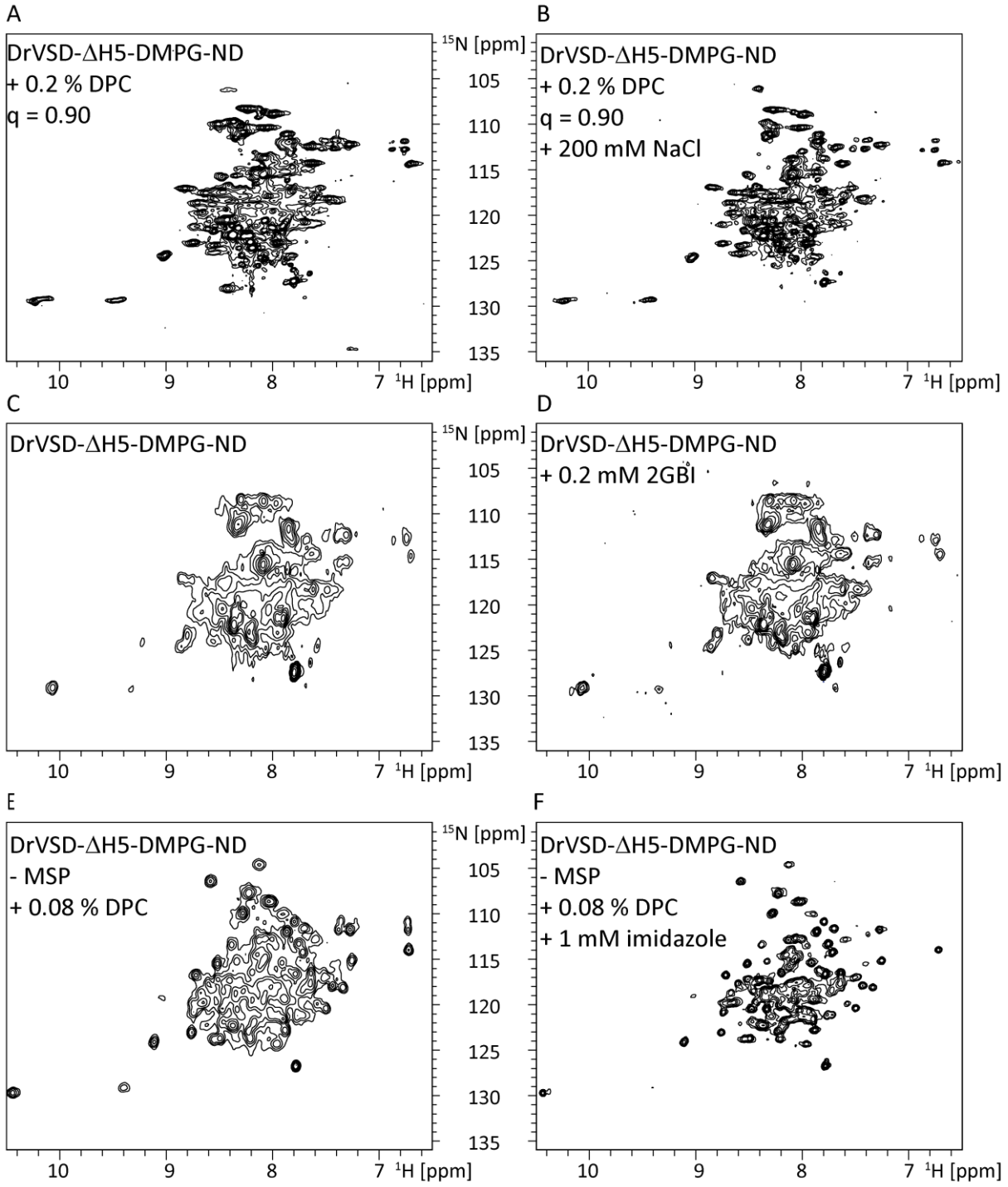

Figure A 8: NMR screening of different conditions for $^{15}N,^{2}H$-labeled His-DrVSD-Strep-ΔH5(-)-DMPG-NDs. Spectra were recorded at 318 K, 800 MHz and in 20 mM HEPES-NaOH pH 7.0, 20 mM NaCl if not otherwise stated. **A** [$^{15}N,^{1}H$]BEST-TROSY spectrum shows DrVSD-NDs titrated with 0.2 % DPC (NS = 432, TD1 = 352). **B** [$^{15}N,^{1}H$]-BEST-TROSY spectrum shows DrVSD-NDs titrated with 0.2 % DPC and additional 200 mM NaCl (NS = 512, TD1 = 180). **C** [$^{15}N,^{1}H$]-BEST-TROSY spectrum shows pure DrVSD-NDs in buffer with 150 mM NaCl (700 MHz, NS = 960, TD1 = 98). **D** [$^{15}N,^{1}H$]-BEST-TROSY spectrum shows DrVSD-NDs in buffer with 150 mM NaCl and additional 0.2 mM 2GBI in 100 % DMSO (700 MHz, NS = 960, TD1 = 74). **E** [$^{15}N,^{1}H$]-SOFAST-HMQC spectrum shows DrVSD in 0.08 % DPC after Ni^{2+}-IMAC purification whereby the scaffold protein was removed while retaining lipid molecules stayed attached in buffer with 150 mM NaCl (NS = 384, TD1 = 160). **F** [$^{15}N,^{1}H$]-BEST-TROSY spectrum shows DrVSD in 0.08 % DPC after Ni^{2+}-IMAC purification whereby the scaffold protein was removed while retaining lipid molecules stayed attached in buffer with 150 mM NaCl with additional 1 mM imidazole, mimicking the inhibitor (700 MHz, NS = 256, TD1 = 224).

7.3 Fluorescence-based assay validation for cell-free-synthesized proteins

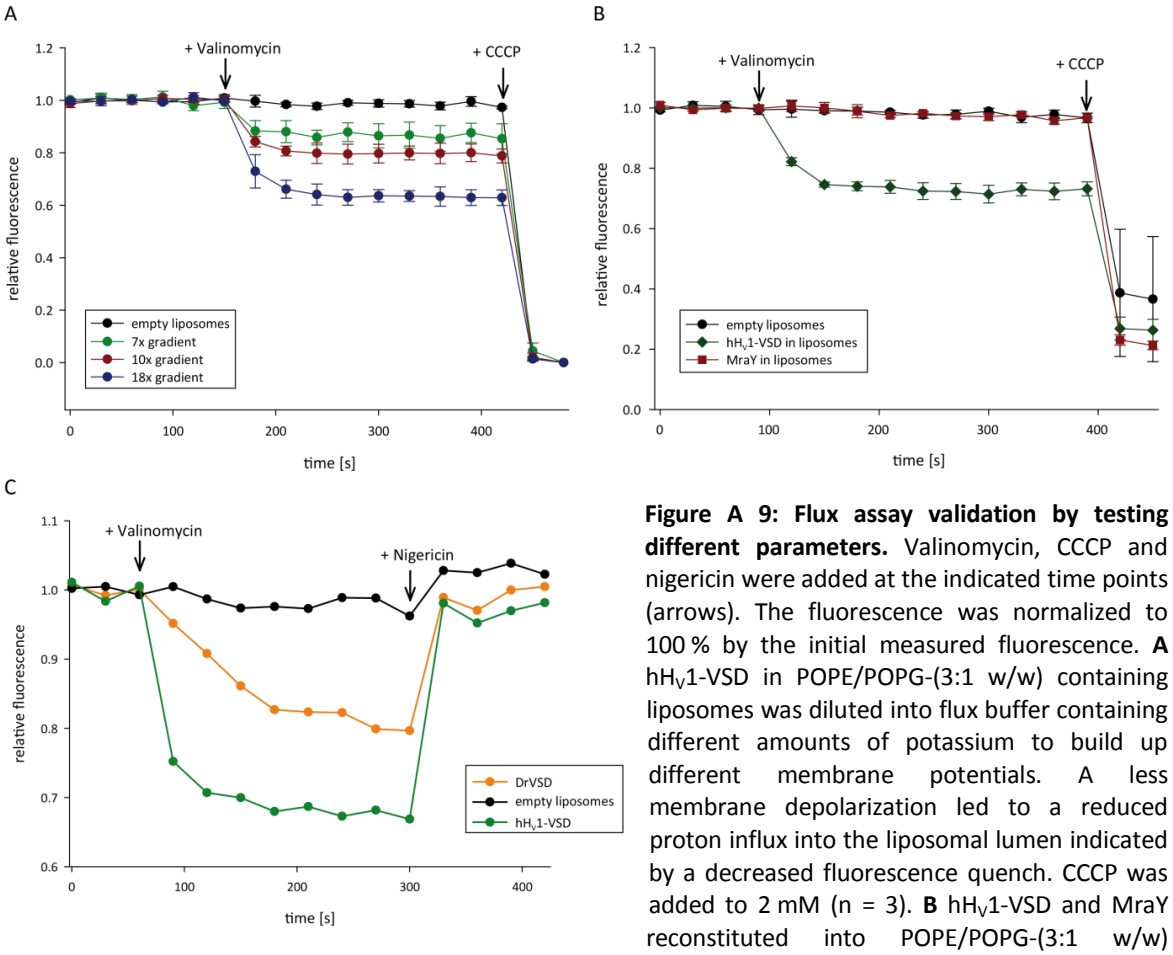

Figure A 9: Flux assay validation by testing different parameters. Valinomycin, CCCP and nigericin were added at the indicated time points (arrows). The fluorescence was normalized to 100 % by the initial measured fluorescence. **A** hH_V1-VSD in POPE/POPG-(3:1 w/w) containing liposomes was diluted into flux buffer containing different amounts of potassium to build up different membrane potentials. A less membrane depolarization led to a reduced proton influx into the liposomal lumen indicated by a decreased fluorescence quench. CCCP was added to 2 mM (n = 3). **B** hH_V1-VSD and MraY reconstituted into POPE/POPG-(3:1 w/w) containing liposomes were diluted 1:20 into flux buffer. The quench effect as described for hH_V1-VSD could not be observed for MraY. CCCP was added to 2 mM (n = 3). **C** hH_V1-VSD and DrVSD reconstituted into POPE/POPG-(3:1 w/w) containing liposomes were diluted 1:20 into flux buffer. The addition of nigericin led to an electroneutral potassium/proton exchange across the lipid bilayer causing a recovery of the fluorescence signal. Nigericin was added to 6 µM.

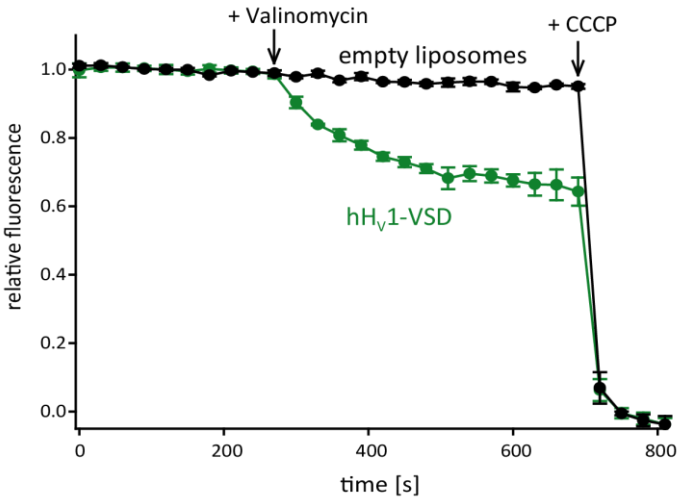

Figure A 10: Flux assay analysis of hH_V1-VSD directly synthesized in POPE/POPG-(3:1 w/w) containing liposomes in L-CF mode. Liposomes were directly added to the CF set-up and ultracentrifuged after 16 h incubation at 30 °C. Afterwards the liposome pellet was washed twice with liposome buffer and used in the flux assay procedure. The flux assay was performed by diluting the proteoliposomes 1:20 into flux buffer. After 240 s incubation, 20 nM valinomycin were added. After a further incubation of 480 s, CCCP was added to a final concentration of 2 mM ("wrong" concentration used). The fluorescence intensity was recorded at 480 nm (emission: 410 nm) and normalized by $(F_{obs}-F_{min})/(F_{max}-F_{min})$ whereby F_{max} is the average value of the maximum baseline prior to valinomycin addition and F_{min} is the average value of the minimum baseline after CCCP addition (n = 3).

Declaration about cooperation partners

Except where stated otherwise by reference or acknowledgment, the work presented was generated by myself under the supervision of my advisors during my doctoral studies.

All contributions from colleagues are explicitly referenced in the thesis. The material listed below was obtained in the context of collaborative research:

Fig. 19: SEC and NMR analysis of hH_V1-VSD in DH(7)PC micelles; Fig. 20: SEC and NMR analysis of hH_V1-VSD in LPPG micelles; Fig. 21: SEC and NMR analysis of hH_V1-VSD in DPC/LDAO (2:1) and DPC micelles; Fig. 30: Effects of DPC titration on VSD-NDs; Fig. 31: Detailed investigation of DPC titration effects on DrVSD-NDs; Fig. 38: Stability screening of refolded VSDs by SEC and NMR analyses; Fig. 39: NMR spectra comparison of DrVSD with the new codon-optimized DrVSD1 construct; Fig. A 1: Spectra of hH_V1-VSD in DH(7)PC micelles; Fig. A 2: Spectrum of His-DrVSD-Strep in 0.08 % DPC after IMAC purification; Fig. A 4: NMR screening of VSDs in different environments after TCA precipitation; Fig. A 5: NMR analyses of $^{15}N,^{2}H$-labeled hH_V1-VSD in different NDs; Fig. A 7: NMR screening of different conditions for $^{15}N,^{2}H$-labeled hH_V1-VSD-ΔH5(-)-DMPG-NDs; Fig. A 8: NMR screening of different conditions for $^{15}N,^{2}H$-labeled His-DrVSD-Strep-ΔH5(-)-DMPG-NDs; Dr. Frank Löhr (Institute of biophysical chemistry, AK Dötsch, Goethe-University Frankfurt a.M.), FL: NMR measurements, BH: sample preparation, conceptualization, formal analysis, data interpretation

Fig. 24: LILBID-MS analyses of VSDs in different detergents; Fig. 29: LILBID-MS analyses of hH_V1-VSD- and DrVSD-ND complexes; Oliver Peetz (Institute of physical and theoretical chemistry, AK Morgner, Goethe-University Frankfurt a.M.); OP: LILBID measurement and data evalutation (Software package), BH: sample preparation, conceptualization, formal analysis, data interpretation

Fig. 25: Analyses of VSDs aggregation using DLS, NTA and RMM, Dr. Bernd Tartsch and Dr. Marcus Epe (Malvern instruments limited company), BT: measurement and data evaluation (Software package) of the DLS and NTA experiments, ME: measurement and data evaluation (Software package) of the RMM experiment, BH: sample preparation, conceptualization, formal analysis, data interpretation

Fig. 28: TEM observations of VSDs co-translationally-inserted into NDs, Simone Prinz (Department of Prof. Dr. Kühlbrandt, MPI of Biophysics Frankfurt a.M.), SP: grid preparation, measurement and data evaluation (Software package), BH: sample preparation, conceptualization, formal analysis, data interpretation

Fig. 32: ITC analysis of VSDs titrated with the inhibitor 2GBI, Dr. Marco Marenchino (Malvern instruments limited company), MM: measurement and data evaluation (Software package), BH: sample preparation, conceptualization, formal analysis, data interpretation

Fig. 33: Sucrose gradient centrifugation analyses of reconstituted proteins, Dr. Erik Henrich (Institute of biophysical chemistry, AK Dötsch, Goethe-University Frankfurt a.M.), EH: provision of the MraY-contianing plasmid and liposomes with DMPC/DOPMME lipid mixture, BH: sample preparation, conceptualization, performance of the experiments, formal analysis, data evalutation and interpretation

Fig. 37: Refolding of KcsA and VSDs, Dr. Christopher Hein (Institute of biophysical chemistry, AK Dötsch, Goethe-University Frankfurt a.M.), CH: provision of the KcsA-containing plasmid, BH: sample preparation, conceptualization, performance of the experiments, formal analysis, data evalutation and interpretation

Whenever a figure, table, or text is identical to a previous publication, it is stated explicitly in the thesis that copyright permission and/or co-author agreement has been obtained. The following parts of the thesis have been previously published:

- Chapter “1.4 Protein synthesis using cell-free gene expression”

- Figure(s) “Figure 7: Different cell-free expression modes for membrane proteins in a preparative scale home-made continuous-exchange reaction container.”, “Figure 20 D: SEC and NMR analysis of hH_V1-VSD in LPPG micelles.”, “Figure 29: LILBID-MS analyses of hH_V1-VSD- and DrVSD-ND complexes”, “Figure 40: Upgrades in the nanodisc technology field”, “Figure A 1: Spectra of hH_V1-VSD in DH(7)PC micelles”